Ozone Science

A Canadian Perspective on the Changing Ozone Layer

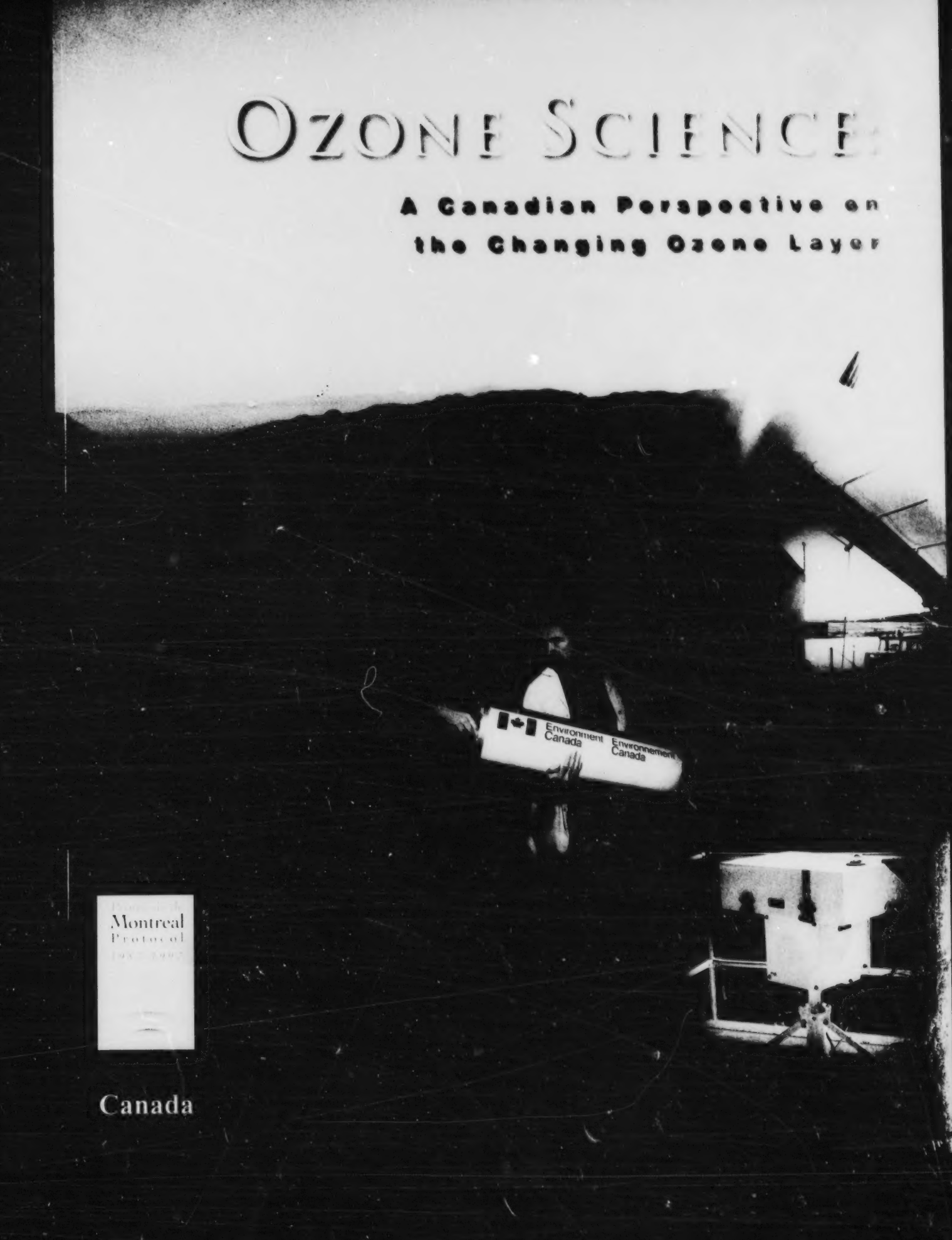

Montreal Protocol

Canada

Cover:

The main cover photograph shows the Eureka Observatory as seen from the north in February 1997 (photo courtesy of John Bird, Institute for Space and Terrestrial Science, Toronto). In the insets:

- A 400,000 cubic metre helium balloon is launched in July 1997, carrying the Environment Canada Atmospheric Environment Service (AES) sunphotospectrometer (SPS) to an altitude of 35 km. Together with the Jet Propulsion Laboratory's ATMOS interferometer solar absorption instrument, the SPS measured atmospheric profiles of ozone, aerosols, and other atmospheric constituents (photo courtesy of R.J. Salawitch, Jet Propulsion Laboratory).
- The ATMOS/SPS payload hangs from the launch crane before flight. The ATMOS balloon flight was undertaken in support of the Polaris ER-2 mission (photo courtesy of R.J. Salawitch, Jet Propulsion Laboratory).
- Bob Hall and Clive Midwinter of the AES install instruments for the Composition and Photodissociative Flux Measurement experiment on board NASA's ER-2 high-altitude research aircraft.
- A Brewer spectrophotometer of the United States Environmental Protection Agency takes observations in Shenandoah Park, Virginia, in May 1997 (photo courtesy of Albert Maione, Sci-Tec Inc., Saskatoon).

CARD 97-3

Copyright © Environment Canada, 1997

Egalement disponible en français

Project Coordinators
Angus Fergusson (Environment Canada)
Harry Hirvonen (Environment Canada)

Consultant
Andrew J. Forester, Dartside Consulting

Design and Production Coordination
Kim Massicotte, CH Design

Printed and bound in Canada by
the University of Toronto Press

Printed on recycled paper

Ozone Science: A Canadian Perspective on the Changing Ozone Layer

edited by

D.I. Wardle, J.B. Kerr, C.T. McElroy, and D.R. Francis

Environment Canada

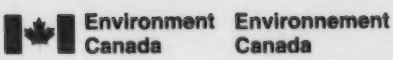

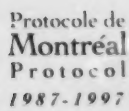

Contents

Summary 1

Introduction 9

Chapter 1:

The Distribution of Ozone and Ozone-Depleting Substances in the Atmosphere and Observed Changes
D.W. Tarasick (Environment Canada) and V.E. Fioletov (Environment Canada) 15

Chapter 2:

The Influence of Dynamical Processes on Ozone Abundance
T. Shepherd (University of Toronto) 41

Chapter 3:

Ozone Chemistry: Simulation and Depletion
J.C. McConnell (York University) and D.J. Chartrand (York University) 57

Chapter 4:

The Influence of Ozone and Other Factors on Surface Radiation
V.E. Fioletov (Environment Canada) and W.F.J. Evans (Trent University) 73

Chapter 5:

UV-B Effects

Human Health
R. Gallagher (British Columbia Cancer Agency) 92

Agriculture
M. Morrison (Agriculture and Agri-Food Canada) 94

Forests
K. Percy (Natural Resources Canada) and S. Cameron (Natural Resources Canada) 97

Freshwater and Wetland Ecosystems
H. Vaughan (National Water Research Institute) and B. Pauli (Canadian Wildlife Service) 101

Marine Ecosystems
J. Cullen (Dalhousie University) 103

Materials
R. Alward (McGill University) and M. Kamal (McGill University) 105

Appendix

Acronyms and Abbreviations 117
Glossary 118

The tenth anniversary of the 1987 signing of the Montreal Protocol is an event to be celebrated because the protocol has been the basis of a successful effort by the international community to control and greatly reduce the emission of ozone-depleting substances into the atmosphere. A serious threat to the global environment has been addressed and appropriate measures have been taken. This report provides a brief overview of the state of ozone science 10 years after the signing. Compiled by Canadian scientists, it draws on both Canadian and international research to outline our current understanding of ozone depletion and its effects. It also highlights Canadian results and data, where appropriate, and emphasizes items of special Canadian concern, such as ozone depletion in the Arctic and the impacts of UV changes on forests and freshwater ecosystems.

The Distribution of Ozone and Ozone-Depleting Substances in the Atmosphere and Observed Changes

The main features of the climatology of total ozone were discovered by G.M.B Dobson by 1930. These were the dependence on latitude and season and the day-to-day changes that are associated with meteorological conditions. A more extensive climatology extending from the ground to all levels in the stratosphere is now available as a result of the use of many new techniques. These measure the distribution of ozone with altitude as well as the total amount both from the ground and from a variety of platforms, including balloons, aircraft, rockets, and satellites. The severe depletion in the Antarctic during the spring, known as the ozone hole, was discovered in 1985, and a few years later midlatitude depletion was recognized. A significant and developing depletion in the Arctic spring has also been observed during the last few years. Atmospheric concentrations of ozone-depleting substances have been measured for some decades and now show definitive evidence of the effect of the Montreal Protocol.

- Canada began total ozone measurements at five stations in the early 1960s and has been operating twelve ground-based ozone observing stations equipped with Brewer spectrophotometers since 1992. The total ozone data are used for trend studies, for forecasting ozone and UV radiation, and for characterization and calibration of satellite measurements.
- The four-station Canadian ozonesonde network was initiated in the mid-1960s. Currently sondes are flown at least weekly from six locations. All the sonde and ground-based data are available from the World Ozone and Ultraviolet Radiation Data Centre (WOUDC) which Environment Canada operates for the WMO.
- The Stratospheric Ozone Observatory at Eureka (80°N, 86°W), which is part of the WMO/UNEP Network for Detection of Stratospheric Change(NDSC), was opened

in 1992. It houses lidars for measuring ozone and aerosols, Fourier transform spectrometers, and other spectrometers for measuring stratospheric composition. The Ontario Institute for Space and Terrestrial Physics and the Japanese Meteorological Agency and Communications Research Laboratory are partners with Environment Canada in conducting these experiments.

- Annual average ozone values over Canadian stations have declined by about 6% from pre-1980 averages. The decline is greatest in spring and least in the fall. Sonde measurements show that the main loss is in the lower stratosphere.
- Sonde measurements over Canada have shown that free (i.e., unpolluted) tropospheric air has suffered a similar loss of ozone to that in the stratosphere during the past 15 years. However, European sonde data show some increases during the 1980s.
- The ozone values in 1993 were lower than in any other year over southern Canada and over the midlatitudes in general. The decline, which is attributed to the effects of the eruption of Mt. Pinatubo in 1991, occurred in the lower stratosphere and, at least over Canada, throughout the troposphere.
- Ground and balloon-based measurements over the Canadian Arctic from the Eureka NDSC observatory, Resolute, and Alert, as well as satellite measurements, show the development of strong depletion during the past few years, especially in the spring of 1997. However, the lowest Arctic ozone values are still much higher than the low values in the Antarctic.
- The Canadian Meteorological Centre's daily forecast of the total ozone field over Canada is based on measurements of total ozone by the twelve Canadian Brewer spectrophotometers and the output from the Numerical Weather Prediction model. The forecast, based on statistical relationships, has a very low error.
- Measurements show that atmospheric concentrations of CFC-11 at Alert and Point Barrow have begun to decline and that the rate of increase in CFC-12 is much reduced.

The Influence of Dynamical Processes on Ozone Abundance.

Transport of ozone by the Brewer-Dobson circulation from its main source region in the equatorial midstratosphere to its regions of greatest abundance, in the lower stratosphere at middle and high latitudes, is a key determining factor in establishing the observed distribution of ozone. The height of the tropopause is also a determining factor for the total ozone amount, since the tropopause is ozone poor while the stratosphere is relatively ozone rich. These are dynamical factors that affect the ozone directly. Different scales of mixing affect concentrations of ozone and other constituents; modelling of chemical reactions may be inaccurate if the spatial resolution of the model is not fine enough to capture the smaller scale effects.

Dynamics act indirectly on the chemistry of ozone by causing changes in temperature, which affect the rates of most chemical reactions (some more than others). Of particular importance is the effect of temperature on the formation of polar stratospheric clouds, and the enhancement that these cause of chlorine concentration and ozone destruction. Understanding of atmospheric dynamics has developed through advances in numerical modelling coupled with increasingly detailed measurements of ozone and other trace constituents, but a number of problems remain.

- The spatial structure of the tropopause directly affects the total abundance and latitudinal distribution of ozone, but our understanding of how this structure is established is mostly qualitative and our ability to characterize, let alone predict, interannual variability and trends is extremely limited.
- Although we have a basic understanding of the origin of the Brewer-Dobson circulation and its seasonal cycle, significant theoretical gaps remain, especially with respect to the tropics. There is considerable potential for interannual variability and decadal-scale trends in the Brewer-Dobson circulation associated with corresponding variability in the driving mechanisms. Such variability places a major limitation on our predictive capability.
- It has recently become evident that the transport and mixing characteristics of the tropics are qualitatively different from those of the midlatitudes. To a first approximation, the tropical stratosphere regime comprises a large-scale systematic upwelling modified by mixing across a permeable subtropical transport barrier. Adequate characterization is not yet possible because of the difficulty in determining the upwelling rate and the current lack of accurate wind measurements in the tropics.
- The lowest part of the tropical stratosphere appears to be a particularly complex region of the atmosphere which plays a critical role in determining the global structure of stratospheric transport and mixing , yet it is a region that remains poorly understood. For example, most current conceptual models completely ignore the effect of longitudinal asymmetries such as the monsoon circulation.
- There is now a good understanding of why wintertime polar ozone depletion is much less and more variable from year-to-year in the Arctic than in the Antarctic. Quantita-

tive evaluation is limited by uncertainties in the cause and magnitude of the polar downwelling (which affects polar temperatures) and in our understanding of planetary wave drag.

- It has been shown recently that simulation of the amount of ozone destruction in the Arctic winter is highly sensitive to an adequate representation of small-scale structure in chemical fields. Similar considerations presumably apply to midlatitudes and represent a major challenge for quantitative modelling.
- The laminae seen in ozonesonde profiles have been clearly linked to filamentation processes associated with planetary wave breaking at the edge of the polar vortex. Dynamical lifetimes of these filaments/laminae are estimated to be at least two weeks, comparable to estimated chemical lifetimes of ozone filaments in midlatitudes.

Ozone Chemistry: Simulation and Depletion

Stratospheric ozone originates almost entirely as a result of the action of sunlight on normal diatomic oxygen molecules, mostly at altitudes above about 25 km and in the tropics. Ozone is also produced through reactions involving volatile organic compounds(VOCs) and nitrogen oxides, but these are mainly of significance in the troposphere. The reaction of atomic oxygen with ozone was once thought to be the only ozone loss mechanism in the stratosphere. However, various anthropogenic and natural long-lived gases such as N_2O, CFCs, halons, and methyl bromide and chloride are dissociated in the stratosphere into products that are effective catalytic destroyers of ozone molecules. These reactive molecules include NO and NO_2, Cl and ClO, OH and HO_2, and Br and BrO. Their concentrations are limited by the formation of reservoir species, such as HNO_3, $ClONO_2$, and HCl, that may dissociate, but not necessarily quickly, to give back the reactive molecules. The relative concentrations of the reactive molecules and the reservoir species which do not destroy ozone determine the effectiveness of ozone destruction. They are strongly influenced by polar stratospheric clouds (PSCs), which facilitate the conversion of reservoir species to reactive halogens as, to a lesser degree, do sulphate aerosols in the midlatitudes. Adequately representing the properties and behavior of PSCs and sulphate aerosols is therefore an important challenge for simulation models. Types of models that are in use range from the zero-dimension, chemistry-only, box models to modified atmospheric general circulation and numerical weather prediction models (AGCMs and NWPs) that incorporate interactive ozone photochemistry. Models serve as tools to diagnose the processes that are occurring in the atmosphere and can be used to make predictions, provided that they are validated and their characteristics are consistent with the known properties of the atmosphere.

- The development of techniques and computer hardware during the past decade has resulted in the ability to carry chemical reaction sets that were once tractable only in box or 1D models into higher dimensional models.
- 3D chemical transport models (CTMs) are models in which the chemical constituents are carried by winds that are generated in AGCMs or NWP models. They do not include feedback from chemical composition to the dynamics. Several advanced AGCMs, including the Canadian Middle Atmosphere Model (CMAM), now incorporate chemistry interactively, so that the feedback from chemistry to dynamics is included.
- NWP models, which are similar to ACGMs but have finer resolution, can also now include interactive chemistry. The Canadian NWP, the Spectral Finite Element Model (SEF), is now carrying gas phase chemistry and heterogeneous reactions are being added. The SEF model, with the addition of new data assimilation methods that are being developed for chemical constituents, is the ideal tool for simulating the Arctic spring stratosphere.
- Current models reproduce the behaviour of atmospheric ozone quite well, but loss rates in the upper stratosphere are overestimated. Also, discrepancies between modelled and observed ratios of active to reservoir chlorine have not yet been resolved.
- Most current models underestimate the ozone loss in the lower stratosphere, which is the major component of the change in total ozone. Some models that give reasonable simulations of the observed loss in total ozone do not reproduce the vertical profile satisfactorily.
- The eruption of Mt. Pinatubo provided a unique opportunity to study the role of sulphate aerosols in ozone chemistry. It is believed that the thermal effects of the enhanced aerosol concentrations may have altered transport patterns so as to enhance ozone destruction and that the conversion of N_2O_5 to HNO_3 on the aerosol surfaces perturbed the chemistry so as to enhance depletion by halogens.
- Simulation of the Antarctic spring depletion by current models appears satisfactory and is somewhat insensitive to the details of the heterogeneous conversion chemistry; this insensitivity is related to the ozone loss being nearly complete in substantial parts of the stratosphere.

- Simulation of the Arctic spring depletion is less satisfactory, the calculated loss being approximately 60% of the observed value according to one recent simulation. The discrepancy may be due to the model's inability to capture small-scale mixing effects. As well, the winter stratospheric temperatures that are used in these simulations may be in error by small amounts that are nevertheless significant for PSC formation.
- Aircraft that fly in the stratosphere and upper troposphere can affect the chemistry there through their emission of nitrogen oxides (NO_x) and water. Both of these will tend to increase the prevalence of PSCs and so enhance ozone destruction. NO_x itself can increase both the loss rate and the production of ozone, and adequate estimation of these competing processes requires characterization of the transport between and within the stratosphere and troposphere of a quality that is not yet available.
- The increased UV-B (290–315 nm) radiation in the troposphere resulting from the depletion of stratospheric ozone could increase tropospheric concentrations of OH. Such an increase would, in turn, increase removal rates for several greenhouse gases, such as methane, CO, and the CFCs. The effects of increased UV-B on tropospheric ozone are complex and uncertain. Ozone concentrations might increase in populated areas with higher concentrations of VOCs and NO_x while decreasing in the less polluted background air.
- The cooling of stratospheric temperatures that is associated with global warming may make PSCs more numerous and thereby counteract the expected recovery of ozone as the amount of stratospheric halogens declines. Evidence of decreasing trends in stratospheric temperatures has been questioned, but in the past few Arctic winters ozone values and stratospheric temperatures have been particularly low. The loss of ozone may itself have augmented the low temperatures and caused the vortex breakup to be delayed.
- Important factors that are not yet treated effectively in atmospheric modelling are: gravity waves and their effect on the middle atmosphere circulation, detailed transport processes in the upper troposphere and lower stratosphere, microphysical aerosol processes that are involved in heterogeneous chemistry in both the troposphere and the stratosphere, and the effects of aerosols on climate through radiation and the formation of clouds.
- It is assumed that, as stratospheric chlorine begins to decline in the next decade, ozone amounts will begin to recover, albeit slowly, shortly thereafter. It is imperative to continue monitoring to determine whether this scenario unfolds in this manner.

The Influence of Ozone and Other Factors on Surface Radiation.

Atmospheric ozone is important as it interacts both with solar radiation and with the thermal radiation that is emitted by the earth's surface and the atmosphere. It screens the surface from solar UV radiation that would otherwise prove harmful to living organisms, causes heating in the stratosphere, and acts as a "greenhouse" gas. The depletion of ozone during the past two decades has allowed more UV-B radiation to reach the ground than would otherwise have happened. The extent of this increase and the variability of ground-level UV radiation and its causes are the focus of current research, since estimation of the biological effects of ozone depletion may require knowledge of both these factors. The effects of UV on people are largely determined by behaviour, and public awareness programs can help people avoid excessive exposure. Ozone-depleting substances are also greenhouse gases, and their presence in the atmosphere and the recent changes in atmospheric ozone affect global warming.

- Changes in the UV are usually expressed as trends in monthly or seasonal averages, although certain biological effects may depend more on peak values during critical stages in life cycles than on the total irradiation. Also, for biological effects that are more complex than skin reddening, there may be problems in representing the effectiveness of UV radiation by simple action-spectra weighted integrals.
- About 100 station years of UV irradiance data can be accessed from the World Ozone and Ultraviolet Radiation Data Centre (WOUDC). Most of the stations have more than five years of data.
- The dependence of clear-sky UV irradiance on ozone is well established. When the sky is overcast, the irradiance throughout the spectral range 300–325 nm is reduced by approximately the same amount at all wavelengths, provided that the transmision is greater than about 15%. Consequently, the ozone amount can be easily derived from the spectrum. The accuracy of one technique developed for this purpose is 3% for daily averages of total ozone.
- With heavily overcast skies, the transmitted spectrum carries the signature of a greater amount of ozone. This is consistent with the enhancement of ozone absorption in the cloud by multiple scattering. Apparent ozone amounts up to 1000 DU have been observed when the cloud transmission is down to about 1%.

- Sulphur dioxide absorbs strongly in the UV-B region. High amounts of absorption by SO_2 are often evident in the UV irradiance spectra from Kagoshima in Japan. This is caused by the plume from the nearby volcano, Sakurajima. The SO_2 absorption associated with the plume can reduce the UV Index by as much as 25%. However, throughout the year the average reduction is only 1–2%. No other stations in the WOUDC exhibit significant absorption by SO_2.
- The effect of ground reflectance on UV radiation has been investigated at seven Canadian locations by comparing data with and without snow on the ground. It was found that the enhancement due to snow cover varies from 8% at Halifax to 39% at Resolute. The range of results reflects differences in terrain around these stations.
- An eleven-year time series of the accumulated spectral irradiation during summer has been derived from spectral irradiance measurements at Toronto that were started in 1986. The irradiation at 324 nm shows a small downward trend, while at 300 nm there is an upward trend of about 1% per year. The ratio of the irradiation at 300 nm to that at 324 nm closely follows the average summer ozone values. This suggests that the main cause of the upward trend at 300 nm is ozone depletion.
- There has been considerable progress in simulating UV irradiance from related atmospheric variables and satellite measurements. These developments should be useful in extending the current climatology of UV and in constructing past climatology.
- The downward thermal radiation at the earth's surface from ozone and several ozone-depleting gases has been measured in southern Canada. The results confirm that ozone-depleting substances are making a significant contribution to global warming.
- The UV Index program, which produces daily forecasts of UV radiation and is designed to help people avoid excessive exposure, was started in Canada in 1992. Similar programs are now operated in several other countries. The Ozone Watch program, also started in 1992, provides Canadians with weekly information on the ozone layer.

UV-B Effects

Increased UV flux to the earth's surface has properly heightened concerns over the impact on human health, given that it is well-known to cause a variety of skin cancers, eye conditions, and other problems. Although the potential health impacts are serious, many aspects of the epidemiology and pathology of UV exposure are relatively well understood; however, the situation with respect to non-human biota is more complex. Ecosytems and biomes have adapted over long periods to a particular range of UV-B, and any change in the regimen must *a priori* influence their stability, geographical range, and possibly survival. Whether changes wrought by an increase in UV flux will be profound or subtle, minor or dramatic, beneficial or inconsequential depends on many factors, most of which are poorly understood. There is, therefore, a pressing need to measure, monitor, and understand the effects of enhanced UV-B irradiance on biological communities if we are to be able to predict the impacts that will occur in the next 30–40 years and manage the consequences.

Human Health

Within Canada, most UV effects research has centred on skin cancer and eye damage, but only minimal effort has been devoted to studies of immune suppression and infectious diseases.

- Recent Australian and Canadian research has shown that members of lower socioeconomic occupations with substantial outdoor exposure have a lower risk of malignant melanoma and basal cell carcinoma than those engaged in indoor, professional, managerial, and technical occupations, who receive only intermittent exposure to the sun.
- Squamous cell carcinoma appears to be related to cumulative exposure.
- Acquired (non-congenital) skin moles (nevi) are an indicator of elevated risk for malignant melanoma. Australian and Canadian researchers have shown a direct relationship between mole density and solar UV exposure. Generally, the risk of melanoma increases with mole density.
- Persons with light skin colour, red hair, and a propensity to burn in the sun are at greater risk of basal and squamous cell carcinoma.
- UV radiation may suppress the human immune response, increasing the risk of skin cancer and bacterial and viral infection (including the re-activating of smallpox and herpes lesions).
- Acute, long-term, and chronic eye conditions may become more prevalent if UV exposure increases.
- Avoidance of the sun, use of sun screens, and wearing UV-protective glasses are important prophylactic measures.

Ecosystems

Alterations in UV irradiance can affect primary production in all ecosystems, terrestrial and aquatic, natural, managed or exploited with a potential cascade of effects. Current understanding of these processes does not enable confident prediction of the impacts.

There has been little systematic research on the impact of enhanced levels of UV-B on Canadian flora and fauna. A few studies of some agricultural and commercial forest species

provide limited insight into the problem, but it is difficult to extrapolate from these to predict impacts on whole ecosystems.

It is important that the effects of both chronic increases in irradiance leading to cumulative doses, and also episodic peaks or events that may coincide with critically vulnerable stages in life cycles, be evaluated. Further, the influence of ozone depletion must also be considered in conjunction with the effects of other stressors such as global warming, acidification, and the presence of toxic chemicals, making it essential that UV-B impact studies be integrated with existing ecological research, monitoring, and assessment programs.

Agriculture

- Ultraviolet radiation damages DNA, cell membranes, and organelles (e.g., chloroplasts). Plants have a capacity to repair damaged DNA, and some can protect themselves by synthesizing UV-absorbing pigments and by modifying key metabolic enzymes. Harm occurs when the radiation dose causes damage beyond a plant's capacity for repair and protection.
- Crop damage is manifest as a decline in yield, reduced fertility with fall in seed and fruit production, drop in marketable quality, and ecological effects such as changes in crop-weed interactions and pasture mixtures.
- While the extrapolation from controlled environments to field conditions remains an issue, research is consistent in identifying that individual varieties differ in their sensitivity to UV-B, as measured by changes in photosynthesis, growth, yield, and reproduction. Most Canadian crops have low or intermediate sensitivity to moderate increases in UV-B radiation. Impacts on forage and vegetable crops have been equivocal. Of over 100 varieties of 12 important crop species, 40% were unaffected by UV-B equivalent to a 20% decrease in the ozone layer and 60% were affected in some fashion. Soybean, tomato, and canola losses may be expected, possibly totalling hundreds of millions of dollars annually. Maize does not appear to be vulnerable to anticipated increases in UV.
- UV-B may accelerate the rate of decomposition of straw and chaff, with potentially beneficial effects in arid environments and under minimum-till conditions.

Forests

- Although forests are of major economic, social, and natural importance, little is known about their susceptibility to enhanced UV-B radiation.
- Trees are long-lived and will be exposed to increased UV-B over decades. Short-term effects have been reported, and there is some indication of cumulative, chronic impacts. Multiyear experiments with long-lived species are desirable.
- The impacts of UV radiation appear to be less serious on species native to high elevations and adapted to greater irradiance.
- Impacts of enhanced UV radiation should be considered in conjunction with the effects of other stressors such as climate change and acidification. Studies of the interactive effects of UV-B and CO_2 enrichment on the growth and physiology of conifer seedlings suggest that future conifer seedling growth and competitive ability will be altered by the changing environment.
- The only field study to have been done so far on UV-B effects on trees in North America attributed sun-scalding of white pine foliage in Ohio and Ontario to elevated ambient UV-B levels. Recent research has also shown that epicuticular wax chemical composition in certain conifer species is affected by UV-B exposure in a manner that inhibits photosynthesis.
- The 50-year window of significant ozone depletion has sufficient potential to affect Canadian forest productivity on a large scale, with far-reaching consequences that are not yet apparent.

Freshwater and Wetland Ecosystems

- Shallow freshwater ecosystems are particularly vulnerable to enhanced levels of UV radiation, showing changes in primary productivity, nutrient cycling, community structure, and modification to the transport and speciation of toxic chemicals in the food-chain.
- UV penetration of surface waters is attenuated by the presence of dissolved organic carbon (DOC), and changes in DOC levels have a greater effect on the vulnerability of freshwaters to UV than changes in stratospheric ozone. In boreal lakes, where global warming and lake acidification have caused a sharp decline in DOC, UV-B penetration into the water column has increased between 22% and 60%.
- Even at current ambient levels, UV-B inhibits some species of zooplankton from frequenting their preferred position in the water column.
- Under experimental conditions, enhanced levels of UV radiation depressed algal production but affected the zooplankton that fed on the algae to a proportionately greater extent. As a result, the accumulated algal biomass increased, even though primary production was reduced. Because a key link in the food chain had been weakened, less production was transferred to higher trophic levels. The implications for aquatic ecosystems are disturbing.
- Concern has been expressed over synergisms between UV-B, climate change, lake acidification, fungal infections, and toxic chemicals that could affect amphibia. However, Ontario amphibians do not seem to have been affected by current levels of radiation, despite the apparent vulnerability of eggs and larvae.

Marine ecosystems

- Direct impacts of UV-B on microbial processes and higher trophic levels have been demonstrated, but the cumulative effects of ozone depletion on marine ecosystems are, as yet, unpredictable. Potential responses include changes in species composition, shifts in food webs (with collateral impacts on fisheries), and possibly climatic changes.
- Increases in UV-B alter the growth, survival, and biogeochemical activities of many microbes, plants, and animals in the sea. Damage to DNA directly influences survival, but UV-B also affects spatial orientation (and hence vertical migration) of phytoplankton, nitrogen metabolism, photosynthesis, larval mortality, and processes ranging from viral infection to hatching success in fish eggs.
- The sensitivity of physiological processes to solar UV-B requires a biological weighting function (BWF, also called an action spectrum) to quantify the effective irradiance. BWFs need to be determined for a greater number of biological functions and estimates need to be made of the range in variation of BWFs for each process, as these appear to be highly variable between species.
- Biological effects of UV-B have been detected tens of metres into the water column, most notably the inhibition of short-term photosynthesis in Antarctic phytoplankton. Quantitative estimates of the inhibition of photosynthesis by UV radiation are converging as research continues.
- Some toxic dinoflagellates show UV-photoprotective mechanisms that might give them a competitive edge, perhaps leading to a greater dominance of toxic or nuisance algae.
- Increases in UV-B may favour species of phytoplankton that produce dimethyl sulphide (DMS), a gas involved in cloud formation, and thus contribute to climate change.
- Interpretations of UV effects in Canadian waters require recognition of the fundamental differences that exist between the Antarctic and waters of the northern hemisphere, including the Arctic. Consequently, basic research on marine ecosystems in Canadian waters is essential.

Materials

UV radiation causes significant and deleterious changes to many materials used in outdoor applications. Any increase in UV flux to the earth's surface will degrade infrastructure and so generate significant costs for repair and replacement.

- Canadian research has addressed the effects of UV on polymers, wood and paper, building materials, paints and coatings, and textiles and clothing, although the main thrust has been on the evaluation of radiation resistance of materials used in outer space and of clothing materials.
- UV-B radiation damages synthetic polymers and other materials, but the mechanisms are not well understood at the molecular level and the combined impacts of both short and long wavelength radiation and other environmental variables adds further complexity to the issue.
- Bleached pulp and paper products made by inexpensive processes are discoloured by UV radiation. Canadian researchers have made significant advances in understanding how this occurs. The ability to reduce discolouration could greatly expand the market for this class of paper.
- Non-plastic building materials such as roofing membranes and outdoor sealants are currently being studied with respect to their resistance to UV but not specifically in the context of enhanced, ozone-related irradiance.

102-05474/

INTRODUCTION

MONTREAL PROTOCOL — THE ACHIEVEMENT AND THE CHALLENGE

The signing of the Montreal Protocol on September 16, 1987, was a remarkable and significant event in modern diplomatic history, one of those rare occasions when individual nations subordinated economic self-interest to the achievement of a common planetary goal. The event was even more remarkable when one considers that it was accomplished in spite of scientific uncertainties about detailed aspects of the depletion process and without immediate evidence of impacts on ecosystems and human health. That an agreement was eventually reached was due not only to an extraordinarily successful collaboration between scientists and policymakers but also to the enormous strides made by the international scientific community in expanding the boundaries of ozone science. The solidity of their achievement can be seen in the very real progress that has been made since 1987 in reducing emissions of ozone-depleting substances

Canada has been concerned about stratospheric ozone depletion since the issue was first raised by scientists in the 1960s and 1970s, and our interest in ozone science goes back even further, to the 1950s, when the first Canadian ozone monitoring programs were established. Over the past couple of decades our involvement in ozone science and contributions to it have been considerable. The Brewer ozone spectrophotometer, now the principal instrument for ground-based ozone measurements, was developed here. Our network of monitoring stations is one of the largest in the world, and, as the home for the World Ozone and Ultraviolet Radiation Data Centre, we are responsible for archiving ozone measurements from around the world. Canada is also proud to have been one of the original parties to the Montreal Protocol and to be among the many countries that have met or exceeded their obligations under the protocol and its amendments.

The present document provides a brief overview of the state of ozone science in 1997, on the 10th anniversary of the Montreal Protocol. Compiled by Canadian scientists, it draws on both Canadian and international research to outline our current understanding of ozone depletion and its effects. It also highlights Canadian research results and data, where appropriate, and emphasizes items of special Canadian concern, such as ozone depletion in the Arctic and the impacts of UV changes on forests and freshwater ecosystems.

The Road to Montreal

The possibility of anthropogenic interference with the ozone layer was raised as early as 1964, when John Hampson of the Canadian Armaments and Research Development Establishment noted the potential for ozone damage as a result of water vapour emissions from rockets and high-flying aircraft. Over the ensuing decade, proposals for the development of supersonic commercial aircraft that would fly in the lower stratosphere brought further attention to the issue, as did the debate over the environmental effects of nuclear weapons. In 1974, however, two articles were published that brought an entirely new dimension to the problem of ozone depletion. The first of these, published in the *Canadian Journal of Chemistry* by Richard Stolarski and Ralph Cicerone of the University of Michigan, described a process by which chlorine from rocket exhausts could catalyze the destruction of large amounts of ozone in the stratosphere over a period lasting many decades. Independently and almost simultaneously,

two University of California researchers, Mario Molina and Sherwood Roland, voiced similar concerns about chlorine-catalyzed ozone loss but suggested the existence of a much larger source of anthropogenic chlorine in the stratosphere. In an article in *Nature* they argued that many widely used industrial chlorofluorocarbons (CFCs) had the potential to migrate into the stratosphere, where they would eventually break down as a result of exposure to intense ultraviolet radiation and release significant quantities of chlorine.

The combined implications of these articles were disturbing. Society appeared to face a choice between preserving the integrity of the ozone layer, which prevents biologically destructive levels of ultraviolet radiation from reaching the earth's surface, or preserving the economic benefits provided by CFCs, a valuable and otherwise benign group of chemicals that had become essential to a broad range of applications, including refrigeration and the manufacture of foams and electronic components. The potential risks to ecosystems and human health were large and unprecedented, while the costs of abandoning CFCs appeared considerable. In addition, although ozone destruction by chlorine catalysis was highly plausible, there was as yet no empirical evidence of ozone loss in the stratosphere. A further complication was added in 1975 when S.C. Wofsy, M.B. McElroy, and Y.I. Yung of Harvard University showed that bromine, used in fire-retarding halons, was also a potent destroyer of ozone. Not surprisingly, the issue ignited a major controversy, both within the scientific community and beyond.

University, government, and industry scientists in various centres around the world responded by intensifying their research activities. The immediate problem was to validate – or invalidate – the new theories of ozone destruction and assess their implications over a wide range of potential impacts. Given the considerable natural variability of ozone concentrations, both geographically and temporally, detecting the imprint of an anthropogenic disturbance and verifying the processes involved were not easy tasks. As researchers uncovered new information about the chemistry and dynamics of the middle atmosphere, the problem became more complex and uncertainties increased. Modelling of processes affecting ozone amounts proved extremely difficult, partly because of limitations of computer power and partly because of uncertainties about reaction rates and other critical aspects of the depletion mechanisms. Consequently, initial projections of depletion by CFCs showed little consistency. Nevertheless, by the mid-1980s, knowledge of ozone-related processes had expanded considerably. When the United Nations Environment Programme (UNEP) and the World Meteorological Organization (WMO) released their first major international ozone assessment in 1986, the report was able not only to provide a comprehensive analysis of the threat from CFCs 11 and 12 but also to identify additional substances that had the potential to deplete stratospheric ozone. In addition, it drew attention to the fact that many of these substances were extremely powerful greenhouse gases whose presence in the atmosphere also had serious implications for global warming and climate change.

At the national level, reaction to the threat of ozone depletion varied considerably. It was strongest in those countries where media interest and vocal environmental movements ensured a place for the issue on the political agenda. Fact-finding commissions were established and research activities intensified in a number of these countries to provide governments with more information about the nature and implications of the problem. By 1978 a few countries had concluded that it would be prudent to curtail the least essential uses of CFCs until there was greater certainty about the risks involved in their use. Thus, the United States banned the use of CFCs in nonessential aerosol sprays in March of that year, and Canada, Norway, and Sweden shortly followed suit. The European Community, after initially rejecting Dutch and later German proposals for CFC restrictions, agreed in 1980 to a more modest 30% cutback in aerosol use.

The ozone issue, however, was fundamentally an international problem, and it could only be resolved by international action. The initiative for promoting this action was taken at a relatively early date by the United Nations Environment Programme, under the leadership of its executive director at the time, Mostafa Tolba. In 1976 UNEP had called for an international conference to discuss an international response to the ozone issue. The conference, held in Washington in March 1977, drafted a "World Plan of Action on the Ozone Layer," which gave UNEP the responsibility for promoting and coordinating international research and data gathering activities. At the same time, a Coordinating Committee on the Ozone Layer, under UNEP direction, was formed to oversee periodic international assessments of the depletion problem.

The possibility of establishing international controls over the production and use of CFCs was first raised a month later at another international meeting in Washington but attracted insufficient support at the time and on subsequent occasions over the next few years. In April 1981, however, UNEP's Governing Council authorized the organization to begin working towards an agreement to protect the ozone layer. The first step in this process was taken in January 1982, when 24 countries met in Stockholm and agreed to launch an "Ad Hoc Working Group of Legal and Technical Experts for the Preparation of a Global Framework Convention for the

Protection of the Ozone Layer." In 1983, the so-called Toronto Group (named after the site of its first meeting and consisting of Canada, Finland, Norway, Sweden, Switzerland, and later the United States) recommended a global ban on nonessential uses of CFC aerosol sprays and proposed that a separate regulatory protocol be developed and adopted simultaneously with the framework convention.

Efforts to complete a framework agreement came to fruition in March 1985 with the signing of the Vienna Convention for the Protection of the Ozone Layer. The participating countries agreed to take measures to protect the ozone layer (although these were not spelled out) and made arrangements for international cooperation in the areas of research, monitoring, and exchange of data on the state of the ozone layer and emissions and concentrations of CFCs and other chemicals. The convention was not accompanied by a regulatory protocol, but under a separate resolution UNEP was authorized to begin negotiations on a legally binding protocol that would be ready in 1987.

Although Vienna was an important milestone, the international consensus needed to support an effective control protocol was still lacking. It was therefore decided to convene two workshops in 1986 to review some of the key economic and scientific issues. Working informally as private citizens rather than as members of national delegations, experts from the UN, governments, industry, universities, and environmental groups met first in Rome and later in Leesburg, Virginia. Though many points of contention remained unresolved, the meetings nevertheless succeeded in building a broader basis of understanding for the negotiations to follow. One of the more important ideas to emerge from these discussions was the concept of an interim protocol – one that did not have to provide a definitive solution to all outstanding problems but allowed for periodic reassessment and revision in the light of changing facts and expanding scientific knowledge.

The actual negotiation of the protocol began in Geneva in December 1986. Subsequent meetings in Vienna and again in Geneva helped to narrow the outstanding differences, but when the delegates convened in Montreal on September 8, 1987, important disagreements remained over such basic issues as the chemicals to be controlled, the use of production or consumption as the basis for restrictions, the extent of the controls and the timing of their implementation, the choice of a base year, and arrangements for developing countries. It was only after further intensive negotiation that agreement was finally reached on the 16th.

The conclusion of such an important and unprecedented agreement owes much to the skill and persistence of those who negotiated it, but a number of other important factors contributed to this achievement. The role of the international scientific community was particularly vital. Although scientists were unable to eliminate many of the uncertainties that surrounded and still surround the stratospheric ozone issue, they were successful in reducing the range of uncertainty and in building a compelling case for action. Chance played a role as well, most notably with the discovery of the Antarctic ozone hole in 1985. The ozone hole did not confirm existing theories about the destruction of the ozone layer – it only raised new questions – but it did create a greater awareness among opinion leaders and the public that something serious was happening to the atmosphere and that precautionary action was necessary. An agreement also became much more likely after 1986, when the American chemical industry, one of the larger producers of CFCs in the world, abandoned its opposition to controls. Finally, it was the very flexibility of the agreement that made it acceptable to many of the parties. It did not attempt the impossible task of solving so complex a problem in one step. Instead, it set up a mechanism for continuing review, so that policy could be refined in the light of new realities and the best available information. Indeed, one of its most important achievements was that it created a mechanism for continuing action. As Mostafa Tolba pointed out, the Montreal Protocol was a starting point, "the beginning of the real work to come."

Mileposts: 1987–1997

The past decade has seen a number of very significant advances in ozone science, both in terms of improvements in research and monitoring capabilities and actual advances in our understanding of ozone depletion and its effects on radiation at the earth's surface. One of the most important developments occurred in the late 1980s, when intensive research efforts unravelled the mystery of the Antarctic ozone hole and uncovered the role of polar stratospheric clouds (PSCs) and hetereogeneous chemistry in its genesis. By 1990, important evidence about ozone trends in other parts of the world was also becoming available, and depletions of about 5% per decade were detected over the northern midlatitudes. After the eruption of Mount Pinatubo in 1991, it became apparent as well that sulphate aerosols injected into the stratosphere by volcanic activity could cause significant depletion. More recently, there has been evidence that significant depletions have been occurring in the Arctic as a result of

heterogeneous reactions on PSCs. In 1993, the expected link between ozone depletion and increases in UV radiation at the surface was finally confirmed through the analysis of spectral data. The study, by Environment Canada scientists, has recently been extended to cover an 11-year period ending in 1996. It shows a positive trend of approximately 1% per year in the summer radiation at 300 nm.

Other noteworthy scientific advances of the past decade include:

- a greater understanding of the transport of ozone and other trace gases as a result of the identification of the role of small-scale filamentary structures in mixing processes in the upper troposphere and lower stratosphere
- the application of new techniques for measuring ozone and other atmospheric constituents from the ground, balloons, and satellites
- advances in chemical modelling, including the ability to incorporate chemical processes in general circulation models and forecast models
- a substantial increase in the number of stations making spectral UV measurements and in the length of the data record
- an evaluation and, in some cases, verification by measurements of the effects of CFCs and other ozone-depleting substances on radiative forcing and climate change
- evidence of a possible link between climate change and ozone depletion in the Arctic
- better understanding of the effects of clouds, sulphur dioxide, and albedo on UV irradiance

Improvements in our understanding of depletion processes as well as further evidence of ozone loss has precipitated a significant tightening and extension of the protocol's regulatory regime. The original agreement had required a 50% reduction in CFC use by mid-1998 and a freeze of halon consumption at 1986 levels by 1992, but amendments passed at meetings in London (1990) and Copenhagen (1992) targeted these substances for virtual elimination and then advanced the phase-out dates to the end of 1994 for halons and the end of 1995 for CFCs. In addition, carbon tetrachloride and methyl chloroform, HCFCs and HBFCs (used as substitutes for CFCs and halons), and methyl bromide were brought under regulatory control. Carbon tetrachloride, methyl chloroform, and HBFCs were scheduled for elimination by the end of 1995, while consumption of HCFCs was scheduled to be eliminated by 2030. Further meetings in Vienna (1995) and Costa Rica (1996) led to reductions in the use of methyl bromide and agreement to end its use entirely by 2010.

Present Trends

The greatest and most dramatic ozone loss has occurred during early spring over the Antarctic, where total ozone values have dropped by more than 65% since 1975. Ozone losses over the Arctic for this period have been less severe, because of differences in circulation patterns, but are still in the area of 12%. In the midlatitudes, ozone has been declining at a rate of about 5% per decade.

The accompanying maps show the differences between ozone amounts over Canada at the time of the signing of the Montreal Protocol in 1987 and a decade later in 1997. The decline in ozone values between the two six-month periods is greatest (as much as 12%) in the high Arctic and lowest (about 3%) over the southeast. However, in 1996 Arctic ozone values were briefly about 30% below normal, while during the spring of 1997 they were as much as 45% below normal over the high Arctic and about 7% below normal over the midlatitude regions of the country. The exceptionally large depletion in the Arctic during the past spring is likely the result of unusual upper wind and temperature patterns that may, in turn, be related to the radiative effects of increased concentrations of greenhouse gases.

Meanwhile, as a result of the Montreal Protocol, the rate at which atmospheric concentrations of CFCs have increased has slowed noticeably since about 1990 and, in the case of CFC-11, concentrations have actually begun to decrease. As concentrations of CFCs and other ozone-depleting substances in the stratosphere decline, concentrations of chlorine and bromine should follow suit. If the provisions of the Montreal Protocol are fully obeyed by all the parties, the current stratospheric chlorine concentration of 3.5 parts per billion (ppb) is expected to peak within the next few years and then decrease gradually, returning to its natural level of 1.0 ppb some time after 2100.

Given the expected decreases in concentrations of ozone-depleting substances and stratospheric chlorine and bromine, when can we expect the ozone layer to recover, and when will we be able to detect that a recovery is under way? The accompanying graph shows how ozone has decreased from 1965 to 1996. It then compares, in a simplified fashion, what might happen if our current assumptions about ozone depletion are correct, and the Montreal Protocol and its amendments are fully implemented, with an alternative scenario in which concentrations of ozone-depleting substances remain unchanged at 1997 levels. Although the scientific basis for the graph is minimal, it does illustrate that evidence of a clear trend towards increasing ozone amounts may not emerge until after 2005 or 2010. In reality, however,

How Has the Ozone Layer Over Canada Changed Since 1987?

Total Ozone. January-June 1987

Total Ozone. January-June 1997

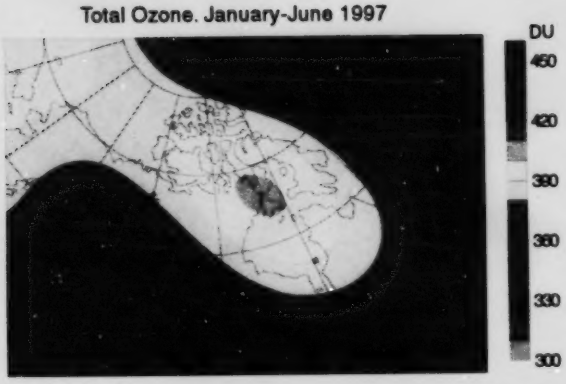

Difference (%). January-June 1997 vs. 1987

The upper map shows average ozone levels over Canada for January–June 1987, while the middle map shows the same information for January–June 1997. The percentage differences between the two periods are plotted in the lower map, which shows declines ranging from 3% over southern Canada and about 4% over the Prairies up to 12% in the high Arctic. Although these differences are consistent with decadal trends, a comparison of other years, such as 1985 and 1995, would yield different results. The maps have been constructed from both ground-based and satellite measurements.

When Might the Recovery of the Ozone Layer Be Detectable?

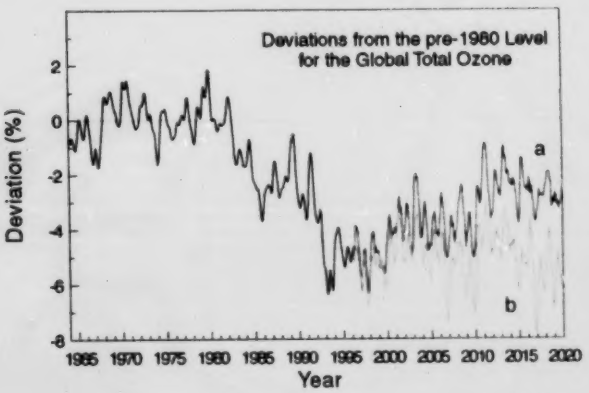

The graph shows the global total ozone record from 1964 to 1996 and two hypothetical projections based on different scenarios. Branch (a), which expresses the best case, assumes that the Montreal Protocol and its amendments will be fully implemented and that concentrations of chlorine and bromine will decline according to the projections contained in the 1994 UNEP Assessment. It also assumes that ozone depletion has been due only to known ozone-depleting substances. Branch (b) is based on the assumption that concentrations of all ozone-depleting substances remain at their 1997 levels.

Although these projections are relatively crude, they do illustrate that several years will be needed to detect the start of any recovery and several more to estimate its extent. The actual recovery scenario is likely to be somewhere between these two cases because the protocol may not be fully adhered to by all parties and other factors or as yet unidentified substances may be contributing to depletion.

The graph is derived from a very simple statistical model of seasonally dependent, chlorine-induced depletion, modified by the addition of random noise and the quasi-biennial and solar cycles in ozone.

such evidence may be delayed even further because compliance with the protocol may not be complete and there are still uncertainties in our understanding of the science. These uncertainties also make it difficult to predict confidently when ozone concentrations will finally return to natural levels. As the recent and unexpectedly large Arctic depletions indicate, the ozone issue can still produce surprises.

The Future Agenda

Reliable forecasts of a future ozone recovery ultimately depend on the comprehensive and accurate modelling of atmospheric chemistry and dynamics. At the present time, however, our models generally underestimate the amount of ozone depletion that has actually occurred and cannot accurately simulate all aspects of ozone distribution with altitude, location, and time of year. These limitations suggest that there may be gaps in our knowledge of ozone chemistry and atmospheric dynamics. They may also point to the presence of other as yet unidentified ozone-depleting substances in the stratosphere. In addition, the unexpected extent of recent ozone depletions in the Arctic indicate a need for further study of the Arctic atmosphere and, in particular, of the effects on it of increased concentrations of greenhouse gases. It is now fairly certain that increased concentrations of these gases have caused stratospheric cooling, and a cooler Arctic stratosphere would generally offer a more favourable environment for ozone destruction. Finally, although many of the effects of enhanced UV radiation on biological systems are reasonably well known, our knowledge is far from complete, and it is possible that additional damage mechanisms remain to be identified. Also, the implications of ecological interactions and other environmental stresses in connection with UV effects have yet to be explored in detail.

In spite of the truly remarkable progress that has been made in ozone science over the past decade, the problem of ozone depletion has not yet been solved. Our challenge for the next decade, therefore, is to fill in these gaps in our knowledge of chlorine- and bromine-induced depletion while expanding our understanding of the effect of other factors on ozone amounts. At the same time, we must continue our efforts to monitor and detect the recovery of the ozone layer and expand our work on the biological effects of enhanced UV radiation.

The successful implementation of this agenda over the next 10 years will give us a much better basis for ensuring the ultimate recovery of the ozone layer and for developing effective responses for the protection of human health and ecosystem vitality in the meantime. It will also enhance our understanding of the complex interactions of radiative, dynamical, and photochemical processes that drive the atmosphere and thus give us better tools with which to predict how the atmosphere will respond to other perturbations that may occur in the future.

The Distribution of Ozone and Ozone-Depleting Substances in the Atmosphere and Observed Changes

1.1 Global Ozone Measurement and Monitoring

Ozone (O_3), an allotrope of ordinary oxygen (O_2), is the most important trace constituent in the stratosphere. Although it is present in relative concentrations of no more than a few parts per million, it is such an efficient absorber of ultraviolet radiation that it is the largest source of heat in the atmosphere at altitudes between about 10 and 50 km. UV absorption by ozone causes the temperature inversion that is responsible for the existence of the stratosphere. Ozone is also an important radiator, with strong emission bands in the 9.6 mm infrared region. In the UV-B region (290–315 nm) it absorbs with an efficiency that increases exponentially with decreasing wavelength, and so strongly that at 290 nm the radiation at the ground is reduced by more than a factor of 10^4 from that above the ozone layer (see Chapter 4). This strong variation of absorption efficiency with wavelength in the UV-B region is the basis of the Dobson and Brewer operational methods of measuring ozone.

Ozone is the main source of the highly reactive OH radical, which causes the removal of many organic molecules from the atmosphere. In the troposphere, it is also a pollutant, which means that its natural concentration is augmented by anthropogenic sources. Because its extra oxygen bond can be easily broken, ozone is a strong oxidant that is both corrosive to materials and toxic to plants and animals. A principal component of urban smog, it is produced in and downwind of urban centres by photochemical reactions involving volatile organic hydrocarbons (VOCs) and oxides of nitrogen (NO_x) (see Chapter 3). Intrusions of stratospheric air are also a significant source of ozone in the troposphere (see Chapter 2). Globally, the distribution and climatology of tropospheric ozone appear to be highly variable and have not yet been well established by comprehensive measurements. Although this is a very important area of current research, this document will deal primarily with the state of current knowledge of ozone in the stratosphere.

Regular measurments of the ozone content of the atmosphere were initiated in the early 1920s by G.M.B. Dobson using spectrographic instruments. He built his first version of what is now known as the Dobson ozone spectrophotometer in 1927. It makes precise measurements of the relative intensities of sunlight at pairs of wavelengths in the UV spectrum; the total ozone column[1] is deduced from these measurements and the known absorption coefficients of ozone at the wavelengths of measurement. Canada acquired a Dobson in 1948. Until the 1950s there were only about 20 regularly operating stations in the world, most of which were located in the northern hemisphere. Some of these had already interrupted their measurement programs in the late 1950s. At this time the reason for studying ozone was the hope that research into stratospheric motion, of which ozone was a useful tracer, would lead to improved models for forecasting the weather. It is for this reason that we have such a comprehensive data base of ozone measurements for the 1960s and 1970s, well before ozone depletion became a scientific issue. Systematic ozone observations using common observational methods and calibration procedures laid out by the International

1 Equivalent thickness of the ozone layer, expressed as a vertical column of pure ozone. The standard unit is the Dobson Unit, equal to 10^{-5}m at 0°C and sea level pressure (STP). The global average of total ozone is approximately 300 DU, equivalent to a thickness of 3 mm.

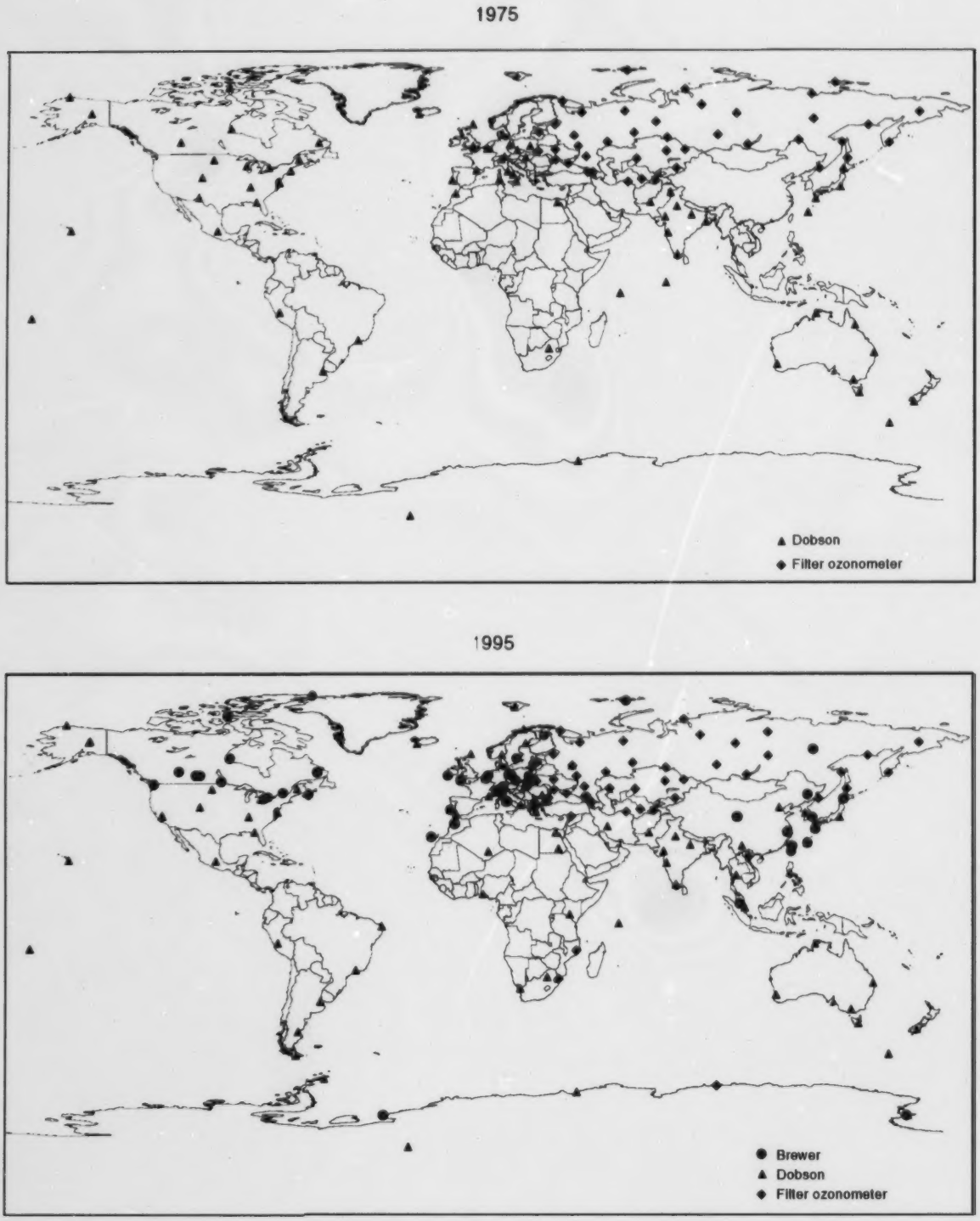

Figure 1.1 Geographical distribution of ground-based ozone measurement stations in 1975 and 1995.

Ozone Commission in collaboration with the World Meteorological Organization (WMO) were started in preparation for the International Geophysical Year (1957–1958). These standard procedures formed the basis of the Global Ozone Observing System, which presently has more than 160 continuously operating stations. Three main types of instruments are used for routine total ozone observations: Dobson and Brewer spectrophotometers that can measure total ozone with up to 1% accuracy [e.g., Kerr et al.1988] and the less accurate M-83 and M-124 filter ozonometers [e.g., Bojkov et. al. 1994]. Figure 1.1 shows the geographical distribution of stations. The World Ozone and UV Radiation Data Centre, the international repository for all ground-based measurements of ozone, is housed at Environment Canada in Toronto.

A relatively small number of stations make regular measurements of the vertical profile of ozone concentration using balloon-borne ozonesondes. Two principal types of ozonesonde exist: the Brewer-Mast [Brewer and Milford 1960] and the ECC [Komhyr 1969]. Both types measure the ozone concentration *in situ*, via its reaction with an aqueous solution of potassium iodide. The technique is very sensitive and can give very fine vertical resolution. It is also capable of excellent accuracy, but sensitivity to contamination as well as errors arising from improper handling or occasional mechanical defects in the sonde itself render it less reliable than optical methods. For this reason sonde data are compared, whenever possible, with Brewer or Dobson total ozone measurements.

Only a few stations have been making regular measurements since before the 1980s. Since ozone loss now appears to have started sometime between 1970 and 1980, their records are of particular significance. The time series of ozone soundings from these stations represent some of the longest records of ozone measurement that exist, as well as the only time series of measurements in the free troposphere and the most precise vertically resolved measurements in the lower stratosphere. The stations with important long-term records are: Hohenpeissenberg and Lindenberg (Germany), Payerne (Switzerland), Uccle (Belgium), Boulder, Wallops Island (contiguous United States), Barrow (Alaska), Hilo (Hawaii), Resolute, Churchill, Goose Bay, and Edmonton (Canada), Tateno and Sapporo (Japan), and the South Pole and Syowa in Antarctica. A much larger number of stations have started making soundings more recently, and a number of other stations have important but intermittent records. Regular ozone soundings have been made since 1966 in Canada and are currently made weekly at six stations. Additional flights are made during times of special interest, like the Arctic spring.

Umkehr observations are made by using an ultraviolet spectrophotometer to measure the intensity of light from the zenith sky at various wavelengths over a range of solar zenith angles between 60° and 90°. As the sun sets (or rises) the mean scattering height of radiation changes as a result of the attenuation of the direct and scattered radiation by ozone absorption and Rayleigh scattering. Since both ozone absorption and Rayleigh attenuation increase toward shorter wavelengths, the mean scattering height moves upward more rapidly as a function of the solar zenith angle for shorter wavelengths than it does for longer wavelengths. The short-wavelength light, which is scattered higher in the atmosphere, travels along a path which passes, on average, through less ozone. The variation of the intensity of light as a function of wavelength and zenith angle can therefore be used to determine the vertical profile of ozone, provided that the ozone distribution remains constant throughout the period.

The vertical resolution of the Umkehr method is about two scale heights (5–10 km) in the stratosphere [Mateer and Dutsch 1964; Mateer and Deluisi 1992; McElroy and Kerr 1995]. The Umkehr method is relatively insensitive to the distribution of ozone in the lower atmosphere (0 to 15 km). Figure 1.2 [McElroy and Kerr 1995] shows the performance of the Brewer Umkehr as compared with the mean profile inferred from measurements made by lidar, ozonesondes, and a microwave radiometer. It can be seen that the Umkehr retrieval performs very well in the 20–40 km altitude range and provides useful information to 45 or 50 km.

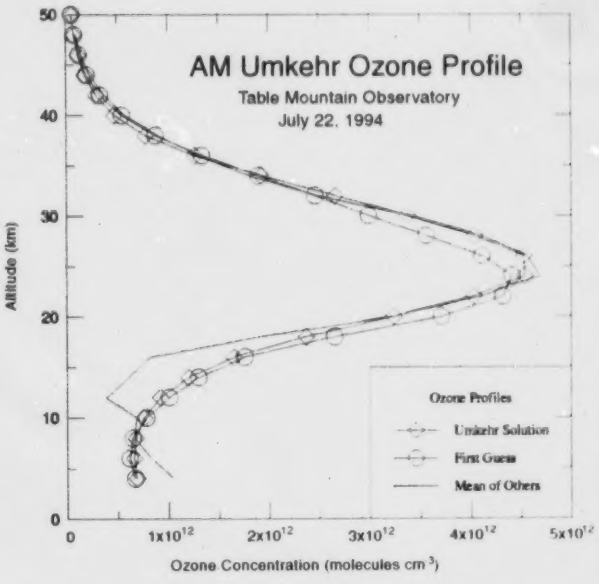

Figure 1.2 Comparison of an Umkehr-derived profile with the mean of other profile measurements (two lidars, one sonde, and one microwave) [McElroy and Kerr, 1995].

Umkehr observations have been made since the effect was first studied by Götz [Götz et al. 1934] in the 1920s, and Umkehr observations are included as a regular part of the automated observing schedules of the Brewer spectrophotometer. Analysis of these data for trends in the vertical distribution of ozone at higher altitudes is complex, and although such studies have been published for Dobson observations [Mateer and Dutsch 1964; Deluisi et al. 1989; WMO 1994] up to now, much less has been done with data from the newer Brewer instruments [Hahn et al. 1995; McElroy et al. 1997].

Dobson ozone spectrophotometers were installed at five sites in Canada between 1957 and 1964. These were replaced in the mid-1980s by the automated Brewer ozone spectrophotometer, developed by scientists at Environment Canada. The Brewer compares the intensities of five UV-B wavelengths in order to better correct for the influence of absorbers other than ozone. It is now in use at some 90 sites worldwide. Brewer instruments have been installed recently at seven additional sites in Canada (Table 1; Figure 1.3). Data from the Brewer network are delivered in quasi-real time to the operational weather forecast centre for use in producing the daily ozone and UV Index forecast. Modified versions of the Brewer spectrophotometer are also being used to monitor NO_2 column amounts at several sites and to make spectrally resolved UV-B measurements at all Canadian sites. With its great geographical area, Canada has one of the largest ground-based ozone measurement networks in the world.

Table 1: Canadian Ground-Based Ozone Measurement Sites

Station	Total Ozone	Other Instrumentation
Alert	Brewer (1989)	Ozonesondes (1987)
Churchill	Brewer (Dobson 1964)	Ozonesondes (1973)
Edmonton	Brewer (Dobson 1957)	Ozonesondes (1970)
Eureka	Brewer (1992)	Ozonesondes, lidars, FTIR spectrometers Fabry-Perot spectrometers, radiometers
Goose Bay	Brewer (Dobson 1962)	Ozonesondes (1969)
Halifax	Brewer (1992)	
Montreal	Brewer (1993)	
Resolute	Brewer (Dobson 1957)	Ozonesondes (1966)
Saskatoon	Brewer (1988)	
Saturna	Brewer (1990)	
Toronto	Brewer (Dobson 1960)	Lidar, 1991. [ISTS]
Regina	Brewer (1994)	
Winnipeg	Brewer (1992)	

Date indicates the start of regular observations. All sites are operated by Environment Canada, except that of the Toronto lidar of the Institute for Space and Terrestrial Science (ISTS), which also operates the ozone lidar at Eureka.

Figure 1.3 Canadian ground-based ozone measurement stations in 1997.

The Network for the Detection of Stratospheric Change (NDSC) is a set of high-quality, ground-based, remote-sounding research stations for observing and understanding the physical and chemical state of the stratosphere. Ozone and key ozone-related chemical compounds and parameters are targeted for measurement. The NDSC is a major component of the international upper atmosphere research effort and has been endorsed by national and international scientific agencies, including the International Ozone Commission, the United Nations Environment Programme (UNEP), and the WMO. Following five years of planning, instrument design, and implementation, the NDSC began network operations in January 1991. The goals of the network are:

1 To make observations so that changes in the physical and chemical state of the stratosphere can be determined and understood and, in particular, so that changes in the ozone layer can be detected and their causes identified as early as possible.
2 To provide an independent calibration of satellite sensors of the atmosphere.
3 To obtain data that can be used to test and improve multi-dimensional stratospheric chemical and dynamical models.

A high-Arctic stratospheric ozone observatory was built by Environment Canada in 1992 near the Eureka weather station on Ellesmere Island. This observatory is a centre for atmospheric research in the Arctic and a primary component of the NDSC. It is used by researchers from Canadian Universities, Japan, and the USA as well as Environment Canada. Observations are carried out with two lidar systems, one designed for obtaining vertical profiles of ozone and temperature [Donovan et al. 1996] and the other for determining the vertical structure of aerosols from volcanic eruptions or in the form of polar stratospheric clouds and Arctic haze. Ozone is being monitored also by means of a modified Brewer spectrophotometer and ozonesondes launched from the Eureka weather

Figure 1.4 The Eureka NDSC High-Arctic Stratospheric Ozone Observatory. (Photo by Luc Sarrazin and Greg Sorensen.)

station. Fourier Transform Infra-Red (FTIR) spectrometers are used to determine the column amounts of several atmospheric gases of importance in the ozone chemistry, such as hydrofluoric and hydrochloric acid [Donovan et al. 1997].

Since 1970 satellites have provided a global picture of total ozone and (to a lesser extent) its vertical distribution. The Backscatter Ultraviolet (BUV) instrument, launched on board the Nimbus 4 satellite in April 1970 is a source for several years of early total ozone data [Stolarski et al. 1997]. Since 1978 the Total Ozone Mapping Spectrometer (TOMS) instruments on Nimbus 7, Meteor 3 [Herman and Larko 1994], and recently on Earth Probe and ADEOS have provided a record of high-resolution daily global total ozone data that now extends over more than 17 years. Long-term records of ozone observations are available from several other satellite instruments: the Solar Backscatter Ultraviolet (SBUV) (1979) and SBUV/2 (several since 1984), the Stratospheric Aerosol and Gas Experiment (SAGE) and SAGE II (1979 and 1984), and the Tiros Operational Vertical Sounder (TOVS) instruments, as well as several instruments on the Upper Atmosphere Research Satellite (UARS). More recently (1996) the Global Ozone Monitoring Experiment (GOME) on the European ERS-2 platform has begun making both global total ozone and profile measurements. Early space-based ozone measurements often compared poorly with ground-based data. However, extensive intercomparison with ground-based and other space-based instruments and careful work with instrument characterization have improved data reduction algorithms to the point where space-based measurements of total ozone are now reported to be compatible with those of the best-calibrated ground-based stations [McPeters and Labow 1996].

Canada participates in space-based monitoring of ozone through scientific and technical collaboration with other countries and cooperative agreements on data and cost sharing with meteorological and space agencies in the United States and Europe. The Canadian OSIRIS ozone spectrometer, due to be launched aboard the Swedish satellite ODIN in 1998, is one example of such collaboration. Canada has also shared some of the cost of the European ENVISAT platform (to be launched in 1999), which contains three instruments for measuring ozone and related chemical species. In addition, several Canadian instruments to study the chemistry and dynamics of ozone are proposed as part of the Canadian Space Agency's Long-Term Space Plan III.

Measurements made *in situ*, by large-payload high-altitude balloons and more recently by high-altitude aircraft, while not usually suitable for the monitoring activities described above, have played and continue to play a very important role in improving our understanding of the detailed chemistry of stratospheric ozone. The advantages of these platforms are that a large number of simultaneous measurements may be made, since many different instruments may be accomodated, and that direct, *in situ*, rather than remote sensing techniques may be used. Such measurements provide data that are directly comparable to outputs from photochemical models of the ozone layer and that are essential for their verification. A series of campaigns with the NASA ER-2 aircraft provided dramatic confirmation of the hypothesis that chlorine-catalyzed chemistry was responsible for the Antarctic ozone hole by demonstrating the anticorrelation of ClO and ozone during the hole's development [Anderson et al. 1989; Brune et al. 1989]. The goal of this program is to measure all of the chemical species that are important in controlling the ozone budget in the stratosphere, and their sources and sinks, and to make measurements of sufficient precision to understand and separate the roles of chemistry and transport. Recent campaigns have concentrated on midlatitude chemistry and that of the Arctic [Brune et al. 1990; other references within].

Canada has participated in a number of balloon campaigns [Evans et al., 1977, 1982, 1985; Hilsenrath et al. 1986] and participates in the ER-2 program through its contribution of a UV/visible spectrometer to make spectrally resolved absolute intensity measurements of solar radiation at photochemically active wavelengths and to measure ozone above the aircraft. The instrument has made more than 100 flights to date [McElroy 1995; McElroy et al. 1995].

Data assimilation is a statistical technique that is an essential feature of any modern numerical weather prediction system, and it is now being applied to ozone observations in the stratosphere by several groups worldwide [Fisher and

Lary 1995; Levelt et al. 1996]. The goal in data assimilation is to produce an optimal estimate of the value of an atmospheric state variable (such as ozone concentration) by combining observations, weighted inversely by their estimated error covariances, with prior estimates of that variable, weighted by their estimated error covariances. The prior estimates contain information from previous observations, from other measurements, or from measurements of related quantities (e.g., temperature or potential vorticity). This information is carried in an atmospheric model that expresses the physical, dynamical, and chemical relationships between these sources of prior information and the target variable. This is a powerful technique that can interpolate with great success in areas where data are sparse and correct (or highlight) both measurement and model deficiencies or inconsistencies. Both models and methods for minimizing the total error of estimation are increasing rapidly in sophistication.

Middle atmosphere modelling and data assimilation are also major research activities in Canada. The development of data assimilation algorithms for the instruments described above is underway in a collaborative effort between Environment Canada and several Canadian universities. Ozone and wind data will be assimilated via the Middle Atmosphere Model (CMAM), as well as the operational global forecast model [Tarasick et al. 1996a]. Similar ozone data assimilation research programs are underway in Europe, the U.S., and Australia. Increased knowledge of ozone circulation and dynamics is expected to lead to better understanding of stratospheric ozone variability and change (see Chapter 2). Moreover, because ozone is the major chemical and radiative constituent of the middle atmosphere, its inclusion in models may also lead to improvements in climate modelling for global change issues and in forecast skill for weather models, particularly in the medium and longer ranges.

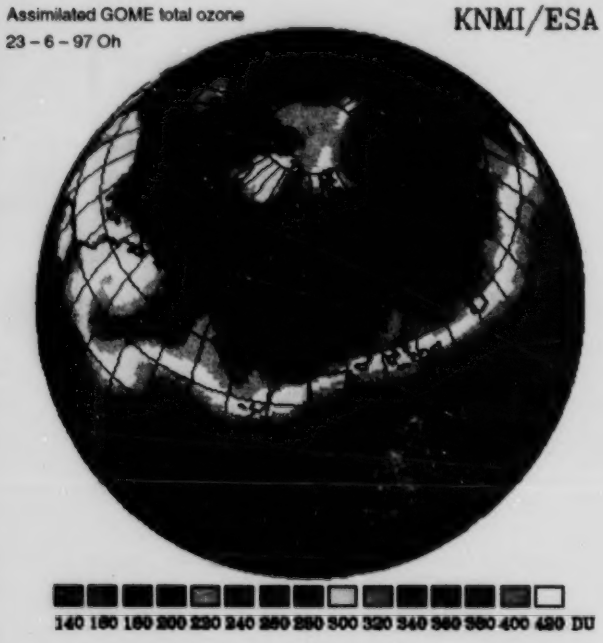

Figure 1.5 GOME data assimilation. (Royal Netherlands Meteorological Institute, KNMI)

1.2 Distribution, Climatology, and Natural Variation

1.2.1 Total Ozone Distribution

The main features of the global total ozone distribution were discovered during the first years of regular observations in the 1920s [Dobson et al. 1926, 1929, 1930]. The most important feature is a strong latitudinal gradient of total ozone, with lower values over the equator and tropics and higher values over middle and high latitudes (Figure 1.6). This gradient has a well-pronounced annual cycle, reaching a maximum in spring and a minimum in fall. The annual cycle in total ozone at a given point thus has an amplitude that is a function of latitude, with maximum amplitudes found at about 60° north and south latitude. In the tropics seasonal variations are small, with ozone maxima in summer; in the equatorial region there are essentially no seasonal variations.

The explanation for this behaviour, also deduced by Dobson and confirmed by Brewer [1949] from aircraft measurements of water vapour, is that the high values at extra-tropical latitudes are a result of transport from the tropical source region. Ozone is formed, primarily in the tropics at altitudes above about 30 km, via the action of ultraviolet light from the sun upon molecular oxygen. While the highest relative concentrations are found here, the more moderate values of 1–2 ppmv found at about 15 km actually make a much greater contribution to the total column ozone, because the density of the atmosphere is greater by an order of magnitude at the lower altitude. Mixing ratios in the lower stratosphere are higher at midlatitudes and toward the poles (Figure 1.7). This latitudinal distribution is made possible by the relatively long lifetime (months to years) of ozone in the lower stratosphere, and the Brewer-Dobson circulation (see Chapter 2) that transports stratospheric ozone from the tropics toward the poles and downwards at high latitudes. This circulation is both strongest and most variable in winter, and the highest total column amounts and the most variability are found in the winter stratosphere below 20 km.

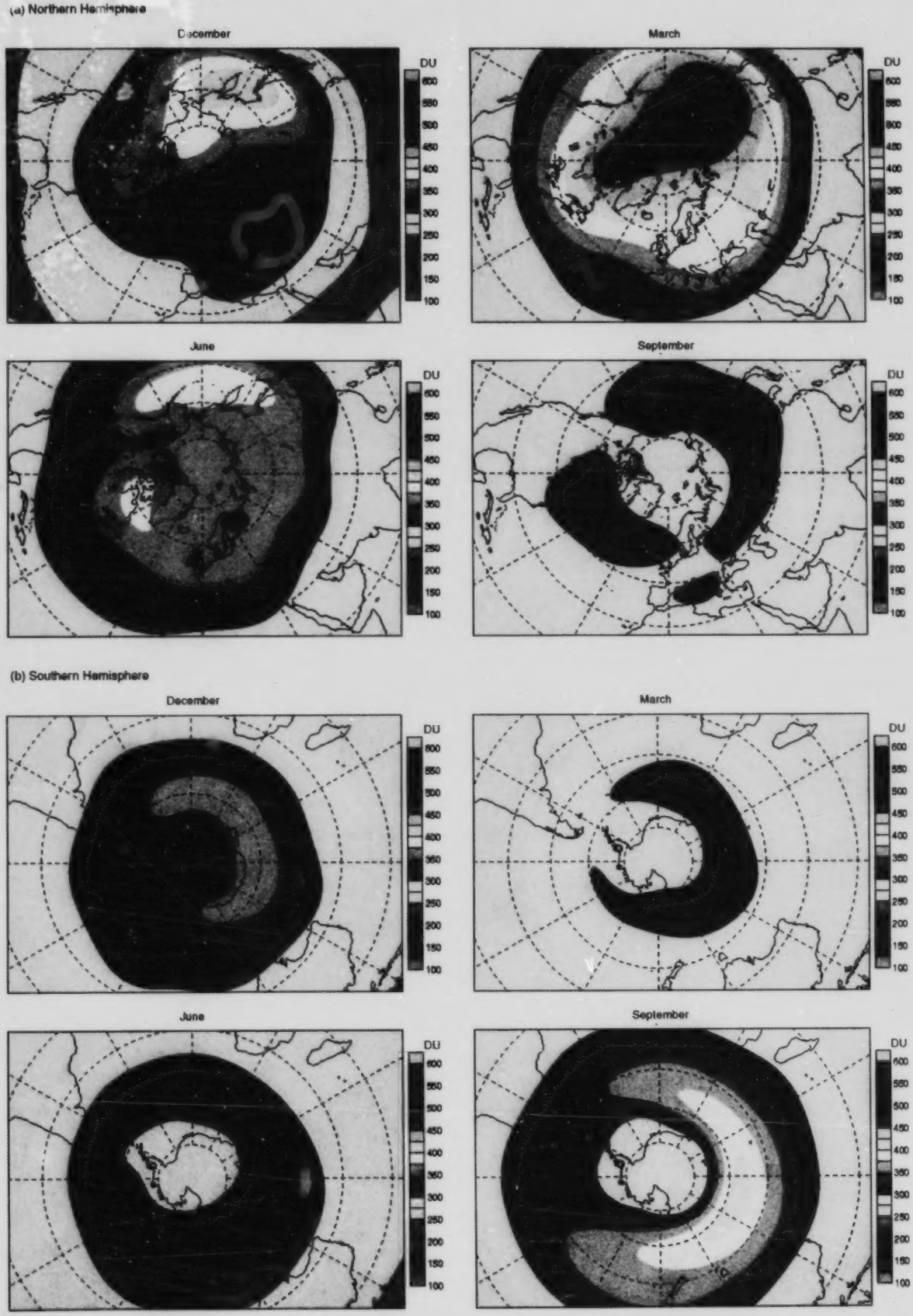

Figure 1.6 Global total ozone for the northern and southern hemispheres. (a) Northern hemisphere: average values for the period 1979–1988. (b) Southern hemisphere: average values for the period 1979–1988, except for the Antarctic where the period is 1960–1980.

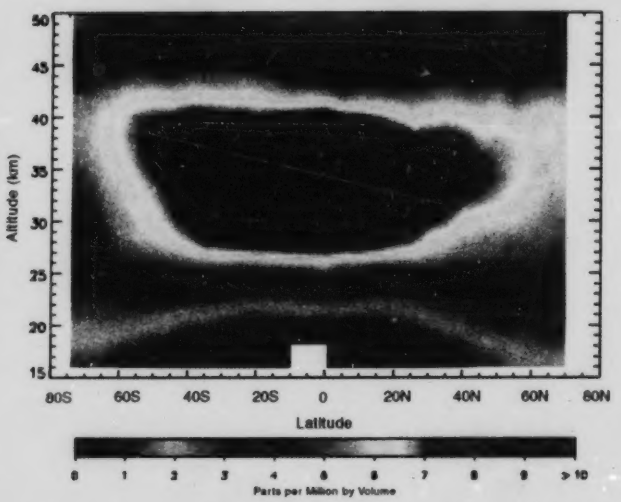

Figure 1.7 Average values of ozone mixing ratio as a function of altitude and latitude for March 1990. Data from SAGE II.

Expansion of the global ozone network during and after the International Geophysical Year (1957–1958) made it possible to analyse ozone climatology and to find longitudinal features in the ozone distribution such as the spring ozone maximum over the Canadian Arctic [London et al. 1976]. The global total ozone climatology has also been deduced from satellite data [e.g., Bowman and Krueger 1985]. More recently, Randel and Wu [1995] prepared a detailed atlas of total ozone, its variability and its vertical distribution, using SBUV and SBUV/2 data for the period 1978–1994.

Ozone variability also depends on season and latitude. It is lower in equatorial regions and over the tropics and higher over middle and high latitudes, especially in winter and spring. Standard deviations from the annual cycle for daily means are about 4–5% in low latitudes, and, over middle and high latitudes, vary from 7–8% in fall to 12–15% in late winter and early spring.

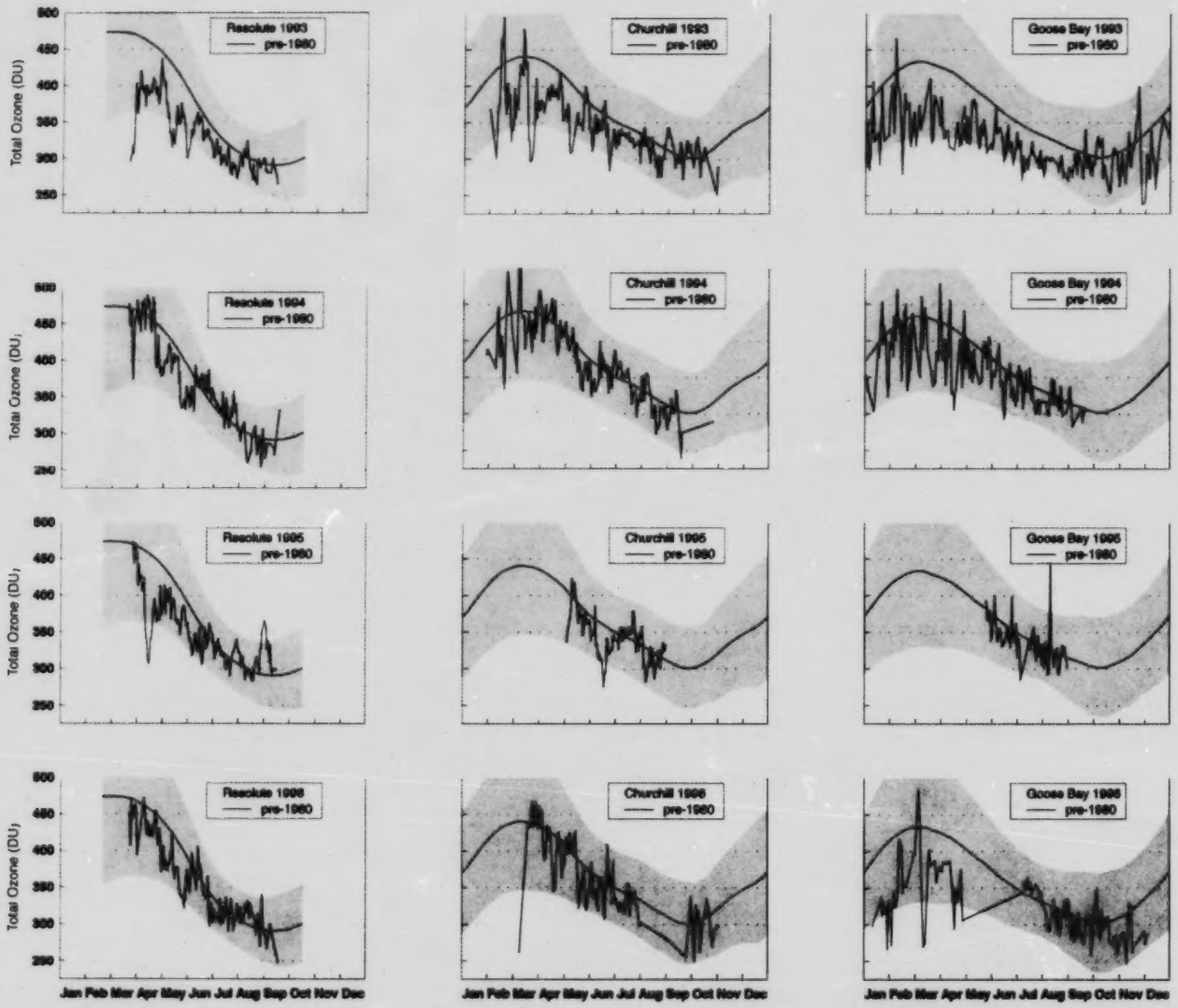

Figure 1.8 shows daily averages of total column ozone at five Canadian stations. Only direct-sun observations (the most reliable) have been used. Both the range of variation of the ozone column (which is greater in winter) and the seasonal cycle are evident. The data are plotted against the average of all values measured prior to 1980, indicated by the (smoothed) curve. Here, as elsewhere, we use the pre-1980 period as a baseline for the "natural" atmosphere. The shaded area shows the 2σ range of variation for this period (95% of observations made prior to 1980 fall within this range). In the top row of figures one may see clearly the record low ozone levels observed at all Canadian stations in early 1993 [Kerr et al. 1993].

The total ozone distribution over Canada is typical of that for the northern middle and high latitudes: the annual cycle has its maximum in March and its minimum in October, and spring ozone values in high latitudes are higher than over middle latitudes. Figure 1.9 shows the average total ozone distribution over Canada for the period 1979–1988. The maps were prepared using TOMS satellite data, with the addition of Dobson and Brewer moon observations for the polar night areas [Fioletov 1993]. The spring ozone maximum is evident in Figure 1.9. Over the Canadian Arctic station at Resolute, total ozone can reach values as high as those observed anywhere else on the globe (~600 DU). In September the latitudinal gradient of ozone is much smaller.

1.2.2 Vertical Ozone Distribution

The vertical profile of ozone can be expressed either by the mixing ratio, usually in parts per million or billion by volume, or by the concentration, typically in molecules per cubic centimeter or in Dobson units per kilometre, or by the partial pressure of ozone, usually in nanobars (10^{-6} hPa). The partial pressure and product of concentration and absolute temperature are proportional.

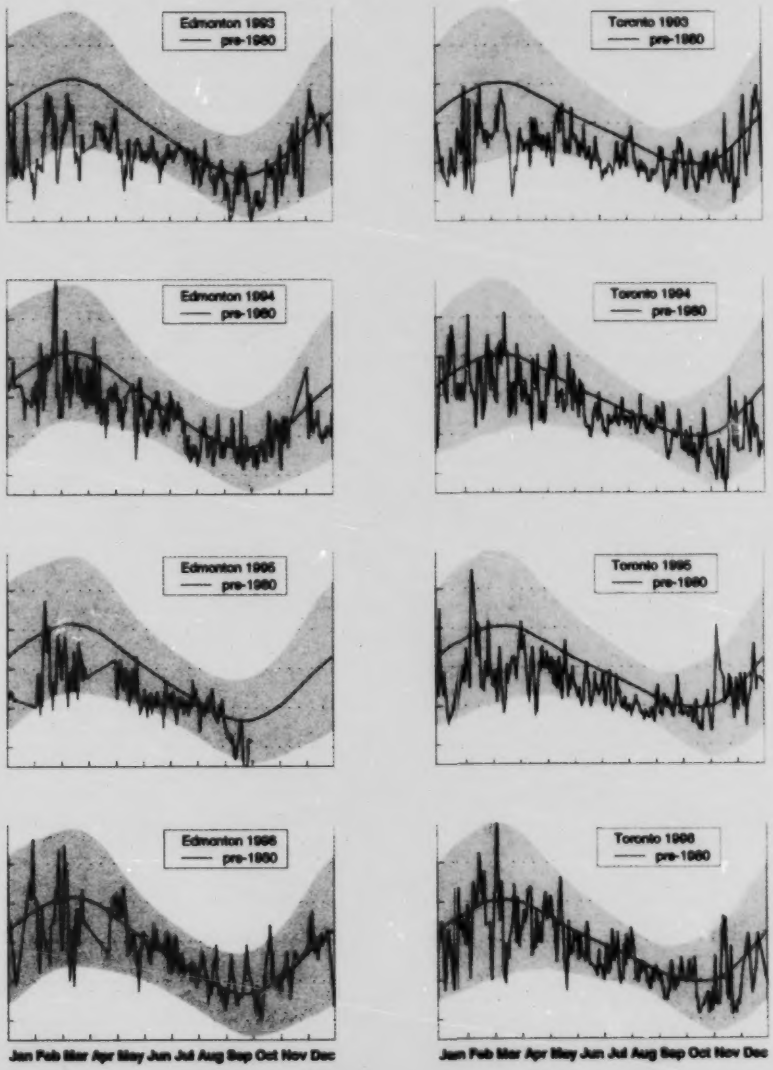

Figure 1.8 Daily observations of total column ozone at five Canadian stations, 1993–1996. The 60-day (smoothed) average of all observations made prior to 1980 is also shown. Spring values are generally lower than the pre-1980 average. The smoothing is performed with a 60-day full-width, half-maximum, triangular filter, similar to that described in Section 1.3.1.

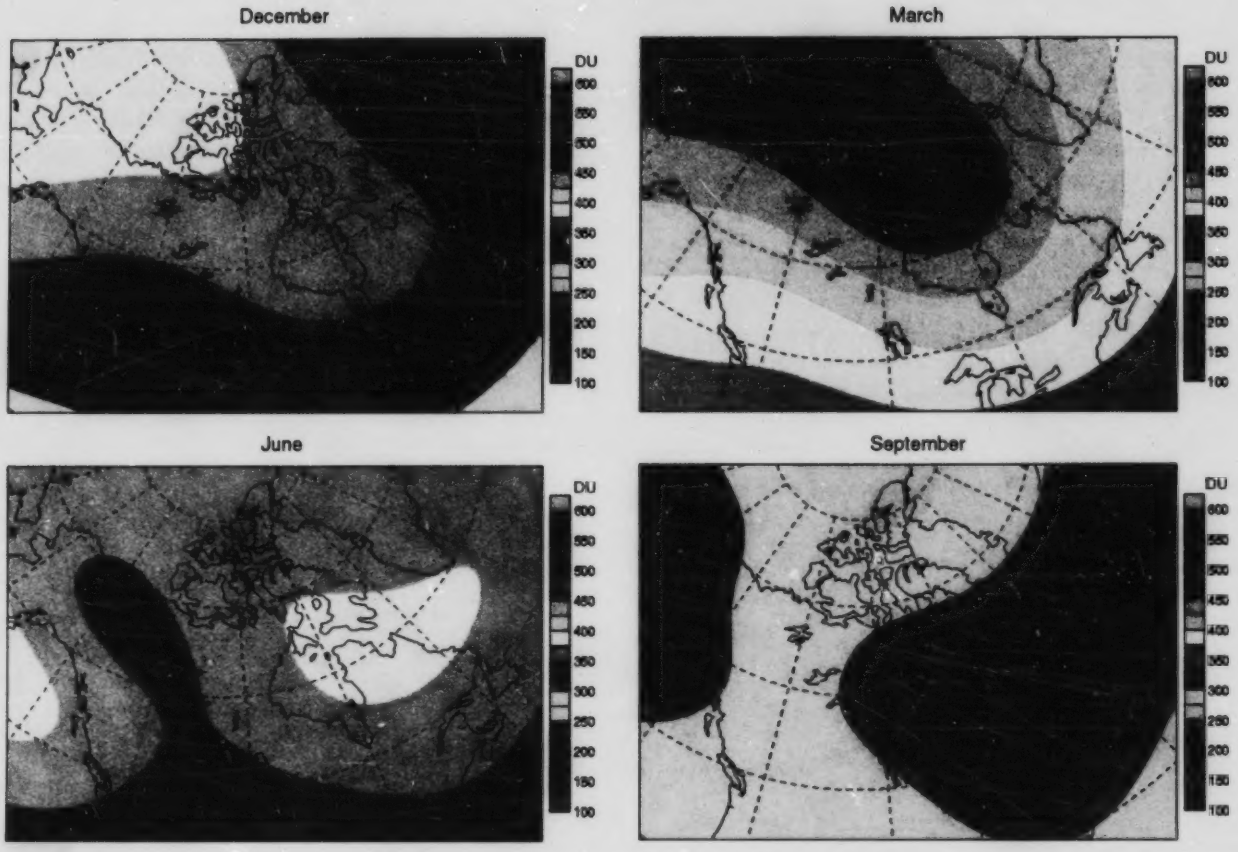

Figure 1.9 Average total ozone distribution over Canada for the period 1979–1988 for (a) December, (b) March, (c) June, (d) September.

Figure 1.10 shows typical spring and fall ozone vertical profiles for Edmonton (53°N) and Resolute (78°N), along with the corresponding temperature profiles. The ozone mixing ratio is relatively constant in the troposphere, so that the ozone concentration (partial pressure) falls with increasing altitude until the tropopause (indicated by the minimum in temperature) is reached. Ozone concentration increases rapidly with altitude in the lower stratosphere, to a maximum near 100 hPa. The maximum at Resolute is larger and occurs at a slightly lower altitude.

The March profiles show strongly layered structures known as ozone laminae (see Chapter 2).

In the summer and fall the maxima are much smaller and occur at higher altitudes (because the tropopause is also higher). Figure 1.11 shows the average vertical distribution of ozone concentration for these same sites as a function of time of year.

1.2.3 Natural Ozone Variations

As Figure 1.8 indicates, ozone concentrations are highly variable on time scales of a few days or more. Day-to-day fluctuations in total ozone, especially over middle and high latitudes, can be quite large, in some cases 100 DU or more. These variations are clearly due to atmospheric dynamics. The stratosphere rides on top of the troposphere and is necessarily greatly influenced by pressure and temperature variations (i.e., synoptic-scale weather systems) in that more massive region of the atmosphere. The ozone laminae in Figure 1.10 are evidence of large-scale horizontal transport, while the total ozone variations are most strongly correlated with tropopause height.

Examination of longer time series reveals, in addition to the annual cycle, longer-term persistent variability from several sources [e.g., Angell and Korshover 1973]. The quasi-biennial oscillation (QBO) in ozone amounts is apparently

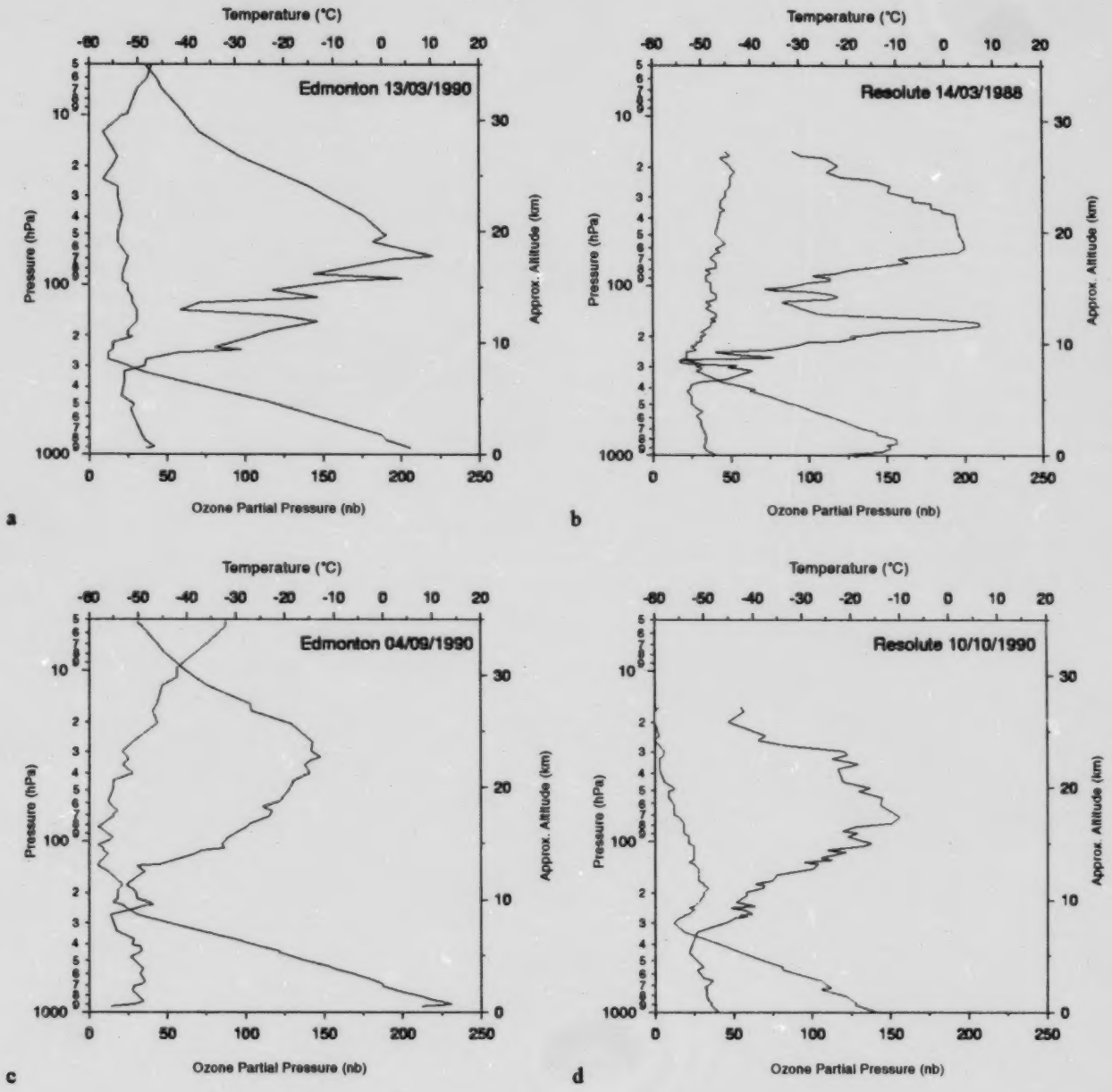

Figure 1.10 Vertical profiles of ozone partial pressure and temperature over (a) Edmonton, 13 March 1990, (b) Resolute, 14 March 1988, (c) Edmonton, 4 September 1990, and (d) Resolute, 10 October 1990.

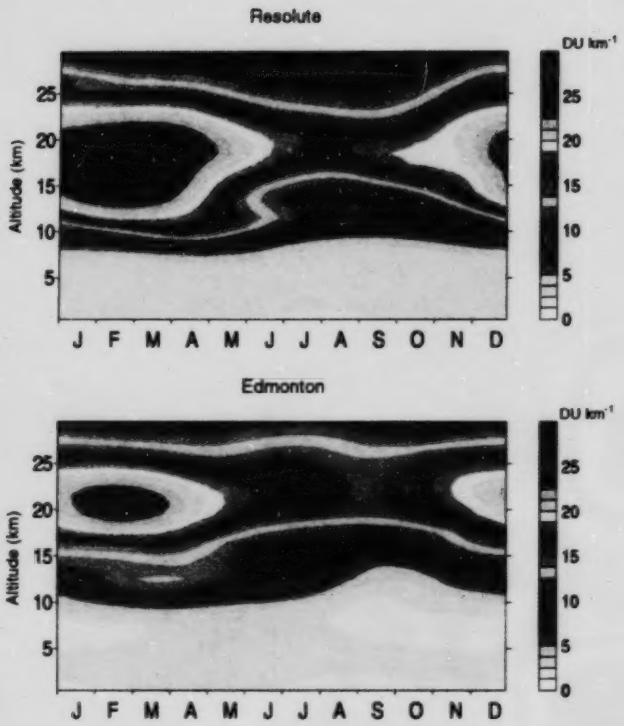

Figure 1.11 Annual variation of ozone density (in DU km^{-1}, based on pre-1988 long-term means) as a function of altitude for **(a)** Resolute Bay (78°N), **(b)** Edmonton (53°N).

caused by changes in the rate of meridional transport of ozone, induced by the quasi-biennial oscillation of the equatorial stratospheric wind. The period of the ozone QBO is about 27–28 months, although it may vary from 20 to 30 months. This is the dominant fluctuation in ozone after the annual cycle at low latitudes; its phase at middle and high latitudes is opposite to that in the tropics. The border between the two regimes is located between 10° and 15° in both hemispheres [Bowman 1989; Hamilton 1989; Chandra and Stolarski 1991; Hasebe 1994]. The amplitude of the QBO signal in the extraequitorial ozone record depends on the season [e.g., Randel and Cobb 1994, Yang and Tung 1994, Bojkov and Fioletov 1995]. It is usually in the 2–4% range [Hasebe 1983; Lait et al. 1989; Gray and Ruth 1993], although it can probably be higher in winter at high latitudes [e.g., Yang and Tung 1994].

The 11-year solar cycle causes the ozone production rate to vary with variations of solar activity. Although the variation in total solar output over the cycle is only about 1%, the change in output in the UV region is several times greater. The amplitude of the effect in total ozone is 1–2% [WMO 1989; Chandra and McPeters 1994, Huang and Brasseur 1993; Chandra 1991; Reinsel et al, 1987] and 5–7% in the upper stratosphere [Chandra and McPeters 1994].

A number of studies [Zerefos et al. 1992, Shiotani and Hasebe 1994; Randel and Cobb 1994] have found a significant El Niño Southern Oscillation (ENSO) signal in equatorial and tropical total ozone, with a characteristic time scale of about four years. Shiotani [1992] has shown a longitudinal difference in the ENSO signal over the equator: during El Niño events there are positive anomalies over the western Pacific and negative anomalies over the eastern Pacific. The anomaly pattern is reversed during La Niña events. In addition, zonal mean values for ozone in the equatorial region are smaller during El Niño events than in La Niña events. There is some evidence that an ENSO-related signal can be seen at extratropical latitudes [e.g., Randel and Cobb 1994], primarily over the Pacific, where the amplitude of the signal can be as much as 6% during strong ENSO events.

1.3 Trends in Total Ozone and its Vertical Distribution

1.3.1 Long-Term Ozone Changes

Since the mid-1980s substantial changes in the ozone layer have been detected. The discovery of the ozone hole in Antarctica [Farman et al. 1985] was the first unequivocal evidence of stratospheric ozone depletion. At that time total ozone levels in spring over Antarctica had dropped to 200 DU from the 300–350 DU levels prevailing in the 1960s and 1970s. Since that time, the hole has become, in general, deeper and wider each year. In the 1990s minimum ozone values of 110–120 DU were seen in Antarctica almost every year, and the total area with spring ozone values below 220 DU exceeded 20 million km^2. Total ozone values less than 100 DU were measured in both 1993 and 1994, with the record low value of 88 DU measured on September 28, 1994. In 1996 a minimum ozone value of 111 DU was recorded, while the area of the hole was almost as large as in the peak year of 1993 [NASA 1996]. Ozonesonde data have shown total destruction (>99%) of ozone from 14 to 19 km during ozone hole episodes in recent years [WMO 1994].

Figure 1.12 shows the mean latitude-time cross-section for the periods 1964–1980 and 1984–1993 [Bojkov and Fioletov 1995]. The hemispheric differences in the ozone distribution are clearly visible in the winter-spring months: in both time periods there is 50–75 DU less ozone at 60°S in October than at 60°N in March. This is probably because of the lower level of planetary wave activity in the southern hemisphere (see Chapter 2), which, in turn, is a consequence of the fact that there is much less land in the southern hemisphere. Losses of about 25 DU between the two time periods, at 60° in each hemisphere in winter, are also apparent. The most dramatic change is south of 75°S in October, where the development of the Antarctic ozone hole can be seen clearly.

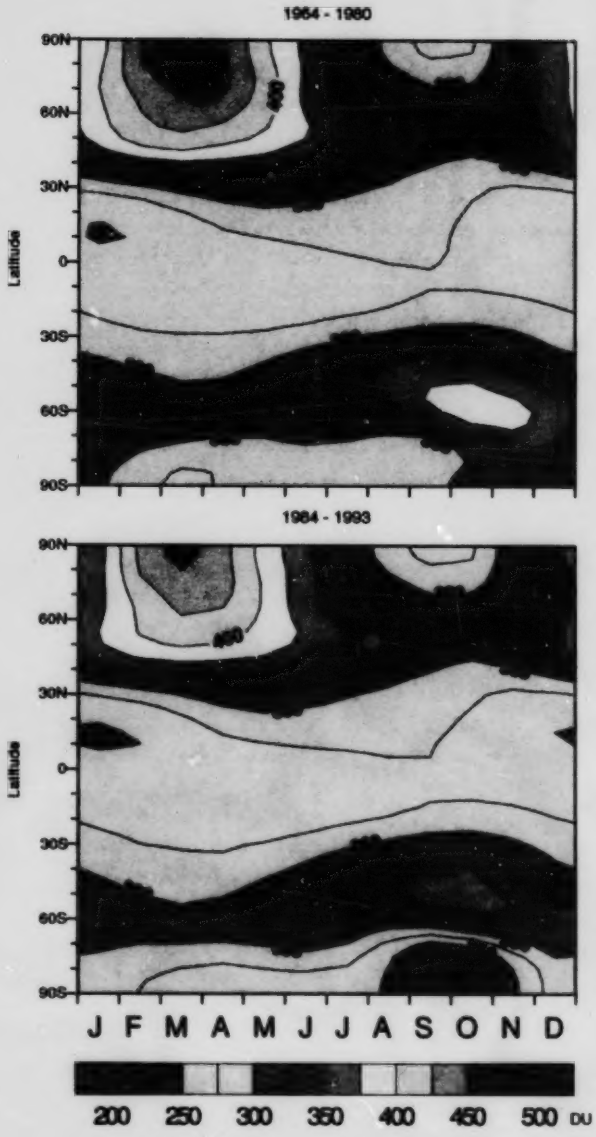

Figure 1.12 Mean total ozone (DU) as a function of latitude and season for 1964–1980 and 1984–1993. (Updated from Bojkov and Fioletov [1995].)

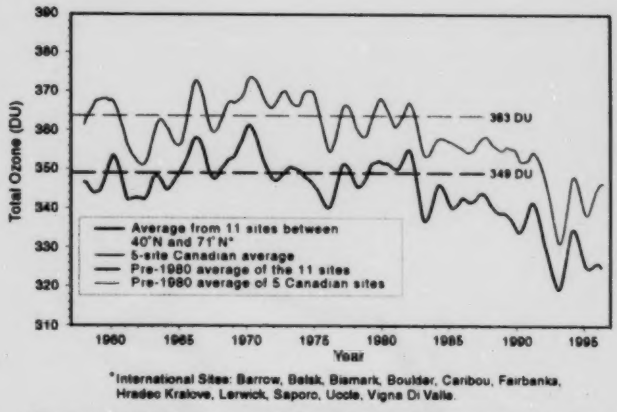

Figure 1.13 Total ozone over 5 Canadian stations and over 11 other midlatitude sites (smoothed, 1-year triangular filter).

Ozone decline over midlatitudes is much weaker than in the Antarctic, although it can be clearly seen from the long-term data records. Figure 1.13 shows the medium- and long-term variation of total ozone over Canada, compared with that of other northern midlatitude sites. The upper curve represents the average of daily total ozone measurements at the five Canadian stations (adjusted in the 1957–1964 period for the fact that not all stations were then operating), the lower curve the average of measurements from the other stations. In each case the smoothed seasonal variation (e.g., the solid curve in Figure 1.8) has been subtracted from the individual daily values, and then the remainder has been smoothed with a 365-day full-width half-maximum triangular filter[2] [Kerr 1991].

The two curves are similar, both in the overall trend and in their variation at time scales of two to five years. The natural year-to-year variation (as evidenced by the values prior to 1980) is of the order of a few percent. The fact that total ozone values are systematically higher over Canada is a manifestation of latitudinal and longitudinal differences in the global ozone distribution. These differences are a result of persistent meteorological features, caused by differences in topography that affect the propagation of planetary waves (see Chapter 2). Both curves demonstrate a decline in total ozone values by about 6% since the late 1970s. Similar trends are seen at other midlatitude stations and from space. In the equatorial belt there are no significant ozone changes [WMO 1994], although a temporary 2–3% total ozone decline is evident after the Mount Pinatubo eruption [e.g., Chandra 1993] .

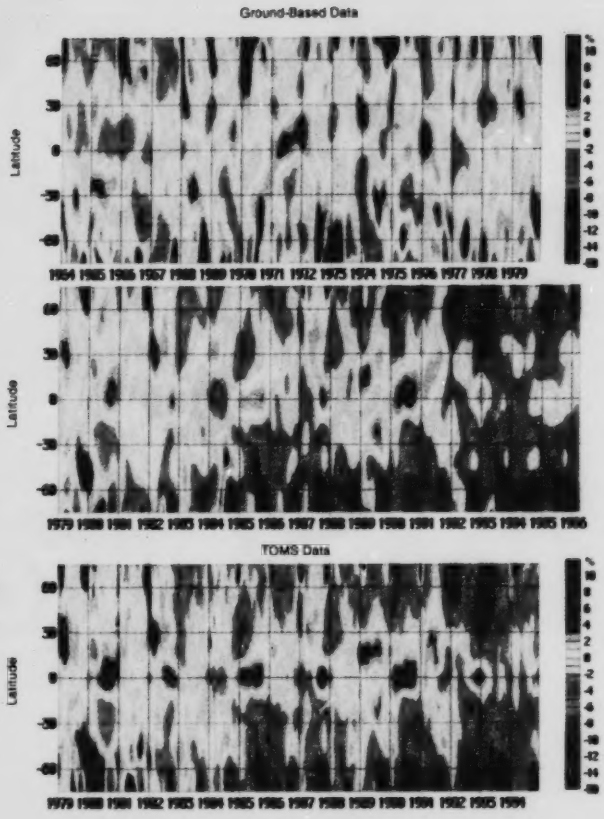

Figure 1.14 Latitude-time cross-section of deviations (%) in total ozone from the long-term mean, 1964–1980. (After Bojkov and Fioletov [1995].)

Figure 1.14 shows total ozone deviations from the long-term (1964–1980) mean, for the periods 1964–1979 and 1979–1996, calculated from ground-based and TOMS data. Both systems show a similar picture of ozone decline during the last 15–20 years. Very significant losses (>30%) are seen in the south polar region after 1980. Losses in the Arctic are smaller than in the Antarctic: typically about 12% in the winter-spring column ozone [Bojkov et al. 1995; McPeters et al. 1996]. This difference is known to be associated with the differences between the Arctic stratosphere vortex and the Antarctic stratosphere vortex [Manney and Zurek 1993]. In the Antarctic, the vortex and the cold temperatures within it persist longer into spring than is the case with the less circular and generally weaker and warmer Arctic vortex. The combination of low temperature (<–80°C) and sunlight, which allows rapid destruction of ozone, occurs to a much greater extent in Antarctica than in the Arctic.

Except in 1993, losses have been smaller (4–6%) at midlatitudes, but a clear downward trend is visible after about 1980. In the tropics the effect of the QBO can be clearly seen. Following the record ozone lows in the northern hemisphere winter of 1992–1993, values closer to normal are seen in 1994. Large negative ozone deviations are visible again in the 1994–1995 winter over northern tropical, middle, and high latitude areas. In the winter of 1995–1996 large negative deviations can be seen over northern high latitudes but not at middle latitudes. One may also see that deviations during the 1960s and 1970s are less significant, and do not show the dramatic trends of the 1980s and 1990s.

Figure 1.15 shows deviations from the long-term (1966–1987) means of vertical ozone distribution over Canada. The data are from weekly ozonesonde flights at the six Canadian stations. Deviations are in DU km^{-1}. The data have been smoothed by a 3-month running mean (boxcar filter). The pattern of low total ozone values during recent years is evident, and from these data it is also apparent that the major losses are in the lower stratosphere. Similar patterns can be seen in sonde data from Asia (Japan) and Europe (Figure 1.20).

Although ozone decline at midlatitudes was anticipated, the fact that the major losses have occurred in the lower stratosphere was surprising, since atmospheric ozone chemistry models employing gas phase reactions with chlorine (see Chapter 3) predict, at most, a decline of about 1% in total ozone since 1980 [Brasseur 1992; McElroy et al. 1992]. Additionally, the bulk of this decline was predicted by those models to occur in the upper stratosphere, near 40 km. Since midlatitude stratospheric temperatures are too warm to permit the formation of Polar Stratospheric Clouds (PSCs, see Chapter 3), the low temperature heterogeneous chemistry responsible for the Antarctic ozone hole cannot occur there. Contributing factors to the midlatitude loss are destruction via heterogeneous reactions on sulphate aerosols injected into the stratosphere from several large volcanic eruptions in the past decade [WMO 1991, 1994]; destruction via heterogeneous

[2] Each point on the smoothed curve is therefore a weighted average of the (deseasonalized) original data: i.e., if S_i and R_i are the values of the smoothed curve and the deseasonalized raw data respectively at day i, then

$$S_i = \frac{\sum_{n=-730}^{730} R_{i+n} W_n}{\sum_{n=-730}^{730} W_n}, \quad W_n = \frac{730-|n|}{730}, \quad \text{if } R_{i+n} \text{ exists,}$$

$$= 0, \quad \text{otherwise.}$$

This has the effect of suppressing short-term variations.

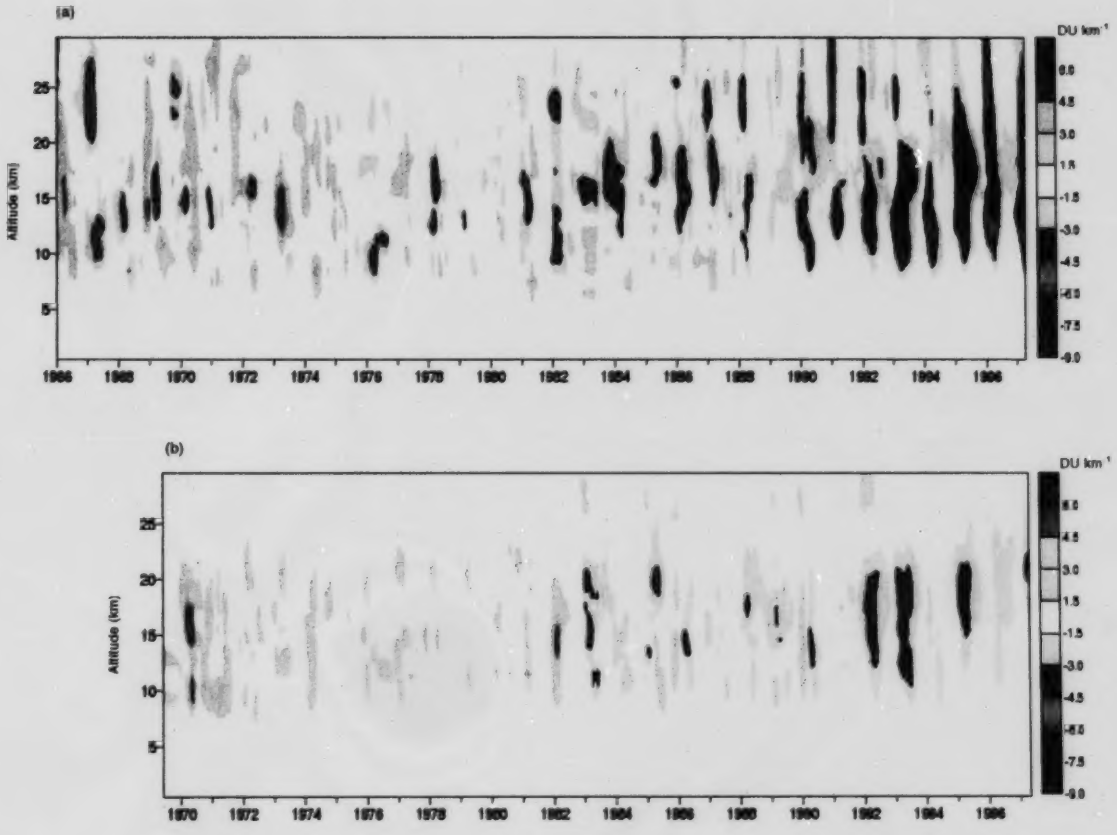

Figure 1.15 Deviations from the 1966–1987 means of ozone in DU km^{-1} over **(a)** Canadian Arctic stations (Resolute, Eureka, and Alert) and **(b)** Canadian midlatitude sites (Edmonton, Goose Bay, and Churchill). Values shown are 3-month running means.

reactions on PSCs in the Arctic winter stratosphere, with subsequent transport to lower latitudes; and possible changes in dynamics, such as the warming of the global troposphere. In addition, a possible side effect of global warming is a cooling of the Arctic stratosphere leading to an enhanced rate of ozone destruction by heterogeneous processes [Austin et al. 1992].

1.3.2 Recent Occurrences of Low Ozone Values

In 1992 and 1993 very low ozone values were observed almost everywhere from the equator to the poles [Gleason et al. 1993, Schoeberl et al. 1993, Chandra 1993, Kerr et al. 1993]. Over Canada the dramatic losses in the spring of 1993 were at that time the largest ever seen [Kerr et al. 1993]. Total ozone values were 10–17 % below normal, and the peak loss was 30% at 16 km. Record low average total ozone values for the period January–April were observed at three of the four midlatitude stations where measurements have been made since the 1960s. These extreme values were not seen in the spring of 1994, however, and the phenomenon is attributed to the effects (dynamical and/or chemical) of the eruption in the Philippines in June 1991 of Mt. Pinatubo, which injected more SO_2 into the stratosphere than any other volcano this century [Brasseur and Granier 1992; Labitzke and McCormick 1992; Schoeberl et al. 1993; Solomon et al. 1996].

In March of 1997 Canadian stations in the Arctic recorded large depletions in total column ozone relative to long-term station mean values. These losses, the largest ever seen in 40 years of ozone monitoring in the Canadian Arctic, exceeded the dramatic losses of 1993. Monthly mean ozone concentration values at 16 km were 40% lower than long-term means, and deviations in total ozone were more than 45% (4σ) for some individual days [Fioletov et al. 1997; Newman et al. 1997]. The net ozone loss was similar to that which occurred in recent years in the Antarctic, although the amount of ozone remaining is still much greater. (In 1997, ozone in the Arctic declined from an undisturbed value of 450 DU to below

300 DU, while in Antarctica values have typically declined from 300 DU to about 100 DU.) The low ozone values in the Arctic were associated with very low temperatures, apparently owing to a reduced eddy flux of heat into the polar vortex [Newman et al. 1997]. This may imply reduced transport of ozone as well. However, polar stratospheric clouds were observed frequently from the observatory at Eureka as were high values of chlorine monoxide in the first two weeks of March [Donovan et al. 1997; Santee et al. 1997]. This suggests that, as in the Antarctic spring, the low temperatures within the arctic stratosphere vortex led to the formation of PSCs, permitting the generation of chlorine monoxide, which in the presence of sunlight rapidly destroys ozone (see Chapter 3). There were also very cold temperatures and low ozone values during the February–March period of 1996.

Total ozone maps and maps of ozone deviations in percent for March 1993 and March 1997 are shown in Figure 1.16. While the 1993 ozone loss was widespread over Canada, that of 1997, while much more pronounced in the Arctic, was not observed at midlatitudes. This may also be seen from Figure 1.15.

1.3.3 Total Ozone Trends

Figure 1.17 shows trends from a large number of ground-based total ozone measuring stations (Dobson and Brewer) located between 60°S and 60°N, and possessing good calibration histories. The station records are those used in the recent UNEP Assessment [WMO 1994], with the addition of data for 1995 and 1996. The Canadian stations with long-term records (Toronto, Edmonton, Goose, and Churchill) are indicated by solid circles. A regression model that allows for annual, QBO, and solar cycle variations and assumes a linear trend beginning in 1979 [Bojkov et al. 1995] was used to estimate trends.

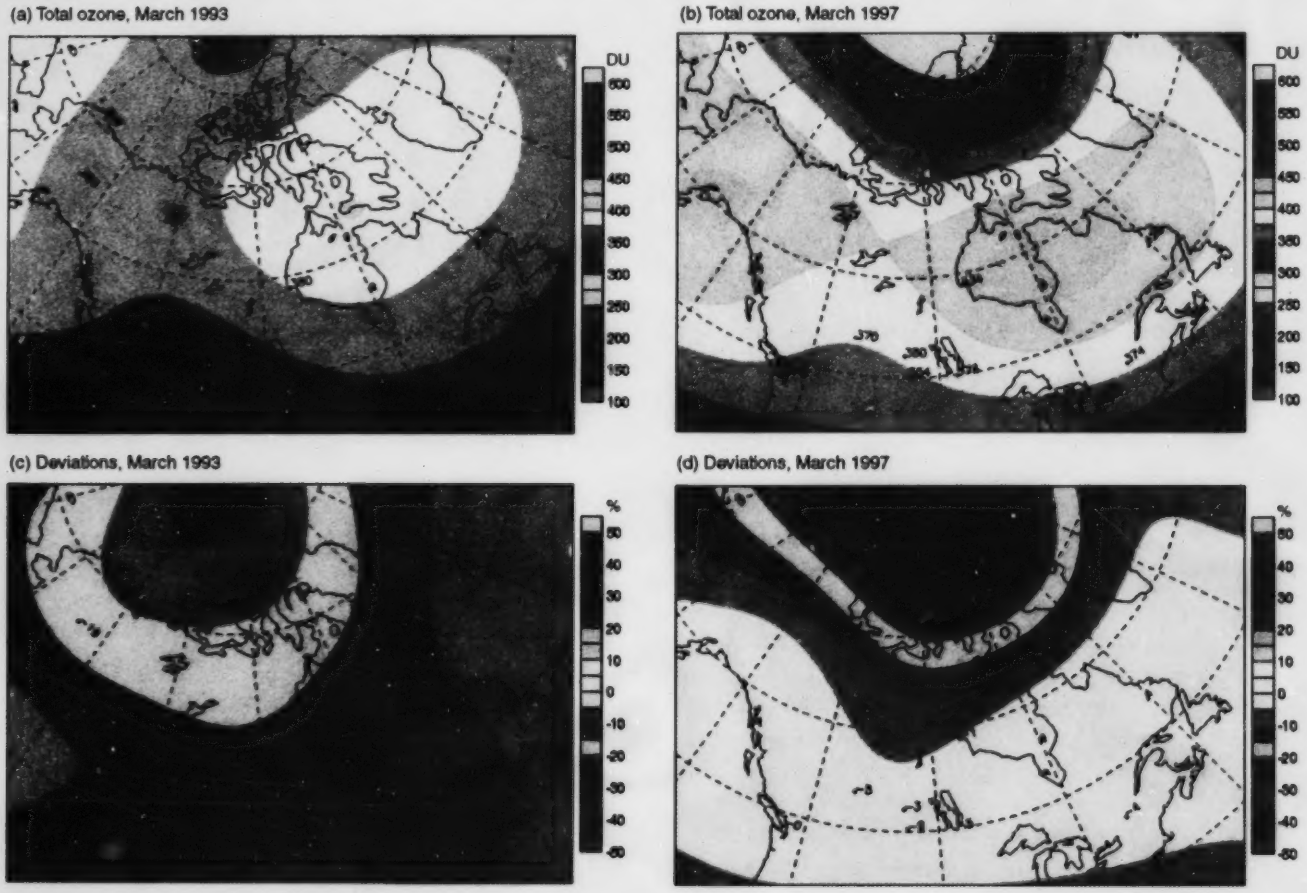

Figure 1.16 Total Ozone over Canada: (a, b): average values for March 1993 and March 1997; (c, d): percentage differences from the 1979–1988 average.

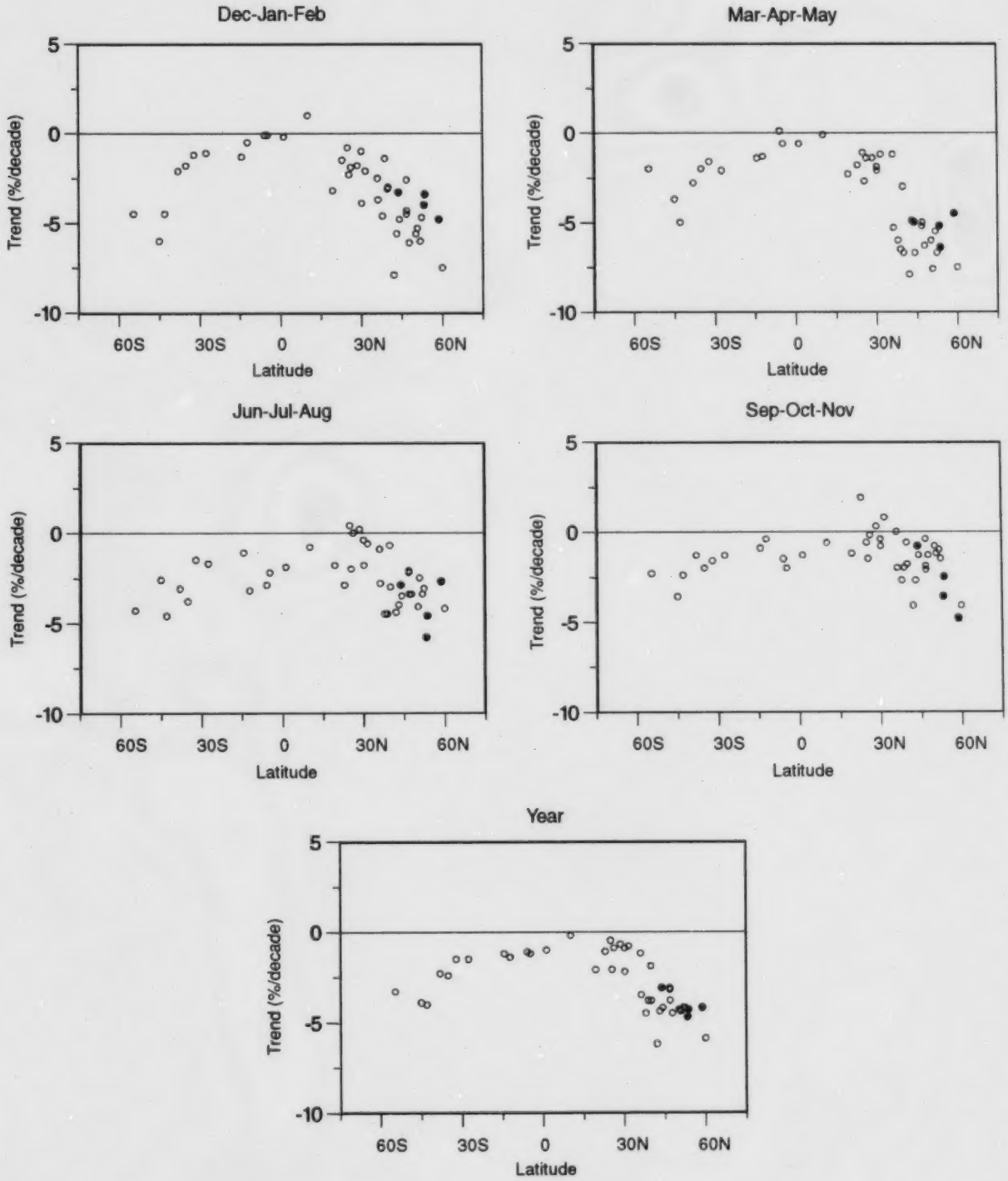

Figure 1.17 Decadal trends in annual and seasonal total ozone averages by latitude, from ground-based data.

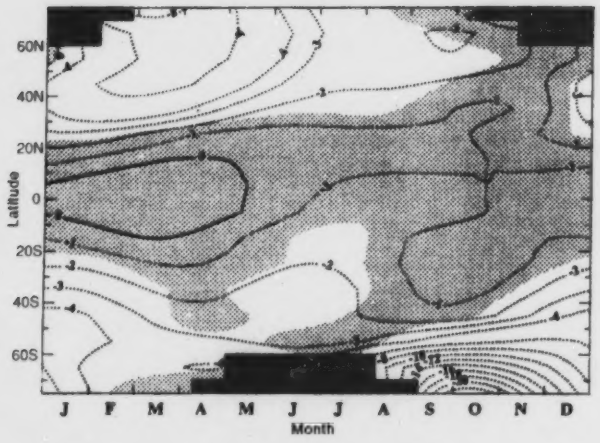

Figure 1.18 Trends in total ozone from TOMS (percentage change per decade), 1978–1994. (From McPeters et al. [1996].)

Examination of the station trends of Figure 1.17 and the satellite data of Figure 1.18 reveals the major latitude and seasonal trend patterns. Midlatitude trends are only slightly different in the two hemispheres. The annual average at 45°S is slightly less (about 4% vs 5% per decade), the seasonal variation is weaker, and the peak occurs later in relation to the spring equinox than at 45°N. The trends are largest poleward of 45°. The strongest decline, more than 20% per decade in the southern polar region during the austral spring, reflects the development of the Antarctic ozone hole.

Trends are not statistically significant between 20°N and 20°S. The tendency toward large negative springtime trends can also be seen in Figure 1.8; the recent measurements fall below the pre-1980 values primarily in the early part of the year. Since ozone is generally much higher at this time of year, these early springtime losses are less serious with respect to human UV exposure than would be summertime losses of similar magnitude. However, the reverse may be the case for aquatic ecosystems as well as crops and other vegetation, which may be more sensitive in the early spring (see Chapter 5).

Deseasonalized annual averages of total ozone for five Canadian stations with long-term records are shown in Figure 1.19 as a deviation in percent from the pre-1980 average. All data are direct-sun observations. No correction has been made for QBO, solar cycle, or other effects. Interannual variability of the order of ±5% is evident, as is the general decline in average ozone values from 1980 onwards. After 1982 the annual deviations are negative, with few exceptions, at all stations, and a tendency toward even lower values in the 1990s is apparent at all stations. The best-fit linear trend to the 1980–1996 data is shown, as well as the 95% confidence limits (dotted curves) for that trend. The trend is negative and statistically significant at the 95% confidence level at all stations.

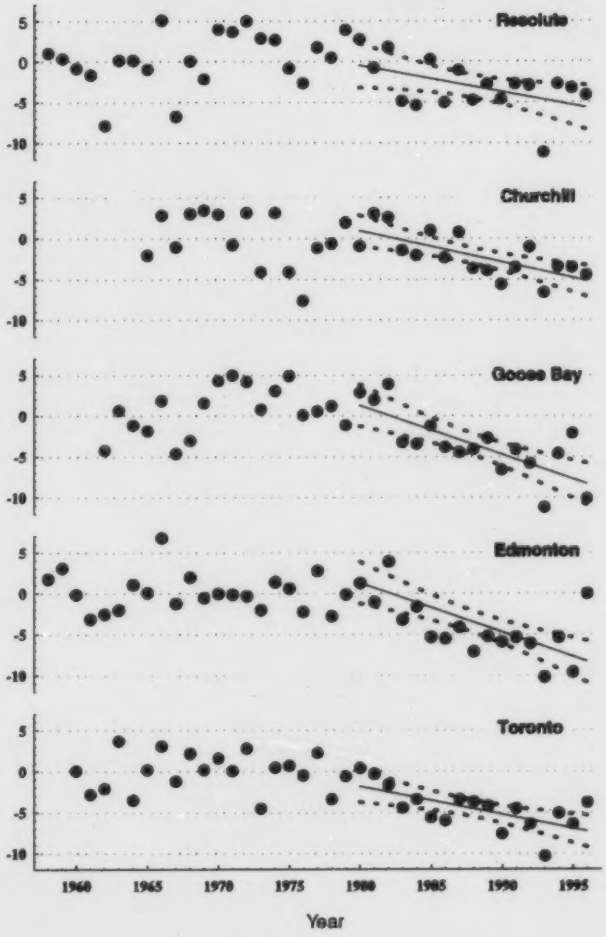

Figure 1.19 Trends in total ozone at Canadian stations. The trend toward lower values in the 1980s and 1990s is indicated. The calculated trends are all statistically significant at the 95% level.

1.3.4 Trends in the Vertical Distribution of Ozone

Figure 1.20 shows deviations from the long-term (1974–1988) means of vertical ozone distribution over Canada, Europe, and Japan. The data are from ozonesonde flights at Hohenpeissenberg and Lindenberg (Germany), Payerne (Switzerland), Churchill, Goose Bay, and Edmonton (Canada), and Sapporo and Tateno (Japan) [Bojkov and Fioletov 1997]. The annual cycle has been removed. Deviations are in ozone partial pressure (nanobars, or 10^{-6} hPa). The data have been smoothed by a 3-month running mean (boxcar filter). A high degree of variability is evident, but with few positive deviations and strong negative deviations after 1982 in all three regions. Most notable are the large negative deviations in 1993 (in all regions) and in 1995 (in Canada and Japan).

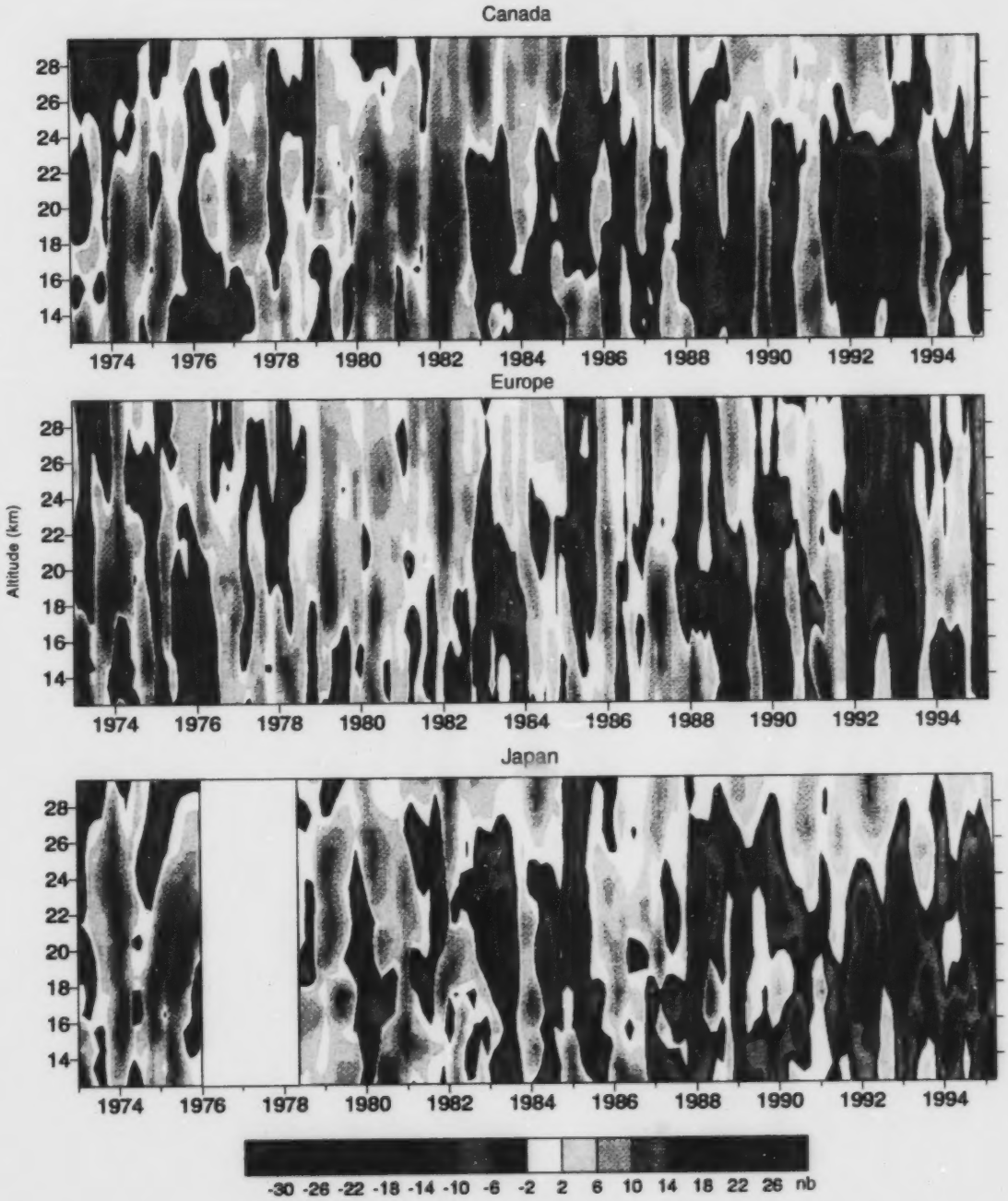

Figure 1.20 Ozone deviations from the long-term (1974–1988) means over Canada, Europe and Japan, expressed as ozone partial pressure (nanobars, or 10^{-6} hPa). The data have been smoothed by a 3-month running mean (boxcar filter). (From Bojkov and Fioletov [1997].)

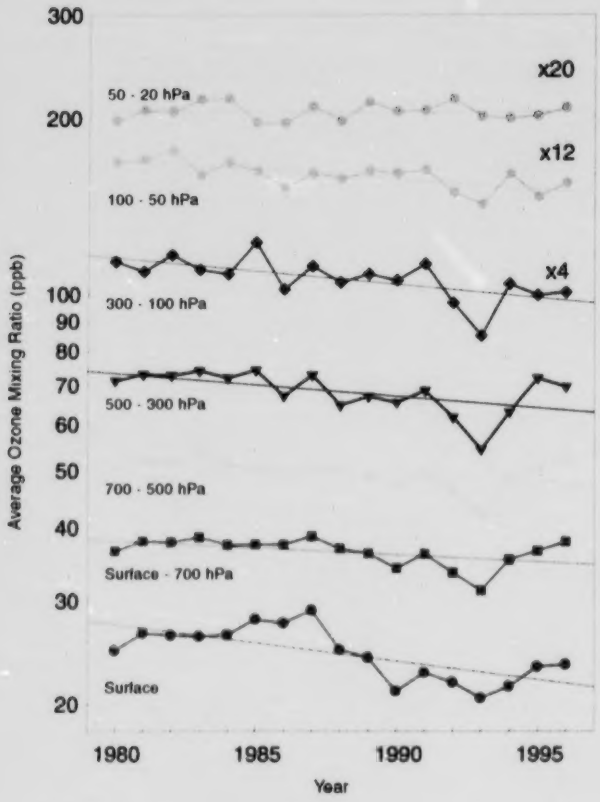

Figure 1.21 Trends in ozone mixing ratio over Canada (5-station average), from ECC ozonesonde data, 1980–1996. Data for Alert (1988–1996) have been included, after adjustment to the four-station mean for that period. Values for the top three plots should be multiplied by the indicated factors to get the correct mixing ratio.

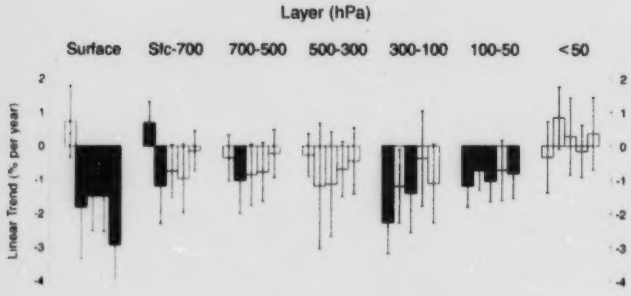

Figure 1.22 Trends in ozone mixing ratio at five Canadian sites, from ECC ozonesonde data, 1980–1996, for six layers and the surface. Stations in each group (left to right): Alert, Resolute, Churchill, Goose Bay, Edmonton. Trends significant at the 95% level are indicated by dark shading.

Figure 1.21 presents the average trends in ozone at different pressure heights over Canada. The atmosphere has been divided into six layers: surface–700 hPa, 700–500 hPa, 500–300 hPa, 300–100 hPa, 100–50 hPa, and 50–20 hPa. Annual average values of the ozone mixing ratio are shown for each layer. The lower two stratospheric layers show the expected decline, as seen throughout the northern hemisphere. The three tropospheric layers also show a similar decline. This behaviour is found at other North American sonde stations [Oltmans et al. 1997], but it contrasts with results from Europe and Japan [Oltmans et al. 1997; Claude et al. 1996; Logan 1994] that show similar negative trends in the stratosphere but positive trends up to the late 1980s in the troposphere.

The steady decrease of mixing ratio from the lower stratosphere to the surface is consistent with the hypothesis that stratospheric injection is a major source of tropospheric ozone in remote northern regions, as has been suggested by studies of tropopause folding using ozonesondes [Oltmans et al. 1989] and recent studies using aircraft [Bachmeier et al. 1994; Browell et al. 1994]. Comparison of the long-term trends is also suggestive: the three free tropospheric layers show essentially the same behaviour as the lower two stratospheric layers. Moreover, the year-to-year variations in all five layers show some correlation. In particular, the large losses in the lower stratosphere in 1993 [Kerr et al. 1993] and subsequent recovery are also reflected in similar losses and recoveries in all three tropospheric layers and possibly even at the surface. Other mechanisms than stratospheric injection have been suggested to explain this correlation in remote northern regions: one possibility is increased *destruction* of ozone in the upper troposphere by higher levels of UV-B radiation penetrating a reduced stratospheric layer [Taalas et al. 1997; Madronich and Granier 1994].

Figure 1.22 shows trends derived for the same atmospheric layers for each of five Canadian sonde stations. (Eureka has been omitted as the record is too short.) The sonde data were integrated within these layers to produce values for the partial ozone column in each layer, which were then converted to an average mixing ratio in parts per billion (ppb). The mixing ratio time series were deseasonalized, and then, as the sonde record is not entirely regular in time, they were binned by month. In order to avoid the effects of autocorrelation within the year on the error estimates of the derived trends, these monthly averages were further averaged into annual averages on which a simple linear regression was then used to derive trends.

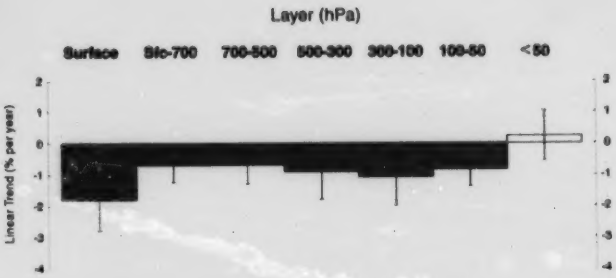

Figure 1.23 Trends in ozone mixing ratio averaged over the five Canadian stations. Data for Alert (1988–1996) have been included, after adjustment to the four-station mean for that period. Trends significant at the 95% level are indicated by dark shading.

Except for Alert at the surface and in Layer 1, all stations show primarily negative trends. The trends for the five-station average (Figure 1.23) are all negative in the troposphere, including the trends in surface ozone (derived from the measurements made by the sondes at the point of launch). All are statistically significant at the 2σ level. Overall, surface trends are nearly twice as large as those in the three free tropospheric layers [Tarasick et al. 1995, 1996b].

1.4 Forecasting Day-to-day Changes in Total Ozone

It has been known since the 1920s that total ozone variations are highly correlated with synoptic scale meteorological disturbances, particularly at extratropical latitudes [Dobson and Harrison 1926; Dobson et al. 1929, 1930, 1946]. Detailed examination of weather patterns and total ozone amounts reveals some simple relationships between them [Reed 1950; Vaughan and Price 1991; Wirth 1993]. For example, high total ozone is associated with an upper air trough, and low total ozone with a ridge, and ozone is observed to increase and decrease with the passage of cold and warm fronts respectively. Total ozone has been shown to be correlated with lower stratospheric temperatures, geopotential heights, and winds [Ohring and Muench 1959], with tropopause pressure (or height) [Schubert and Munteanu 1988], and with isentropic potential vorticity near the tropopause [Vaughan and Begum 1989; Allaart et al. 1993]. Knowledge of these relationships was the basis for the development of Environment Canada's Ozone/UV-B Forecast Model, which uses the output from the operational forecast model at the Canadian Meteorological Centre to forecast total ozone and thence UV-B (see Chapter 4). The ozone forecast model that became operational in 1993 [Burrows et al. 1995] is based on multiple regressions of historical values of total ozone and meteorological variables. The initial forecast produced by the regression equations is corrected, using knowledge of current ozone measurements at the 12 Canadian Brewer sites and their forecasted values from the previous day, to produce the final forecast. Figure 1.24 shows that, in general, the model has performed extremely well, with typical root mean square errors of only approximately 10 DU.

The model's good performance is in large part due to the simple correction procedure that it uses. Research is currently in progress to improve the stratospheric part of the Canadian Meteorological Centre's global forecast model and to include ozone as a model variable. A three-dimensional optimal data assimilation system (3DVAR) is also under development, along with the necessary algorithms to assimilate ozone data, both from satellite instruments such as GOME and from the Canadian ground-based network.

1.5 Trends in Ozone-Depleting Substances and Stratospheric Chlorine

The Montreal Protocol, which by mid-1997 had been signed by 163 countries, has established controls on the major ozone-depleting substances. Under the terms of the protocol and the subsequent London and Copenhagen amendments, the industrialized countries agreed to cease production of halons by the end of 1993 and of CFCs, carbon tetrachloride, and methyl chloroform by the end of 1995. Following meetings in Vienna (1995) and Costa Rica (1996), agreement was reached on gradual reductions in the use of methyl bromide and on its complete phase-out by 2010.

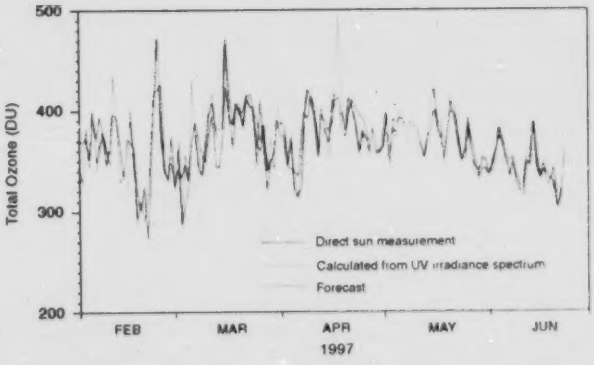

Figure 1.24 Ozone forecasts at Montreal: Total column ozone measured by Brewer at Montreal versus the ozone predicted by the forecast model at CMC.

Assuming that the Montreal Protocol provisions are obeyed, it is estimated that the amount of chlorine in the stratosphere, currently about 3.5 parts per billion, will peak within the next five years and that it will decrease thereafter. It should reach the 1980 level of 2.0 ppb by 2050 and the natural level of 1.0 ppb some time after 2100 [WMO 1991, 1994]. Uncertainties in the extent to which countries adhere to their obligations under the protocol as well as modelling uncertainties will no doubt cause these estimates to be revised many times before then.

Chlorine concentrations in the stratosphere follow those in the troposphere with a time lag of three to five years. Observations of tropospheric CFCs at Barrow and Alert are shown in Figure 1.25. CFC-11 and CFC-12 are destroyed in the atmosphere at a rate of about 2% and 1% per year respectively. The measurements for both show strong evidence of decreasing rates of emission into the atmosphere. In the case of CFC-11, the emission rate is now less than the destruction rate, and the concentration is therefore declining. With CFC-12, the rate of increase has been much reduced since about 1990. It is encouraging that tropospheric concentrations of these CFCs are already clearly showing the effects of the Montreal Protocol controls.

That ozone depletion has been caused by increasing chlorine and bromine amounts in the stratosphere is beyond doubt, and it is therefore reasonable to assume that ozone depletion should diminish as the chlorine and bromine content of the stratosphere declines. However, other factors such as different anthropogenic gases or possibly global warming may be significant contributors to ozone depletion. Current models do not reproduce observed ozone depletion well enough to rule out a contribution from these factors. Thus, stratospheric chlorine or bromine or any combination of these is a proxy for ozone depletion but not necessarily an accurate or complete one. Also, because there is a much greater variability in ozone than stratospheric chlorine, any recovery in ozone will take many more years to detect than a corresponding one in the chlorine values.

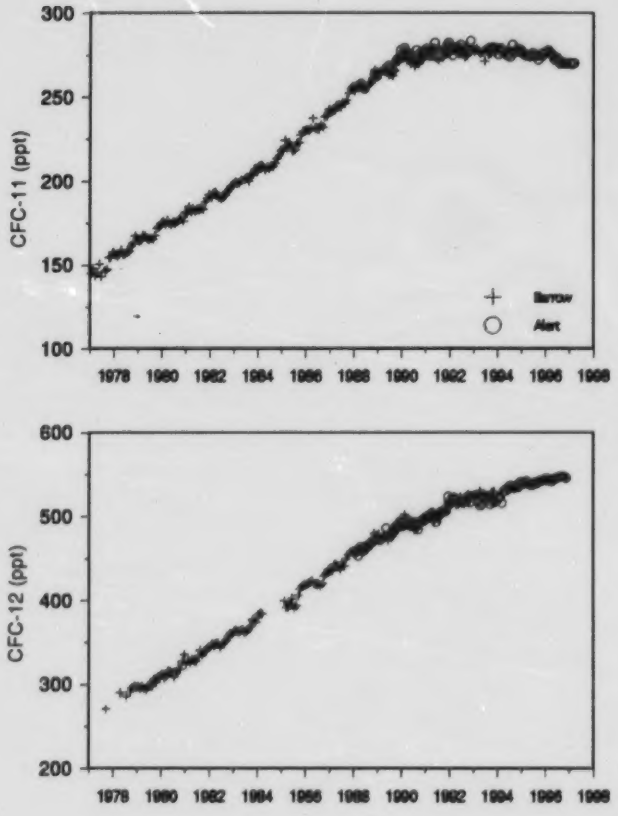

Figure 1.25 Measurements of tropospheric CFC concentration, from flask samples taken at Alert, N.W.T., and Barrow, Alaska. (Courtesy J.W. Elkins, NOAA.)

References

Allaart, M.A., H. Kelder, and L.C. Heijboer, 1993. On the relation between ozone and potential vorticity. *Geophys. Res. Lett.*, **20**, 811–814.

Anderson, J.G., W.H. Brune, S.A. Lloyd, D.W. Toohey, S.P. Sander, W.L. Starr, M. Loewenstein, and J.R. Podolske, 1989. Kinetics of O_3 destruction by ClO and BrO within the Antarctic vortex: An analysis based on in situ ER-2 data. *J. Geophys. Res.*, **94**, 9837–9846.

Angell, J. K., and J. Korshover, 1973. Quasi-biennial and long-term fluctuations in total ozone. *Mon. Weather Rev.*, **101**, 426–443.

Angell, J.K., and J. Korshover, 1976. Global analysis of recent total ozone fluctuations. *Mon. Weather Rev.*, **104**, 63–75

Austin J., N. Butchart, and K. P. Shine, 1992. Possibility of an Arctic ozone hole in a doubled-CO_2 climate. *Nature*, **360**, 221–225.

Bachmeier, E.V., M.C. Shipman, E.V. Browell, W.B. Grant, and J.M. Klassa, 1994. Stratospheric/tropospheric exchange affecting the northern wetlands regions of Canada during summer 1990. *J. Geophys. Res.*, **99**, 1793–1804.

Bojkov, R.D., and V.E. Fioletov, 1995. Estimating the global ozone characteristics during the last 30 years. *J. Geophys. Res.*, **100**, 16,537–16,551.

Bojkov, R. D., V.E. Fioletov, and A.M. Shalamjansky, 1994. Total ozone changes over Eurasia since 1973 based on reevaluated filter ozonometer data. *J. Geophys. Res.*, **99**, 22,985–22,999.

Bojkov R.D., L. Bishop and V.E. Fioletov, 1995. Total ozone trends from quality-controlled ground-based data (1964–1994). *J. Geophys. Res.*, **100**, 25,867–25,876.

Bojkov, R.D., and V.E. Fioletov, 1997. Changes of the lower stratospheric ozone over Europe and Canada. *J. Geophys. Res.*, **102**, 1337-1347.

Bowman, K.P., 1989. Global patterns of the quasi-biennial oscillation in total ozone. *J. Geophys. Res.*, **99**, 3328–3343.

Bowman, K.P. and A.J. Krueger, 1985. A global climatology of total ozone from the Nimbus-7 Total Ozone Mapping Spectrometer (TOMS). *J. Geophys. Res.*, **90**, 9767–9776.

Brasseur, G.P., 1992. Natural and anthropogenic perturbations of the stratospheric ozone layer. *Planet. Space Sci.*, **40**, 403–412.

Brasseur, G., and C. Granier, 1992. Mount Pinatubo aerosols, chlorofluorocarbons, and ozone depletion. *Science*, **257**, 1239–1242.

Brewer, A.W., 1949. Evidence for a world circulation provided by the measurements of helium and water vapour distribution in the stratosphere. *Quart. J. R. Met. Soc.*, **75**, 351–363.

Brewer, A.W., and J.R. Milford, 1960. The Oxford-Kew sonde. *Proc. Roy. Soc. A*, **256**, 470–495.

Browell, E.V., M.A. Fenn, C.F. Butler, W.B. Grant, R.C. Harriss, and M.C. Shipman, 1994. Ozone and aerosol distributions in the summertime troposphere over Canada. *J. Geophys. Res.*, **99**, 1739–1755.

Brune, W.H., J.G. Anderson, and K.R. Chan, 1989. In situ observations of ClO in the Antarctic: ER-2 aircraft results from 54° to 72°N latitude. *J. Geophys. Res.*, **94**, 16649–16663.

Brune, W.H., D.W. Toohey, J.G. Anderson, and K.R. Chan, 1990. In situ observations of ClO in the arctic stratosphere: ER-2 aircraft results from 59° to 80°N latitude. *Geophys. Res. Lett.*, **17**, 505–508

Burrows, W., M. Vallee, D.I. Wardle, J.B. Kerr, L.J. Wilson, and D.W. Tarasick, 1995. The Canadian UV-B and Total Ozone Forecast Model. *Met. Apps.*, **1**, 247-265.

Chandra, S., 1991. The solar UV–related changes in total ozone from a solar rotation to a solar cycle. *Geophys. Res. Lett.*, **18**, 837–840.

Chandra, S., 1993. Changes in stratospheric ozone and temperature due to the eruptions of Mt. Pinatubo. *Geophys. Res. Lett.*, **20**, 33–36.

Chandra, S., and R.S. Stolarski, 1991. Recent trends in stratospheric total ozone: Implications of dynamical and El Chichon perturbations. *Geophys. Res. Lett.*, **18**, 2277–2280.

Chandra, S., and R.D. McPeters, 1994. The solar cycle variation of ozone in the stratosphere inferred from Nimbus 7 and NOAA 11 satellites. *J. Geophys. Res*, **99**, 20665–20671.

Claude, H., U. Kohler, and W. Steinbrecht, 1996. New trend analyses of the homogenized total ozone records at Hohenpeissenberg. *Proc. Quad. Ozone Symp.*, L'Aquila, Italy, 12–21 September, 1996, in press.

Danielson, E.F., 1983. Ozone Transport. Pages 161–194 in *Ozone in the Free Atmosphere*. R.C. Whitten and S.S. Prasad, eds. Princeton: Van Nostrand Reinhold.

Deluisi, J.J., D.U. Longnecker, C.L. Mateer, and D.J. Wuebbles, 1989. An analysis of northern middle-latitude Umkehr measurements corrected for stratospheric aerosols for 1979–1986. *J. Geophys. Res.*, **94**, 9837–9846.

Dobson, G.M.B., and D.N. Harrison, 1926. Measurements of the amount of ozone in the earth's atmosphere and its relation to other geophysical conditions: Part I. *Proc. Roy. Soc. London*, **A110**, 660–693.

Dobson, G.M.B., D.N. Harrison, and J. Lawrence, 1929. Measurement of the amount of ozone in the earth's atmosphere and its relation to other geophysical conditions: Part III. *Proc. Roy. Soc. London*, **A122**, 456–486.

Dobson, G.M.B., H.H. Kimball, and E. Kidson, 1930. Measurement of the amount of ozone in the earth's atmosphere and its relation to other geophysical conditions, Part IV. *Proc. Roy. Soc. London*, **A129**, 411–433.

Dobson, G.M.B., A.W. Brewer, and B.M. Cwilong, 1946. Meteorology of the lower stratosphere. *Proc. Roy. Soc. London*, **A185**, 144–175.

Donovan, D.P., J.C. Bird, J.A. Whiteway, T.J. Duck, S.R. Pal, A.I. Carswell, J.W. Sandilands, and J.W. Kaminski, 1996. Ozone and aerosol observed by lidar in the Canadian Arctic during the winter of 1995/96. *Geophys. Res. Lett.*, **23**, 3317–3320.

Donovan, D. P., H. Fast, Y. Makino, J.A. Whiteway, J.W. Kaminski, V. Savastiouk, J.C. Bird, A.I. Carswell, J. Davies, T.J. Duck, C.T. McElroy, R.L. Mittermeier, S.R. Pal, and D. Velkov,1997. Ozone, chlorine oxide, and polar stratospheric clouds observed over the NDSC observatory at Eureka during spring 1997. *Geophys. Res. Lett.*, **24**, in press.

Evans, W.F.J., J.B. Kerr, C.T. McElroy, R.S. O'Brien, B.A. Ridley, and D.I. Wardle, 1977. The odd nitrogen mixing ratio in the stratosphere. *Geophys. Res. Lett.*, **4**, 235–238.

Evans, W.F.J., J.B. Kerr, C.T. McElroy, R.S. O'Brien, and J.C. McConnell, 1982. Measurement of NO_2 and HNO_3 during a stratospheric warming at 54°N in February 1979. *Geophys. Res. Lett.*, **9**, 493–496.

Evans, W.F.J., C.T. McElroy, and I.E. Galbally, 1985. The conversion of N_2O_5 to HNO_3 at high latitudes in winter. *Geophys. Res. Lett.*, **12**, 825–828.

Farman, J.C., B.G. Gardiner and J.D. Shanklin, 1985. Large losses of ozone in Antarctica reveal seasonal ClO_x/NO_x interaction. *Nature*, **315**, 207–210.

Fisher, M., and D.J. Lary, 1995. Lagrangian four-dimensional variational data assimilation of chemical species. *Quart. J. R. Met. Soc.*, **121**, No. 527 Part A, 1681–1704.

Fioletov, V.E., 1993. Total ozone "normal" values and mapping algorithm used in the atlas. Pages 17–28 in *Atlas of GO_3OS total ozone maps for the northern hemisphere winter-spring of 1992–1993*. WMO Ozone Rep. 34. Geneva: World Meteorological Organization.

Fioletov, V.E., J.B. Kerr, D.I. Wardle, J. Davies, E.W. Hare, C.T. McElroy and D.W. Tarasick, 1997. Long-term decline of ozone over the Canadian Arctic to early 1997 from ground-based and balloon sonde measurements. *Geophys. Res. Lett.*, **24**, in press.

Gleason, J. F., P. K. Bhartia, J. R. Herman, R. McPeters, P. Newman, R. S. Stolarski, L. Flynn, G. Labow, D. Larko, C. Seftor, C. Wellemeyer, W. D. Komhyr, A. J. Miller, and W. Planet, 1993. Record low global ozone in 1992. *Science*, **260**, 523–526.

Götz, F.W.P., A.R. Meetham, and G.M.B. Dobson, 1934. The vertical distribution of ozone in the atmosphere. *Proc. Roy. Soc. London*, **A145**, 416–446.

Gray, L.J., and S. Ruth, 1993. The modeled latitudinal distribution of the ozone quasi-biennial oscillation using observed equatorial winds. *J. Atmos. Sci.*, **50**, 1033–1046.

Hahn, J.F., C.T. McElroy, E.W. Hare, W. Steinbrecht, and A.I. Carswell, 1995. Intercomparison of Umkehr and differential absorption lidar stratospheric ozone measurements. *J. Geophys. Res.*, **100**, 25899–25911.

Hamilton. K., 1989. Interhemispheric asymmetry and annual synchronization of the ozone quasi-biennial oscillation. *J. Atmos. Sci.*, **46**, 1019–1025.

Herman, J. R., and D. Larko, 1994. Low ozone amount during 1992–1993 from Nimbus 7 and Meteor 3 total ozone mapping spectrometers. *J. Geophys. Res.*, **99**, 3483–3496.

Hasebe, F., 1983. Interannual variations of global ozone revealed from NIMBUS 4 BUV and ground-based observations. *J. Geophys. Res.*, **88**, 6819–6834.

Hasebe, F., 1994. Quasi-biennial oscillations of ozone and diabatic circulation in the equatorial stratosphere. *J. Atmos. Sci.*, **55**, 729–745.

Hilsenrath, E., W. Attmannspacher, A. Bass, W. Evans, R. Hagemeyer, R.A. Barnes, W. Komhyr, K. Mauersberger, J. Mentall, M. Proffitt, D. Robbins, S. Taylor, A. Torres and E. Weinstock, 1986. Results from the balloon intercomparison campaign (BOIC). *J. Geophys. Res.*, **91**, 13137–13152.

Hofmann, D.J., and S. Solomon, 1989. Ozone destruction through heterogeneous chemistry following the eruption of El Chichon. *J. Geophys. Res.*, **94**, 5029–5041.

Huang, T.Y.W., and G.P. Brasseur, 1993. Effect of long-term solar variability in a two-dimensional interactive model of the middle atmosphere. *J. Geophys. Res*, **98**, 20413–20427.

Kerr, J. B., 1991. Trends in total ozone at Toronto between 1960 and 1991. *J. Geophys. Res.*, **96**, 20703–20709.

Kerr, J.B., I. A. Asbridge, and W.F.J. Evans, 1988. Intercomparison of ozone measured by Brewer and Dobson spectrophotometers at Toronto. *J. Geophys. Res*, **93**, 11129–11140.

Kerr, J.B., D.I. Wardle, and D.W. Tarasick, 1993. Record low ozone values over Canada in early 1993. *Geophys. Res. Lett.*, **20**, 1979–1982.

Komhyr, W.D., 1969. Electrochemical concentration cells for gas analysis. *Ann. Géophys.*, **25**, 203–210.

Labitzke, K., and M.P. McCormick, 1992. Stratospheric temperature increases due to Pinatubo aerosols. *Geophys. Res. Lett.*, **19**, 207–210.

Lait, L.R., M.R. Schoeberl, and P.A. Newman, 1989. Quasi-biennial modulation of the Antarctic ozone depletion. *J. Geophys. Res.*, **94**, 11559–11571.

Levelt, P.F., M.A.F. Allaart, and H.M. Kelder, 1996. On the assimilation of total-ozone satellite data. *Ann. Géophys.*, **14**, 1111–1118.

Logan, J.A., 1994. Trends in the vertical distribution of ozone: an analysis of ozonesonde data. *J. Geophys. Res.*, **99**, 25553–25585.

London, J., R. D. Bojkov, S. Oltmans, and J. I. Kelly, 1976. *Atlas of the global distribution of total ozone, July 1957–June 1967*, NCAR Tech. Note/TN/113 STR, Boulder, Colorado: National Center for Atmospheric Research.

Madronich, S., and C. Granier, 1994. Tropospheric chemistry changes due to increased UV-B radiation. Pages 3–10 in *Stratospheric Ozone Depletion/UV-B Radiation in the Biosphere*. NATO ASI Series I18. R.H. Biggs and M.E.B. Joyner, eds. Berlin: Springer-Verlag.

Manney, G. L., and R. W. Zurek, 1993. Interhemispheric comparison of the development of the stratospheric polar vortex during the fall: A 3-dimensional perspective for 1991–1992. *Geophys. Res. Lett.*, **20**, 1275–1278.

Mateer, C.L., and J.J. Deluisi, 1992. A new Umkehr inversion algorithm. *J. Atmos. Terr. Phys.*, **54**, 537–556.

Mateer, C.L., and H.U. Dutsch, 1964. *Uniform Evaluation of Observations From the World Ozone Network*. Boulder, Colorado: National Center for Atmospheric Research.

McElroy, C.T., 1995. A spectrometer for the measurement of direct and scattered solar irradiance from on-board the NASA ER-2 high-altitude research aircraft. *Geophys. Res. Lett.*, **22**, 1361–1364.

McElroy, C.T., and J.B. Kerr, 1995. Table Mountain ozone intercomparison: Brewer ozone spectrophotometer Umkehr observations. *J. Geophys. Res.*, **100**, 9293–9300.

McElroy, M.B., R.J. Salawitch and K. Minschwaner, 1992. The changing stratosphere. *Planet. Space Sci.*, **40**, 373–401.

McElroy, C.T., C. Midwinter, D.V. Barton, and R.B Hall, 1995. A comparison of J-values from the compostion and photodissociative flux measurement with model calculations. *Geophys. Res. Lett.*, **22**, 1365–1368.

McElroy, C.T., J.F. Hahn, and E.W. Hare, 1997. Determining high-altitude trends in ozone from Brewer Umkehr observations made at Canadian stations. *Proc. Quad. Ozone Symp.*, L'Aquila, Italy, 12–21 September 1996, in press.

McPeters, R. D., and G.J. Labow, 1996. An assessment of the accuracy of 14.5 years of Nimbus 7 TOMS Version 7 ozone data by comparison with the Dobson network. *Geophys. Res. Lett.*, **23**, 3695–3698.

McPeters, R. D., S. M. Hollandsworth, L. E. Flynn, J R. Herman, and C. J. Seftor, 1996. Long-term ozone trends derived from the 16-year combined Nimbus 7/Meteor 3 TOMS Version 7 record, *Geophys. Res. Lett.*, **23**, 3699–3702.

Michelangeli, D.V., M. Allen, and Y.L. Yung, 1989. El Chichon volcanic aerosols: impact of radiative, thermal, and chemical perturbations. *J. Geophys. Res.*, **94**, 18429–18443.

NASA, 1992. *The Atmospheric Effects of Stratospheric Aircraft: A First Program Report*. NASA Reference Publication 1272. Washington, D.C.: National Aeronautics and Space Administration.

NASA, 1993. *The Atmospheric Effects of Stratospheric Aircraft: A Second Program Report*. NASA Reference Publication 1293. Washington, D.C.: National Aeronautics and Space Administration.

NASA, 1996. "1996 Antarctic Ozone Hole Below Record Size," *NASA HQ Public Affairs Office Press Release*, October 25, 1996. Washington, D.C.: National Aeronautics and Space Administration.

Newman P. A., J. F. Gleason, and R. S. Stolarski, 1997. Anomalously low ozone over the Arctic. *Geophys. Res. Lett.*, **24**, in press.

Oltmans, S.J., W.E. Raatz, and W.D. Komhyr, 1989. On the transfer of stratospheric ozone into the troposphere near the north pole. *J. Atmos. Chem.*, **9**, 245–253.

Oltmans, S.J., A.S. Lefohn, H.E. Scheel, J.A. Harris, H. Levy II, I.E. Galbally, E-G. Brunke, C.P. Meyer, J.A. Lathrop, B.J. Johnson, D.S. Shadwick, E. Cuevas, F.J. Schmidlin, D.W. Tarasick, J.B. Kerr, and O. Uchino, 1997. Trends of ozone in the troposphere. *Geophys. Res. Lett.*, forthcoming.

Ohring, G., and H.S. Muench, 1959. Relationships between ozone and meteorological parameters in the lower stratosphere. *J. Meteor.*, **17**, 195–206.

Prather, M., 1992. Catastrophic loss of stratospheric ozone in dense volcanic clouds. *J. Geophys. Res.*, **97**, 10187–10191.

Randel, W. J., and J.B. Cobb, 1994. Coherent variations of monthly mean total ozone and lower stratosphere temperatures. *J. Geophys. Res.*, **99**, 5433–5474.

Randel, W. J., and F. Wu, 1995. *Climatology of stratospheric ozone based on SBUV and SBUV/2 data:1978-1994*, NCAR Technical Note NCAR/TN-412+STR. Boulder, Colorado: National Center for Atmospheric Research.

Reed, R.J., 1950. The role of vertical motion in ozone-weather relationships. *J. Meteor.*, **7**, 263–267.

Reinsel, G.C., G.C. Tiao, A.J. Miller, D.J. Wuebbles, P.S. Connell, C.L. Mateer and J.J. DeLuisi, 1987. Statistical analysis of total ozone and stratospheric Umkehr data for trends and solar cycle relationship. *J. Geophys. Res.*, **92**, 2201–2209.

Reinsel, G. C., G.C. Tiao, D.J. Wuebbles, J.B. Kerr, A.J. Miller, R.M. Nagatani, L. Bishop, and L.H. Ying, 1994. Seasonal trend analysis of published ground-based and TOMS total ozone data through 1991. *J. Geophys. Res.*, **99**, 5449–5464.

Santee, M. L., G. L. Manney, L. Froidevaux, R. W. Zurek, and J. W. Waters, 1997. MLS observations of ClO and HNO_3 in the 1996–97 Arctic polar vortex. *Geophys. Res. Lett.*, **24**, in press.

Schoeberl, M.R., P.K. Bhartia, and E. Hilsenrath, 1993. Tropical ozone loss following the eruption of Mt. Pinatubo. *Geophys. Res. Lett.*, **20**, 29–32.

Schubert, S.D., and M.J. Munteanu, 1988. An analysis of tropopause pressure and total ozone correlations. *Mon. Weather Rev.*, **116**, 569–582.

Shiotani, M., 1992. Annual, quasi-biannual, and El Nino-Southern Oscillation (ENSO) time-scale variations in equatorial total ozone. *J. Geophys. Res.*, **97**, 7625–7633.

Shiotani, M. and F. Hasebe, 1994. Stratospheric ozone variations in the equatorial region as seen in Stratospheric Aerosol and Gas Experiment Data. *J. Geophys. Res.*, **99**, 14575–14584.

Solomon S., R.W.Portmann, R.R. Garcia, L.W. Thomason, L.R. Poole, and M.P. McCormick, 1996. The role of aerosol variations in anthropogenic ozone depletion in the northern hemisphere. *J. Geophys. Res*, **101**, 6713–6727.

Stolarski, R., R. Bojkov, L. Bishop, C. Zerefos, J. Staehelin, and J. Zawodny, 1992. Measured trends in stratospheric ozone. *Science*, **256**, 343–349.

Stolarski, R., G.J. Labow, and R. D. McPeters, 1997. Springtime Antarctic total ozone measurements in the early 1970s from the BUV instrument on Nimbus 4. *Geophys. Res. Lett*, **24**, 591–594.

Taalas, P., J. Damski, E. Kyrö, M. Ginzburg, and G. Talamoni, 1997. Effect of stratospheric ozone variations on UV radiation and on tropospheric ozone at high latitudes. *J. Geophys. Res.*, **102**, 1533–1539.

Tarasick, D.W., J.B. Kerr, D.I. Wardle, J.J. Bellefleur and J. Davies, 1995. Tropospheric ozone trends over Canada: 1980–1993. *Geophys. Res. Lett.*, **22**, 409–412.

Tarasick, D.W., G. Brunet, R. Daley, P. Gauthier, and W.E. Ward, 1996a. A Canadian middle atmosphere initiative, *Proc. Quad. Ozone Symp.*, L'Aquila, Italy, 12–21 September 1996, in press.

Tarasick, D.W., J.B. Kerr, D.I. Wardle, J.J. Bellefleur, S. Bunka and J. Davies, 1996b. Tropospheric ozone trends at Canadian stations: 1980–1995, *Proc. Quad. Ozone Symp.*, L'Aquila, Italy, 1996, in press.

Tie, X., G.P. Brasseur, B. Briegleb, and C. Granier, 1994. Two-dimensional simulation of Pinatubo aerosol and its effect on stratospheric ozone. *J. Geophys. Res.*, **99**, 20545–20562.

Vaughan, G., and D.A. Begum, 1989. Correlation between ozone and potential vorticity. Pages 91–94 in *Ozone in the Atmosphere: Proceedings of the Quadrennial Ozone Symposium 1988*. R.D. Bojkov and P. Fabian, eds. Hampton, Virginia: Deepak.

Vaughan, G., and J.D. Price, 1991. On the relation between total ozone and meteorology. *Quart. J. R. Met. Soc.*, **117**, 1281–1298.

Wirth, V., 1993. Quasi-stationary planetary waves in total ozone and their correlation with lower stratospheric temperature. *J. Geophys. Res.*, **98**, 8873–8882.

WMO, 1989. *Scientific Assessment of Stratospheric Ozone: 1989*. World Meteorological Organization Global Ozone Research and Monitoring Project, Report No. 20. Geneva: World Meteorological Organization.

WMO, 1991. *Scientific Assessment of Stratospheric Ozone: 1991*. World Meteorological Organization Global Ozone Research and Monitoring Project, Report No. 25. Geneva: World Meteorological Organization.

WMO, 1994. *Scientific Assessment of Stratospheric Ozone: 1994*. World Meteorological Organization Global Ozone Research and Monitoring Project, Report No. 37. Geneva: World Meteorological Organization.

Yang, H., and K.K. Tung, 1994. Statistical significance and pattern of extratropical QBO in column ozone. *Geophys. Res. Lett.*, **21**, 2235–2238.

Zerefos, C. S., A.F. Bais, T.C. Ziomas, and R.D. Bojkov, 1992. On the relative importance of quasi-biennial oscillation and ENSO in the revised total ozone records. *J. Geophys. Res.*, **97**, 10135–10144.

The Influence of Dynamical Processes on Ozone Abundance

2.1 Introduction

Ozone abundance is affected by dynamical processes in two important ways: first, through temperature and, second, through transport and mixing. Although the two aspects are related in practice – temperature is affected by the same dynamical processes that control transport and mixing – it is useful to maintain a distinction between them. Accordingly, the first section of this chapter addresses our present understanding of the dynamical structure of the stratosphere, while the second section addresses the global structure of transport and mixing. Subsequent sections focus on specific regions of the stratosphere, in terms of their role in determining ozone abundance.

2.2 The Dynamical Structure of the Stratosphere

The stratosphere is the region of the atmosphere between approximately 10 km and 50 km altitude, containing roughly 20% of the mass of the atmosphere. It is distinguished, as its name suggests, by a strong vertical stratification, or layering, that inhibits vertical motion. The existence of the stratosphere is a consequence of the ozone layer. Although the strongest heating of the atmosphere occurs from the earth's surface, there is a secondary heating maximum throughout the ozone layer. Rapid vertical heat transfer by convection in the lowest part of the atmosphere, referred to as convective adjustment, leads to a layer of weak stratification (the troposphere), capped by a layer of strong stratification (the stratosphere). The boundary between the two is the tropopause. The global mean height of the tropopause is thus determined by a balance between the amount of stratospheric ozone, the surface temperature, and the vertical temperature structure of the troposphere (which involves the distribution of water vapour and clouds). It follows that changes in any of these quantities can be expected to lead to changes in the global mean height of the tropopause.

The height of the tropopause varies significantly with latitude. It is greatest in the tropics, where it is typically around 18 km, and decreases to around 8 km as one moves toward the poles. Part of this variation can again be explained on radiative-convective grounds: since surface heating is strongest in the tropics, the depth of convective adjustment is greater there. However, there are two other contributing effects that act in the same direction. First, there is a persistent mean meridional mass circulation in the stratosphere that draws air upward in the tropics and pushes it downward in the extratropics. Second, although the photochemical production of ozone takes place primarily in the tropics, significant quantities of ozone are transported poleward, thus affecting the latitudinal distribution of radiative heating. Both effects – which turn out to be closely related (see Section 2.3) – act to raise the tropopause in the tropics and to lower it in the extratropics. In addition, there is a sharpening of the tropopause slope in midlatitudes associated with the subtropical jet stream, which is controlled by tropospheric synoptic-scale weather systems. Thus, the latitudinal structure of the tropopause reflects a complex interplay between the mass circulation of the stratosphere, the ozone distribution, upper-tropospheric synoptic-scale disturbances, and the latitudinal temperature gradient of the lower troposphere. Once again, water vapour and clouds play a critical role in the latter. Our understanding of how these different processes interact to determine the structure of the tropopause is qualitative at best.

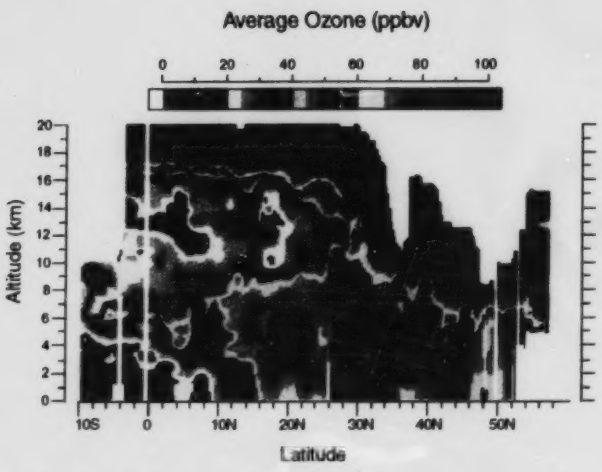

Figure 2.1 Composite latitudinal ozone distribution obtained with an airborne lidar over the western Pacific during the NASA Pacific Exploratory Mission conducted in February-March 1994 (private communication, E.V. Browell, NASA Langley Research Center, Hampton, Virginia, U.S.A.). The strong gradient region (yellow to black) follows the tropopause.

There is a very direct connection between the spatial distribution of ozone and the spatial structure of the tropopause. Figure 2.1 shows a cross-section of ozone taken from airborne lidar measurements. Comparatively high values of ozone are found in the stratosphere, and comparatively low values in the troposphere. On short (i.e., several day) timescales, the tropopause acts as a deformable material surface. When the tropopause descends, the fraction of stratospheric air above that location increases, thereby increasing total ozone; when the tropopause ascends, there is a corresponding decrease in total ozone. This correlation is well established on short timescales associated with dynamical variability in the tropopause height. On longer timescales, other effects come into play. Nevertheless, this highlights the fact that the structure of the tropopause has a significant impact on ozone distribution and must be accounted for in any assessment of ozone changes.

The elevated tropical tropopause implies that a local minimum in lower stratosphere temperatures will occur in the tropics – the reverse of the situation in the troposphere. This feature is present in all seasons and is associated (via thermal-wind balance) with the subtropical jet stream. At higher altitudes, the latitudinal temperature structure has a dramatic seasonal dependence. Ozone that has been transported poleward provides a major source of radiative heating in the sunlit polar summer, which maintains the relative warmth of polar temperatures relative to tropical values, and is reflected in the easterly zonal winds of the summer hemisphere stratosphere. In the winter hemisphere, in contrast, the lack of radiative heating over the polar night leads to extremely cold temperatures and the formation of an intense westerly polar vortex. Thus, in polar regions, the seasonal cycle of temperature consists of a cooling trend in the fall and a warming trend in the spring.

The cold temperatures of the polar night are mitigated by adiabatic heating arising from the compression of the descending, poleward-moving air. However, there are important contrasts between the Antarctic and Arctic wintertime regimes. In the Antarctic, the wintertime mass circulation is comparatively weak and fairly steady, with little interannual variability, although the effect of the quasi-biennial oscillation (QBO) is discernible. In the Arctic, in contrast, the wintertime mass circulation is much stronger, and far more variable; this leads to warmer temperatures on average than those found in the Antarctic winter, with episodic intense warming events known as stratospheric sudden warmings. These characteristics are demonstrated in Figure 2.2, which shows time series of mid-stratospheric polar temperatures over the Antarctic and Arctic from observations and from the Canadian Middle Atmosphere Model [Shepherd 1995; Beagley et al. 1997].

An understanding of this behaviour requires consideration of what determines the mean meridional mass circulation. To a first approximation, the adiabatic heating (or cooling) associated with sinking (or rising) air is balanced by radiative cooling (or heating). Although one might be tempted to conclude that the radiative cooling or heating is the *cause* of the vertical motion (e.g., air rises where radiation is warming it), it is now well established that, on a global scale and over seasonal timescales, it is rather the opposite: the observed local radiative imbalances are themselves caused by the mean meridional mass circulation [Andrews et al. 1987; see also Shepherd 1995]. This can be seen in several ways. First, the mass circulation of the stratosphere is essentially thermally indirect: air rises where it is relatively cold (the tropics) and sinks where it is relatively warm (the extratropics). Thus, the energetic forcing of the stratosphere must be mechanical rather than thermal. Second, the rotation of the Earth acts to inhibit mean meridional (north-south) motion. In order to maintain a mean meridional mass circulation, a zonal (east-west) mechanical force is required to balance the zonal Coriolis force that acts on meridional motion. (To put this another way, tropical air has more angular momentum than polar air, so to move air from one region to the other a zonal force must be applied to either increase or decrease its angular momentum.) This zonal mechanical force is provided by the drag force associated with the breaking and dissipation of wave motions propagating into the stratosphere from the more massive troposphere. In the stratosphere, most of this drag force is associated with large-scale planetary waves, with

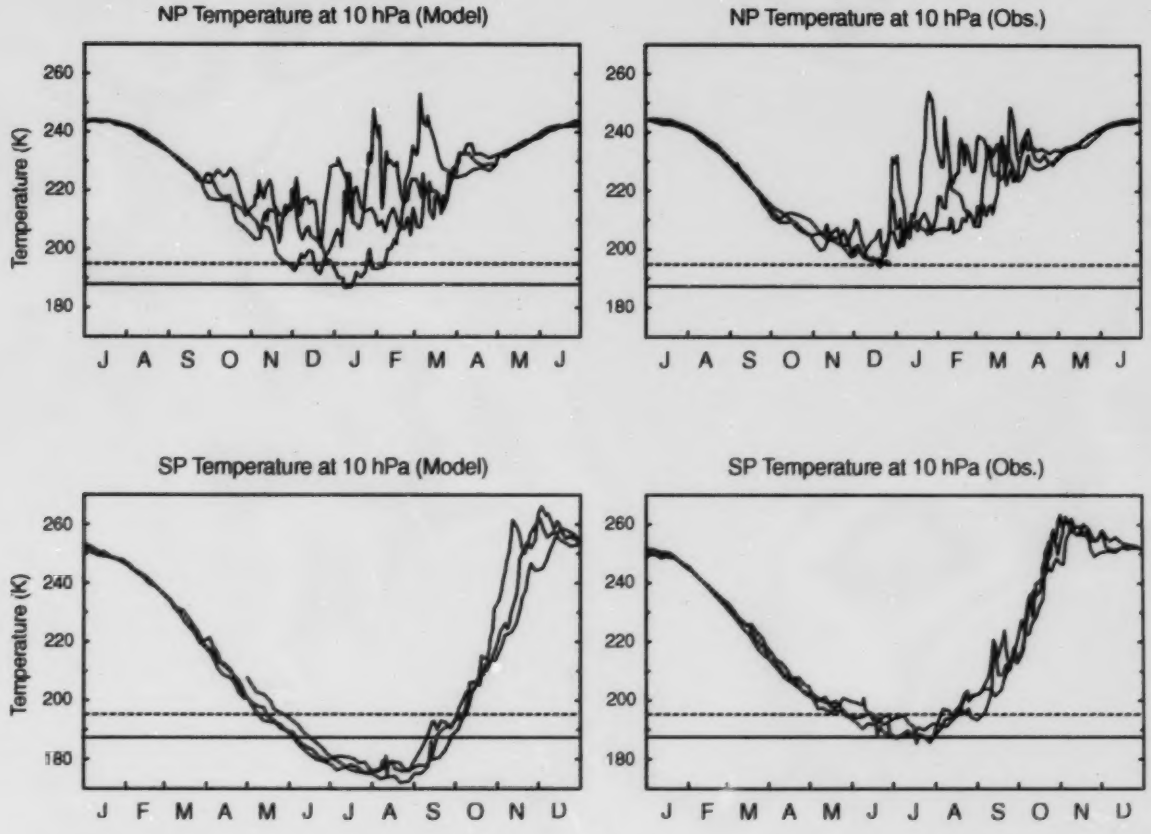
NP Temperature at 10 hPa (Model)
NP Temperature at 10 hPa (Obs.)
SP Temperature at 10 hPa (Model)
SP Temperature at 10 hPa (Obs.)
Temperature (K)
260
240
220
200
180
J A S O N D J F M A M J
J F M A M J J A S O N D

Figure 2.2 Annual variation of temperature at 10 hPa over the North Pole (NP) and South Pole (SP), centred in midwinter, for the Canadian Middle Atmosphere Model and observations. In each case, three different years are shown; the observations correspond to UK Meteorological Office analyses during 1993–1995. The temperature thresholds of 195 K and 188 K for Type 1 and Type 2 polar stratospheric clouds are indicated with dashed and dotted lines respectively. (Figure provided by John Koshyk, University of Toronto.)

a secondary contribution from smaller-scale inertia-gravity waves. It is the difference in the strength and variability of the stratospheric wave drag between the northern and southern hemispheres (resulting from their different surface topography) that accounts for the difference in the strength and variability of the wintertime mass circulation between the Arctic and Antarctic.

Although there is a consensus on the essential validity of the above picture, our quantitative understanding of it and predictive ability remain poor. For example, the most sophisticated atmospheric general circulation models are plagued by systematic errors in their polar temperatures, most notably the so-called "cold pole" problem in the Antarctic winter, which can be seen in Figure 2.2. The origin of this discrepancy is not known, though it is believed to be associated with missing gravity-wave drag [Garcia and Boville 1994]. If true, this implies a serious fundamental uncertainty in our quantitative understanding and predictive capability, since gravity-wave drag is extremely poorly constrained from either observations or theory. The magnitude of the temperature discrepancy in the Antarctic, 10 K or more, is enough to compromise quantitative modelling of ozone depletion; in practice, it is corrected through forced adjustment to observed winds and temperatures, but such "relaxational" corrections have been shown to be problematical in the context of climate-change modelling [Shepherd et al. 1996].

In our present climate, the difference between Antarctic and Arctic mid-stratospheric wintertime temperatures has enormous effects on the respective amounts of ozone loss, because the difference range happens to straddle the critical temperatures required for the formation of polar stratospheric clouds (PSCs; see Chapter 3). If, for example, the mean temperatures were 10 K higher in the Antarctic or 10 K lower in the Arctic, then the difference in ozone loss between the hemispheres would presumably be much less. (Of course, polar temperatures are only part of what matters for polar

ozone loss; confinement by the polar vortex is also critical, as will be discussed in Section 2.5.) The high degree of variability of Arctic wintertime polar temperatures, not only within each season but also from one year to another, is responsible for the considerable interannual variability of Arctic ozone loss. As noted above, the variability of Arctic wintertime polar temperatures is directly attributable to dynamical variability. Since dynamical variability is poorly understood, and difficult to predict for any given year, this places a major limitation on our quantitative understanding of present and future Arctic ozone loss.

2.3 The Global Structure of Transport and Mixing

The ozone distribution provided one of the earliest pieces of observational evidence for the transport of trace species in the stratosphere [Dobson 1956]. Since most ozone production occurs in the tropics but the largest values of total ozone are found in the extratropics, there must, therefore, be systematic poleward transport out of the tropics. This inference is consistent with the observed low values of stratospheric water vapour, from which Brewer [1949] concluded that air must enter the stratosphere through the region of extremely low temperature at the tropical tropopause: the so-called "cold trap". The stratospheric transport circulation implied by these observations – the "Brewer-Dobson" circulation – rises in the tropics, moves poleward, and (by mass conservation) descends back into the troposphere in the extratropics. Confirmation of this picture by global observations is comparatively recent, as it is dependent on satellite measurements – most notably those from the Upper Atmosphere Research Satellite (UARS) launched by NASA in 1991. An example of such measurements is shown in Figure 2.3.

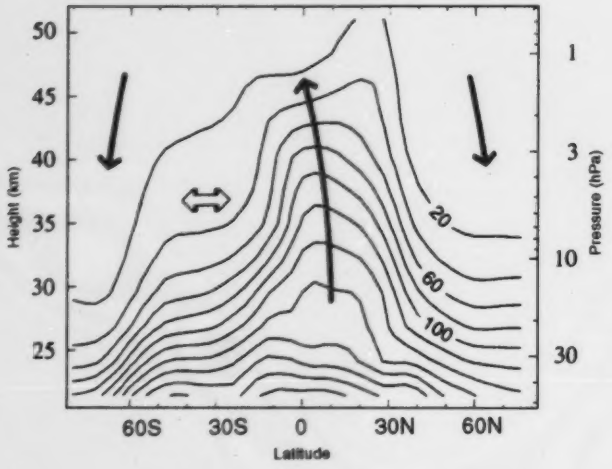

Figure 2.3 Longitudinally averaged structure of nitrous oxide (N_2O) mixing ratio (in parts per billion by volume) during 1–20 September 1992 as measured by the CLAES instrument on UARS. Heavy solid lines denote the mean stratospheric circulation in the latitude-height plane, and the horizontal arrows denote the location of quasi-horizontal mixing by planetary waves. (From Randel et al. [1993].)

The inferred structure of the Brewer-Dobson transport circulation is broadly consistent with the mean meridional mass circulation inferred from purely dynamical considerations. In one sense this is no surprise: the mass circulation describes the mean movement of air across (quasi-horizontal) isentropic surfaces (i.e., surfaces, of constant potential temperature, which determine stratification; air from everywhere on such a surface would, if compressed to the same pressure, acquire the same temperature and density). Thus, the mass circulation is linked in a fundamental way to the bulk vertical motion of air parcels. However, it must be emphasized that the mass circulation is an Eulerian diagnostic (the mean is taken at a fixed latitude); it is therefore distinct, and can be quite different, from the mean circulation defined by the movement of trace species, which is a Lagrangian diagnostic (the mean is taken following air parcels). An example in which the difference between the two circulations is particularly important is described in Section 2.5.

A central feature of the Brewer-Dobson circulation is its pronounced seasonal cycle; although there is tropical upwelling all year long, the poleward motion (and polar downwelling) occurs predominantly in the winter hemisphere. This behaviour is exhibited in Figure 2.4, which shows the seasonal cycle of the mean meridional mass circulation in the Canadian Middle Atmosphere Model [Beagley et al. 1997]. (Reliable estimates of the mass circulation from observations are difficult to obtain. As for a tracer-based transport circulation, even its definition is problematical.) It must be emphasized that the tropical upwelling rates are quite slow, so that an air parcel confined to the tropics takes more than a year to ascend through the ozone production region into the upper stratosphere; thus tracer distributions such as that shown in Figure 2.3 for nitrous oxide reflect the annual mean of the circulation shown in Figure 2.4, modified by more rapid quasi-horizontal mixing.

At a certain level, it may be said that we understand the origin of the Brewer-Dobson circulation and its seasonal cycle [Holton et al. 1995]. Planetary waves propagate westward relative to the mean wind, and thus exert a westward (i.e., negative) zonal force where they break. This westward force drives poleward motion in both hemispheres, which induces upwelling in the tropics and downwelling in the extratropics. The seasonal cycle in the Brewer-Dobson circulation is likewise a consequence of the seasonal cycle in stratospheric planetary-wave drag [Rosenlof 1995]; most planetary-wave

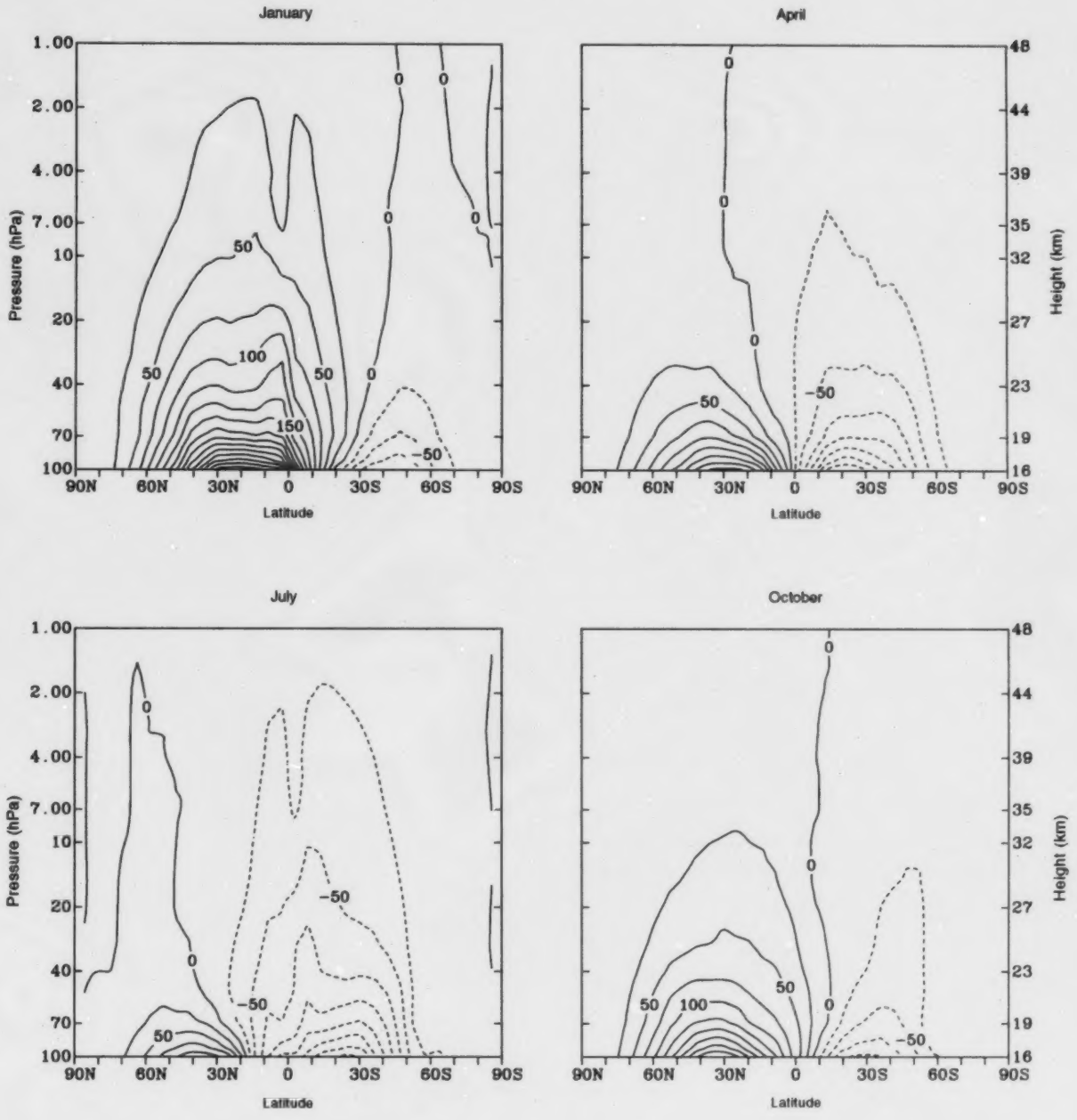

Figure 2.4 The seasonal cycle of the mean meridional mass circulation of the Canadian Middle Atmosphere Model. Each panel represents the average over three different simulated years of the monthly mean for January, April, July, or October. Contours denote mass streamlines, and correspond to rising motion in the tropics and sinking motion in the extratropics. The contour interval is 25 kg m^{-1} s^{-1}. (Figure provided by John Koshyk, University of Toronto.)

drag occurs in the winter hemisphere. A similar relationship must also hold on longer timescales. It follows that the interannual variability in northern hemisphere planetary-wave drag reflected in Arctic wintertime temperatures (see Section 2.2), and the potential for its systematic change over decadal timescales, has concomitant implications for variability and change in the Brewer-Dobson circulation and hence in the ozone distribution. But even if dynamical variability could be predicted, there remain significant gaps in our quantitative understanding of how this relates to ozone transport. Most notably, the argument outlined above relies on the tacit equivalence of the Brewer-Dobson, mean mass (i.e., radiatively balanced), and wave-drag-driven circulations. Although these circulations are certainly related, they are far from identical, and their differences are not yet understood on a quantitative level. This issue is discussed in more detail later in the context of tropical upwelling (Section 2.4) and polar downwelling (Section 2.5).

There are a number of different circulation timescales that are relevant to the determination of ozone abundance. For ozone-depleting substances with tropospheric sources and stratospheric sinks, one may define a residence time based on the decay timescale required to account for observed stratospheric concentrations. Such residence times are clearly different for different chemical species; they reflect both the decay processes themselves and the time it takes for the species to reach the altitudes where the decay occurs. Many substances have stratospheric residence times of decades or longer. A stratospheric age timescale may also be defined, based on the time lag between tropospheric values of long-lived species and their value at a certain location in the stratosphere. For a tracer with linearly increasing tropospheric values, this provides a well-defined age that is a tracer-independent quantity [Hall and Plumb 1994]; it is estimated to be between one and two years in the lower extratropical stratosphere, and greater than four years in the upper stratosphere. (The contours of age look rather like the nitrous oxide contours in Figure 2.3.) These timescales are of the same order of magnitude as those obtained on the basis of the mean meridional mass circulation alone, without mixing [Rosenlof 1995], but they have a very different spatial distribution. There is, however, no straightforward connection between this definition of age and the time lags of species with nonlinear time dependence, especially those with a strong seasonal cycle. In principle, all transport information (for long-lived species) is contained in the "age spectrum" [Hall and Plumb 1994], but the age spectrum is only well-defined for stationary transport and mixing statistics; it is not clear how robust the concept is in the presence of annual and interannual variability in the dynamics. For species affected by stratospheric sources and sinks, the age spectrum provides incomplete information, because one needs to know the distribution of transport pathways.

Traditionally, transport and mixing in the stratosphere has been approached as an advective-diffusive problem [Andrews et al. 1987], with tracer distributions such as those of Figure 2.3 regarded as a balance between the slope-steepening effects of the mean meridional mass circulation and the slope-flattening effects of quasi-horizontal mixing. While this is probably a reasonable description in midlatitudes, like all mixing-length approaches it depends on a spatial scale separation between (large) tracer scales and (small) eddy scales. Thus it is problematical in regions where the size of the eddies is greater than the tracer-gradient length scale, as occurs in strong gradient regions such as the edge of the polar vortex, the edge of the tropics, and the tropopause. The traditional mixing-length approach also fails to account for the robust transport barriers that provide such strong tracer gradients in the first place, as will be discussed in more detail below. (Although these are not perfect barriers, but rather quasi-barriers, the term "transport barrier" will be used hereafter for conciseness.) The role of the wintertime polar vortex in isolating vortex air, thereby allowing heterogeneous chemical processing to occur, was recognized early on as an essential ingredient in polar ozone loss [Schoeberl and Hartmann 1991]. More recently, with the availability of high-quality tropical measurements, analogous transport barriers have been identified at the edge of the tropics [Trepte and Hitchman

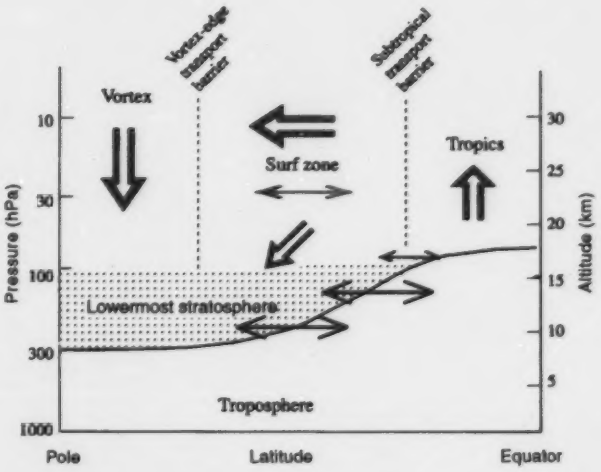

Figure 2.5 Schematic of transport and mixing in the winter hemisphere of the lower stratosphere. Heavy single-headed arrows indicate the mean mass circulation, and thin double-headed arrows indicate strong mixing. Vertical dashed lines represent transport barriers. The solid curve denotes the tropopause, while the stippled region denotes the lowermost stratosphere, in which isentropic surfaces intersect the troposphere.

Figure 2.6 Time-height section of $2(CH_4)+(H_2O)$, the variable part of total hydrogen, between 12°S and 12°N, measured by the HALOE instrument on UARS. The vertically propagating oscillation is indicative of tropical ascent. (From Mote et al. [1996].)

1992; Fahey et al. 1996]. The lowest part of the extratropical stratosphere is also a distinctive region, because it is "ventilated" by isentropic surfaces that intersect the troposphere [Holton et al. 1995]. Accordingly, the current picture of stratospheric transport and mixing is far more complex than it was a decade ago, and in some ways more fragmented. A schematic of the various elements in the picture is provided in Figure 2.5.

2.4 Tropics

The tropics play an important role in establishing ozone abundance in a number of ways. First, the tropical stratosphere is the principal source region for ozone, which the Brewer-Dobson circulation then transports into the extratropics. Second, the lower tropical stratosphere represents the principal stratospheric gateway for ozone-depleting substances. A current issue of great concern in this respect is the potential impact of NO_x emissions from proposed high-altitude civil aircraft flying in the extratropical lower stratosphere [NASA 1995]. If the NO_x gets directly entrained into the tropical ascent region, instead of being diluted in the troposphere, then the potential for ozone destruction is enormously greater (see Chapter 3). Third, the temperature of the tropical tropopause regulates the amount of water vapour in the stratosphere through Brewer's "cold trap" effect, and this affects the temperature threshold for PSC formation. In this way, a long-term trend in the tropical tropopause temperature could have an indirect impact on ozone destruction.

A significant development of the past few years has been the realization that the ascent that occurs in the tropical branch of the Brewer-Dobson circulation is relatively isolated. This was first seen in aerosol measurements following the eruption of Mount Pinatubo in 1991 [Trepte and Hitchman 1992; Grant et al. 1994], which showed limited transport of aerosol into the extratropics above about 22 km. Further evidence of a subtropical transport barrier is evident in latitudinal profiles of the chemical correlations of long-lived species [Fahey et al. 1996], which suggest distinct mixing regions in the tropics and extratropics. But perhaps the most dramatic evidence comes from satellite measurements of water vapour in the tropical lower stratosphere, which reveal a meridionally confined, vertically propagating oscillation, shown in Figure 2.6; Mote et al. [1996] argue that this represents the imprint of the annual cycle of tropical tropopause temperatures on the water vapour content of the air being carried up by the mean meridional circulation – in other words, an annual modulation of the "cold trap" effect, carried upwards.

However, there is considerable variability in the existence and strength of the subtropical transport barriers; they depend on season, and are significantly modulated by the QBO. This is consistent with the notion that they are explainable in terms of the spatial structure of the horizontal velocity field: transport barriers correspond to quasi-zonal streamlines, without stagnation points [Polvani et al. 1995]. It is well established that the midlatitude stratosphere is disturbed by breaking planetary waves, forming a "surf zone" [McIntyre and Palmer 1983]. The nature of this breaking is consistent with the predictions of Rossby-wave critical-layer theory. A particularly striking example is shown in Figure 2.7, at about 21 km

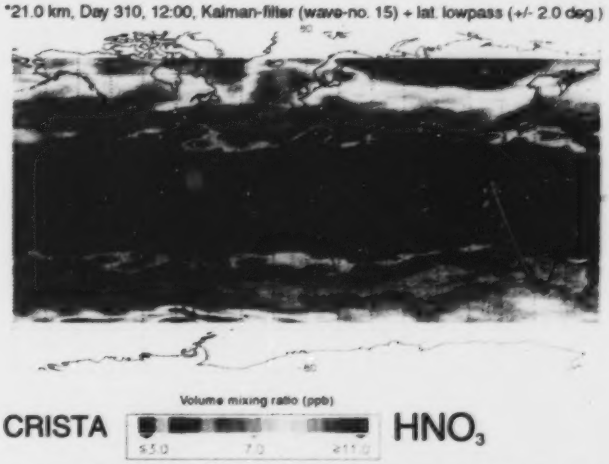

Figure 2.7 Horizontal cross-section of HNO_3 at about 21 km altitude on 6 November 1994, measured by the CRISTA instrument on the Space Shuttle (personal communication, D. Offermann, Wuppertal University, Germany). The field shows several cat's-eye structures in the northern subtropics.

altitude; the tracer field exhibits the characteristic "cat's eye" structure of a Rossby-wave critical layer. Within the cat's eyes, strong horizontal mixing occurs, but on either side of the cat's eyes, tracer contours remain quasi-zonal [Ngan and Shepherd 1997a]. From this perspective, the subtropical transport barrier represents the tropical limit of the midlatitude surf zone. (Similarly, the polar vortex transport barrier represents the polar limit of the surf zone; see Section 2.5.) Its existence, therefore, depends on whether or not breaking planetary waves extend into the tropics. This, in turn, depends on the amplitude and phase speed of the planetary waves and the meridional shear of the underlying zonal flow. Both depend on season, while the latter also depends on the phase of the QBO.

Because of the subtropical transport barriers, the transport and mixing characteristics of the tropics are qualitatively different from those of midlatitudes. An extreme idealization is that of a "tropical pipe" [Plumb 1996], where tropical air is assumed to ascend with no exchange with midlatitudes. Certainly the water vapour signal shown in Figure 2.6 suggests there is some validity to this concept. However, detailed chemical modelling within the tropics shows that the observed vertical profiles of chemical species cannot be reconciled with a strict interpretation of the tropical pipe; some dilution from midlatitudes is required [Avallone and Prather 1996], especially below 22 km or so. There have been a number of recent attempts to quantify the amount of dilution by balancing the dilution against vertical upwelling and chemical processing [e.g., Volk et al. 1996]. Most calculations estimate that, at altitudes above 22 km, 50% or more of the air in the tropical upwelling region is of midlatitude origin. Such calculations are subject to considerable uncertainty. First, they rely on an extreme idealization of lateral exchange between two homogeneous mixing regions; second, they depend quite sensitively on the estimate of the tropical upwelling rate.

The upwelling rate cannot be directly measured, and must be inferred from the estimated radiative heating rates in the tropics. (The vertical propagation rate of an annual cycle, such as that seen in water vapour in Figure 2.6, is not the same as the mean upwelling rate if there is significant dilution [Hall and Waugh 1997].) However, this is a very difficult calculation, as it depends on a small difference of large terms, and is thus prone to sampling errors – especially in the lower stratosphere where radiative timescales are long. The solution is also generally non-unique. A number of recent studies [e.g., Rosenlof 1995] have used the UARS data set to attempt to make accurate estimates of the upwelling rate, and while there is broad agreement in the results, uncertainties remain at about the 50% level in the lower stratosphere and increase as one approaches the tropopause.

A further difficulty is that one cannot assume a simple balance between radiative heating and vertical upwelling in the tropics, because of inertial adjustment that is expected to occur in response to radiatively forced inertial instability [Dunkerton 1989]. (This is the horizontal analogue of convective adjustment in the vertical.) The way in which these processes interact to determine tropical temperatures in the real stratosphere has yet to be established at a quantitative level suitable for diagnostic analysis. The resulting difficulty in relating radiative heating to vertical upwelling provides a major limitation on our understanding of the tropical branch of the Brewer-Dobson circulation.

While most interest has focused on lateral inmixing into the tropics from midlatitudes, one expects this process also to be associated with lateral outmixing. There is clear evidence of outmixing events in the middle stratosphere, corroborated by tracer advection calculations [Randel et al. 1993]. Aerosol measurements also suggest significant outmixing in the lower stratosphere [Grant et al. 1994]. Figure 2.8 shows an aerosol cross-section from the Lidar In-Space Technology Experiment (LITE), which flew on the space shuttle [McCormick 1996]. Given that stratospheric aerosol is injected in the tropics (most notably from the eruption of Mount Pinatubo in 1991), this figure shows poleward spreading just above, and following, the tropopause. In addition, measurements of water vapour [Dessler et al. 1995], carbon dioxide [Boering et al. 1994], and ozone [Folkins and Appenzeller 1996] in the midlatitude

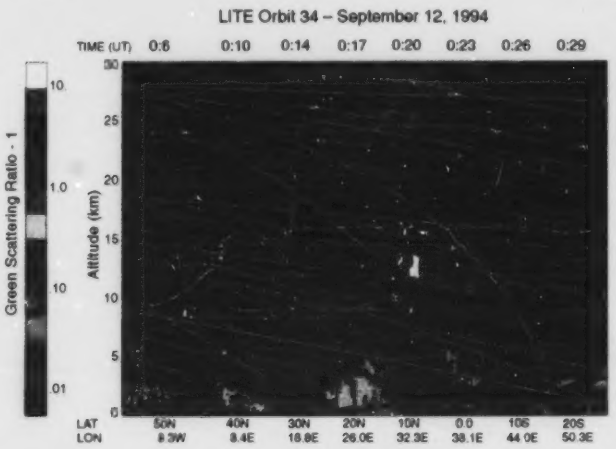

Figure 2.8 Aerosol scattering ratio cross-section on 12 September 1994 measured by the LITE experiment on the Space Shuttle [Hoff and Osborn 1996]. The aerosol layer in the lower stratosphere is largely due to the remnants of the Mount Pinatubo eruption in 1991 (green); in the lower troposphere, high concentrations of aerosol from Europe to east of Africa can be seen near the surface (red-yellow). The thin line indicates the location of the tropopause from US NMC data.

lower stratosphere point to a direct transport pathway from the tropical upper troposphere/lower stratosphere into the midlatitude lower stratosphere, which amounts to a "short-circuiting" of the Brewer-Dobson circulation. In fact, the lowest part of the tropical stratosphere is revealing itself as a particularly complex part of the atmosphere, which plays a critical role in determining the global structure of stratospheric transport and mixing. It remains one of the most poorly understood regions of the atmosphere. In particular, the way in which the rapid convective dynamics of the tropical troposphere connect to the slower dynamics of the tropical stratosphere, over what is properly regarded as a tropical tropopause layer (rather than a simple interface), represents a major gap in our theoretical understanding. For example, most current conceptual models completely ignore the effect of strong longitudinal asymmetries such as the monsoon circulation.

It should be emphasized that inmixing and outmixing are distinct processes. They are equivalent in the limit of small eddies, as is assumed in traditional mixing-length approaches, but – as noted in Section 2.3 – the subtropical transport barriers represent precisely the opposite situation, where large eddies act on a sharp tracer gradient. The scales involved are exemplified by Figure 2.7. If planetary-wave breaking is largely unidirectional, then one can have significant outmixing with little inmixing, or vice-versa; it is well established that this is the case in the wintertime polar vortex (see Section 2.5). Our understanding in the tropics is much more limited, in comparison, because of the current unavailability of reliable wind measurements in the tropical stratosphere. Estimates of stratospheric winds are largely derived from temperatures, assuming gradient-wind balance, but this balance breaks down in the tropics. A high priority for future measurement capabilities in the stratosphere is the development of reliable wind measurements, in order to provide better constraints on our understanding of transport and mixing. While direct wind measurements would be the most obvious solution, there is some hope that advanced data assimilation techniques might be able to obtain reliable wind information from the time evolution of tracer fields, such as that shown in Figure 2.7.

2.5 Wintertime Polar Vortex

The strong polar vortex that develops in the winter hemisphere provides the basic dynamical setting for polar ozone loss. The strength of the vortex is directly related, by thermal-wind balance, to the cold temperatures required for ozone-depleting heterogeneous chemistry; at the same time, the vortex provides a transport barrier that isolates the polar air from midlatitude dilution. As noted in Section 2.2, these effects are much more pronounced in the Antarctic than in the Arctic, for reasons that are reasonably well understood, and this accounts for the fact that the most dramatic polar ozone loss has occurred in the Antarctic.

From the perspective of transport and mixing, there are many useful parallels between the wintertime polar vortex and the tropics. In both cases, the Brewer-Dobson circulation provides one-way vertical transport (up in the tropics, down in the polar vortex), while a transport barrier is established at the relevant edge of the midlatitude surf zone. As in the tropics, the polar-vortex transport barrier is not perfect, and much interest has focused on quantifying the extent of inmixing and outmixing. Our quantitative understanding of transport and mixing processes is, however, considerably greater for the wintertime polar vortex than it is for the tropics for a number of quite different reasons. First, since the discovery of the Antarctic ozone hole there have been numerous aircraft missions directed at polar regions (both Arctic and Antarctic). Second, global wind measurements are far more reliable in the polar regions than they are in the tropics, thus making possible the calculation of detailed air-parcel trajectories. Third, much tighter theoretical constraints are available on the mean meridional mass circulation in the polar case, because of the strong meridional gradient in angular momentum [Holton et al. 1995].

One of the principal difficulties in quantifying transport and mixing in and around the wintertime polar vortex has been the definition of the vortex edge. The dynamical edge is generally considered to be the location of the maximum gradient in potential vorticity. Since this is a highly derived quantity, and therefore difficult to measure (especially on an aircraft flight track), researchers tend to use the maximum zonal velocity instead. The distinction appears to make quantitative rather than qualitative differences in transport diagnostics. A kinematical edge can be defined in terms of the structure of the velocity field, as the edge of the region of quasi-zonal streamlines without stagnation points. This should correspond most closely to a transport barrier. Observations often show the dynamical and kinematical edges to be distinct entities. In fact, the kinematical edge is just the outer limit of a barrier region of finite extent [Bowman 1993]. This behaviour is represented in Figure 2.9, which shows the evolution of tracer particles on a single (quasi-horizontal) isentropic surface in the Canadian Middle Atmosphere Model. If the barrier region extends well into the vortex, this creates the possibility of further edges in tracer fields within the vortex itself. In particular, measurements sometimes reveal a chemical edge inside the vortex, associated with chemical processing in the polar night within a confined region.

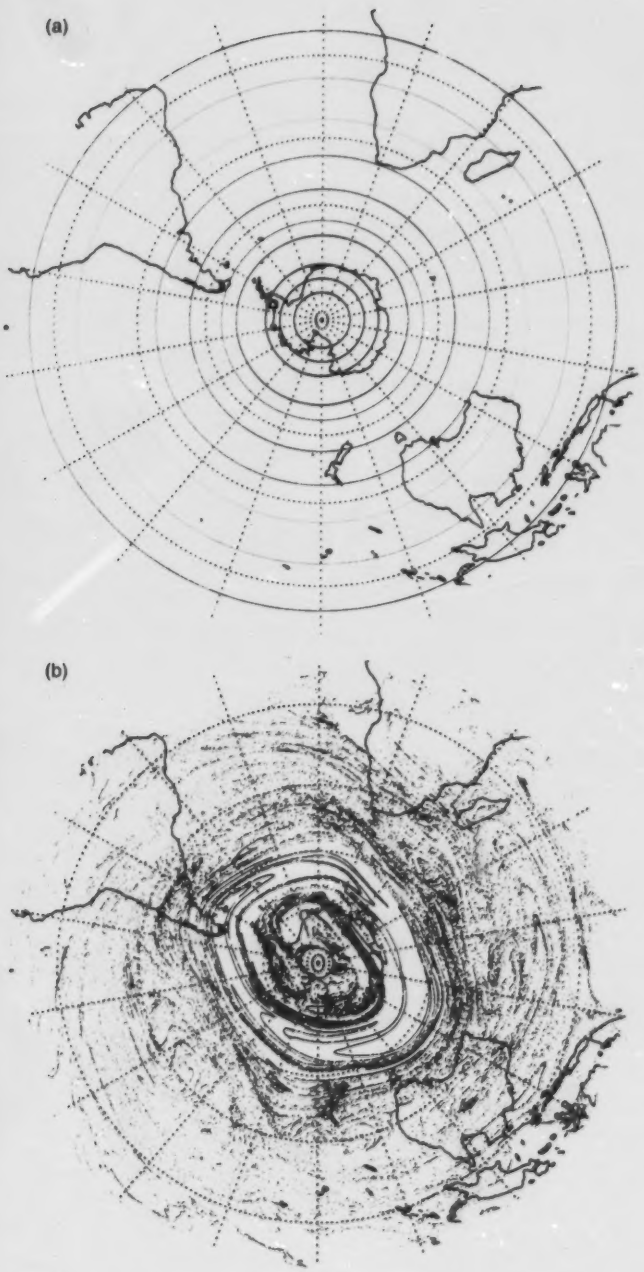

Figure 2.9 Evolution of passive tracer particles in the lower stratosphere during the southern hemisphere winter (July) from the Canadian Middle Atmosphere Model. (a) shows the initial distribution, and (b) the distribution after 30 days using quasi-horizontal winds interpolated onto the 450 K isentropic surface, which is located at about 17 km altitude. Thus, diabatic motion is neglected in this calculation. The particle evolution reveals strong mixing in the midlatitude "surf zone" (including the presence of several large cat's-eye structures), coexisting with comparatively regular behaviour in the outer part of the vortex, manifested in quasi-zonal wrapping of lines of particles. (Figure provided by Keith Ngan, University of Toronto.)

A striking feature of the polar vortex is that mixing very much tends to be outward rather than inward [Waugh et al. 1994]. Inmixing does occur on occasion in the Arctic, but it is associated with rare, large-amplitude perturbations that provide a major disruption of the vortex [Plumb et al. 1994] and are thus connected to sudden warmings such as those seen in Figure 2.2. There has been some debate in recent years over exactly how much outmixing occurs, especially in the Antarctic. This is a critical issue for ozone depletion, because the amount of ozone loss over a winter season is directly proportional to how much air can be chemically processed; a leaky vortex can support higher ozone destruction. (On the other hand, a leaky vortex requires greater vortex downwelling, which would warm the vortex and thus perhaps limit ozone destruction.) Mass conservation constraints from the mean meridional circulation appear to limit the amount of outmixing in the Antarctic middle stratosphere (down to about 16 km) to an amount consistent with the vortex being flushed out only once over the period of ozone loss. Similar kinds of considerations are of less relevance for the Arctic, because it is rarely intact through the winter season. Considerable uncertainty remains, however, with regard to the characterization of transport and mixing in the subvortex region (below about 16 km).

Because of mixing, there is an important distinction between the descent provided by the mean meridional mass circulation, which is in balance with mean radiative cooling, and the Lagrangian-mean descent of long-lived chemical species. Satellite measurements of chemical species [Russell et al. 1993] show clear evidence of unmixed descent in the Antarctic vortex, maximizing at the pole, which is consistent with air-parcel trajectory calculations [Fisher et al. 1993]. However, radiative cooling – and thereby the descent rate of the mass circulation – is greatest not over the pole, but over the vortex edge. This difference in the location of the peak descent rates can be understood by recognizing that the vortex edge represents a region of significant lateral mixing. Air parcels initially located at the vortex edge do not remain there, but perform large excursions into the midlatitude surf zone where they experience much less radiative cooling. Hence, the descent rate of the (Eulerian) mean mass circulation at the vortex edge is a significant overestimate of the actual Lagrangian descent of air parcels. It is worth remarking that this phenomenon arises from the fact that the diabatic cooling rate varies strongly (with latitude) over the length scale characterizing the air parcel motion; in the opposite, small-eddy limit – which is that assumed in traditional mixing-length approaches – the two descent rates would have to be essentially equivalent.

As noted in Section 2.2, dynamical variability of the wintertime polar vortex is much greater in the Arctic than in the Antarctic, and temperatures sufficiently cold to allow PSC formation therefore occur far less often. Consequently, Arctic ozone depletion is comparatively more limited and more variable from year to year. It may be that predictions of ozone loss in the Arctic will never be possible, because of the inherent unpredictability of wintertime dynamical variability. Nevertheless, it is still important to achieve sufficient understanding of the relevant dynamical processes so that reasonable bounds can be placed on the range of variability of Arctic ozone destruction. Understanding at this level remains poor. Even when constrained by observed winds and temperatures, stratospheric models with sophisticated ozone chemistry have been unable to account for the observed amounts of Arctic ozone depletion, with shortfalls in the range of 40%. Edouard et al. [1996] have argued that this discrepancy can be explained by insufficiently fine horizontal resolution in the models. Because the catalytic halogen species may be concentrated in filamentary structures, and because the chemistry of ozone depletion is strongly nonlinear with respect to the concentrations of those species, the rate of ozone destruction may therefore be underestimated if such structures are not well represented. (In other words, the same amount of halogen destroys ozone more rapidly when it is concentrated in intense filaments rather than spread out over a broad region.) Such considerations are of most relevance in the Arctic, because of the incompleteness of the ozone destruction; in the Antarctic, where polar ozone destruction is essentially complete, the rate is not relevant to the final result.

It should be emphasized that although models may require fine spatial resolution in order to represent chemical tracers, they do not necessarily require equally high resolution for the dynamical fields, because it is only the large-scale wind field that appears to be relevant to the development of realistic small-scale structure in the tracer field. This is quite consistent with our understanding of quasi-horizontal stirring and mixing (see also Section 2.6), and – it may be added – with the existence of transport barriers. A possible exception concerns the effect of small-scale temperature inhomogeneities on PSC formation, which has not yet been quantified.

The implications of inadequate spatial resolution in models are complex, because there are competing effects. If the spatial resolution is too coarse, and the tracer fields too diffuse, then reactions between distinct air masses (for example, following an intrusion of midlatitude air into the polar vortex) will occur too quickly, before the actual (i.e., the fine-grained) air masses have actually mixed. On the other hand, when they finally do mix, if the tracer concentrations are too diffuse, then the resulting chemical effects will be underestimated. Such considerations are especially relevant to the important question of the possible impact of polar ozone chemistry on midlatitude ozone (see Section 2.6).

2.6 Midlatitudes

The greatest uncertainties in our present understanding of observed ozone changes have to do with the cause of midlatitude changes. There are many ways in which dynamical processes can be expected to be relevant. First, the height and structure of the midlatitude tropopause has a direct bearing on total ozone abundance. Second, the strength of the Brewer-Dobson circulation controls the transport of ozone from the tropical source region into the midlatitudes, and also controls the rate of mean descent through the lowermost stratosphere into the upper troposphere [Holton et al. 1995]. Third, the transport of chemically processed air out of the wintertime vortex – either in a major vortex-breaking event, such as a sudden warming, or in the final breakdown of the vortex – provides a strong chemical perturbation in midlatitudes. The last example contains competing effects; although breakdown and flushing out of the vortex ultimately limit ozone loss, there are short-term losses in midlatitudes as processed air reaches to lower latitudes and receives more sunlight. The extent of midlatitude ozone loss can be expected to depend sensitively on how rapidly this processed air gets diluted in the surf zone, which, like the vortex breakdown itself, depends on the large-scale flow.

The arguments given in Section 2.5 concerning the scale dependence of halogen-induced chemical ozone loss in the Arctic apply equally to midlatitudes, if not more so. Such scale dependence reflects the fact that large-scale, quasi-horizontal motion is the dominant contributor to mixing in the stratosphere, and that "stirring" by such motion generically leads to filamentary structure. An example from the lower stratosphere is shown in Figure 2.10. Stratospheric mixing is, therefore, quite opposite to diffusive mixing: homogenization is achieved first at large scales, and only subsequently at small scales; extremes in the concentration field are preserved even as small scales develop; and the advective development of small scales is a precondition for mixing. Because of the nonlinearity of ozone chemistry, it thus becomes crucial to achieve a good understanding of the small-scale structure of ozone and of ozone-depleting substances.

The existence of widespread filamentary structure in the stratosphere, as shown in Figure 2.10, is well established from measurements and has been clearly linked to large-scale advection acting on the sharp gradients characterizing the vortex edge [Waugh and Plumb 1994]. On the other hand, vertical profiles of ozone taken by ozonesondes have long

(a)

(b)

Figure 2.10 (a) Pattern of selected potential vorticity contours on the 320 K isentropic surface at 1200 UT on 14 May 1992, derived using the passive contour advection technique. The calculation begins 96 hours earlier (on 10 May 1992) from analyzed potential vorticity. **(b)** The satellite radiance image taken at the same time as (a) confirms the physical reality of the predicted filamentary and vortical structures. (From Appenzeller et al. [1996a].)

shown evidence of "laminae," namely isolated layers of anomalous values [Dobson 1973]; some examples are provided in Figure 2.11. Until recently, it had been widely assumed that these laminae result from inertia-gravity waves – though it was never clear why a wave would produce a vertically isolated, layered perturbation to an ozone profile. (Interestingly, *subtropical* laminae have been linked for some time to quasi-horizontal advective intrusions of tropical air [e.g., Andrews et al. 1987, Section 9.5.1].) It is rather surprising that the connection between filaments and laminae has only recently been made, because they are clearly two sides of the same coin: because of vertical shearing of the large-scale quasi-horizontal flow, the filaments seen in tracer structure at a given level are just the horizontal manifestations of sloping sheets of tracer, whose vertical manifestations are laminae. This explanation of ozone laminae has recently been established by several groups [e.g., Orsolini 1995]. The process has been quantified by Haynes and Anglade [1997], who argue that for conditions characteristic of the lower stratosphere, the asymptote of the ratio of the horizontal to the vertical length scales, in the long-time limit, should be somewhere around 250. The limiting process is small-scale vertical diffusion.

The existence of ozone filaments and laminae is consistent with the fact that horizontal spectra of ozone calculated from aircraft profiles in the stratosphere exhibit roughly a k^{-2} power-law scaling, where k is the horizontal wavenumber [Bacmeister et al. 1996]. The most obvious explanation of this scaling is that it is the singularity spectrum arising from the presence of a finite number of jumps in ozone concentration, associated with filamentation of the vortex edge [Ngan and Shepherd 1997b]. (The same scaling is found for the TOMS data [Sirovich et al. 1995], where it is presumably associated with the vortex edge itself.) The scaling holds down to the smallest resolvable length scales, of about 0.5 km, which suggests that we have yet to determine the ultimate scale at which three-dimensional effects overcome two-dimensional advection in the stratosphere. This sets a lower limit on vertical diffusion, and on the mix-down time for passive tracers; the latter must be about two weeks or greater. This is comparable to the estimated chemical lifetime of ozone filaments in midlatitudes [von der Gathen et al. 1995].

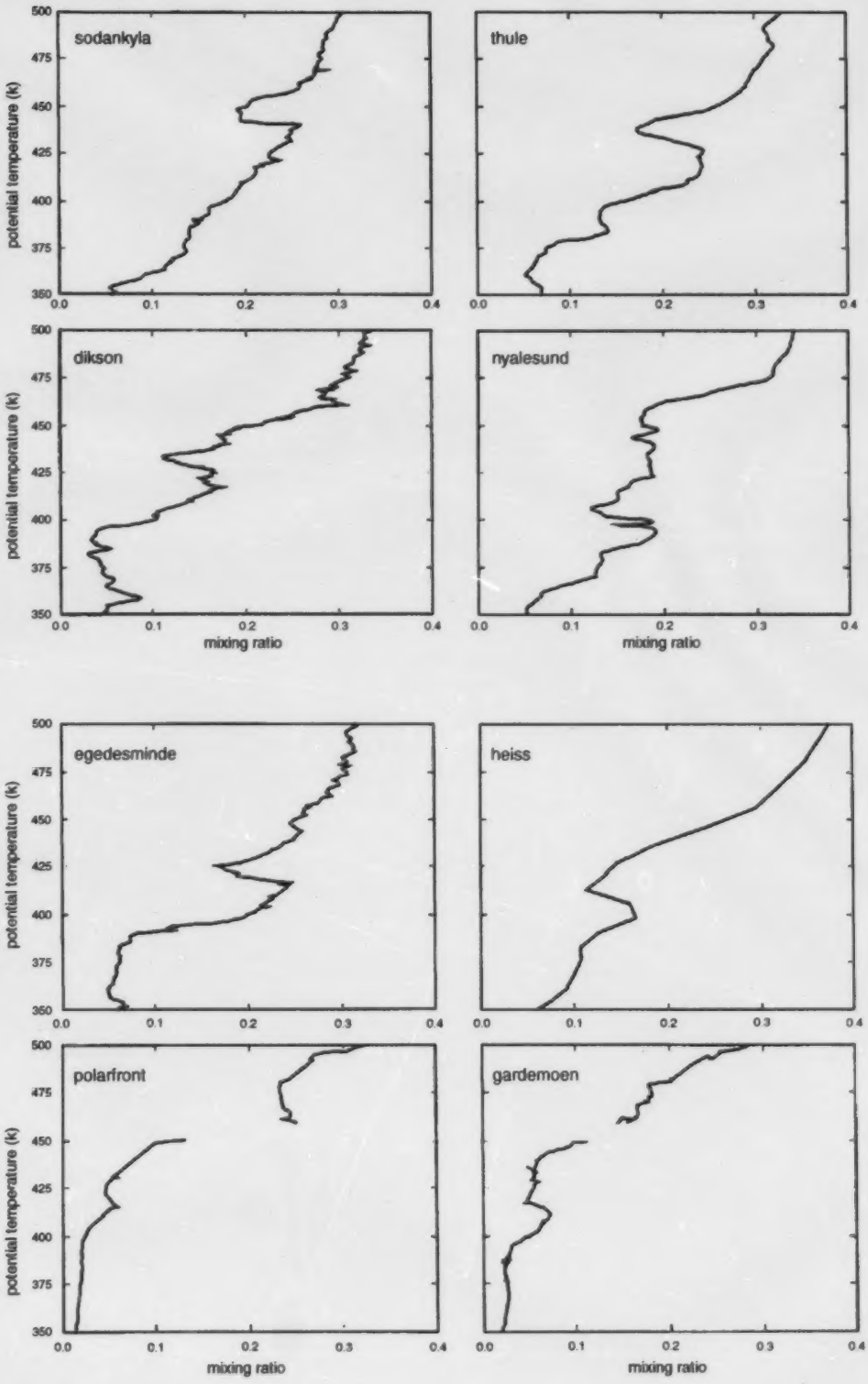

Figure 2.11 Ozone mixing-ratio profiles (in 10 parts per million by volume) taken over northern Europe and the northern Atlantic by ozonesondes on 29 January 1992. Height is measured by potential temperature (K). (After Orsolini [1995].)

When they first develop, ozone filaments will be associated with anomalous values of potential vorticity, because both ozone and potential vorticity are materially conserved on short timescales. However, the potential vorticity signature of these filaments will be increasingly damped – not diffused – by radiative cooling as their vertical scale decreases. Haynes and Ward [1993] have estimated the resulting horizontal cut-off scale in the lower stratosphere to be around 50 km, which is considerably larger than the cut-off scale estimated above for tracer filaments. (Tracers are not directly affected by radiative processes.) It follows that one should expect to find chemical filaments with no corresponding potential-vorticity signature. Such structures have indeed been found in the lowermost stratosphere in water vapour [Dessler et al. 1995] and in ozone [Folkins and Appenzeller 1996].

Any global budget of ozone in the extratropical lower stratosphere must take account of ozone transport into and out of this region. A recent diagnostic analysis by Appenzeller et al. [1996b] has shown that there is a seasonal cycle in the structure of the tropopause that leads to a seasonal cycle in the mass of the extratropical lower stratosphere; in the northern hemisphere (though not in the southern hemisphere) there is a corresponding lag between the mass flux in and the mass flux out, which must be accounted for in order to explain the seasonal cycle of stratosphere-troposphere exchange seen in tracers.

In order to determine the cause of midlatitude ozone depletion, it is essential to quantify the relative role of dynamical effects, chemical destruction, and the short-term impact of aerosol from volcanic eruptions (which complicates the recent record). Purely advective dynamical effects should be capable of quantification, but others are far more complex: for example, the impact of temperature changes on heterogeneous chemistry, or the impact of changes in the frequency of sudden warmings, or in the timing of the final vortex breakdown, on the propagation of polar ozone loss into midlatitudes. Such coupled dynamical-chemical processes are the most difficult to unravel. Since they may well have strong sensitivity to horizontal resolution (i.e., strong scale dependence), they are also extremely difficult to quantify with any confidence.

References

Andrews, D.G., J.R. Holton, and C.B. Leovy, 1987. *Middle Atmosphere Dynamics.* Academic Press, New York, 489 pp.

Appenzeller, C., H.C. Davies, and W.A. Norton, 1996a. Fragmentation of stratospheric intrusions. *J. Geophys. Res.*, **101**, 1435–1456.

Appenzeller, C., J.R. Holton, and K.H. Rosenlof, 1996b. Seasonal variation of mass transport across the tropopause. *J. Geophys. Res.*, **101**, 15071–15078.

Avallone, L.M., and M.J. Prather, 1996. Photochemical evolution of ozone in the lower tropical stratosphere. *J. Geophys. Res.*, **101**, 1457–1461.

Bacmeister, J.T., S.D. Eckermann, P.A. Newman, L. Lait, K.R. Chan, M. Loewenstein, M.H. Proffitt, and B.L. Gary, 1996. Stratospheric horizontal wavenumber spectra of winds, potential temperature, and atmospheric tracers observed by high-altitude aircraft. *J. Geophys. Res.*, **101**, 9441–9470.

Beagley, S.R., J. de Grandpré, J.N. Koshyk, N.A. McFarlane, and T.G. Shepherd, 1997. Radiative-dynamical climatology of the first-generation Canadian Middle Atmosphere Model. *Atmos.-Ocean*, in press.

Boering, K.A., B.C. Daube, Jr., S.C. Wofsy, M. Loewenstein, J.R. Podolske, and E.R. Keim, 1994. Tracer-tracer relationships and lower stratospheric dynamics: CO_2 and N_2O correlations during SPADE. *Geophys. Res. Lett.*, **21**, 2567–2570.

Bowman, K.P., 1993. Large-scale isentropic mixing processes of the Antarctic polar vortex from analyzed winds. *J. Geophys. Res.*, **98**, 23013–23027.

Brewer, A.W., 1949. Evidence for a world circulation provided by the measurements of helium and water vapour distribution in the stratosphere. *Quart. J. Roy. Met. Soc.*, **75**, 351–363.

Dessler, E.J. Hintsa, E.M. Weinstock, J.G. Anderson, and K.R. Chan, et al., 1995. Mechanisms controlling water vapor in the lower stratosphere: "A tale of two stratospheres". *J. Geophys. Res.*, **100**, 23167–23172.

Dobson, G.M.B., 1956. Origin and distribution of polyatomic molecules in the atmosphere. *Proc. Roy. Soc. Lond. A*, **236**, 187–193.

Dobson, G.M.B., 1973. The laminated structure of the ozone in the atmosphere. *Quart. J. Roy. Met. Soc.*, **99**, 599–607.

Dunkerton, T.J., 1989. Nonlinear Hadley circulation driven by asymmetric differential heating. *J. Atmos. Sci.*, **46**, 956–974.

Edouard, S., B. Legras, F. Lefèvre, and R. Eymard, 1996. The effect of small-scale inhomogeneities on ozone depletion in the Arctic. *Nature*, **384**, 444–447.

Fahey, D.W., S.G. Donnelly, E.R. Kein, R.S. Gao, R.C. Wamsley, L.A. Del Negro, E.L. Woodbridge, et al., 1996. In situ observation of NO_y, O_3, and the NO_y/O_3 ratio in the lower stratosphere. *Geophys. Res. Lett.*, **23,** 1653–1656.

Fisher, M.A., A. O'Neill, and R. Sutton, 1993. Rapid descent of mesospheric air into the stratospheric polar vortex. *Geophys. Res. Lett.*, **20,** 1267–1270.

Folkins, I., and C. Appenzeller, 1996. Ozone and potential vorticity at the subtropical tropopause break. *J. Geophys. Res.*, **101,** 18787–18792.

Garcia, R.R., and B.A. Boville, 1994. "Downward control" of the mean meridional circulation and temperature distribution of the polar winter stratosphere. *J. Atmos. Sci.*, **51,** 2238–2245.

Grant, W.B., E.V. Browell, J. Fishman, V.G. Brackett, R.E. Veiga, D. Nganga, A. Minga, B. Cros, C.F. Butler, M.A. Fenn, C.S. Long, and L.L. Stowe, 1994. Aerosol-associated changes in tropical stratospheric ozone following the eruption of Mount Pinatubo. *J. Geophys. Res.*, **99,** 8197–8211.

Hall, T.M., and R.A. Plumb, 1994. Age as a diagnostic of stratospheric transport. *J. Geophys. Res.*, **99,** 1059–1070.

Hall, T.M., and D.W. Waugh, 1997. Timescales for the stratospheric circulation derived from tracers. *J. Geophys. Res.*, **102,** 8991½n 9001.

Haynes, P.H,. and J. Anglade, 1997. The vertical-scale cascade in atmospheric tracers due to large-scale differential advection. *J. Atmos. Sci.*, **54,** 1121–1136.

Haynes, P.H., and W.E. Ward, 1993. The effect of realistic radiative transfer on potential vorticity structures, including the influence of background shear and strain. *J. Atmos. Sci.*, **50,** 3431–3453.

Hoff, R.M., and M.T. Osborn, 1996. Overview of the Lidar In-Space Technology Experiment (LITE). In *ELITE-94: The European LITE Correlative Measurement Campaign,* European Space Agency Report ESA WPP–107.

Holton, J.R., P.H. Haynes, M.E. McIntyre, A.R. Douglass, R.B. Rood, and L. Pfister, 1995. Stratosphere-troposphere exchange. *Rev. Geophys.*, **33,** 403–439.

McCormick, M.P., 1996: The Flight of the Lidar In-Space Technology Experiment (LITE). Pages 141–144 in *Advances in Atmospheric Remote Sensing with Lidar* (A. Ansmann, R. Neuber, P. Rairoux and U. Wandinger, eds.), Springer-Verlag, Berlin.

McIntyre, M.E., and T.N. Palmer, 1983. Breaking planetary waves in the stratosphere. *Nature,* **305,** 593–600.

Mote, P.W., K.H. Rosenlof, M.E. McIntyre, E.S. Carr, J.C. Gille, J.R. Holton, J.S. Kinnersley, H.C. Pumphrey, J.M. Russell III, and J.W. Waters, 1996. An atmospheric tape recorder: the imprint of tropical tropopause temperatures on stratospheric water vapor. *J. Geophys. Res.*, **101,** 3989–4006.

NASA, 1995. *1995 Scientific Assessment of the Atmospheric Effects of Stratospheric Aircraft.* National Aeronautics and Space Administration Reference Publication 1381. National Aeronautics and Space Administration, Washington.

Ngan, K., and T.G. Shepherd, 1997a. Chaotic mixing and transport in Rossby-wave critical layers. *J. Fluid Mech.*, **334,** 315–351.

Ngan, K., and T.G. Shepherd, 1997b. Comments on some recent measurements of anomalously steep N_2O and O_3 tracer spectra in the stratospheric surf zone. *J. Geophys. Res.*, in press.

Orsolini, Y.J., 1995. On the formation of ozone laminae at the edge of the Arctic polar vortex. *Quart. J. Roy. Met. Soc.*, **121,** 1923–1941.

Plumb, R.A., 1996. A "tropical pipe" model of stratospheric transport. *J. Geophys. Res.*, **101,** 3957–3972.

Plumb, R.A., D.W. Waugh, R.J. Atkinson, M.R. Schoeberl, L.R. Lait, P.A. Newman, E.V. Browell, A.J. Simmons, and M. Loewenstein, 1994. Intrusions into the lower stratospheric Arctic vortex during the winter of 1991/92. *J. Geophys. Res.*, **99,** 1089–1105.

Polvani, L.M., D.W. Waugh, and R.A. Plumb, 1995. On the subtropical edge of the stratospheric surf zone. *J. Atmos. Sci.*, **52,** 1288–1309.

Randel, W.J., J.C. Gille, A.E. Roche, J.B. Kumer, J.L. Mergenthaler, J.W. Waters, E.F. Fishbein, and W.A. Lahoz, 1993. Stratospheric transport from the tropics to middle latitudes by planetary wave mixing. *Nature,* **365,** 533–535.

Rosenlof, K.H., 1995. The seasonal cycle of the residual mean meridional circulation in the stratosphere. *J. Geophys. Res.*, **100,** 5173–5191.

Russell, J.M., III, A.F. Tuck, L.L. Gordley, J.H. Park, S.R. Drayson, J.E. Harries, R.J. Cicerone, and P.J. Crutzen, 1993. HALOE Antarctic observations in the spring of 1991. *Geophys. Res. Lett.*, **20,** 719–722.

Schoeberl, M.R., and D.L. Hartmann, 1991. The dynamics of the stratospheric polar vortex and its relation to springtime ozone depletions. *Science,* **251,** 46–52.

Shepherd, T.G., 1995. The Canadian MAM project. *CMOS Bull.*, **23**(1), 3–12.

Shepherd, T.G., K. Semeniuk, and J.N. Koshyk, 1996. Sponge-layer feedbacks in middle atmosphere models. *J. Geophys. Res.*, **101**, 23447–23464.

Sirovich, L., R. Everson, and D. Manin, 1995. Turbulent spectrum of the Earth's ozone field. *Phys. Rev. Lett.*, **74**, 2611–2614.

Trepte, C.R., and M.H. Hitchman, 1992. Tropical stratospheric circulation deduced from satellite aerosol data. *Nature*, **355**, 626–628.

Volk, C.M., J.W. Elkins, D.W. Fahey, R.J. Salawitch, G.S. Dutton, J.M. Gilligan, M.H. Proffitt, M. Loewenstein, J.R. Podolske, K. Minschwaner, J.J. Margitan, and K.R. Chan, 1996. Quantifying transport between the tropical and mid-latitude lower stratosphere. *Science*, **272**, 1763–1768.

von der Gathen, P., M. Rex, N.R.P. Harris, D. Lucic, B.M. Knudsen, G.O. Braathen, H. DeBacker, et al., 1995. Observational evidence for chemical ozone depletion over the Arctic in winter 1991–92. *Nature*, **375**, 131–134.

Waugh, D.W., and R.A. Plumb, 1994. Contour advection with surgery: a technique for investigating fine-scale structure in tracer transport. *J. Atmos. Sci.*, **51**, 530–540.

Waugh, D.W., R.A. Plumb, R.J. Atkinson, M.R. Schoeberl, L.R. Lait, P.A. Newman, M. Loewenstein, D.W. Toohey, and C.R. Webster, 1994. Transport out of the lower stratospheric Arctic vortex by Rossby wave breaking. *J. Geophys. Res.*, **99**, 1071–1088.

Ozone Chemistry: Simulation and Depletion

Throughout much of the atmosphere the abundance of ozone molecules is the result of a balance between production by UV radiation from the sun and chemical loss. However, in those regions of the stratosphere where most of the ozone resides, such a balance does not obtain. Instead, as Chapter 2 has already demonstrated, the distribution of ozone is shaped largely by atmospheric transport. In this chapter the general gas phase and heterogeneous chemistry of stratospheric ozone and its depletion are discussed. Additionally, the different types of models used to simulate and analyse stratospheric ozone are described.

Some attention is also given to measurement programs, since these are of particular importance to the validation of the models used to forecast future ozone levels. Finally, the chapter explores our current understanding of the impacts of aircraft on stratospheric ozone as well as climate-related impacts such as the effects of changes in the output of solar UV radiation on stratospheric chemistry.

3.1 Stratospheric Ozone Chemistry

3.1.1 Gas Phase Chemistry

By far the largest source of O_3 in the stratosphere is the photolysis of molecular oxygen, in which solar radiation of wavelength 240 nm and shorter breaks the O_2 bond.

$$O_2 + h\nu \rightarrow 2O \quad (1)$$

The oxygen atoms that are produced rapidly form ozone

$$O + O_2 + M \rightarrow O_3 + M \quad (2)$$

which is in turn photolyzed.

$$O_3 + h\nu \rightarrow O + O_2 \ (\lambda < 900 \text{ nm}) \quad (3)$$

The continual repetition of the last two steps results in the heating of the stratosphere but no loss of ozone. Since ozone production is driven by solar radiation, most ozone is produced over tropical regions, with the maximum occurring at about 40 km as is shown in Figure 3.1a.

Ozone may also be produced in the troposphere and lower stratosphere by the "smog" reactions

$$NO + HO_2 \rightarrow NO_2 + OH \quad (4)$$

$$NO_2 + h\nu \rightarrow NO + O \quad (5)$$

$$O + O_2 + M \rightarrow O_3 + M \quad (6)$$

which are catalyzed by NO. The O_2 bond in HO_2 is broken by reaction 4. However, the reactions

$$CO + OH \rightarrow CO_2 + H \quad (7)$$

$$H + O_2 + M \rightarrow HO_2 + M \quad (8a)$$

regenerate the HO_2, so that the net effect is essentially the oxidation of CO to produce ozone:

$$\text{net:} \quad CO + 2O_2 \rightarrow CO_2 + O_3$$

A major ozone loss results from the reaction of O and O_3 with each other.

$$O + O_3 \rightarrow 2O_2 \quad (8b)$$

Other major ozone loss processes result from catalytic cycles involving other minor species, from both biogenic and anthropogenic sources, that are transported upwards from the troposphere. However, volcanos and subsonic and supersonic aircraft also inject material directly into the stratosphere. Important species whose breakdown products act to catalyze O_3 destruction are H_2O, N_2O, CH_4, CH_3Cl, and CFCs, CH_3Br, and halons. These are transformed into more active forms such as NO, NO_2, OH, HO_2, Cl, ClO, Br, and BrO, which participate in catalytic cycles (largely) of the form

$$X + O_3 \rightarrow XO + O_2 \quad (8c)$$

$$O + XO \rightarrow X + O_2 \quad (8d)$$

$$\text{net:} \quad O + O_3 \rightarrow 2O_2$$

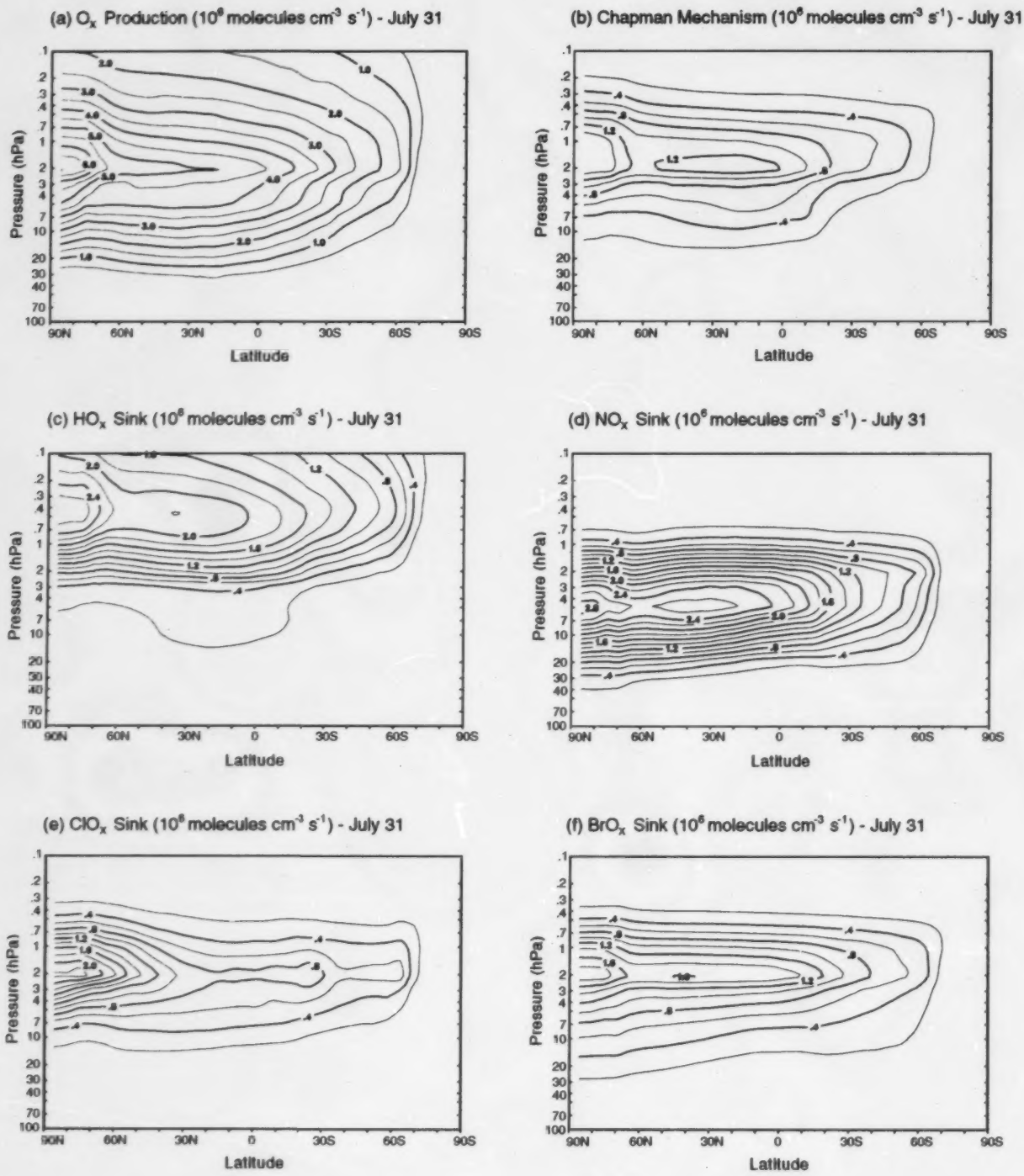
(a) O_x Production (10^6 molecules cm^{-3} s^{-1}) - July 31
(b) Chapman Mechanism (10^6 molecules cm^{-3} s^{-1}) - July 31
(c) HO_x Sink (10^6 molecules cm^{-3} s^{-1}) - July 31
(d) NO_x Sink (10^6 molecules cm^{-3} s^{-1}) - July 31
(e) ClO_x Sink (10^6 molecules cm^{-3} s^{-1}) - July 31
(f) BrO_x Sink (10^6 molecules cm^{-3} s^{-1}) - July 31
Pressure (hPa)
Latitude
90N
60N
30N
0
30S
60S
90S

Figure 3.1 The ozone budget (10^6 molecules cm^{-3} s^{-1}) for July from the CMAM: (a) O_3 production from O_2 photolysis. Loss processes for ozone: (b) Chapman loss O + O_3 (c) HO_x reactions, (d) NO_x reactions, (e) ClO_x reactions, (f) BrO_x reactions. (After de Grandpré et al. [1997].)

The last of these steps is slow due to the low abundance of atomic oxygen in the lower stratosphere. Consequently, the rate of destruction of ozone by catalytic cycles such as these is limited by low O abundances. The X represents several species, such as NO, OH, HO_2, Cl, and Br.

Another important cycle is represented by the following sequence, which is important in the lower stratosphere:

$$OH + O_3 \rightarrow HO_2 + O_2 \quad (9)$$

$$HO_2 + O_3 \rightarrow OH + 2O_2 \quad (10)$$

The above reaction sequences account for a large fraction of the non-heterogeneous loss.

Gas phase loss rates for July, taken from the Canadian Middle Atmosphere Model (CMAM), are shown in Figures 3.1b–f. By comparing Figures 3.1a and the remainder of the panels, we can see that above about 30 km at tropical and middle latitudes O_3 is in quasi-photochemical equilibrium. Below this, in the lower tropical stratosphere, excess chemical production is transported from the tropics to higher latitudes to maintain a distribution much as shown in Figure 2.1, which is discussed in detail in Chapter 2.

Each of the radicals mentioned above may be considered to be part of a family of species that are transformed one to the other on time scales that are relatively short compared to those for dynamical processes. For example, the NO_y family consists of NO, NO_2, NO_3, N_2O_5, HNO_3, HNO_4, $ClONO_2$, and $BrONO_2$ The more stable members of the family, such as HNO_3, that do not attack ozone are often called reservoir species. Thus, NO_x (i.e., NO + NO_2) and OH are converted into HNO_3 and N_2O_5, while NO_x and ClO can either combine to form $ClONO_2$ or react to form Cl which is converted to HCl. Due to the formation of these relatively stable reservoir forms, less remains of the (re)active members of each family to react with ozone. (In the case of bromine species, however, none of the species is sufficiently stable to be thought of as a reservoir species.) As we shall see later, it is the disruption of the balance of the reservoir species that leads to increased ozone loss.

The effects of transport are also underlined by Figure 1.12, which shows the variation of the average total ozone with time of year and latitude (for the two periods 1964–1980 and 1984–1993). On the basis of the production shown in Figure 3.1a, we might expect most of the ozone column to be located at the equator. However, higher column amounts occur at higher latitudes and shift following the patterns of stratospheric transport. Tropical ozone remains at approximately 250 DU throughout the year, but values at higher latitudes fluctuate in response to variations in transport and are affected most in the springtime stratosphere. Thus any natural or anthropogenic change in the dynamics of the stratosphere is likely to have an important impact on the ozone column, as is any alteration or perturbation in the chemical composition of the lower stratosphere.

3.1.2 Heterogeneous Chemistry

3.1.2.1 Sulphate Layer

Heterogeneous reactions on and within sulphate aerosols also play an important role in the stratosphere. The main aerosol layer consists of sulphate aerosols (at midlatitudes their composition is approximately 75% H_2SO_4 and 25% H_2O, by weight) formed by the oxidation of SO_2.

$$SO_2 + OH + M \rightarrow HSO_3 + M \quad (11)$$

$$HSO_3 + O_2 \rightarrow HO_2 + SO_3 \quad (12)$$

$$SO_3 + H_2O \rightarrow H_2SO_4 \quad (13)$$

At background levels, the SO_2 appears to be formed largely by the oxidation of COS diffusing from the troposphere. Some SO_2 may possibly be transported into the stratosphere as well.Volcanic SO_2 from "random" eruptions penetrating the stratosphere is also important in maintaining the stratospheric sulphate budget.

Two important reactions occurring on sulphate aerosols at midlatitudes in the lower stratosphere are

$$N_2O_5 + H_2O\ (a) \rightarrow 2HNO_3 \quad (14)$$

and

$$BrONO_2 + H_2O\ (a) \rightarrow HNO_3 + HOBr \quad (15)$$

where (a) means that the species is in the condensed phase of the sulphate aerosol. These hydrolysis reactions are important, since they change the balance of the catalysts active in O_3 destruction. Thus the NO_x/NO_y ratio may decrease due to the conversion of N_2O_5 and $BrONO_2$ to HNO_3. However, while nitrogen-cycle ozone depletion may decrease, ozone losses due to ClO_x and HO_x may increase. Active chlorine species (ClO_x) will increase because less ClO will be tied up as $ClONO_2$, a chlorine reservoir species. Odd hydrogen (HO_x) will increase due to the photolysis of the species formed through reactions 14 and 15, HNO_3 and HOBr.

$$HNO_3 + h\upsilon \rightarrow OH + NO_2 \quad (16)$$

$$HOBr + h\upsilon \rightarrow OH + Br \quad (17)$$

The OH and HO_2 produced will thus enhance ozone loss reactions 9 and 10 above. The enhanced OH mixing ratios also release additional Cl from HCl via

$$OH + HCl \rightarrow H_2O + Cl \quad (18)$$

[Danilin and McConnell 1994, 1995; Lary 1996; Lary et al. 1996; Chartrand and McConnell 1997].

BrO_x/Br_y ratios have been shown to be less sensitive to midlatitude aerosol processing than chlorine analogues because of the larger rate of $BrONO_2$ hydrolysis (reaction 15), compared to similar $ClONO_2$ hydrolysis. Although increased $BrONO_2$ hydrolysis will produce increased OH levels, which will destroy HBr through a process similar to reaction 18 above, increased Br concentrations will lead to an increase in HBr as a result of the reaction

$$Br + HO_2 \rightarrow HBr + O_2 \quad (19)$$

It should, however, be noted that the influence of increased sulphate aerosols on these hydrolysis reactions is subject to saturation effects. Thus, the conversion of NO_x to HNO_3 is ultimately limited by the formation of N_2O_5 via

$$NO_2 + O_3 \rightarrow NO_3 + O_2 \quad (20)$$

$$NO_2 + NO_3 + M \rightarrow N_2O_5 + M \quad (21)$$

with the former reaction being rate limiting. In the case of the $BrONO_2$ hydrolysis (reaction 15), the increase in HNO_3 is limited by the increase in OH loss

$$OH + HNO_3 \rightarrow H_2O + NO_3 \quad (22)$$

where the OH increase occurs as a result of the hydrolysis reaction.

3.1.2.2 Polar Stratospheric Cloud Chemistry

The formation of a strong polar vortex in the winter stratosphere, as described in section 2.2, tends to isolate the polar air from the midlatitude air. Each winter and spring since 1979 a dramatic decrease in the austral ozone column has been observed [Farman et al. 1985] in this vortex region. The vortex forms largely as a result of the infrared cooling that occurs during the winter, causing temperatures to drop well below 200 K, so that H_2SO_4, HNO_3, and H_2O, as well as various mixtures, can freeze or exist as supercooled solutions. In general, when temperatures are above approximately 195 K, there is little dissolved HNO_3 in the sulphate aerosols and the heterogeneous chemistry is similar to that at midlatitudes, although some reactions may be more important due to increased solubilities (see below). As the temperature is further decreased, HNO_3 can dissolve into the sulphate aerosols to form ternary solutions in amounts large enough to almost entirely deplete gas phase HNO_3 levels. The volume of these aerosol solutions can dramatically increase with this large uptake of gaseous HNO_3 and H_2O. It is thought that these supercooled ternary $H_2SO_4/HNO_3/H_2O$ liquid solutions can exist to within a few degrees of the frost point without forming nitric acid trihydrate.(solid $HNO_3 \cdot 3H_2O$ or NAT) and sulphuric acid tetrahydrate ($H_2SO_4 \cdot 4H_2O$ or SAT), which occur in Type I PSCs (polar stratospheric clouds). If the temperature falls below the ice frost point (~188 K), Type 2 PSCs made of water ice can form. As temperatures again rise, adsorption of gas phase HNO_3 onto solid SAT can help to regenerate ternary solutions and melt SAT at temperatures far below its melting point of 210–215 K [Tolbert 1996; Koop and Carslaw 1996]. Due to the low temperatures needed for solid PSCs to form, it is expected that processing on liquid surfaces is more important in the Arctic than the Antarctic.

Heterogeneous reactions on these condensed phases can activate chlorine and bromine while tying up odd-nitrogen as HNO_3(a) [e.g., Tolbert, 1996]. The active chlorine and, to a lesser extent, bromine drive the reactions that form the ozone hole. For example, on the ice crystals, inactive or reservoir forms of the halogen catalysts are freed through the following reaction

$$ClONO_2 + HX\ (ice) \rightarrow HNO_3\ (ice) + XCl(gas) \quad (23)$$

where X = Cl or Br.

Low temperatures are crucial to this process. As the polar lower stratospheric temperatures drop at the end of the fall season, the aerosol reactions become important. For example, the solubility of HCl is very temperature sensitive, and as the temperature drops, HCl begins to dissolve in the ternary solution or sulphate aerosol.These and similar reactions initiate the formation of the ozone hole in the polar late winter (northern hemisphere) and austral springtime. These reactions can occur during the nighttime, and when polar sunrise occurs species such as Cl_2, BrCl, and $ClNO_2$ are readily photolyzed into more labile species such as Cl. One of the main features of ozone loss in polar regions is that it is *not* rate limited by the low abundances of atomic oxygen. One of the main loss mechanisms involves self-reaction of ClO [Molina and Molina 1987]:

$$ClO + ClO \rightarrow Cl_2O_2 \quad (24)$$

$$Cl_2O_2 + h\upsilon \rightarrow Cl + ClO_2 \quad (25)$$

$$ClO_2 + M \rightarrow Cl + O_2 + M \quad (26)$$

$$2 \times (Cl + O_3 \rightarrow ClO + O_2) \quad (27)$$

net: $O_3 + O_3 \rightarrow 3O_2$

As long as temperatures are less than approximately 210 K, then thermal decomposition of Cl_2O_2,

$$Cl_2O_2 + M \rightarrow ClO + ClO + M \quad (28)$$

which does not lead to ozone loss, does not play a major role. In this case the ozone loss rate is proportional to $[ClO]^2$. Thus as more ClO_y is converted to ClO, ozone is destroyed with a quadratic dependence.

Another important ozone loss mechanism is due to the synergistic reaction between BrO and ClO [Clyne and Watson 1977; Yung et al. 1980]:

$$BrO + ClO \rightarrow Br + Cl + O_2 \quad (29)$$

$$BrO + ClO \rightarrow BrCl + O_2 \quad (30)$$

$$BrCl + h\upsilon \rightarrow Br + Cl \quad (31)$$

$$Cl + O_3 \rightarrow ClO + O_2 \quad (27)$$

$$Br + O_3 \rightarrow BrO + O_2 \quad (32)$$

As before, this loss rate is not limited by the abundance of atomic oxygen.

One of the critical regions of ozone loss is the lower stratosphere, a region in which, as noted above, ozone concentrations are strongly influenced by the effects of transport. However, as stressed in Chapter 2, the subtleties of transport in this region are not well defined. Current theories propose that air enters the stratosphere at the tropical tropopause at approximately 17–18 km and rises to about 20–25 km (the so-called "tropical pipe"). This rising air has a distinct tropical

signature and properties, such as the H_2O tape recorder effect [Mote et al. 1996] in which the amount of water flowing into the stratosphere is determined by freezing at the tropopause, thus leaving an imprint of tropical tropopause temperatures on stratospheric water vapour [Brewer 1949]. However, much evidence suggests that there is a two-way exchange of midlatitude air with tropical air [Volk et al. 1996]. In fact, Schoeberl et al. [1997] suggest that the mixing occurs below 20 km.

Thus, we have the potential scenario of pollution from midlatitude supersonic aircraft reaching the tropics and being carried aloft in the tropical pipe, where the pollution can do more serious damage to the ozone layer. The extent, direction, and sensitivity of this transport is uncertain and a matter for concern. It is quite likely that after the Mt. Pinatubo eruption some of the decrease in the ozone field was due to changes in the dynamics of the stratosphere, which consequently altered the transport of ozone and other species [e.g., Tie et al. 1994].

3.2 Observations of Minor Species

One method of validating chemical models of the stratosphere is to compare modelled species to measured quantities with various characteristic time scales. In this section we focus primarily on shorter-lived radical species. Currently there are many international efforts to model these effects and to obtain diagnostic measurements. Some of the important measurement campaigns with global scope are (a) those involving the Upper Atmosphere Research Satellite (UARS) (*J. Geophys. Res.*, 98 (D6), 1993; *J. Geophys. Res.*, 101, July 1996; *J. Atmos. Sci.*, 51 (20), October 1994) and (b) the ER2 campaigns such as SPADE, ASHOE, and STRAT. (e.g., *Geophys. Res. Lett.*, 21 (23), November 1994, special issue; Volk et al. [1996]). At the present time the GOME (Global Ozone Monitoring Experiment) program [Burrows et al. 1993] is also making stratospheric measurements.

Direct comparison of measurements with models is important for validation. However, analysing ratios of species provides a powerful method of deriving further information from both measurements and models. Figure 3.2 shows an example taken from ER-2 flights [Volk et al., 1996]. In this figure O_3 is used as the baseline gas. The black dots represent data from the tropics, while the light grey dots represent data taken at midlatitudes. The different ratios reveal the different histories of the air parcels. Thus, as the air rises over the tropics both NO_y and O_3 increase as they approach their source region. However, at midlatitudes the slope of the correlation curve is much steeper, indicating a more direct connection between the O_3 and NO_y sources. Much has been learned from analysis such as this, and there is more to be discovered.

The preceding paragraph outlines the importance and the

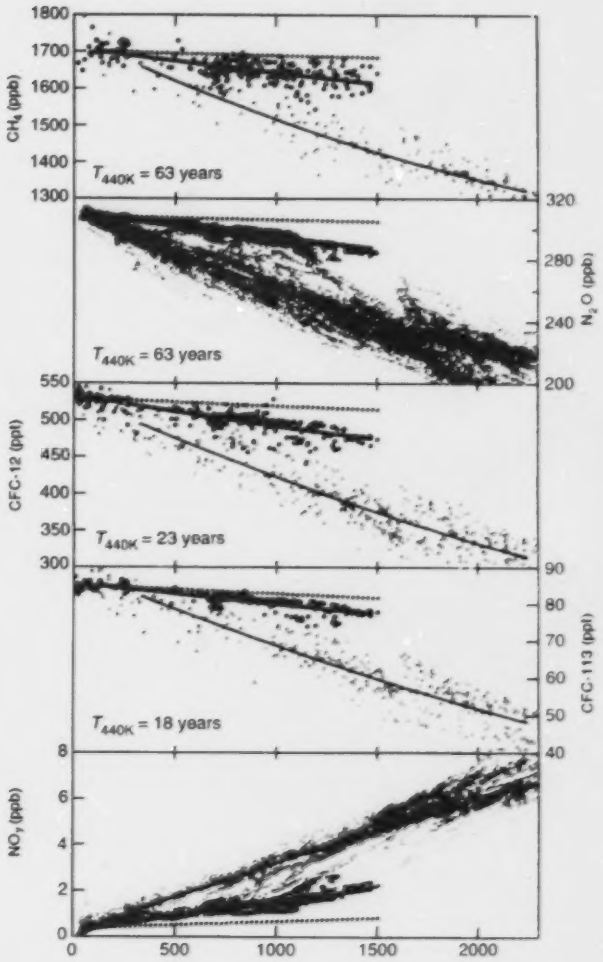

Figure 3.2 Correlations of mixing ratios for longer-lived species versus O_3 in the tropics (black dots) and at midlatitudes (light grey dots). Thick dotted lines represent the unmixed case. For N_2O and NO_y, mean midlatitude correlations are derived from nonparametric loss fits of each species versus potential temperature, T. Effective lifetimes at T = 440 K are as indicated. (After Volk et al. [1996].)

uncertainty of transport into the stratosphere in the tropics. Even more uncertain, perhaps, is the transport of material in the midlatitudes. In terms of the picture painted in Chapter 2 and reviewed by Holton et al. [1995], midlatitude transport most likely occurs in one direction only. However, recent measurements of chemical tracers such as CO, which are diagnostic of tropospheric air, suggest that the lowest few kilometres of the stratosphere can be affected by air convected upwards from the lower troposphere [Lelieveld et al. 1997]. This is certainly an area that requires more evaluation.

3.3 Modelling

Modelling helps us to understand the workings of the atmosphere and allows us to forecast the effects of changes in external forcings such as solar variability, volcanic emissions, or the addition of greenhouse gases. There are various types of models, ranging from box to three-dimensional (3D), each of which offers us different insights into the workings of the atmosphere.

Box models are just that: one looks at a box or parcel of air and investigates the impact of sunlight. They are used principally for analysing chemistry in the atmosphere, particularly on time scales of less than a day. They can be used either at a single point or in a trajectory mode where the box or air parcel is transported (usually unmixed) by the wind system. One of the most powerful aspects of box models is that they allow a focus on the chemistry without the complicating (but real-life) details of dynamics. Box models have been used very effectively in connection with the SPADE, ASHOE/MAESA, and STRAT experiments. These experiments make use of a comprehensive suite of instruments on board an ER-2 flying at an altitude of about 20 km in the stratosphere. Some of the data from the SPADE flights are shown in Figure 3.3 [Salawitch et al. 1994]. The data points show measurements of a number of constraining species. The solid lines in the figure are the modelled values obtained by following the air parcel at that location back several days. (This is also a data assimilation method and is discussed later.)

As can be seen from this figure, the current quality of the measurements is such that disagreement greater than 20% can be a cause for concern that something is missing in the chemistry. One particular example, pertaining to OH, is shown in the first panel of Figure 3.3. The disagreement between the measurements and model output at sunrise pointed to the need for a readily photolyzable source of OH. This turned out to be HOBr, produced by the heterogeneous processing of $BrONO_2$ during the night in the sulphate particles omnipresent at ER-2 altitudes [Lary et al. 1996]:

$$BrONO_2 + H_2O \rightarrow HOBr + HNO_3 \qquad (15)$$

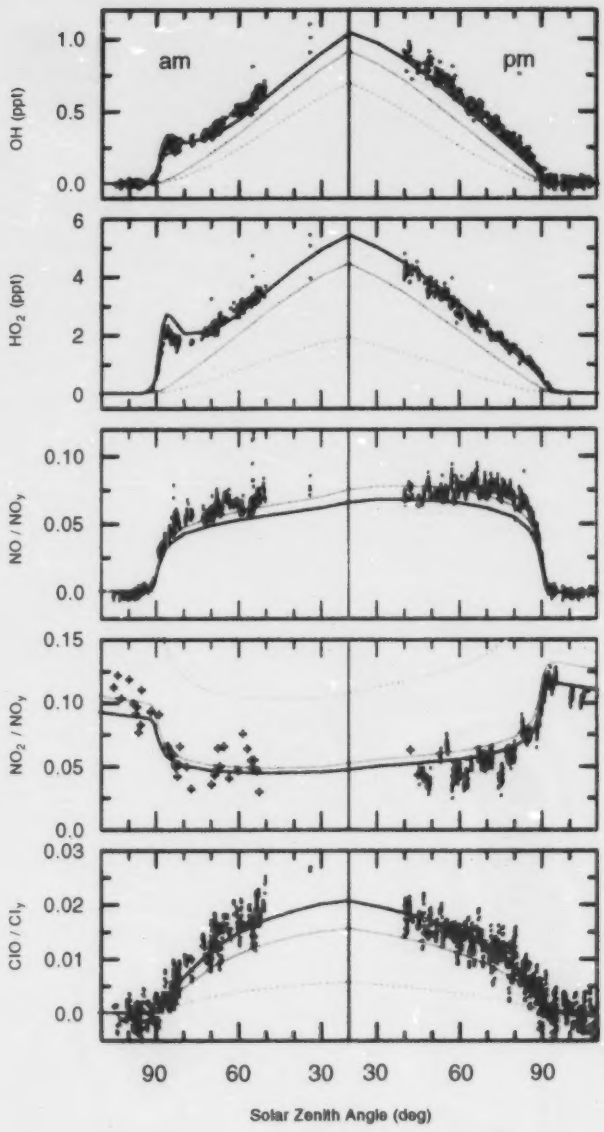

Figure 3.3 Diurnal variation of OH, HO_2, NO/NO_y, NO_2/NO_y, and ClO/Cl_y as measured by the JPL (crosses) and NOAA (dots) instruments and plotted as a function of the solar zenith angle. Measurements were taken from two ER-2 flights on May 11 (sunrise) and May 12 (sunset) near 37° N and at 63 hPa. NO_2 concentrations were between 240 and 260 ppb. Also shown are the results from a constrained data assimilation model. The dotted curve is for homogeneous gas phase chemistry; the lower solid curve in the OH, HO_2 and ClO/Cl_y panels includes the heterogeneous chemistry shown in reaction 14. The upper curve for the same panels includes the effects of reactions 14 and 15. (After Salawitch et al. [1994].)

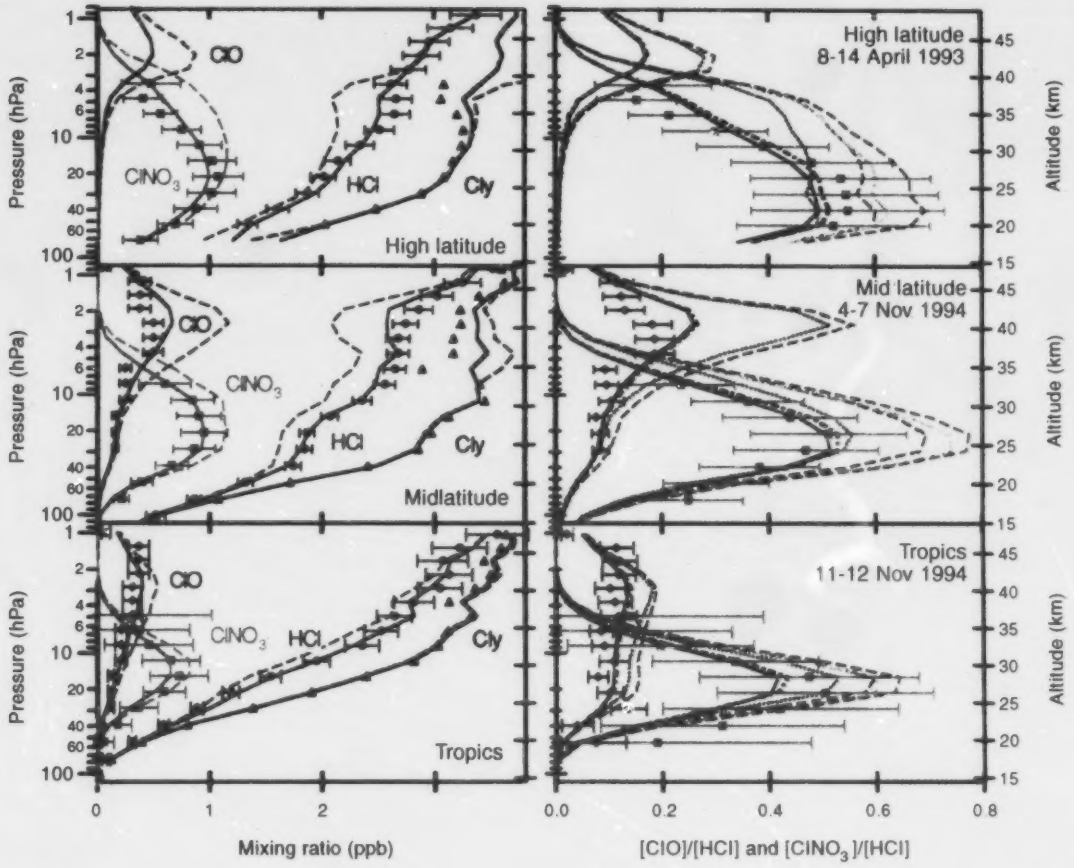

Figure 3.4 Comparison of modelled and measured $ClNO_3$, HCl, Cl_y (estimated), and ClO mixing ratios and ClO/HCl and $ClNO_3$/HCl concentration ratios. Model results are represented by lines, measurements by symbols. The vertical axis is pressure; approximate altitude is also shown. Model cases are for a variety of rates, including the standard case as described in Michelsen et al. [1996]. The top panel shows concentrations at sunrise, the middle and bottom panels at sunset. (After Michelson et al. [1996].)

The HOBr accumulated during the night was then photolyzed at sunrise, releasing a burst of OH

$$HOBr + h\upsilon \rightarrow HO + Br \qquad (33)$$

Another example of the importance of box models is their application to the analysis of ATMOS (Atmospheric Trace Molecule Spectroscopy) data from the space shuttle [Michelsen et al., 1996]. These observations have indicated that our knowledge of the partitioning of chlorine is incomplete (Figure 3.4) and that other chemical reactions are required to understand the data. Because the partitioning at midlatitudes takes place over several weeks and conditions within the air parcels are believed to be relatively uniform, a box model can be used with some assurance to study the relevant processes. Since the amount of active chlorine stored in reservoirs is important, the results of these analyses will have a significant impact on our understanding of the role of chlorine in the ozone chemical budget.

A recent balloon experiment and analysis [Osterman et al. 1997] has also pointed to deficiencies in our understanding of ozone production at altitudes of 40–50 km where transport should not be important. The experiment, which provided accurate measurements of OH, HO_2, NO , ClO and other radicals and precursors mentioned earlier, showed that ozone loss exceeded production by some 35% at these altitudes, thus revealing a serious discrepancy in our current understanding of the the ozone production and loss scheme at these altitudes and indicating a serious flaw in our comprehension of ozone chemistry.

One-dimensional (in height) chemical diffusion models represent the atmosphere as a series of boxes stacked vertically and connected by diffusive processes. In the past, these have proved very useful for preliminary and exploratory estimates of atmospheric chemistry, since much more chemistry could be incorporated in these models than in more complex models that had to account for a wider array of physical processes. However, it has become clear that the atmosphere is too complex to be understood simply in terms of a vertically connected column. In addition, computer power has burgeoned over the past 10 years to the point where chemistry that was once tractable only in a box or 1D model can readily be carried in higher dimensional models.

The next level of complexity is addressed by models that use two spatial variables. These are known as two-dimensional (2D) models, and there are two main types. In the first type, the simulation is on a vertical slice of the atmosphere, usually a meridional plane, and the spatial variables might be height and latitude. In the other type, the simulation is over a horizontal or quasi-horizontal surface such as an isentropic surface, and the variables might typically be latitude and longitude. Models of the first type carry more dynamical information than 1D models but are limited by the lack of longitudinal (zonal) variation. However, they can be readily run for much longer periods than current 3D models, and so scenarios encompassing time periods of hundreds of years can be investigated (see, for example, Tie et al. [1994] for one such model).

Horizontal models in 2D using surfaces (usually potential temperature surfaces) that approximate the motion of air parcels on a time scale of a few weeks have proved very important in advancing our understanding of the detailed development of the filamentary structures discussed in Chapter 2 and their impact on atmospheric chemistry. New studies performed at very high spatial resolution [Edouard et al. 1996; Chipperfield et al. 1997] of Arctic ozone depletion, for example, have underlined the uncertainty in the modelling of ozone depletion that arises as a result of scale-dependent diffusion. A major advantage of these models is that they allow investigation of chemical and dynamical processes on a scale not accessible by more complex models.

With the increase in computational power, three-dimensional (3D) models will be a very important tool for future work. At the present time, 3D models with full chemistry can be used to investigate long-term scenarios that even only 10 years ago or less were at the limit of feasibility of 2D models. Various types of 3D models can be distinguished. There are, for example, 3D chemical transport models (CTMs) that solve the continuity equation for many chemical species: thus, the species can be transported around by wind fields and allowed to interact with each other. The wind fields and other meteorological data that are used can be derived from weather forecast models or atmospheric general circulation models (AGCMs). However, chemical changes in these models do not feed back on dynamics and transport or heating.

AGCMs are 3D models that extend from the surface to the middle atmosphere and higher and have detailed representation of physical and dynamical processes but limited horizontal resolution (~300–500 km). These models can now be run with interactive chemistry and are used to understand and explore the terrestrial climate and its response to perturbations, natural and anthropogenic. Weather forecast models are much like AGCMs but are run at much higher horizontal resolutions (~50–100 km) in order to resolve detailed weather patterns. They are usually used to simulate (forecast) the weather on time scales from days to a few months at most. Interactive chemistry has also been added to these models in order to investigate the effect of stratospheric ozone on long-range forecasting and to attempt to improve the forecasting of ozone loss over the Arctic.

Canada is making significant contributions to the modelling of the middle atmosphere. The Canadian Middle Atmosphere Model (CMAM), is being built by a university and government consortium involving the University of Toronto, York University, the University of Quebec at Montreal (UQAM), McGill University, Dalhousie University, the Atmospheric Environment Service's Canadian Centre for Climate Modelling and Analysis (AES-CCCma), and the Institute for Space and Terrestrial Science (ISTS). The CMAM is a three-dimensional global general circulation model that has a vertical domain extending from the surface to an altitude of about 100 km [Beagley et al. 1997]. The starting point for the development of CMAM was the CCCma-GCM II [McFarlane et al. 1992]. The modelling of the physics and dynamics of the original model has been modified to cope with the exigencies of the stratosphere and mesosphere. The heating parameterization has been improved [Fomichev and Blanchet 1995], and gravity wave parameterizations have been added [Hines 1997; Medvedev and Klaassen 1995]. Chemistry has also been added and experiments have been run with interactive chemistry [de Grandpré et al. 1997]. The current capabilities of the model [Shepherd 1995; Beagley et al. 1997; de Grandpré et al. 1997] are comparable to those of the most advanced models developed elsewhere.

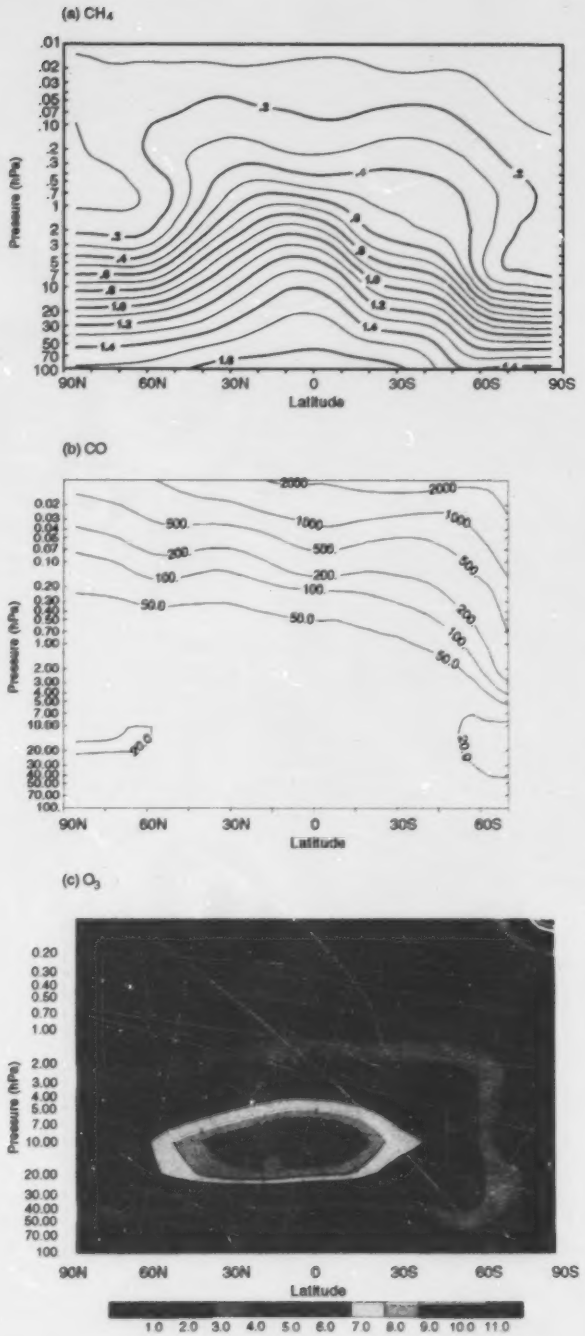

Figure 3.5 (a) August zonal mean cross-section of CH_4 mixing ratios (ppmv) from the CMAM model. (b) June zonal mean cross-section of daytime CO mixing ratios (ppbv) (70°S–90°N) from the CMAM model. (c) July zonal mean cross-section of O_3 mixing ratios (ppmv). (From de Grandpré et al. [1997].)

Some of the results shown in Figure 3.5 give an idea of the extent of the modelling results and may be compared with measurements. Panel (a) shows stratospheric CH_4, for which the current version of the model does a reasonable job of modelling the measured distribution as observed by UARS [cf. de Grandpré et al. 1997]. Other diagnostic tools such as time series of species ratios for N_2O, O_3, NO_2, and CO_2, as mentioned in section 3.2, will be used to analyse the model's transport characteristics [e.g., Volk et al. 1996 and references therein]. Panel (b) in Figure 3.5 shows the daytime distribution of carbon monoxide (CO) for June in the stratosphere and mesosphere and illustrates the downward motion in the winter polar vortex region. This result is also in quite good agreement with the UARS CO measurements of Lopez-Valverde et al. [1996]. Panel (c) shows the O_3 field developed by the model, and it compares quite well with measured values (Figure 1.7).

As noted in Chapter 1, Canada was one of the first countries to introduce ozone and UV-B forecasts [Burrows et al. 1994]. However, there is now also a fledgling research capability to do limited chemical- and transport-based ozone forecasts for a fairly complete suite of stratospheric chemicals. In the past year gas phase chemistry has been added to the Canadian Meteorological Centre's Spectral Finite Element (SEF) forecast model [Sandilands et al. 1996], and heterogeneous chemistry is currently being added. Such a model will allow improved forecasts of ozone depletion in the Arctic, particularly if used with chemical data assimilation.

3.4 Data Assimilation

Data assimilation employs a variety of techniques to turn four-dimensional (4D) non-synoptic (often satellite) data into a global 4D time series. In the past the technique has generally been limited to meteorological data, and most data assimilation has been 3D in nature for fixed synoptic times. However, recent efforts have been directed to the assimilation of chemical data [e.g., Fisher and Lary 1995]. Through this process the information in the measurement data may be validated by use of a good dynamical model, or alternatively the data can be fed back into the model to improve the representation of dynamics. In other words, chemistry can aid dynamics and vice-versa. In this manner, we can improve our knowledge of the ozone field by incorporating sonde, lidar, and satellite measurements.

The Middle Atmosphere Initiative (MAI) [Tarasick et al. 1996] is a new data assimilation project that has recently begun in Canada under the aegis of AES, with university

support and the interest of the Canadian Space Agency (CSA). Compared to the expense of a satellite mission, data assimilation is a means of obtaining a great deal of added value for a relatively modest increase in cost. Although the current focus of the MAI is the stratosphere, associated tropospheric projects, such as the data assimilation of MOPITT tropospheric CO data, are also being undertaken.

3.5 Ozone Loss Calculations

As noted above, models are important both as diagnostic and prognostic tools. To be useful as prognostic tools, however, they require validation. Comparison with observations is one stage of this process. Frequently this is an interactive process, with observations pointing to limitations in the modelling process (as we have noted above) or modelling underscoring inconsistencies in the observations. We have already discussed some of the intercomparisons above, and here we discuss the ability of the models to reproduce the measured trends in ozone depletion.

Certainly current models do quite well in reproducing the general behaviour of ozone in the atmosphere. Nevertheless, as we have stressed above, there still appears to be a disagreement between calculated and measured ozone levels near the stratopause, with the models overestimating ozone loss by about 30% [e.g., Osterman et al., 1997]. Careful comparison has also revealed discrepancies between modelled and observed ratios of active to reservoir species for Cl_y. However, the use of rates tuned to yield a better simulation of the ratio of ClO to HCl does produce trends that are more consistent with observations. Clearly more laboratory work needs to be done to clarify this situation.

In the lower stratosphere the situation is reversed, in that the models do not calculate sufficient ozone loss. There is some disagreement between the different measurements, such as those from SAGE, SBUV, and sondes. However, ozone losses calculated by the models are all too small in the 15–20 km region. Whether this is a problem with chemistry or transport (to date, the only long-term simulations of this region have been 2D) remains to be seen. In addition, many 2D models have not been run with heterogeneous bromine chemistry.

Both 2D and 3D models [e.g., Jackman et al. 1996; Rasch et al. 1995] are able to produce reasonable simulations of stratospheric column ozone amounts. Figure 3.6 shows the results from a 2D simulation of column ozone for the last 20 years [Jackman et al. 1996]. However, the simulations of vertical profiles are far from being perfect, and certainly it appears as if limitations in our representation of the transport are

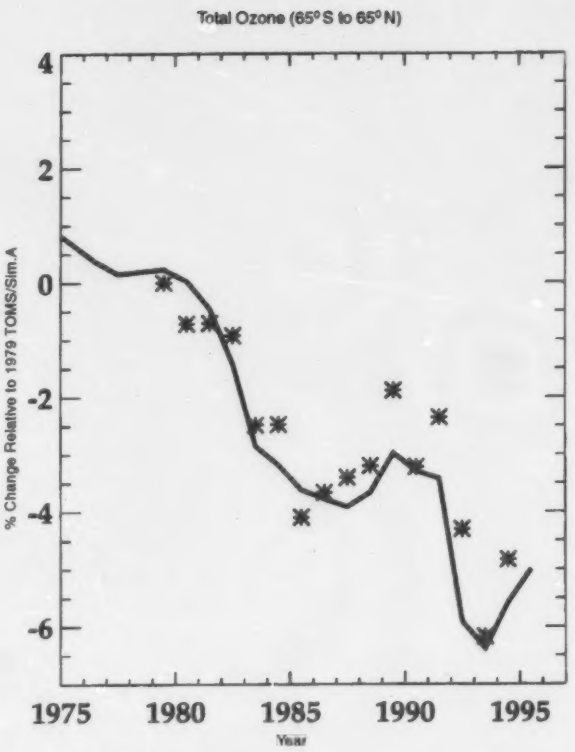

Figure 3.6 Total ozone changes (%) between 1975 and 1995 for annually averaged values integrated between 65°S and 65°N for TOMS version 7 (stars) and GSFC 2D model simulation (solid line). (From Jackman et al. [1996].)

constraining our ability to better simulate stratospheric ozone (see Chapter 2).

A tremendous natural experiment began on June 15, 1991, with the eruption of Mt. Pinatubo, resulting in the deposition of more than 20 MT of SO_2 into the stratosphere and the subsequent generation of sulphate aerosols. Simulations of this phenomenon indicate that the presence of these aerosols led to the heating of the stratosphere and cooling of the troposphere [Jiang et al. 1997; Hansen et al. 1992]. Ozone was also affected by virtue of the perturbation of the nitrogen reservoirs by the conversion of N_2O_5 into HNO_3 (reaction 14) within the sulphate aerosols, which in turn affected the Cl_x and to some extent the Br_x reservoirs. Furthermore, because of the generation of HOBr by reaction 15 and production of OH by reaction 17, the lower stratospheric budget was greatly perturbed [Danilin and McConnell 1995; Lary et al. 1996; Chartrand and McConnell 1997]. Additionally, the heating altered the transport patterns and the dynamical lifetimes of the ozone, and as a result loss processes could act for longer periods.

Generally the models estimate ozone loss in the Antarctic relatively well. Moreover, these estimates do not appear to be too sensitive to differences in detail in the representation of the hetereogeneous chemistry mechanism: as long as processing converts HCl and $ClNO_3$ to Cl_2 and other photolabile species, then there will be substantial O_3 loss.

In the Arctic the situation seems less clear. The details of the processing of the reservoir species, as calculated from the ozone loss, appear to be more important. For example, ozone loss as calculated by some groups appears to be too low by about 40% (see references in Edouard et al. [1996]), whereas Bregman et al. [1997] suggest that the measured depletion and modelling are in reasonable agreement. Furthermore, as we have noted above, this may indicate a problem with the limited resolution of the CTMs used to date rather than a limitation of our knowledge of the chemistry [Edouard et al. 1996]. In addition, because the Arctic temperatures are higher than those in the Antarctic, knowledge of temperatures appears to be much more critical for calculating Arctic ozone depletion: a few degrees can make a substantial difference in the extent of processing. In particular, there is uncertainty regarding the lowest values at which polar stratospheric clouds will form in the Arctic. For example, Pullen and Jones [1997] have compared objectively analysed (OA) temperatures from the UK Meteorological Office with independent sonde measurements and find that the OA temperatures are often too high by 1°–2° at the lowest values. Similar offsets are found for the lowest ECMWF (European Centre for Medium Range Weather Forecasting temperatures in the Arctic [Knudsen 1996]. Also, it is not clear if most models capture the different temperature scales within the Arctic: for example, PSCs can be induced by flow over mountains. But this is a mesoscale phenomenon and has not been directly addressed in most models to date. This effect is quite different from the scale effects introduced by the filamentation processes associated with dynamics.

Similar problems will beset the application of AGCMs to the ozone depletion problem over polar regions, since they will not capture specific events but rather the climatology of events. On the more positive side, they will allow an investigation of the interactions to play out in detail within the model on time scales not achievable by forecast models. More importantly, AGCMs offer the only means at present for probing the future of the ozone layer and climate-related effects.

One aspect of the ozone depletion problem that underlines the necessity of being able to simulate *both* dynamical and chemical processing is that of dilution effects. In the polar regions during the springtime (or just before in the Arctic), there is substantial depletion of ozone as a result of chemical destruction. At the end of spring, when the vortex breaks down, midlatitude ozone is transported into the vortex region and replenishes the loss. However, the depleted air is transported to lower latitudes and will modify the ozone budget in these regions. The ability to capture the details of this process accurately in a detailed simulation does not yet exist but must certainly be developed for the next generation of models.

3.6 Other Issues

3.6.1 Aircraft Impacts

As discussed in Chapter 2, determining the extent of the exchange of midlatitude and tropical air in the lower stratosphere is going to be a critical test of the models. It will also be a deciding factor in assessing the effects of a fleet of supersonic aircraft [Stolarski and Wesoky 1995]. In addition, O_3 is an important radiatively active gas in the vicinity of the tropopause [e.g., Ramaswamy et al. 1996], where most of the global O_3 depletion has occurred. Not only is this a region where stratospheric-tropospheric exchange is so uncertain, but it is also one that is currently perturbed by the present subsonic fleet [Thompson et al. 1996].

A report on the potential effects of a fleet of stratospheric aircraft [Stolarski and Wesoky, 1995] has indicated that impact estimates would be lessened by the inclusion of the effects of heterogeneous chemistry in the models. However, this assessment was based on 2D models with limited dynamics (by virtue of the 2D approximations) and without heterogeneous bromine chemistry on sulphates. The representation of heterogenous PSC chemistry was also limited, again by virtue of the zonal averaging inherent in the 2D models.

If a fleet of supersonic aircraft is built in the foreseeable future, then it will have to operate in a climate regime characterized by increasing CO_2 and thus enhanced stratospheric cooling. The increased NO_x, H_2O, and sulphates from these aircraft may result in an increase in the incidence of PSCs and thus more polar ozone loss. At midlatitudes lower temperatures will lead to the increased dissolution of HCl in sulphates, with more processing and ozone loss. Thus, there is a need for more careful modelling with 3D models.

3.6.2 Impacts on the Troposphere

As noted above, the stratosphere acts as a substantial source of ozone for the troposphere. The injection has been known for a long time and appears to be most pronounced in the springtime at high latitudes. Thirty years ago it was thought that this was the main source of tropospheric ozone, except perhaps in urban centres. However, it was gradually realized that the smog reactions shown earlier (reactions 4–8), driven

by volatile organic compounds (VOCs), NO_x (both from natural and anthropogenic sources), and sunlight, are important in the global production of tropospheric ozone. In the troposphere, loss processes for ozone include (1) deposition, mainly on land surfaces but also with slower deposition over water and snow, (2) conversion of NO to NO_2, and these to other NO_y species, which either wash out or deposit to the surface, (3) photolysis to $O(^1D)$ which reacts with water molecules, (4) possible loss in clouds, and perhaps (5) reaction with chlorine atoms at the sea surface.

In the troposphere, decreased levels of stratospheric ozone result in increased levels of UV-B and thus increased production of $O(^1D)$ from the photolysis of ozone. This production of $O(^1D)$ leads, in turn to the increased production of the hydroxyl (OH) radical as well as increased ozone destruction. Since OH reacts with many species in the troposphere, increasing production can have far-reaching effects. Methane, a greenhouse gas, is lost primarily via reaction with OH. CO, a product of anthropogenic combustion and biomass burning, is also lost via reaction with OH. As noted above, NO_2 is a player in the generation of ozone in the troposphere, and it is oxidized by OH to HNO_3. Consequently, an increase in OH could lead to a decrease in tropospheric ozone production.

On the other hand, this has to be weighed against possible increases in ozone, as increased OH levels can lead to more rapid destruction of VOCs and increased ozone production. The net effect of changes in stratospheric ozone on the troposphere will be complex. Tropospheric ozone levels may increase in certain regions due to increased UV-B and sources of NO_X and VOCs. However, in polar regions or other pristine regions with low levels of NO_X increased UV-B will lead to decreases in ozone.

The hydroxyl radical also plays a role in the oxidation of SO_2 to H_2SO_4 and thus in the formation of sulphate aerosols (both in the troposphere and stratosphere). Sulphate aerosols can act as condensation nuclei for the formation of cloud water droplets, thereby indirectly affecting climate. The aerosols also can affect climate directly by reflecting and absorbing solar and infrared radiation.

In addition to its potential effects on the intricate web of tropospheric chemistry (and its connections to climate), the alteration of stratospheric ozone will modify stratospheric heating. This, in turn, is likely to modify stratospheric dynamics and may thus alter the extent of the transport of stratospheric ozone into the troposphere in a manner that appears completely uncertain at the moment.

3.6.3 Climate Connections

Although levels of Cl_x may decrease in the coming years, the occurrence of heterogeneous reactions in the stratosphere could become more widespread as a result of the increased concentration of CO_2, which results in more efficient cooling to space. If, as is likely, cooler stratospheric temperatures result, this will lead to the enhanced solubility of HCl in the stratospheric aerosol and additional transformation of Cl_x to active ClO_x, resulting in enhanced O_3 depletion. Furthermore, the lower temperatures may alter the stratospheric circulation, which will, in turn, have an impact on the O_3 distribution.

The potential reduction in stratospheric temperatures noted in the previous paragraph applies to most latitudes. In the Arctic, it has been suggested that the areas at 50 hPa with temperatures cold enough to stimulate processing of NO_y and Cl_y on PSCs have been increasing in size over the last 31 years [Pawson and Naujokat 1997]. It is difficult to decide whether such a decrease in minimum temperatures is genuine or a reflection of previous limitations of temperature sondes.

It has also been suggested that in the Antarctic the breakup of the vortex has been delayed by 10–12 days over the past 10 years [Chubachi 1997]. This raises the question of whether the decrease of ozone (an infrared gas and solar heating gas) within the vortex has led to the stabilization of the vortex and thus increased the potential for a longer period of ozone loss. This mechanism may have played a role in causing the low Arctic ozone amounts observed in the past few winters.

We have not dealt explicitly with how the atmosphere/biosphere systems are likely to react to changing climate, although we did allude to some indirect effects. It is important to watch, however, for important feedbacks that may previously have been neglected or missed altogether.

3.6.4 Solar Flux Variation and Ozone

In terms of its effects on the ozone column, the most important region of the solar spectrum is the transmission window in the vicinity of 200–220 nm. Since the solar flux varies by a factor of 20–30% in this region [Lean 1989] over a solar cycle, the important variations in the ozone column that result must be allowed for in the extraction of ozone trends and in modelling scenarios that continue over a long period of time.

3.7 Future Directions

Although our understanding of processes affecting stratospheric ozone has increased enormously over the past 25 years, many important issues and questions have yet to be resolved.

- In the stratosphere the issue of gravity wave parameterization is important and must be solved if the middle atmosphere circulation is to be simulated more realistically. Understanding the details of how air is exchanged between the stratosphere and the troposphere is also extremely important, and it is expected that this will be a major area of research.
- At a recent SPARC (Stratospheric Processes and their Role in Climate) workshop held in France in October 1996, it was concluded that upper tropospheric chemistry is also likely influenced by heterogeneous processes. Over the next few years enhanced efforts will be made to include microphysical aerosol processes in stratospheric and tropospheric models in order to provide a more comprehensive understanding of heterogeneous reactions in liquids or on solid surfaces.
- In addition to the chemical aspects, there are also the climate effects of aerosols related to radiation processes and cloud formation.
- Another array of issues concerns the effects on ozone of aircraft, both the current subsonic fleet and the possible supersonic fleet. Will ozone in the lower stratosphere increase or decrease as a result of emissions from these aircraft? How far will the effluent of the supersonic fleet be transported? Have emissions from the current fleet increased tropospheric ozone, and, if so, what are the climate impacts?
- It is assumed that Cl_y in the stratosphere will begin to decrease in the next decade and that ozone will begin to recover, albeit slowly, shortly thereafter. It is imperative to continuing monitoring to determine whether this does indeed happen.

References

Beagley, S.R., J. de Grandpré, J.N. Koshyk, N.A. McFarlane and T.G. Shepherd, 1997. The first generation Canadian Middle Atmosphere Model: model description and climatology. *Atmos.-Ocean,* in press.

Bregman, A., M. van den Broek, K.S. Carslaw, R. Muller, T. Peter, M.P. Scheele, and J. Lelieveld, 1997. Ozone depletion in the later winter lower Arctic stratosphere: observations and model results. *J. Geophys. Res.,* **102,** 10815-10828.

Brewer, A.W., 1949. Evidence for a world circulation provided by the measurements of helium and water vapour distribution in the stratosphere. *Quart. J. R. Met. Soc.,* **75,** 351–363.

Burrows, J.P., K.V. Chance, A.P.H. Goede, R. Guzzi, B.J. Kerridge, C. Muller, D. Perner, U. Platt, J-P Pommereau, W. Schneider, R.J. Spurr, H. van der Woerd, et al., 1993. *Global Ozone Monitoring Experiment interim science report.* Report ESA SP-1151. T.D. Guyenne and C. Readings, eds. Noordwijk, the Netherlands: ESA Publications Division, ESTEC.

Burrows, W.R., M. Vallé, D.I. Wardle, J.B. Kerr, L.J. Wilson, and D.W. Tarasick, 1994. The Canadian operational procedure for forecasting total ozone and UV radiation. *Met. Apps.,* **1,** 247–265.

Chartrand, D.J., and J.C. McConnell, 1997. Heterogeneous bromine chemistry and the ozone budget in the lower midlatitude stratosphere. Working paper, Dept. of Earth and Atmospheric Science, York University, Toronto.

Chipperfield, M.P., E.R. Lutman, J.A. Kettleborough, J.A. Pyle, and A.E. Roche, 1997. Model studies of chlorine deactivation and formation of $ClONO_2$ collar in the Arctic polar vortex. *J. Geophys. Res.,* **102,** 1467–1478, 1997.

Chubachi, S., 1997. Annual variation of total ozone at Syowa Station, Antarctica. *J. Geophys. Res.,* **102,** 1349–1354.

Clyne, M.A.A., and R.T. Watson, 1977. Kinetic studies of diatomic free radicals using mass spectrometry. *J. Chem. Soc. Faraday Trans.,* **1/73,** 1169–1187.

Danilin, M.Y., and J.C. McConnell, 1994. Heterogeneous reactions in a stratospheric box-model: a sensitivity study. *J. Geophys. Res.,* **99,** 25681–25696.

Danilin, M.Y., and J.C. McConnell, 1995. Stratospheric effects of bromine activation on/in sulfate aerosol. *J. Geophys. Res.,* **100,** 11237–11243.

Edouard, S., B. Legras, F. Lefèvre, and R. Eymard, 1996. The effect of small-scale inhomogeneities on ozone depletion in the Arctic. *Nature,* **384,** 444-447.

de Grandpré, J., J.W. Sandilands, J.C. McConnell, S. R. Beagley, P. Croteau, and M. Y. Danilin, 1977. Chemistry in the Canadian Middle Atmosphere Climate Model. *Atmos.-Ocean,* forthcoming.

Farman, J.C., B.G. Gardiner, and J.D. Shanklin, 1985. Large losses of ozone in Antarctica reveal seasonal ClO_x/NO_x interaction. *Nature,* **315,** 207–210.

Fisher, M., and D.J. Lary, 1995. Lagrangian four-dimensional variational data assimilation of chemical species. *Quart. J. R. Met. Soc.,* **121,** 1681–1704.

Fomichev, V.I., and J-P. Blanchet, 1995. Development of the new CCC/GCM long-wave radiation model for extension into the middle atmosphere, *Atmos.-Ocean,* **33,** 513–529.

Hansen, J., A. Lacis, R. Ruedy, and M. Sato, 1992. Potential climate impact of Mount Pinatubo eruption, *Geophys. Res. Lett.,* **19,** 215–218.

Hines, C.O., 1997. Doppler-spread parameterization of gravity-wave momentum deposition in the middle atmosphere. Part I: Basic formulation. *J. Atmos. Terr. Phys.,* **59,** 371-386.

Hofmann, D.J., and S. Solomon, 1989. Ozone destruction through heterogeneous chemistry following the eruption of El Chichon. *J. Geophys. Res.,* **94,** 5029–5041.

Holton, J.R., P.H. Haynes, M.E. McIntyre, A.R. Douglass, R.B. Rood, and L. Pfister, 1995. Stratosphere-troposphere exchange, *Rev. Geophys.,* **33,** 404–439.

Jackman, C.H., E.L. Fleming, S. Chandra, D.B. Considine, and J.E. Rosenfield, 1996. Past, present and future modeled ozone trends with comparisons to observed trends. *J. Geophys. Res.,* **101,** 28753–28767.

Jiang, J.H., S.R. Beagley, J.C. McConnell, J. de Grandpré, W.F.J. Evans, and H.W. Barker, 1997. A simulation of Pinatubo aerosol climate effects using the Canadian Climate Centre GCM II. Working paper. Dept. of Earth and Atmospheric Science, York University, Toronto.

Knudsen, B.M., 1996. Accuracy of Arctic stratospheric temperature analyses and the implications for the prediction of polar stratospheric clouds. *Geophys. Res. Lett.,* **25,** 3747–3750.

Koop, T., and K.S. Carslaw, 1996. Melting of $H_2SO_4 \cdot 4H_2O$ particles upon cooling: implications for polar stratospheric clouds. *Science,* **272,** 1638-1641.

Lary, D.J., Gas phase atmospheric bromine photochemistry. *J. Geophys. Res.*, **101,** 1505–1516.

Lary, D.J., M.P. Chipperfield, R. Toumi, T.M. Tenton, 1996. Heterogeneous atmospheric bromine chemistry. *J. Geophys. Res.*, **101,** 1489–1504.

Lean, J., 1989. Contribution of UV irradiance variations to changes in the Sun's total irradiance. *Nature,* **244,** 197–200.

Lelieveld, J., B. Bregman, F. Arnold, V. Burger, P.J. Crutzen, H. Fischer, A. Waibel, P. Siegmund, and P.F.J. van Velhoven, 1997. Chemical perturbation of the lowermost stratosphere through exchange with the troposphere. *Geophys. Res. Lett.*, **24,** 603–606.

Lopez-Valverde, M.A., M. Lopez-Puertas, J.J. Remedios, C.D. Rogers, F.W. Taylor, E.C. Zipf, and P.W. Erdman, 1996. Validation of measurements of carbon monoxide from the improved stratospheric and mesospheric sounder. *J. Geophys. Res.*, **101,** 9929–9955.

McFarlane, N.A., G.J. Boer, J-P. Blanchet, and M. Lazare, 1992. The Canadian Climate Centre second generation GCM and its equilibrium climate. *J. Clim.*, **5,** 1013–1044.

Medvedev, A.S., and G.P. Klaassen, 1995. Vertical evolution of gravity wave spectra and the parameterization of associated wave drag. *J. Geophys. Res.*, **100,** 25841–25853.

Michelson H.A., R.J. Salawitch, M.R. Gunson, C.Aellig, N. Kampfer, M.M. Abbas, M.C. Abrams, et al., 1996. Stratospheric chlorine partitioning: constraints from shuttle-borne measurement of [HCl], [$ClNO_3$], and [ClO]. *Geophys. Res. Lett.*, **23,** 2361–2364.

Molina, L.T., and M.J. Molina, 1987. Production of Cl_2O_2 from the self-reaction of the ClO radical. *J. Phys. Chem.*, **91,** 433-436.

Mote, P.W., K.H. Rosenkof, M.E. McIntyre, E.S. Carr, J.C. Gille, J.R. Holton, J.S. Kinnersley, H.C. Pumphrey, J.M. Russell III, and J.W. Waters, 1996. An atmospheric tape recorder: the imprint of tropical tropopause temperatures on stratospheric water vapor. *J. Geophys. Res.*, **101,** 3989-4006.

Osterman, G. B., R.J. Salawitch, B. Sen, G.C. Toon, R.A. Stachnik, H.M. Pickett, J.J. Margitan, J-F. Blavier, and D.B. Peterson, 1997. Balloon-borne measurements of stratospheric radicals and their precursors: implications for the production and loss of ozone, *Geophys. Res. Lett.*, **24,** 1107–1110.

Pawson, S., and B. Naujokat, 1997. Trends in daily wintertime temperatures in the northern stratosphere. *Geophys. Res. Lett.*, **24,** 575–578.

Pullen, S., and R. L. Jones, 1997. Accuracy of temperature from UKMO analyses of 1994/95 in the Arctic winter stratosphere. *Geophys. Res. Lett.*, **24,** 845–848.

Ramaswamy, V., M.D. Schwarzkopf, and W.J. Randel, 1996. Fingerprint of ozone depletion in the spatial and temporal pattern of recent lower-stratospheric cooling. *Nature,* **382,** 616–618.

Rasch, P.J., B.A. Boville, and G.P. Brasseur, 1995. A three-dimensional General Circulation Model with coupled chemistry for the middle atmosphere. *J. Geophys. Res.*, **100,** 9041–9071.

Salawitch, R.J., S. Wofsy, P. Wennberg, R. Cohen, J. Anderson, D. Fahey, R. Gao, et al., 1994. The distribution of hydrogen, nitrogen, and chlorine radicals: implications for the heterogeneous production of HNO_2. *Geophys. Res. Lett.*, **21,** 2551–2554.

Sandilands, J.W., L. Neary, J.W. Kaminski, H. Ritchie, and J.C. McConnell, 1996. Developing an interactive chemistry solver for inclusion with SEF, the Canadian global weather forecast model. Paper presented at 30th CMOS Congress, Toronto, May 26–31, 1996.

Schoeberl, M.R., A.E. Roche, J.M. Russell III, D. Ortland, P.B. Hays, and J.W. Waters, 1997. An estimation of the dynamical isolation of the tropical lower stratosphere using UARS wind and trace gas observations of the quasibiennal oscillation. *Geophys. Res. Lett.*, **24,** 53–56.

Shepherd, T.G., 1995. The Canadian MAM project. *CMOS Bull.*, **23,** 3–12.

Stolarski, R.S., and H.L. Wesoky (eds.), 1995. *The atmospheric effects of stratospheric aircraft: a fourth program report.* NASA reference publication 1359. Washington: National Aeronautics and Space Administration.

Tarasick, D.W., G. Brunet, R. Daley, P. Gautier, and W.E. Ward, 1966. A Canadian Middle Atmosphere Initiative. XVIII Quadrennial Ozone Symposium, L'Aquila, Italy, 12–21 September 1996.

Thompson, A.M., R.R. Friedl, and H.L. Wesoky (eds.), 1996. *Atmospheric effects of aviation: first report of the subsonic assessment program.* NASA Reference publication 1385. Washington: National Aeronautics and Space Administration.

Tie, X., G. Brasseur, B. Briegleb, and C. Granier, 1994. Two-dimensional simulation of Pinatubo aerosol and its effect on stratospheric ozone. *J. Geophys. Res.*, **99**, 20545–20562.

Tolbert, M.A., 1996. Polar clouds and sulfate aerosols. *Science*, **272**, 1597.

Volk, C.M., J.W. Elkins, D.W. Fahey, R.J. Salawitch, G.S. Dutton, J.M. Gilligan, M.H. Proffit, M. Lowenstein, J.R. Podolske, K. Minschwaner, J.J. Margitan, and K.R Chan, 1996. Quantifying transport between the tropical and mid-latitude lower stratosphere. *Science*, **272**, 1763–1768.

Yung, Y.L., J.P. Pinto, R.T. Watson, and S.P. Sander, 1980. Atmospheric bromine and ozone perturbations in the lower stratosphere. *J. Atmos. Sci.*, **37**, 339–353.

The Influence of Ozone and Other Factors on Surface Radiation

4.1 Introduction

Ozone is important because of its interactions with solar radiation and with thermal radiation emitted by the atmosphere and the earth's surface. Partial absorption by ozone moderates the amount of solar UV radiation that reaches the ground. Increases in exposure to this radiation, particularly in the UV-B range, can be harmful to living organisms. Absorption by ozone and the influences of other variable factors on UV radiation are the main subjects of this chapter.

Ozone is the main source of radiative heating in the stratosphere through its absorption of solar radiation in the UV and the 550–650 nm range of wavelengths. Also, because ozone is a greenhouse gas like carbon dioxide and water vapour, the increases in tropospheric ozone that have occurred during this century have had a warming effect on the planet. On the other hand, the depletion of stratospheric ozone is likely to have partially offset the warming effects of increases in other greenhouse gases during the past two decades. These important roles of ozone are examined thoroughly in the WMO/UNEP and IPCC assessments [WMO 1991, 1994; IPCC 1990, 1994, 1995] but will not be addressed in detail here. In addition, ozone-depleting substances, notably the CFCs, are powerful greenhouse gases by virtue of their having absorption properties at wavelengths in the thermal infrared, where there is little absorption by other atmospheric constituents. These regions, between approximately 8 and 13 μm, are called the atmospheric infrared windows. Under various schemes of comparison it is estimated that CFC-11 and CFC-12 are from 2000 to 4000 times as effective as carbon dioxide as global warming agents. Ground-based measurements of the radiation emitted by several ozone-depleting gases are discussed in Section 4.3.

The effects of UV radiation on humans can be mitigated to some extent by changes in behaviour. The chapter therefore concludes with a discussion of two Canadian-developed programs, the Ozone Watch and the UV Index programs, that promote understanding of ozone depletion and the importance of reducing personal exposure to UV radiation.

4.1.1 Introduction to Ozone and UV Radiation.
Ozone absorbs so strongly in the UV-C range (below 280 nm) that solar radiation at these wavelengths does not reach the earth's surface. As the wavelength increases through the UV-B range (280–315 nm) and into the UV-A (315–400 nm), ozone absorption becomes weaker, until it is undetectable at about 340 nm. Figure 4.1 shows several spectra including the spectrum (A) of solar radiation measured above the atmosphere. The fractions of solar energy above the atmosphere in the UV-B and UV-A ranges are approximately 1.5% and 7% respectively. The figure also shows spectra measured at the ground near midday on two very clear days in mid-June. (These two spectra, curves B and C, are almost indistinguishable.) The fine curve (D) is computed from the extraterrestrial spectrum (A) and the absorption by the average measured ozone amount for the two days. It is above the measured ground-level spectra, but otherwise almost identical to them. One may conclude that, for these two clear days, the ground-level spectra are mostly the result of ozone absorption, with a relatively constant extra attenuation of about 40% due to air molecules and background aerosols.

The spectra in Figure 4.1 thus illustrate the simplest case in which ozone determines the intensity of solar UV radiation at ground level. In general, UV intensity varies considerably as a result of fluctations in cloud cover, ground albedo, aerosols, and other atmospheric constituents. In the context of possible

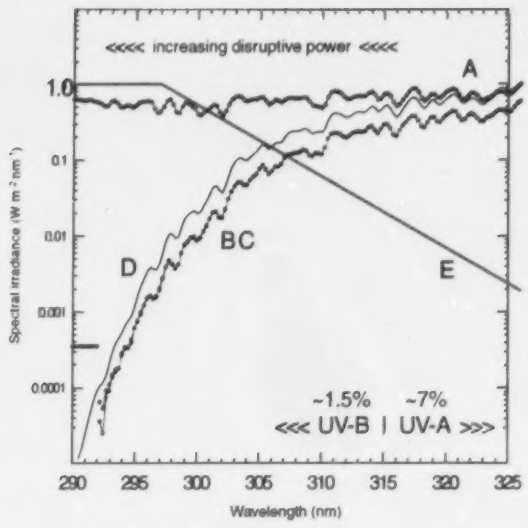

Figure 4.1 The solar spectrum above the atmosphere (A) and at ground level (B,C), ozone absorption (D), and sunburning (E).

biological consequences, the effect of an ozone-related change in the UV environment is likely to depend on how large that change is in comparison to the normal range of natural variability. For this reason, the variability and its causes must be studied more thoroughly.

Changes in UV radiation can be expressed in a variety of ways, and the question of which particular measure is most relevant to a given biological effect is often complex and difficult to resolve. One option is the total UV irradiation received over a specified area during the summer of each year. Over Toronto, for example, as shown later in this chapter, total summer irradiation at 300 nm has changed during the past decade by an amount comparable to the typical year-to-year variability and consistent with the observed ozone change. A statistical study based on satellite data [Lubin and Jensen 1995] reaches a similar conclusion for the change during the past 20 years in the erythemally weighted irradiation (i.e., weighted in terms of skin-reddening effectiveness) for July over southern Canada. Using monthly or seasonal irradiation as in these two examples is convenient but not necessarily correct in relation to a given biological effect, since some effects may be more dependent on peak values of UV encountered during the early growing season. However, statistics of peak values of UV or other derivative statistics have received little or no attention in the literature to date.

A similar question refers to what wavelengths should be considered. Action spectra, as discussed in Chapter 5, deal with the problem of impact variations across a range of wavelengths. An action spectrum, for a particular biological effect, expresses the effectiveness of radiation at each wavelength as a fraction of the effectiveness at a standard wavelength, such as 298 nm in the case of the erythemal action spectrum of the Commission internationale de l'éclairage (CIE). In principle, the wavelength integration of the product of an irradiance spectrum with the action spectrum yields the effectiveness of that spectrum at producing the given effect. For this to be valid, the effect must satisfy two requirements: first, additivity of effects at different wavelengths and, second, reciprocity, which means that the effect must depend on dose (irradiation) rather than dose rate (irradiance). Reciprocity and additivity are probably satisfied for a relatively simple effect like skin reddening, but there is no reason to expect them to be satisfied for other, more complex, effects. In this chapter, only the CIE action spectrum, curve E in Figure 4.1, has been illustrated. For a fairly wide range of atmospheric conditions, the CIE-weighted irradiance increases by approximately 1.2% for a decrease of 1.0% in the ozone value. The ratio 1.2 is called the radiometric amplification factor (RAF) of the CIE spectrum. Recently measured action spectra for plant damage [Quaite et al. 1992] and induction of squamous cell skin cancer in mice [deGruijl and van der Leun 1994] have RAFs that are also close to 1.2, while the full range of reported RAFs is from 0.2 to 4.0 [Madronich 1992].

4.2 Observed Dependencies of UV Changes on Ozone, Sulphur Dioxide, Clouds, Aerosol, and Snow

There is strong evidence to suggest that the total ozone decline in northern midlatitudes has been accompanied by increases in solar UV irradiance at the earth's surface [Kerr and McElroy 1993; Zerefos et al. 1995]. However, UV irradiance depends on many other variables, such as cloud condition, albedo, atmospheric aerosol, and pollution, that make it difficult to measure the effects of ozone decline on irradiance. Establishing a direct link between ozone and UV irradiance and separating the ozone-related component in UV irradiance from other components provides a better understanding of the causes of UV changes. The following are some of the approaches used to quantify that link.

Numerous studies [e.g., Frederick et al. 1993; Eck et al. 1995; Bojkov et al. 1995] show that it is possible to estimate UV irradiance from total ozone data. The reverse process, the derivation of total ozone amounts from UV radiation, is applied by the Dobson and Brewer methods when measuring total ozone using zenith sky radiance. However, to obtain reliable results it is necessary to have a set of parallel zenith sky and direct sun measurements [e.g., Komhyr 1980]. Stamnes et al. [1991] have also suggested the use of a radiative transfer model to derive total ozone from measurements of

horizontal irradiance at two wavelengths, 305 nm and 340 nm.

Total ozone may also be derived using the whole 290–325 nm irradiance spectrum measured by the Brewer spectrometer, and, conversely, the spectrum may be derived from the ozone amount [Fioletov et al. 1997]. A statistical model that relates the spectrum to the ozone amount and that was originally developed for quality control of UV spectral data is the basis of a new algorithm that is used to calculate the ozone value from the irradiance spectrum. This technique has proved to be a useful addition to the direct sun and zenith sky techniques.

UV irradiance measurements made by Brewer spectrophotometers at seven stations (Toronto, Edmonton, Winnipeg, Sapporo, Tateno, Kagoshima, and Naha) for the period 1989–1995 were used to establish the statistical model. The stations have between four and seven years of continuous UV observations and a set of parallel Dobson or Brewer total ozone measurements. All these data are available from the World Ozone and UV data Centre (WOUDC), Toronto.

There are two parts to the statistical analysis on which the model is based. The first is a comparison of irradiance values at all the wavelengths in the spectral range with the irradiance value at 324 nm, where ozone has least (and virtually negligible) absorption. This analysis primarily quantifies the dependence of UV-B irradiance on ozone. The second part of the analysis is the assessment of the absolute irradiance at 324 nm. Variation of irradiance at this wavelength is due to other causes besides ozone.

A discussion of observed dependencies of UV irradiance on ozone and other variables is given in the following sections.

4.2.1 Dependence on Ozone

Figure 4.2 shows the value of the mean logarithm of the ratio between solar irradiance at wavelength λ and irradiance at 324 nm as a function of wavelength and solar zenith angle for total ozone equal to 300 DU. For wavelengths between 305 and 315 nm the Umkehr effect [Götz 1931] is clearly seen: the ratio as a function of increasing zenith angle decreases up to a certain value of zenith angle and increases thereafter.

Comparison of the surface shown in Figure 4.2 with another surface representing a different total ozone value allows the calculation of the sensitivity of UV irradiance to changes in ozone as a function of wavelength and solar zenith angle. The sensitivities for a 1% decrease in ozone are shown in Figure 4.3.

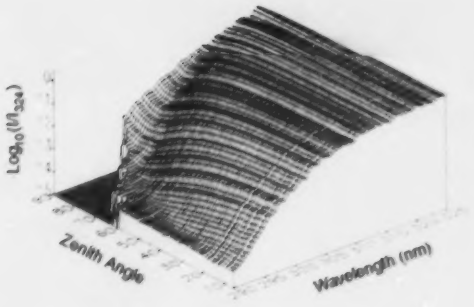

Figure 4.2 Logarithm of ratio between UV-B irradiance at wavelength λ and irradiance at 324 nm for 300 DU of total ozone as a function of zenith angle and wavelength.

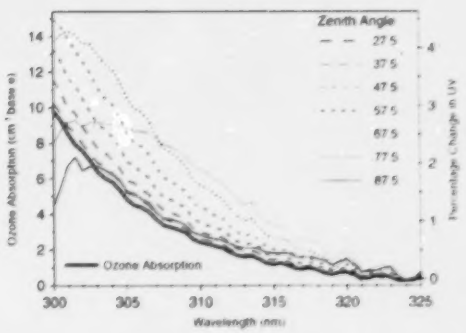

Figure 4.3 Sensitivity of UV irradiance to total ozone amount in percent change per 1% change in total ozone (for a total ozone amount of 300 DU) as a function of wavelength for different zenith angles. The bold continuous line shows the ozone absorption spectrum.

Figures 4.4a and 4.4b show measured and calculated spectra for two cases with approximately the same zenith angles and 324 nm irradiances but different total ozone values (about 250 and 500 DU respectively) and 3σ limits. The ratio of irradiance at any wavelength between 300 and 323 nm to that at 324 nm can be used to derive total ozone. Figures 4.4c and 4.4d show calculated total ozone as a function of wavelength. The accuracy of the retrieval depends on zenith angle and wavelength.

Total ozone was calculated from UV spectra which have been measured at Toronto since 1989. Figure 4.5 shows the monthly average departures from pre-1989 values for the UV spectral calculations compared with those of Brewer and Dobson direct sun measurements and satellite measurements. The agreement between all types of measurements is generally very good.

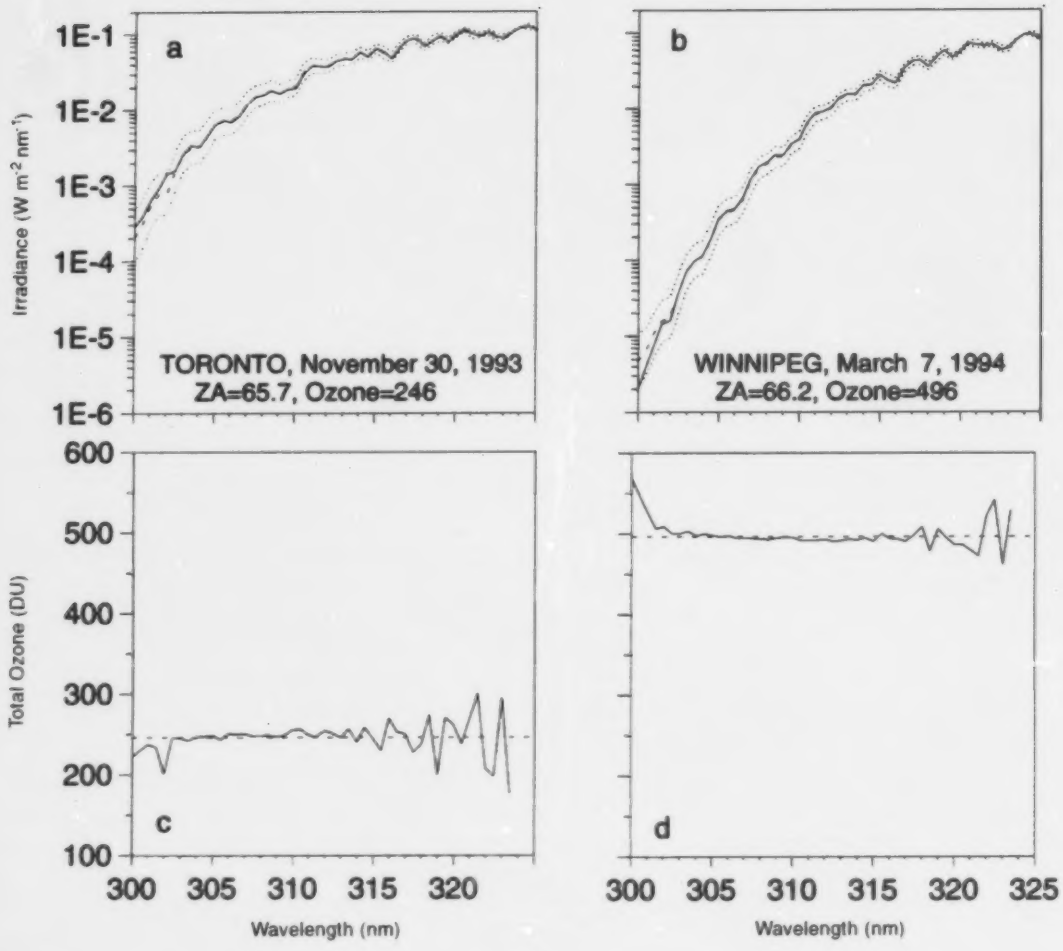

Figure 4.4 (a and b): Examples of two UV irradiance spectra (solid lines) measured for nearly the same zenith angles and 324 nm irradiance but for different total ozone amounts, estimated from Figure 4.2 (dashed lines) and the 3σ envelope (dotted lines). (c and d): Retrieved total ozone as a function of wavelength for the two spectra in (a) and (b), respectively. Dashed lines show direct sun total ozone measured values.

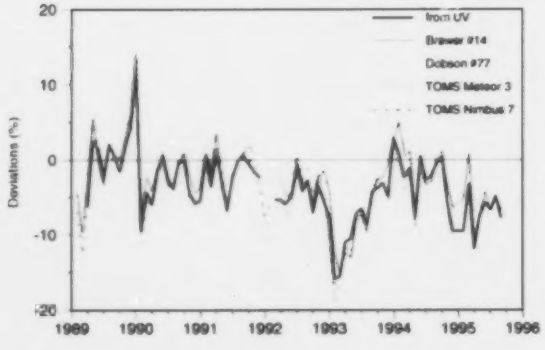

Figure 4.5 Monthly deviations of total ozone from pre-1989 level for Toronto, using Dobson #77 and Brewer #14 direct sun measurements, TOMS Nimbus 7 and Meteor 3 data, and retrieved estimates from Brewer #14 UV measurements.

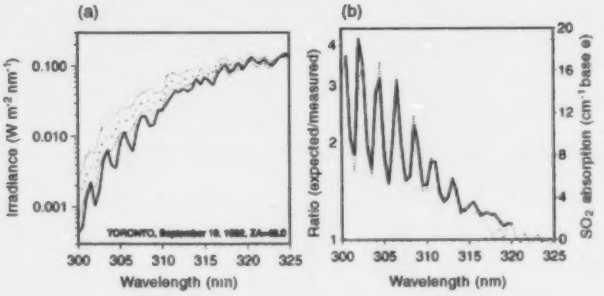

Figure 4.6 (a) Measured irradiance spectrum (solid line) and spectrum calculated from Figure 4.2 (dashed line) with 3σ envelope (dotted lines) for Toronto, September 19, 1992. (b) Ratio between estimated and measured irradiance (dotted line) and SO_2 absorption spectrum (solid line) of McGee and Burris [1987] at 210 K.

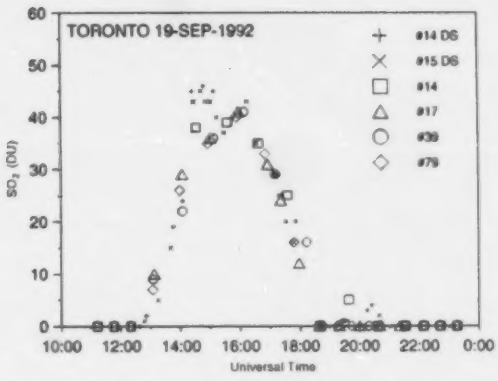

Figure 4.7 Total column sulphur dioxide derived from Brewer direct sun measurements (pluses and crosses) and from UV spectra (squares, triangles, circles, and diamonds) for September 19, 1992, at Toronto. Brewer instrument numbers are shown in the legend.

4.2.2 Dependence on SO_2

Occasionally, the measured UV spectrum will differ substantially from a spectrum predicted by the statistical model. One example is shown in Figure 4.6 (a) for Toronto on September 19, 1992, when the plume from the Mount Spurr, Alaska, volcanic eruption passed over the city [Krueger et al. 1995]. Most of the measured spectrum is outside the 3σ envelope and the difference exceeds 6σ at some wavelengths. The cause of these differences was identified as atmospheric SO_2, which has strong absorption bands in the UV-B spectral region, as shown in Figure 4.6 (b), for the resolution of the Brewer instrument. The ratio between the expected and measured spectra is also plotted. For some wavelengths the measured irradiance was 3 times lower than expected. The features of the ratio, however, reproduce the SO_2 absorption spectrum. Calculation of ozone from this spectrum results in values that overestimate ozone by 50 to 100 DU, depending on wavelength. The amount of SO_2 required to cause the absorption shown in Figure 4.6 is approximately 50 DU.

Figure 4.7 shows results of SO_2 values retrieved from UV spectra and direct sun SO_2 measurements for September 19, 1992, in Toronto. Both methods show the same pattern in SO_2 variations, and the difference between direct sun and global UV spectra methods is less than 20% for the time when maximum values of SO_2 were observed.

A summary of all days with more than 10 and 20 DU of SO_2 is shown for 13 localities in Table 4.1. Only days containing two or more observations at these levels have been included. The high SO_2 amounts over Kagoshima are associated with volcanic eruptions of nearby Mount Sakurajima and will be discussed further below. At all other stations, SO_2 levels above 20 DU were observed only once: that observation was recorded in Toronto when the plume from the Mount Spurr eruption passed overhead. Values between 10 and 20 DU were observed on fewer than 1% of the days, and most of these cases were associated with pollution. Since SO_2 values in the 10–20 DU range reduce the erythemally weighted UV irradiance by only a few percent, the overall effect of SO_2 absorption of solar radiation on UV climatology is likely negligible for all stations except Kagoshima.

The relatively large number of cases with SO_2 above 10 DU in Toronto can be explained by local pollution sources. In addition, more frequent sampling at Toronto, where up to five measurements per hour are made, causes short-term increases of SO_2 to be registered.

The high SO_2 amounts observed over Kagoshima are associated with the Sakurajima volcano, which is 10 km southeast of the observation site and one of the few active volcanoes in Japan. The levels of SO_2 observed there can substantially reduce the level of biologically active ultraviolet radiation. For an SO_2 amount of 50 DU the energy of the erythemally weighted UV spectrum is about 25% less than that for the same atmosphere without SO_2. During the five-year period, SO_2 levels of 50 DU or greater were observed on 65 occasions. Other components of volcanic plumes, such as aerosol and dust, also reduce UV irradiance values.

Table 4.1: List of Stations, Periods of Observation, and Number of Days with High SO_2

Station	Period of Observations	Latitude	Longitude	Number of Days with SO_2 ≥10DU (≥20DU)	Percentage of Total Number of Days with UV Observations
Kagoshima	1991-1995	32°N	131°E	236 (125)*	13.04 (6.92)*
Toronto	1989-1995	44°N	79°W	26 (1)	1.08 (0.04)
Montreal	1993-1995	50°N	74°W	3 (0)	0.32 (0.00)
Saturna	1991-1995	49°N	123°W	5 (0)	0.28 (0.00)
Naha	1991-1995	26°N	128°E	2 (0)	0.11 (0.00)
Churchill	1992-1995	58°N	94°W	1 (0)	0.09 (0.00)
Winnipeg	1992-1995	50°N	97°W	1 (0)	0.08 (0.00)
Edmonton	1992-1995	54°N	114°W	1 (0)	0.08 (0.00)
Saskatoon	1990-1995	52°N	107°W	1 (0)	0.05 (0.00)
Sapporo	1991-1995	43°N	141°E	0 (0)	0.00 (0.00)
Tateno	1991-1995	36°N	140°E	0 (0)	0.00 (0.00)
Halifax	1992-1995	45°N	64°W	0 (0)	0.00 (0.00)
Regina	1994-1995	50°N	105°W	0 (0)	0.00 (0.00)

** Number of days with $SO_2 \geq$ 20DU and number of such days as a percentage of total number are shown in brackets.*

The long-term effect of volcanic SO_2 absorption on UV climatology at the surface may be estimated by multiplying the number of days with high SO_2 by the reduction of UV irradiance due to SO_2. For Kagoshima this is about a 1–2% reduction. The overall effect of the volcano on UV irradiance is likely stronger, however, because other volcanic plume components absorb and scatter solar radiation. The effect would be at least twice as strong if the observatory were located in the path of the prevailing wind from the volcano. However, since no other Japanese stations report SO_2 values more than 20 DU, it is likely that the effects of this volcano are not widespread.

4.2.3 Dependence on Clouds

The effects of clouds on UV-B may be approached by first investigating their effects on irradiance measurements made at 324 nm, a wavelength that is not significantly affected by ozone or SO_2 absorption, Figures 4.8b and 4.8d show the logarithm of UV irradiance normalized to the irradiance value at 324 nm as a function of wavelength and time of day for May 7, 1992 (Figure 4.8b) and May 6, 1992 (Figure 4.8d). Ozone amounts were approximately the same for both days, but cloud conditions were quite different. Figures 4.8a and 4.8c, which show the absolute irradiance for the two days, indicate a significant drop in irradiance values on the afternoon of May 6. The variations of irradiance on May 6 are due to variations in cloud cover. However, as shown in Figures 4.8b and 4.8d, the behaviour of the ratios for these two days is similar. This illustrates that the effects of clouds on global irradiance are approximately the same for all wavelengths in the UV-B.

For most cases the presence of clouds does not affect the retrieval of total ozone values, since the shape of the normalized spectra are nearly unaffected (Figure 4.8b and 4.8d). However, when very thick cumulonimbus clouds are present the shape of the normalized spectra are affected significantly. Figure 4.8f shows the normalized spectra for May 2, 1992, a day when irradiance values at 324 nm dropped to about 1% of the values for clear sky conditions during the passage of thunderstorms. Calculations during these events yield very high levels of ozone (up to 1000 DU). These effects have been reported earlier by Brewer and Kerr [1973] and are likely caused by very long optical path lengths due to extensive scattering in the clouds.

Information about cloud conditions can be obtained from the absolute value of irradiance at 324 nm. Figure 4.9 shows percentiles of irradiance at 324 nm as a function of zenith angle, derived using data from seven stations. Measured values of irradiance at 324 nm may be compared with the curves in Figure 4.9 to estimate cloud thickness. An observation above the 95th percentile curve would be considered to have been made under clear sky conditions. Observations below the 5th percentile curve would have been made under heavy convective clouds. In terms of absolute values of irradiance, the 5th percentile level corresponds to 12–15% of irradiance at 324 nm for clear sky conditions. Values of irradiance at 324 nm under the 1st percentile level are probably from measurements made under very thick cumulonimbus clouds.

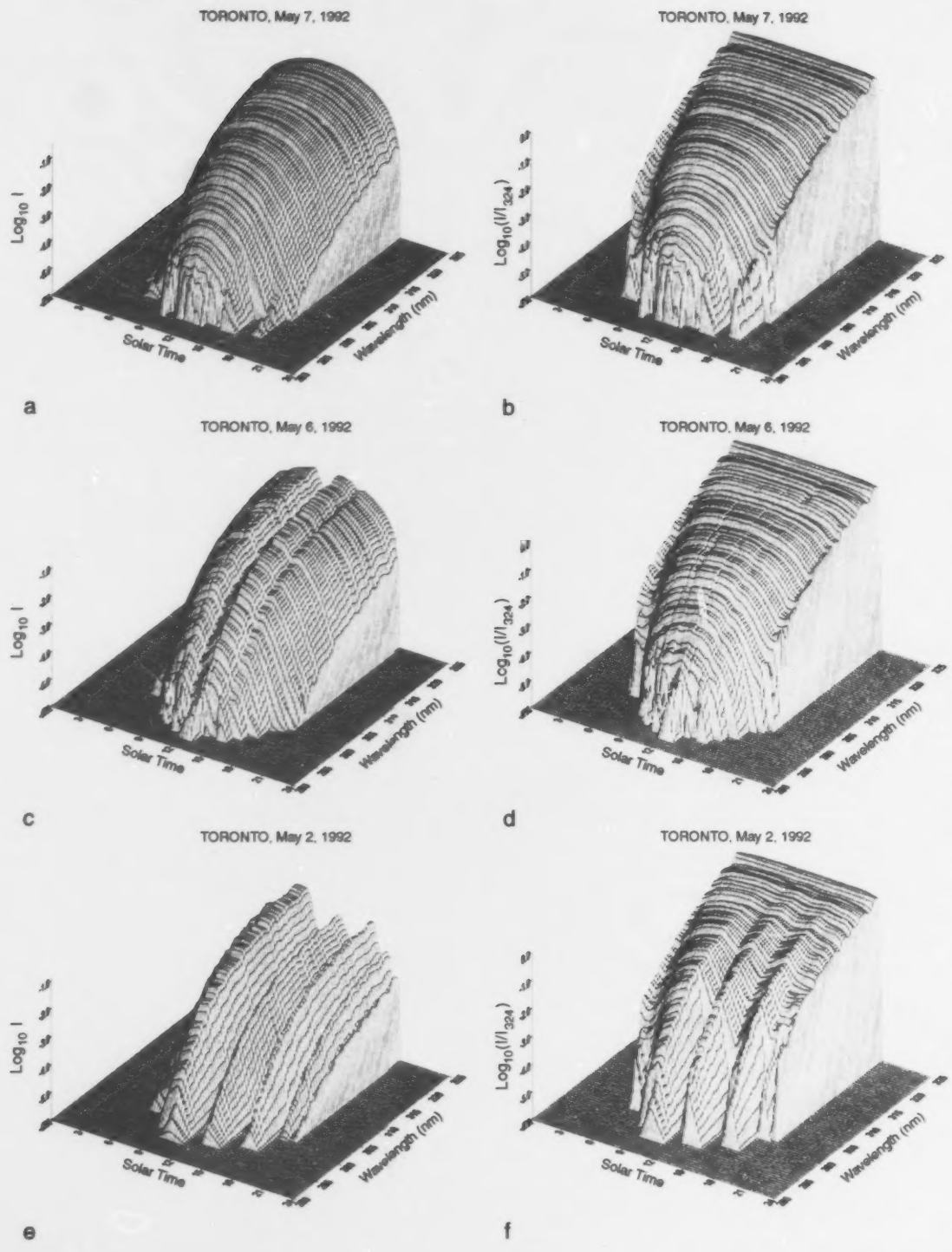

Figure 4.8 The logarithm of the UV irradiance (a, c, e) and the logarithm of UV irradiance normalized to the irradiance value at 324 nm (b, d, f) as a function of wavelength and time of day for May 2, 6, and 7, 1992.

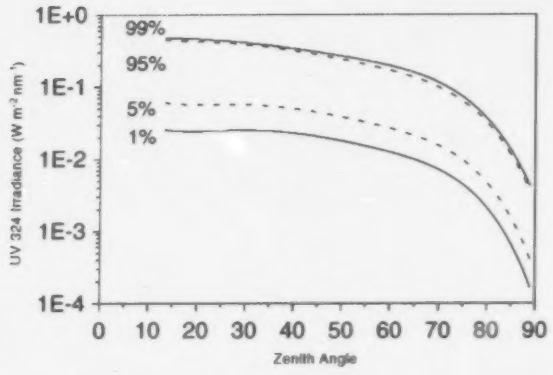

Figure 4.9 Percentiles of UV 324 nm irradiance distribution as a function of zenith angle (the 1% or 1st percentile means that 1% of the observations is below this curve).

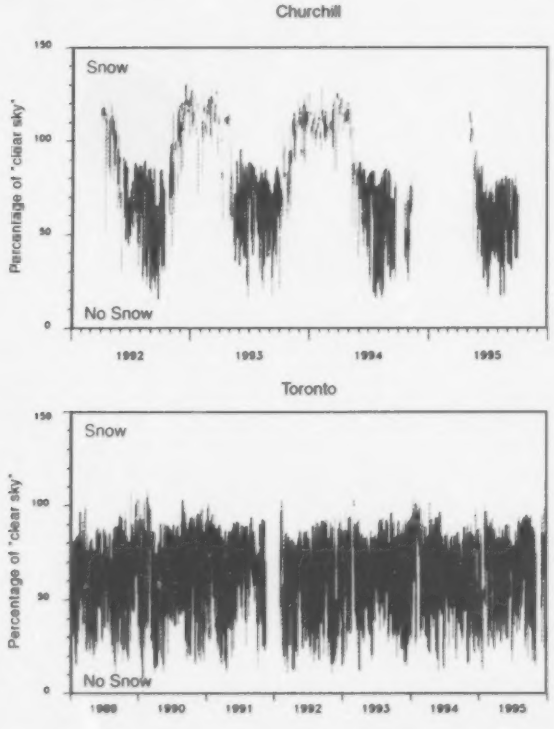

Figure 4.10 Averages of the daily mean adjusted UV 324 nm irradiance for days with and without snow on the ground for Churchill (60°N) and Toronto (44°N).

4.2.4 Dependence on Other Variables

UV irradiance depends on surface albedo, and snow on the ground is the main factor that affects surface albedo in the UV. To estimate the effect of snow on UV irradiance, all Canadian Brewer observations taken under clear sky conditions have been divided into two groups: those taken with snow on the ground and those taken without. Data were used only for conditions when no clouds were reported at nearby weather stations. UV irradiance at 324 nm was used as an indicator of the UV signal. The effect of zenith angle was removed by dividing the UV irradiance values at 324 nm by the 95th percentile value (see Figure 4.9) at the corresponding zenith angle. The daily average of these values represents a relative level of UV irradiance adjusted for zenith angle and is called the "adjusted UV 324 nm irradiance."

Table 4.2 summarizes the averages of the adjusted UV 324 nm irradiance for clear days with and without snow on the ground for seven Canadian Brewer stations. An important result that is evident here is that for clear sky and no-snow conditions the adjusted UV 324 nm irradiance is similar at all stations and snow has significantly different enhancements at different stations likely because of terrain variations.

Figure 4.10 shows the daily average adjusted UV 324 nm irradiance values for all days at Churchill and Toronto. Days with snow (blue) have generally higher values than days without snow (red). The difference between "snow" and "no snow" is more apparent at Churchill, where the nearby flat terrain is likely "whiter" than at Toronto, which has urban surroundings.

The presence of atmospheric aerosols affects the amount of global UV irradiance at the ground. In a study by Kerr [1997], data from clear days over a three-year period (1989–1991) at Toronto were used to quantify the effect of aerosols on UV-B irradiance values. Variations in irradiance values measured with the Brewer instrument were compared with aerosol optical depth measurements for UV-B wavelengths made with the same instrument. The analysis found that aerosols reduce the global irradiance by about 20–30% of the reduction of the direct irradiance. (Thus, if aerosols were to reduce the direct irradiance by 10%, the global irradiance would be reduced by 2–3%.) The reduction has little wavelength dependence and is in reasonable agreement with radiative transfer models for non-absorbing aerosols.

Table 4.2: Averages of the Adjusted UV 324 nm Irradiance for Clear Days With and Without Snow on the Ground

Station	No snow	Snow	Difference (% from "no snow" level)
Resolute	82	111	35
Churchill	84	116	39
Edmonton	84	103	21
Winnipeg	87	111	27
Montreal	80	97	22
Halifax	86	93	8
Toronto	85	95	12

4.2.5 Modelling of Spectral UV Irradiance

Radiative transfer models [e.g. Dave 1964; Stamnes et al. 1988] can be used to estimate spectral UV irradiance from a number of measured parameters, such as total ozone and aerosol and cloud conditions. For clear sky conditions, systematic differences between measurements and models are typically in the order of several percent [Mayer et al. 1997]. These differences are mostly due to errors in the model input parameters (e.g., extraterrestrial radiance) and uncertainties in the absolute calibration and characterization of the spectroradiometer [Mayer et al. 1997]. However, differences between individual measurements and the modelled radiation can be much higher. According to Schwander et al. [1997], typical errors in the input parameters can lead to a 10–20% uncertainty in the global UV irradiance at 300 nm and up to 50% uncertainty at 290 nm. If ozone and SO_2 contents and spectral aerosol characteristics are measured under actual conditions, the uncertainties in input parameters result in an uncertainty of about 5% for spectral integrals of UV irradiance [Schwander et al., 1997].

4.3 Changes in UV Irradiance due to Ozone Depletion

The extent to which ozone has been decreasing over the past two decades has been reported by many researchers, and the results have been summarized in periodic international scientific assessments [e.g., WMO 1991; 1994]. Depletion of stratospheric ozone over Canada has been summarized in Chapter 1 of this report. These assessments have quantified the long-term trends in ozone as a function of latitude and time of year and have summarized findings that relate these changes to enhanced levels of anthropogenic chlorine and bromine in the stratosphere. The long-term trend values are based on the results of analyses of stratospheric ozone measurements that have been made routinely on a global scale for nearly four decades.

Quantifying long-term changes in UV irradiance at the earth's surface is more difficult than detecting long-term changes in ozone, since surface UV irradiance depends on many variables. Although analysis of spectral data can separate changes due to ozone from changes due to other causes (Section 4.1), it is only relatively recently (since the late 1980s) that instruments have been developed with the capability of carrying out routine field measurements of spectral UV irradiance with sufficient accuracy and long-term stability.

4.3.1 Analysis of UV Irradiance Records

Relatively short records of spectral UV irradiance have been studied to determine possible increases that may be caused by decreases in stratospheric ozone. Kerr and McElroy [1993, 1994] analysed daily integrated UV irradiance values and total ozone measured at Toronto between 1989 and 1993 and found significant increases in UV irradiance resulting from a large drop in ozone over the same period. Data from all days were used, so the analysis includes the effects of clouds and other variables. The decrease in ozone occurred mostly in 1993 and was associated with the volcanic eruption of Mt. Pinatubo in June 1991. These significantly perturbed conditions provided an opportunity to quantify the links between changes in UV irradiance and changes in ozone and to demonstrate through the spectral signature that the UV changes were caused by ozone. Figure 4.11 shows the ratios of data from a year with low ozone (1992-1993) to a year with higher ozone (1989-1990) for summer (May to August) and winter (December to March) and compares these ratios with the absorption spectrum of ozone. The spectral absorption features of ozone are clearly evident in the temporal changes in UV irradiance. The study is important because it demonstrates the capability to observe these absorption features in data gathered under all types of weather conditions.

The analysis of the Toronto data set has been extended both into the past (from 1989 to 1986) and into the future (beyond 1993 to 1997). Data prior to 1989 are not as reliable as later data, since the measurements were made over a reduced wavelength range (290–315 nm) and there is more uncertainty in the absolute calibration of the instrument. Nevertheless, when the longer data set (now with 11 years of data) is analysed to determine long-term changes, the relationship of changes in UV irradiance to changes in ozone remains very clear. Figure 4.12a shows the summer daily average values of irradiance at 300 nm (where ozone absorbs strongly) and 324 nm (where ozone has negligible absorption). UV irradiance values from 315 nm to 325 nm prior to 1989 have been calculated from data between 290 nm and 315 nm and the very strong statistically determined correlations between irradiance at the shorter and longer wavelengths. The

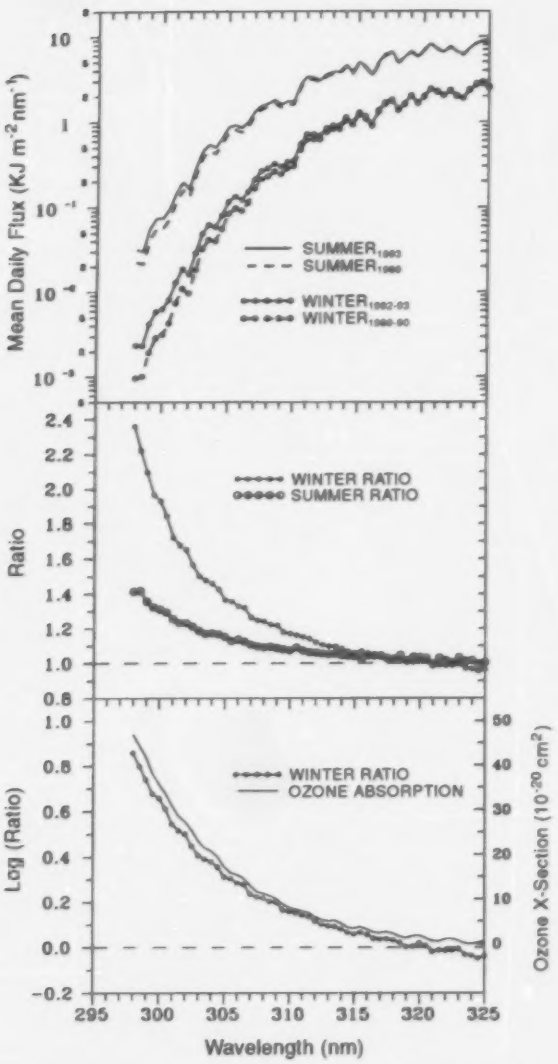

Figure 4.11 Impact of low ozone over Toronto in 1992 and 1993 compared with earlier years. The top panel shows the main daily UV flux as a function of wavelength for the summers of 1989 and 1993 and the winters of 1989–1990 and 1992–1993. The middle panel shows flux ratios for summer (1993 divided by 1989) and for winter (1992–1993 divided by 1989–1990). The bottom panel compares the observed changes as a function of wavelength with the ozone absorption spectrum. The log of the winter ratio is used because the intensity of UV-B radiation depends on the exponent of the absorption coefficient of ozone. (From WMO [1994].)

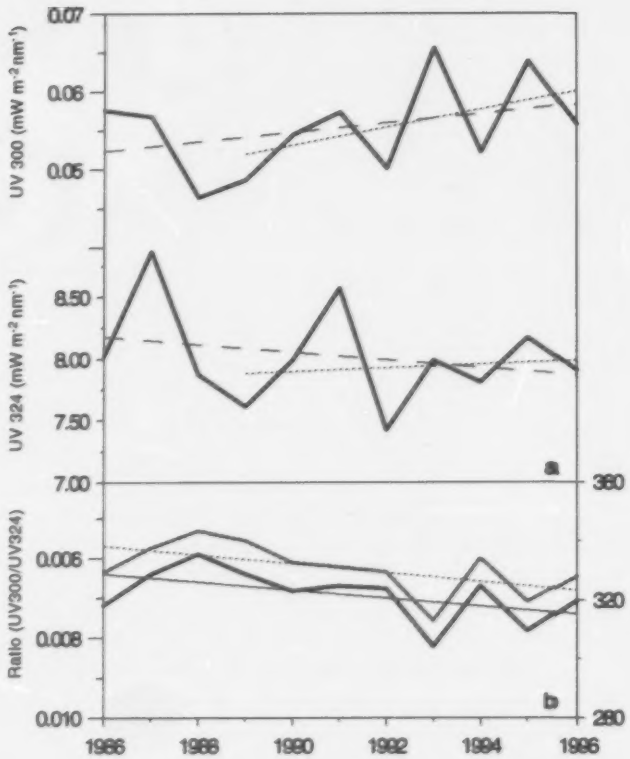

Figure 4.12. (a) The summer daily average values of irradiance at 300 nm (where ozone absorbs strongly) and 324 nm (where ozone has negligible absorption). (b) The ratio between the average daily integrated value of UV irradiance at 300 nm to that at 324 nm for the summer months (May–August). Seasonal mean total ozone is shown by the dotted line. The best fit lines are also plotted.

accuracy of the proxy data at 324 nm is estimated to be about 5% for an individual scan and about 2% for the summertime averages prior to 1989. Both data sets have been fitted with two trend lines: one from 1986 and the other from 1989. The linear fits show a positive trend at 300 nm and near zero (since 1989) or negative (since 1986) at 324 nm. The slopes of the trend lines as a function of wavelength for the data since 1989 are shown as percent per decade in Figure 4.13, with the ozone absorption spectrum for comparison.

Figure 4.12b shows the ratio of irradiance at 300 nm to that at 324 nm (on a decreasing scale) and the average summer total ozone value for each year. The relationship between the average ratio of irradiance at 300 nm to that at 324 nm and average total ozone values is quite evident on a year-to-year as well as a longer-term basis.

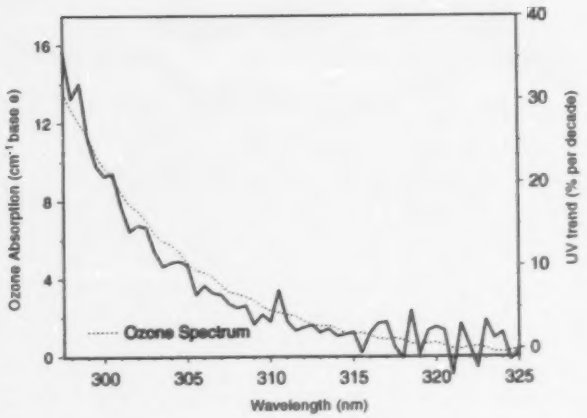

Figure 4.13 UV irradiance trends for May–August for Toronto. The slopes of the trend lines as a function of wavelength for the data from 1989 to 1996 are shown as percent per decade with the ozone absorption spectrum.

4.3.2 Present UV Climatology

There are now about 100 station years of spectral UV irradiance data stored in the WOUDC. Many of the stations have records more than five years long. These data have been used to determine average UV values measured over the length of the records at each site. One example of how these UV "climatologies" may be graphically summarized is shown in Figure 4.14. In this example, the average values of the observed UV Index [Kerr et al. 1994; Burrows et al. 1994; Burrows 1997; see also Section 4.4] are shown as a function of time of day and time of year at Churchill, Canada (59°N), San Diego, USA (32°N), Toronto, Canada (44°N), and Sapporo, Japan (43°N).

Inspection of the diagrams in Figure 4.14 reveals several interesting aspects of UV irradiance. At San Diego, Toronto, and Sapporo, the UV Index is lower near the spring equinox (March 21) than it is near the fall equinox (September 21). This is due to the fact that there is more ozone during spring than there is in fall. In Churchill, however, the UV Index is higher in spring than it is in the fall. This is because the UV levels are enhanced by snow on the ground, which usually disappears in May. Comparison of the four station climatologies clearly shows enhanced UV irradiance at lower latitudes. It also illustrates longer hours of sunshine during summer and shorter hours during winter at high latitudes. Comparison of the climatology at Toronto with that at Sapporo indicates that there can be significant differences in UV levels at two stations with similar latitude. These differences are due to different ozone and/or cloud conditions.

The measured climatologies that are evolving from the growing data base are useful for the study of short-term variations. Figure 4.15 shows the UV Index for individual years at Toronto (44° N, 1993), Ushuaia, Argentina (54° S, 1994), Palmer, Antarctica (64° S, 1993), and Mauna Loa, Hawaii (20° N, 1997). The observed day-to-day fluctuations are much larger than one might infer from the climatology diagrams shown in Figure 4.14. These fluctuations result in larger peak values than are seen in the climatological averages. For example, the climatology for Toronto shows a peak Index of less than 7 in June and July, but the individual observations made in 1993 (when ozone was a record low) show peak values of about 9.5. Figure 4.15 shows that Palmer under the ozone hole in October has UV Index values greater than 10, suggesting very strong sun-burning potential there. The record at Mauna Loa shows that the combination of typically low tropical ozone values with high sun angles and high altitude can result in UV Index values peaking near 16.

4.3.3 Estimating Past UV Climatology

In order to determine long-term changes in UV irradiance that may have occurred since the onset of ozone depletion in the late 1970s, it is necessary to estimate levels of UV irradiance that existed before routine spectral measurements were made. Estimates of past UV levels are the product of a thorough understanding of the dependencies of spectral UV irradiance on geophysical variables (Section 4.1) and the application of these relationships with the aid of radiative transfer models to archived measurements of other variables (e.g., ozone, cloud cover, optical depth, etc.). Work towards reconstructing past UV climatology has been initiated in recent years. These estimated past climatologies may then be compared with those of recent years (Section 4.3.2) to determine long-term changes.

Several studies have been done [e.g., Frederick et al. 1993; Madronich 1992] that calculate changes in UV irradiance from long-term changes in total ozone measured by ground-based or satellite instruments. In deriving estimated changes in UV irradiance, most of these studies have assumed that the effects of clouds and other variables have not changed over time and are therefore representative of changes under clear sky conditions.

More recently Herman et al. [1996] have estimated past UV irradiance values at the surface from measurements made by the Total Ozone Mapping Spectrometer (TOMS). The TOMS instrument uses backscattered radiance measurements at several wavelengths in the UV to determine total ozone from space. The backscattered data may also be used to estimate

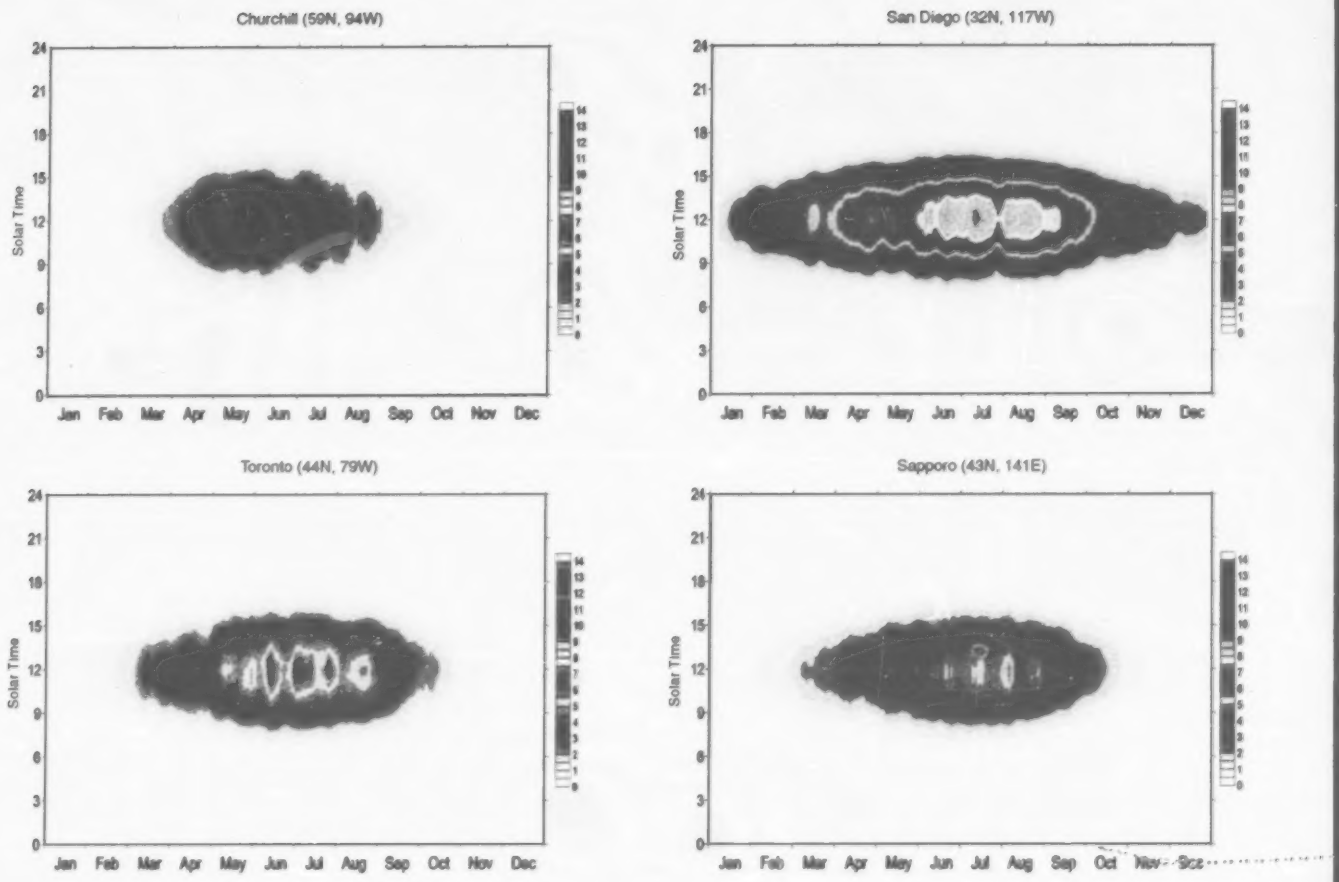

Figure 4.14 UV Index "climatology" for San Diego, Churchill, Toronto, and Sapporo.

cloud thickness and therefore derive the attenuation of surface UV irradiance due to clouds. Comparison of the TOMS-estimated UV surface irradiance with actual ground-based irradiance measurements has played a key part in the development of this approach [Eck et al. 1995]. Although there are still problems to overcome with this method, the potential to provide a realistic estimation of surface UV irradiance values on a daily basis with global coverage back to the late 1970s is quite promising. The possibility of extending the record further back in time at sites where total ozone and cloud cover are measured also exists, although results of such analyses are yet to be reported.

4.4 The Contribution of Ozone-Depleting Gases to Global Warming

The anthropogenic emission of chlorine-bearing gases into the atmosphere has resulted in a significant depletion of the earth's ozone layer and the development of the Antarctic ozone hole. Many of these gases are also strong greenhouse gases that modify the atmospheric radiation so as to make the earth's surface warmer and the stratosphere colder. This is particularly true of CFC-11 and CFC-12, but new alternatives to CFCs, such as HCFC-22 (designed for the replacement of CFC-11 and CFC-12) are also strong greenhouse gases, even though they may not deplete as much ozone. The buildup of carbon dioxide and other greenhouse gases contributes to cooling of the polar stratosphere, which favours the formation of Polar Stratospheric Clouds (PSCs) [Austin 1992]. Consequently, the accumulation of these gases may have increased the severity of ozone depletion in the Antarctic ozone hole

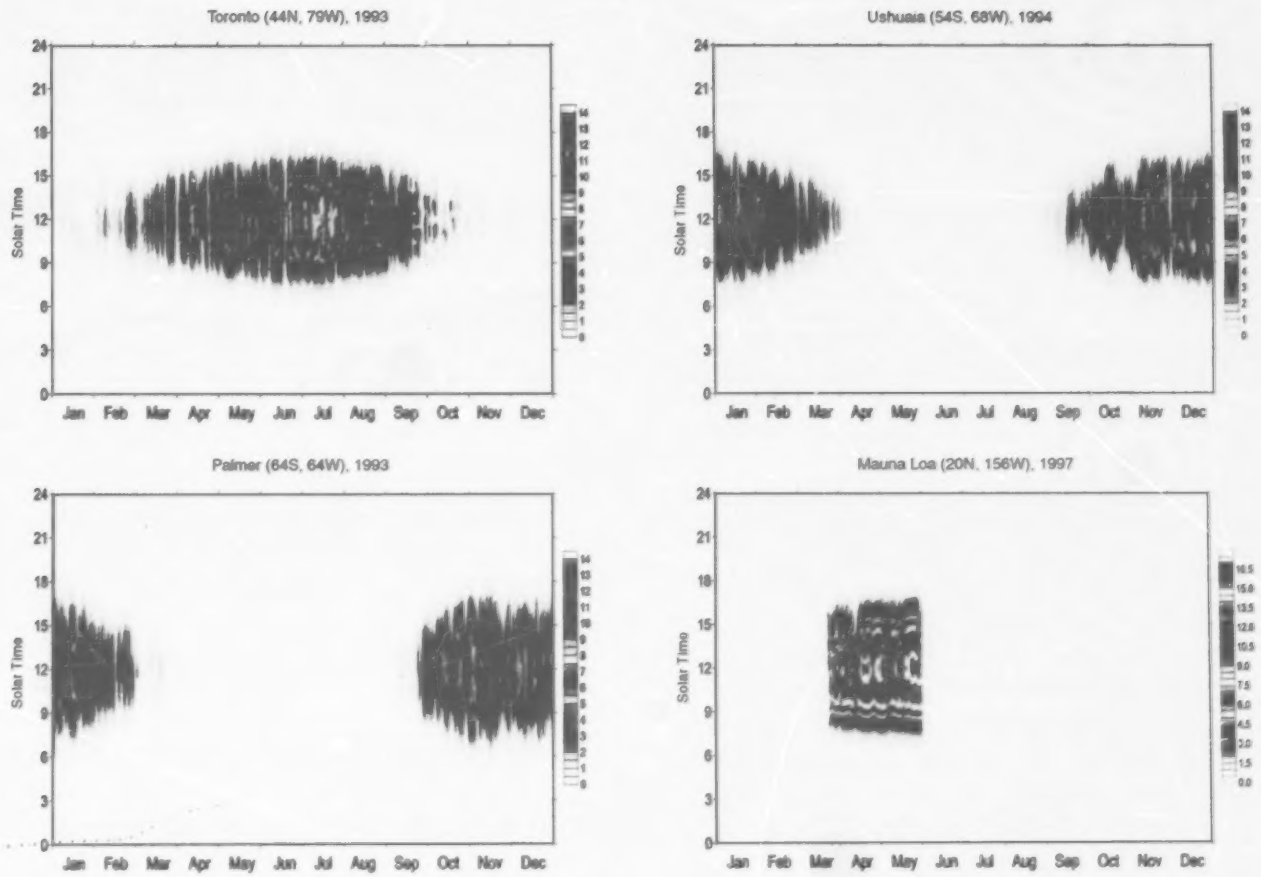
Toronto (44N, 79W), 1993
Ushuaia (54S, 68W), 1994
Palmer (64S, 64W), 1993
Mauna Loa (20N, 156W), 1997
Solar Time
Jan Feb Mar Apr May Jun Jul Aug Sep Oct Nov Dec

Figure 4.15 The UV Index for individual years at Toronto (44°N, 1993), Ushuaia, Argentina (54°S, 1994), Palmer, Antarctica (64°S, 1993), and Mauna Loa, Hawaii (20°N, 1997).

and enhanced Arctic ozone depletion in late winter. In addition, the increase in atmospheric methane concentrations has increased the amount of water vapour in the stratosphere, thus probably enhancing polar ozone depletion by making more water available for PSC formation. The depletion of the stratospheric ozone layer will also cause surface cooling in the polar regions, as discussed later in this section. Hence, the greenhouse gases contribute indirectly in a variety of ways to ozone depletion, which itself mitigates global warming.

In order to evaluate the contributions of the various gases to global warming, the concept of radiative forcing or changes in absorption of the upward long-wave radiation by the atmosphere has been formulated [Ramanathan 1987; IPCC 1994]. Using the radiative forcing at the tropopause as an input, climate models can then estimate the effect of these gases on global temperature. Model calculations of this radiative forcing and the associated fluxes have been conducted by several authors [Dickinson and Cicerone 1986]. Earlier estimates of the greenhouse effect were expressed in terms of the overall loss of radiation to space or of the downward radiation at the surface. It may be noted that, when convection just above the ground is small, the land surface temperature actually responds to the downward greenhouse radiation from the atmosphere in a few hours. The greenhouse radiation is typically about 150 Wm^{-2}; the modelled increases in the greenhouse radiation since pre-industrial times are about 2.2 Wm^{-2}. The increase in downward surface greenhouse radiation for a particular gas is quite similar to the absorption of upward long-wave radiation by that gas, as has been demonstrated by Sinha and Toumi [1996]. Estimates of the radiative fluxes at the tropopause from greenhouse gases at current 1997 concentrations are given in Table 4.3. These are based on the 1990 IPCC report [IPCC 1990]. Although there are extensive model calculations of radiative forcing in the literature, there are few experimental measurements. In what follows, measurements of the surface greenhouse radiation are described and compared with estimates from radiative transfer modelling.

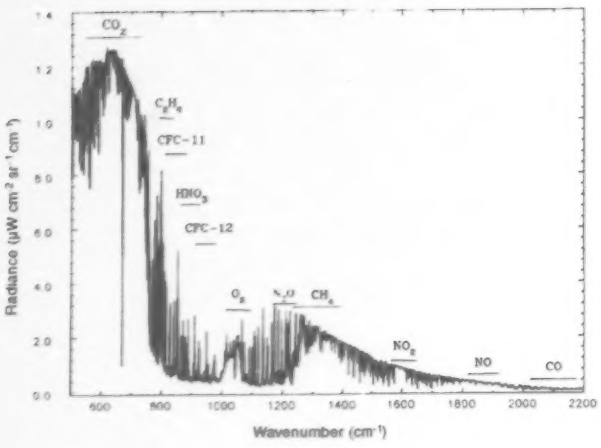

Figure 4.16 A spectrum of downward (greenhouse) radiation at the surface, showing the contributions of several greenhouse gases observed at Peterborough, Ontario, in February 1996.

Table 4.3: Radiative Fluxes at the Tropopause (after IPCC [1990])

Greenhouse Gas	Simulated Flux (Wm^{-2})
H_2O	~90
CO_2	56
CH_4	1.51
N_2O	2.48
Tropospheric O_3	0.70
CFC-12	0.15
CFC-11	0.062

Table 4.4: Measured Greenhouse Fluxes at the Earth's Surface

Greenhouse Gas	Emission Band (cm^{-1})	Measured Flux (Wm^{-2})	Simulated Flux (Wm^{-2})
CFC-11	830–860	0.13	0.12
CFC-12	900–940	0.10	0.090
CFC-12	all bands	0.24	0.22
CFCs-11 & 12	all bands	0.37	0.34
CCl_4	786–806	0.046	0.039
HCFC-22*	780–830	NA	0.030
HNO_3	850–920	0.085	0.060
N_2O	all bands	1.33	1.30
CH_4	1200–1400	0.85	0.80
CO	2000–2200	0.032	0.033
CO_2*	all bands	NA	60.9
O_3	950–1100	6.52	6.39
Tropospheric O_3	950–1100	0.11	0.07

** greenhouse flux is based on simulations only*

A project to measure the increases in greenhouse radiation at the surface has been conducted at a location in Ontario for the past five years. Measurements of the fluxes from the individual gases CFC-11, CFC-12, CCl_4, CH_4, N_2O, HNO_3, CO, and tropospheric ozone have been reported in a series of papers by Evans and Puckrin [1994–1997]. The measurements were made with a standard Fourier-transform infrared (FTIR) spectrometer operated at a resolution of 0.25 cm^{-1}. The investigation has focused on those radiatively active gases that may have a particularly large adverse effect on climate, either because of their high atmospheric concentrations, their large global warming potentials, or a combination of these factors. Figure 4.16 shows a typical spectrum of the downward radiance in the 8–12 μm wavelength range and identifies emissions from several of the greenhouse gases.

The greenhouse radiation from tropospheric ozone was measured by a technique in which the base of cold clouds is used as a cold target. The thermal emission from the warm atmosphere below the cloud is measured against the low background emission from the cold cloud base [Puckrin et al. 1996]. The cloud also screens out the emission from the stratospheric ozone above it. The greenhouse emission from tropospheric ozone in the lower 2 km and the lower 4 km of the atmosphere has been measured at about 0.1 Wm^{-2} on several occasions.

The downward radiation fluxes at the surface from those greenhouse gases measured to date are summarized in Table 4.4. The measurements, except for tropospheric ozone, were made in clear sky, winter conditions at latitude 44°N. The values in Table 4.4 are for average sky conditions, assuming that the sky is overcast 50% of the time. They are 50% of the measured (clear sky) values and can be compared with IPCC values, which generally include the effects of cloud cover. The measurement pertaining to tropospheric ozone was made in moderately polluted air with an ozone concentration of 60 ppbv. Fluxes predicted by the FASCD3 atmospheric transmission code [Anderson et al. 1986] for the actual atmospheric conditions and recent atmospheric gas concentrations [Kaye et al. 1994 ; IPCC 1995] are also shown in Table 4.4. In general there is a good correlation between the measured and simulated radiative fluxes. Only nitric acid and tropospheric ozone show significant deviations between the measured and simulated flux values.

The flux measurements presented in Table 4.4 provide important experimental verification of the radiation that is responsible for global warming and that may be introducing significant changes in the climate system. Continued measurements of the downward greenhouse fluxes over a range of locations and seasons would provide useful information for validating global climate models and resolving the discrepancies that currently exist between them. For example, a

Table 4.5: Contribution of Greenhouse Gases to the Surface Downward Flux Since the Pre-industrial Era

Greenhouse Gas	Pre-industrial Concentration	Current Concentration	Flux Increase (Wm^{-2})	%
Carbon dioxide	275 ppmv	360 ppmv	1.30	60 %
Methane	0.7 ppmv	1.75 ppmv	0.33	15 %
Nitrous oxide	285 ppbv	316 ppbv	0.13	6 %
Tropospheric ozone	30 ppbv	60 ppbv	0.04	2 %
CFC-11	0 pptv	280 pptv	0.13	6 %
CFC-12	0 pptv	530 pptv	0.24	11 %
Total			2.17	100 %

comparison of surface fluxes from 20 models conducted by Ellingson et al. [1995] reported only the CO_2 fluxes, although the combined CH_4 and N_2O flux were reported for one model. That model's reported value of 1.7 Wm^{-2} is broadly consistent with the experimental value of 2.1 Wm^{-2}.

Table 4.5 shows the contribution of greenhouse gases to the increase in the downward greenhouse flux since the pre-industrial period. Simulations using FASCD3 were performed to estimate the greenhouse flux from the various gases, using their respective tropospheric concentrations from two centuries ago [Dickinson and Cicerone 1986]. Most of the simulations of the current fluxes have been verified with the experimental measurements in Table 4.4, so that there is some confidence that these modelled flux increases are representative of Canadian latitudes. In these calculations, the amount of atmospheric water vapour has been assumed to be invariant.

The pre-industrial and current concentrations of gases used in the flux calculations are also summarized in Table 4.5. The current tropospheric ozone amount of 60 ppbv over the first 2 km of the atmosphere is typical of a moderately polluted environment. From Table 4.5 it is apparent that the increase in the carbon dioxide concentration since pre-industrial times has resulted in the largest increase in the radiative forcing at the surface. The chlorofluorocarbons, CFC-11 and CFC-12, contribute the second largest amount to the flux; however, carbon dioxide has increased about 100,000 times more than the combined concentrations of CFC-11 and CFC-12 since the pre-industrial period. The data from Table 4.5 are represented pictorially in Figure 4.17a, which shows the relative contribution of greenhouse gases to the downward greenhouse flux since the pre-industrial period.

Radiative forcing at the tropopause, as taken from IPCC [1995], is shown in Table 4.6 and Figure 4.17b. These radiative forcing contributions are more representative of global averages, although they are of the same magnitude as the surface flux increases in Table 4.5. The estimated total radiative forcing is 2.92 Wm^{-2} with an uncertainty range of 2.4–3.5 Wm^{-2}.

The contribution of water vapour to the increase in greenhouse radiation has not been included, since it is a part of the natural climate feedback. It is possible that tropospheric water vapour has already increased by several percent. The water vapour flux is typically about 90 Wm^{-2}, giving a total greenhouse radiation of about 150 Wm^{-2}. From Table 4.5 it is evident that the greenhouse radiation has increased by about

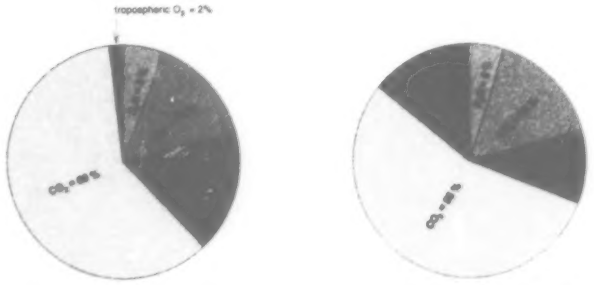

Figure 4.17 (a) Percentage increases in measured surface radiation. (b) Percentage increases in radiative forcing. (From IPCC [1995].)

Table 4.6: Contribution of Greenhouse Gases to Radiative Forcing Since the Pre-industrial Era (after IPCC [1995])

Greenhouse Gas	Pre-industrial Concentration	Current Concentration	Flux Increase (Wm^{-2})	%
Carbon dioxide	275 ppmv	360 ppmv	1.6	55 %
Methane	0.7 ppmv	1.75 ppmv	0.48	16 %
Nitrous oxide	285 ppbv	316 ppbv	0.14	5 %
Tropospheric ozone	25 ppbv	60 ppbv	0.4	14 %
CFCs	0 pptv	1ppbv	0.3	10 %
Total			2.92 (2.4–3.5)	100%

2.2 Wm^{-2} since pre-industrial times. Of this 2.2 Wm^{-2}, nearly 0.5 Wm^{-2} has been attributed by measurements to CFCs. The CFC contribution is mainly due to CFC-11, CFC-12, CCl_4, CFC-22, and CFC-113.

In Table 4.7 some of the factors that may produce cooling of the climate are considered [IPCC 1995]. These cooling factors are important because they may partially compensate for the observed increases in greenhouse radiation and radiative forcing. The depletion of stratospheric ozone causes cooling in the polar regions but not in the tropics. This is because stratospheric ozone both attenuates solar UV radiation that heats the surface and emits infrared (IR) radiation that also heats the surface. If the ozone layer is thinned, more solar UV radiation reaches the surface to heat it but less long-wave IR is emitted. If the long-wave term is larger, its reduction will therefore lead to cooling at the surface. In the winter polar regions, for example, a thinning of the ozone layer causes net cooling of up to 0.2 Wm^{-2} since the short-wave solar UV is very small in this situation. In the tropics the solar UV term is larger, and consequently an ozone thinning actually causes a net heating of the surface of 0.05 Wm^{-2}.

Table 4.7: Cooling Influences (after IPCC [1995])

Stratospheric ozone depletion (5 %)		–0.05 to +0.2 Wm^{-2}
Sulfate aerosols	direct	0.2 to 0.8 Wm^{-2}
	indirect	0 to 1.5 Wm^{-2}
Solar variability		–0.1 to –0.5 Wm^{-2}

4.5 Public Awareness Programs

Environment Canada runs two public awareness programs dealing with ozone conditions: Ozone Watch, which reports current ozone measurements, and the UV Index Program, which gives forecasts of UV radiation.

Ozone Watch was started in March 1992, largely in response to public concerns about low ozone values in the Arctic. The reports are based on measurements at the twelve Canadian Brewer locations. A single percentage is given for each location, describing the mean ozone value over the preceding two weeks in relation to pre-1980 average values. The goal of the program is to present a rough indication of ozone depletion and to show interested people that ozone changes in much the same way as other atmospheric variables. Ozone Watch is put on the wire service every Friday in tabular form. It is also issued as a map with spot values, shown on a commercial weather service (Meteomedia), and posted on an Environment Canada Web site. It is believed to be unique to Canada, and it often generates questions from journalists who may notice low ozone values earlier than anyone else. The Ozone Watch ensures that Environment Canada is not ever seen to be withholding data on ozone.

The UV Index program was started in May 1992. It predicts the strength of UV erythemally weighted irradiance, using a number describing the maximum irradiance that will occur on a given day. The forecast is issued the previous evening and is carried on radio and television and in newspapers. The UV Index itself is an irradiance scale, computed by multiplying the CIE irradiance in Wm^{-2} by 40. Thus, the clear sky value at sea level in the tropics would normally be in the range 10–12 (250–300 mW m^{-2}), while 10 would be an exceptionally high value for northern mid-latitudes. This scale has been adopted by the WMO and WHO and is in use in a number of other countries. UV intensity is also described in terms of ranges running from low (values less than 4) to medium (4–7), high (7–9), and extreme (9+). Media reports use these descriptors as well as actual index values. UV Index forecasts that are sent to the regional offices of Environment Canada list the periods when the index is predicted to be in the highest range. Televised reports on Meteomedia's Weather Channel show a predicted index curve throughout the day and add measured values from local radiometers run by Meteomedia as the observations become available.

The UV forecasts are produced from measurements of ozone on the current day and the output from the Numerical Weather Prediction (NWP) model of the Canadian Meteorological Centre. First, the ozone field is predicted using current (real-time) ozone measurements from the Canadian Brewer network and a statistically derived relation between ozone and the NWP output. The clear sky value at the CIE irradiance is then computed from the predicted ozone. Finally, the clear sky value is adjusted for the expected sky conditions using a statistical prediction of sky cover [*Burrows, et al.*, 1994].

REFERENCES

Anderson, G.P., S.A. Clough, F.X. Kneizys, J.H. Chetwynd, and E.P. Shettle, 1986. *AFGL Atmospheric Constituent Profiles (0–120 km)*, AFGL-TR-86-0110. Cambridge, Mass.: Air Force Geophysical Laboratory.

Austin J., N. Butchart, and K.P. Shine, 1992. Possibility of an Arctic ozone hole in a doubled-CO_2 climate. *Nature*, **360**, 221–225.

Basher, R.E., 1982. *Review of the Dobson spectrophotometer and its accuracy*. WMO Ozone Rep. 13. Geneva: World Meteorological Organization.

Bojkov, R.D., V.E. Fioletov, and S. B.Diaz, 1995. The relationship between solar UV irradiance and total ozone from observations over southern Argentina. *Geophys. Res. Lett*, **22**, 1249–1252.

Brewer, A.W., and J.B. Kerr, 1973. Total ozone measurements in cloudy weather. *Pure Appl. Geophys.*, **106–108**, 928–937.

Burrows W., 1997. Cart regression models for predicting UV radiation at the ground in the presence of cloud and other environmental factors. *J. Appl. Meteorol.*, **36**, 531–544.

Burrows, W., M. Vallee, D.I. Wardle, J.B. Kerr, L.J. Wilson, and D.W. Tarasick, 1994. The Canadian UV-B and total ozone forecast model. *Met. Apps.*, **1**, 247–265.

Dave, J.V., 1964. Meaning of successive iteration of the auxiliary equation of radiative transfer. *Astrophysics J.*, **140**, 1292–1303.

deGruijl, F.R., and J.C. van der Leun, 1994. Estimate of the wavelength dependency of ultraviolet carcinogenesis in humans and its relevance to risk assessment of stratospheric ozone depletion. *Health Physics*, **67**, 319–325.

Dickinson, R.E., and R.J. Cicerone, 1986. Future global warming from atmospheric trace gases. *Nature*, **319**, 109–115.

Eck, T.F., P.K. Bhartia, and J. B. Kerr, 1995. Satellite estimation of spectral UVB irradiance using TOMS-derived total ozone and UV reflectivity. *Geophys. Res. Lett*, **22**, 661-614.

Ellingson, R.G, J. Ellis, and S. Fels, 1991. The Intercomparison of radiation codes used in climate models: long wave results. *J. Geophys. Res.*, **96**, 8923–8953.

Evans, W.F.J., and E. Puckrin, 1994a. An observation of the atmospheric emission spectrum of CFC-11. *Geophys. Res. Lett.*, **21**, 2381–2384.

Evans, W.F.J., and E. Puckrin, 1994b. An observation of the atmospheric thermal emission spectrum of dichlorodifluoromethane. *Can. J. Appl. Spectrosc.*, **39**, 85–90.

Evans, W.F.J., and E. Puckrin, 1995a. An observation of the greenhouse radiation associated with carbon monoxide. *Geophys. Res. Lett.*, **22**, 925–928.

Evans, W.F.J., and E. Puckrin, 1995b. The extraction of the thermal emission band of methane from the longwave spectrum of the atmosphere. *J. Climate*, **8**, 3091–3095.

Evans, W.F.J., and E. Puckrin, 1995c. The measurement and extraction of the n6 atmospheric emission band of CFC-12 from interfering emission features. *Ann. Geophysicae*, **13**, 969–972.

Evans, W.F.J., and E. Puckrin, 1996. A measurement of the greenhouse radiation associated with carbon tetrachloride (CCl_4). *Geophys. Res. Lett.*, **23**, 1769–1772.

Evans, W.F.J., and E. Puckrin, 1997. A wintertime measurement of the greenhouse radiation from nitrous oxide. *Can. J. Appl. Spectrosc.*, forthcoming.

Fioletov, V.E., J.B. Kerr, D.I. Wardle, 1997. The relationship between total ozone and spectral UV irradiance from Brewer observations and its use for derivation of total ozone from UV measurements. Working paper. Atmospheric Environment Service, Downsview, Ontario.

Frederick J.E., P.F. Soulen, S.B. Diaz, I., Smolskaia, C.R. Booth, T. Lucas, and D. Neuschuler, 1993. Solar ultraviolet irradiance observed from Southern Argentina: September 1990 to March 1991, *J. Geophys. Res.*, **98**, 8891–8897.

Götz F. W. P., 1931. Zum Strahlungsklima des Spitzbergen Sommers. *Gerlands Beiträge zur Geophys.*, **31**, 119.

Herman J. R., P.K. Bhartia, J. Ziemke Z. Ahmad, and D. Larko, 1996. UV-B radiation increases (1979–1992) from decreases in total ozone. *Geophys. Res. Lett.*, **23**, 2117–2120.

IPCC, 1990. *Climate Change: The IPCC Scientific Assessment*. J.T. Houghton, G.J. Jenkins, and J.J. Ephraums, eds. Cambridge: Cambridge University Press.

IPCC, 1994. *Climate Change 1994: Radiative Forcing of Climate Change*. J.T. Houghton, L.G. Meira Filho, B.A. Callander, N. Harris, A. Kattenberg and K. Maskell, eds. Cambridge: Cambridge University Press.

IPCC, 1995. *Climate Change 1995. The Science of Climate Change*. J.T. Houghton, L.G. Meira Filho, B.A. Callander, N. Harris, A. Kattenberg and K. Maskell, eds. Cambridge: Cambridge University Press.

Kaye, J.A., S.A. Penkett, and F.M. Ormond, 1994. *Report on concentrations, lifetimes, and trends of CFCs, halons, and related species*. NASA Publication 1339. Washington: National Aeronautics and Space Administration.

Kerr, J.B., 1997. Observed dependences of atmospheric UV radiation and trends. Pages 259–265 in *Solar Ultraviolet Radiation Modelling, Measurements and Effects*. NATO ASI Series, Vol I 52. C. S Zerefos and A. F. Bais, eds. Berlin: Springer-Verlag.

Kerr, J.B., and C.T. McElroy, 1993. Evidence for large upward trends of ultraviolet-B radiation linked to ozone depletion. *Science*, **262**, 1032–1034.

Kerr J.B., and C.T. McElroy, 1994. Analyzing ultraviolet-B radiation: is there a trend? *Science*, **264**, 1342–1343.

Kerr J.B., C.T. McElroy, D.W. Tarasick, and D.I. Wardle, 1994. The Canadian Ozone Watch and UV-B advisory programs. Pages 794–797 in *Ozone in the troposphere and stratosphere*. Proceedings of the Quadrennial Ozone Symposium 1992, NASA Conference Publication 3266. Berlin: Springer-Verlag.

Komhyr, W.D., 1980. *Operations handbook – ozone observations with a Dobson spectrophotometer*, WMO Ozone Report No. 6. Geneva: World Meteorological Organization.

Krueger, A.J., L.S. Walter, P.K. Bhartia, C.C. Schnetzler, N.A. Krotkov, I. Sprod, and G.J.S. Bluth, 1995. Volcanic sulfur dioxide measurements from the total ozone mapping spectrometer instruments. *J. Geophys. Res.*, **100**, 14057–14076.

Lubin, D., and E.H. Jensen, 1995. Effects of clouds and stratospheric ozone depletion on ultraviolet radiation changes. *Nature*, **377**, 710–713.

Madronich S., 1992. Implications of recent total ozone measurements for biologically active ultraviolet radiation reaching the Earth's surface. *Geophys. Res. Lett.*, **19**, 37–40.

Mayer B., G. Seckmeyer, and A. Kyling, 1997. Systematic long-term comparison of spectral UV measurements and UVSPEC modeling results. *J. Geophys. Res.*, **102**, 8755–8767.

Puckrin E., W.F.J. Evans, and T.A.B. Adamson, 1996. Measurement of tropospheric ozone by thermal emission spectroscopy. *Atmos. Environ.*, **30**, 563–568.

Quaite, R.E., B.M. Sutherland, and J.C. Sutherland, 1992. Action spectrum for DNA damage in alfalfa lowers predicted impact of ozone depletion. *Nature*, **358**, 576–578.

Ramanathan, V., L. Callis, R. Cess, J. Hansen, I. Isaksen, W. Kuhn, A. Lacis, F. Luther, J. Mahlman, R. Reck, and M. Schlesinger, 1987. Climate-chemical interactions and effects of changing atmospheric trace gases. *Rev. Geophys.*, **25**, 1441–1487.

Schwander, H., P. Koepke, and A. Ruggaber, 1997. Uncertainties in modeled UV irradiances due to limited accuracy and availability of input data. *J. Geophys. Res.*, **102**, 9419–9429.

Simmonds, P.G., and R.G. Derwent, 1991. Measurements of ozone and other radiatively active gases at Mace Head, Ireland. *Atmos. Environ.* **25A**, 1795–1808.

Sinha, A., and R. Toumi, 1996. A Comparison of climate forcings due to chlorofluorocarbons and carbon monoxide. *Geophys. Res. Lett.*, **23**, 65–68.

Stamnes, K., S-C. Tsay, and K. Jayaweera, 1988. Numerically stable algorithm for discrete-ordinate-method radiative transfer in multiple scattering and emitting layered media. *Appl. Opt.*, **27**, 2502–2509.

Stamnes K., J. Slusser, and M. Bowen, 1991. Derivation of total ozone abundance and cloud effects from spectral irradiance measurements. *Appl Opt.*, **30**, 4418–4426.

WMO, 1991. *Scientific Assessment of Stratospheric Ozone: 1991*. World Meteorological Organization Global Ozone Research and Monitoring Project, Report No. 25. Geneva: World Meteorological Organization.

WMO, 1994. *Scientific Assessment of Stratospheric Ozone: 1994*, World Meteorological Organization Global Ozone Research and Monitoring Project, Report No. 37. Geneva: World Meteorological Organization.

Zerefos C.S., A.F. Bais, C. Meleti, and I.C. Ziomas, 1995. A note on the recent increase of solar UV-B radiation over northern middle latitudes. *Geophys. Res. Lett*, **22**, 1245–1247.

CHAPTER 5

UV-B EFFECTS

5.1 INTRODUCTION

The correlation between the characteristics of the world's biomes and climatic factors such as temperature and precipitation is well understood, but it is only recently that scientists have recognized a similar equilibrium between ecosystem characteristics and UV-B radiation. Studies have shown that both reductions and increases in incoming UV-B result in observable and significant changes in ecosystem characteristics, although in either case the system may continue to function well. As a consequence of the continuing depletion of the stratospheric ozone layer, the amount of UV-B radiation reaching the earth's surface has increased over the past two decades. In response to these increases, fundamental changes to the structures and processes of existing ecosystems, both aquatic and terrestrial, may now be occurring. These changes are subtle and could evolve for many years until a new equilibrium is established. Even if mitigating measures were to succeed immediately in halting further increases in ambient levels of UV-B, ecosystems would continue to adjust for another 30 to 40 years. Whether these fundamental ecological changes will be good, bad, or inconsequential from a human perspective is not yet known. Consequently, there is a need for ecologists to expand their understanding of the role of UV-B in ecological processes and improve their ability to predict and measure natural impacts arising from UV-B increases at the earth's surface as a result of stratospheric ozone depletion.

Concerns about higher levels of UV-B are related not only to absolute increases in ambient levels but also to UV-B peaks that may occur at critical stages in the life cycles of organisms. Although many organisms have developed defence mechanisms to protect themselves from such fluctuations, the egg and larval stages of some species can be particularly susceptible to harm from UV-B peaks.

In Canada, these concerns are compounded by the impact of other environmental stressors, such as global warming, acid rain, land use changes, and toxic chemicals. As a result, UV-B impacts cannot be considered in isolation from these other factors. In any given case, UV-B may be either a causal factor or one of several contributing factors that cumulatively result in undesirable effects. The distinction between the two possibilities is seldom clear. It is essential, therefore, that studies of UV-B impacts on Canadian ecosystems be integrated with existing ecological research, monitoring, and assessment programs.

This chapter discusses the results of recent research on the effects of increased levels of UV-B radiation resulting from stratospheric ozone depletion on human health and terrestrial and aquatic ecosystems. The studies referred to are primarily Canadian and cover not only short-term direct impacts of UV-B but also life processes (e.g., photosynthesis) where the full effects may be evident only after several years of monitoring. Cumulative effects resulting from interactions with other anthropogenic stressors are discussed wherever possible. Where data permit, the potential socioeconomic consequences to Canada are also highlighted.

5.2 Human Health

Concern over stratospheric ozone depletion has led to scientific speculation about the effects of increased exposure to UV on human disease and on the incidence of skin cancers in particular. This concern has led to an enhanced level of research on human UV effects. In this section, some of the major advances taking place between 1987 and 1996 are described briefly by disease categories.

5.2.1 Cutaneous Malignant Melanoma

As several studies published in the early 1980s have shown, the relationship between cumulative sun exposure and melanoma risk is neither simple nor direct. Canadian and Australian scientists have independently hypothesized that melanoma is caused by strong intermittent sun exposure on unacclimatized skin [Elwood and Hislop 1982; Elwood and Gallagher 1983; Holman et al. 1983]. The Western Canada Melanoma Study [Elwood et al. 1985a; Gallagher et al. 1986] and the West Australia Melanoma Study [Holman et al. 1986] both demonstrated associations with indicators of intermittent recreational solar exposure. Furthermore, previous studies had demonstrated a strong and unexpected association between socioeconomic status and risk of melanoma – that is, workers in lower socioeconomic occupations with substantial outdoor exposure paradoxically had lower melanoma risk than members of indoor professional, managerial, and technical occupations. The Western Canada Melanoma Study showed that this gradient of risk was due to greater intermittent recreational sun exposure in the higher socioeconomic groups [Gallagher et al. 1987]. This observation was confirmed a year later in an important study conducted in East Denmark [Østerlind et al. 1988].

A large number of investigations by researchers from Europe [Beitner et al. 1990; Nelemans et al. 1993; Autier et al. 1994], Australia [Green et al. 1986], and the U.S. [Weinstock et al. 1989b; White et al. 1994; Holly et al. 1995] have confirmed the importance of intermittent solar UV radiation as a risk factor for melanoma. Australian and American studies [Khlat et al. 1992; Weinstock et al. 1989b] have also demonstrated the importance of childhood and adolescent exposure to solar UV as factors in adult melanoma risk.

Because reported exposure is subject to substantial error due to faulty memory among study subjects, investigators have used sunburn history as an indicator of strong intermittent solar exposure. Numerous studies have shown sunburn to be related to melanoma risk [Green et al. 1985; Elwood et al. 1985b; Østerlind et al. 1988; MacKie et al. 1989].

5.2.2 Acquired Melanocytic Nevi

Recent epidemiological research indicates that the strongest and most consistent indicator of elevated risk of cutaneous malignant melanoma is the presence of large numbers of acquired melanocytic nevi (skin moles) [Holly et al. 1987; Grob et al. 1990; Garbe et al. 1989; Marrett et al. 1992; Weinstock et al. 1989a]. The finding that many melanomas have histologic evidence of pre-existing nevi has led to major interest in the causes and formation of benign nevi. Although slightly over 1% of the population have nevi present at birth, that is, congenital nevi [Rivers et al. 1990], most nevi develop in childhood. A number of investigations of nevi in children have been carried out to evaluate whether solar UV radiation is involved in the genesis of these lesions.

A study of acquired melanocytic nevi among Vancouver schoolchildren, ages 6–18, revealed that nevus density increased with age in both males and females. Nevus density (nevi per square metre of body surface area) reached a maximum by about age 15, suggesting that the full adult complement of moles is acquired quite early in life [Gallagher et al. 1990a]. Furthermore, among white children, those with the highest nevus density tended to have light skin, were inclined to burn rather than tan in the sun, and were likely to have a history of sunburn [Gallagher et al. 1990b]. These risk factors are similar to those seen in studies of adult melanoma and suggest that sunlight exposure is involved in the genesis of both nevi and melanoma [McLean et al. 1995].

Further research, conducted by Australian and Canadian investigators, showed a direct relationship between latitude of residence and nevus density in Australian schoolchildren [Kelly et al. 1994]. Another Australian study of nevi in preschool age children confirmed the relationship between solar UV exposure and nevus density [Harrison et al. 1994].

Current research in Canada, Europe, and especially Australia is evaluating the use of programs promoting solar avoidance and sunscreen use as a means of reducing the number of nevi that children develop between birth and the teenage years. This research presupposes that nevi are an intermediate step in a continuous spectrum of lesions ranging from normal melanocytes to malignant melanoma. If this assumption is correct, reduction of the nevus density in children should result in lower melanoma rates in adult life.

5.2.3 Non-melanocytic Skin Cancer

Traditionally, the incidence of non-melanocytic skin cancer in white populations was thought to bear a simple direct relationship to cumulative solar UV exposure [Scotto et al. 1983]. This assumption was based largely on studies demonstrating that the incidence of such cancers in white populations

increased with proximity to the equator. However, until recently, relatively few analytic studies of basal cell carcinoma (BCC) and squamous cell carcinoma (SCC), the two principal types of non-melanocytic skin cancer, had been conducted.

Several recent studies have discussed the relationship of BCC and SCC to UV radiation. In Australia Kricker et al. [1995] demonstrated an increased risk of BCC with increased exposure to sunlight on weekends, a surrogate measure of intermittent solar exposure. This increase in risk was most pronounced for solar UV exposure in the late teenage years (15–19). Similar findings were seen in an Alberta study of non-melanocytic skin cancer [Gallagher et al. 1995a], with elevated risks for BCC in subjects with the highest solar exposure before the age of 20. Furthermore, the Canadian and Australian studies demonstrated a stronger effect of solar exposure in subjects with a propensity to burn rather than tan in the sun.

The Canadian study also showed an increased risk of SCC among people with chronic sunlight exposure obtained largely in occupational settings. The strongest effect was related to exposure in the 10 years prior to diagnosis [Gallagher et al. 1995b]. No difference in exposure effect was observed for SCC between those who burned and those who tanned easily in the sun.

Thus, the data for BCC, like those for melanoma, suggest that intermittent sun exposure, particularly in childhood, may be more important in accounting for risk than total cumulative dose. For SCC, in contrast, current evidence suggests that chronic cumulative dose is more important.

Finally, results from a study of non-melanocytic skin cancer conducted in high sunlight areas of Southern Europe [Rosso et al. 1996, Zanetti et al. 1996] confirm the elevated risk of non-melanocytic skin cancer in subjects with light skin colour, red hair, and a propensity to burn in the sun. Because of the greater range of solar UV exposure in this study than in the Canadian study, the investigators were able to produce dose-response curves relating BCC and SCC to accumulated solar exposure. The curves showed an increased risk of SCC occurring only after prolonged accumulated exposure (70,000+ hours), whereas the dose-response curve for BCC rose rapidly with relatively little exposure and then reached a plateau. These findings are consistent with the low-sunlight Canadian data and the Australian data.

5.2.4 *Immune Suppression*

Recent investigations indicate that UV radiation can suppress cellular components of the human immune system. Following exposure to 10–100 mJ cm^{-2} of UV-B, in the absence of sunscreen, the Langerhans cell population is depressed for more than two weeks [Miyagi et al. 1994]. This may be a marker for a potentially significant immunologic defect, particularly in relation to primary contact sensitization. Approximately 100 minutes of midday sun exposure in Italy could suppress resistance to *Listeria monocytogenese* (a bacterial agent that can produce meningitis and other diseases) to a medically significant degree [Garssen et al. 1996]. Other investigations have indicated that use of sunscreens likely does not prevent systemic immunosuppression by UV-B [Wolf et al. 1993]. However, it is difficult to assess the medical significance of studies that have shown immune suppression by UV radiation, as historically humans have spent a great deal of time in the sun and have moved to protect against overexposure only in recent years.

Recent studies have revealed an increase in skin cancers in medically immune-suppressed patients. In a follow-up of kidney transplant patients in Australia, 7% developed a skin cancer after 1 year, 45% after 11 years, and 70% after 20 years [Bouwes-Bavinck et al. 1996]. Other investigations have demonstrated that the increase in nevus counts in kidney transplant children receiving immunosuppressive treatment is greater than in children in control groups [Smith et al. 1993]. Furthermore, children receiving chemotherapy for hematological cancers demonstrated a median increase of 66 nevi per child three years after chemotherapy [Baird et al. 1992]. These data indicate that UV-B increases may be very important to medically immunosuppressed patients, even if the immune-suppressing effects of ultraviolet radiation in the normal healthy population are clinically insignificant.

A different line of investigation suggests that UV irradiation can stimulate synthesis of the interleukins IL-1, IL-6, and IL-8 (factors important in stimulating cell growth and proliferation) and that IL-1 and IL-8 can stimulate growth of subcutaneously injected melanoma B-16 cells in mice [McKenzie et al. 1994]. Furthermore, whole-body UV radiation also appears to stimulate increased IL-1 activity in humans [Granstein and Sauder 1987]. However, it is not clear that this has an effect on the ability in humans to resist tumour growth . Further research is required on basic mechanisms in humans in order to understand which UV effects are of concern in basic disease susceptibility. Currently, the clinical importance of this knowledge is not known.

5.2.5 *Infectious Diseases*

Adverse effects of UV on the course of a number of infectious diseases have been reported since the turn of the century, when Finsen [1901] showed that smallpox lesions were made larger by sun exposure. More recently, it was demonstrated that lesions from Herpes Simplex Virus I and II are reactivated

by UV exposure [Spruance 1985]. There is also speculation that excessive UV exposure may have an adverse effect on patients who are HIV-positive, as UV activates HIV *in vitro* [Zmudzka and Beer 1990]. However, no alteration in CD4+ cell count levels was seen after treatment of HIV patients with 60% of their minimal erythemal dose of UV for dermatologic disease [Warfel et al. 1993].

Global climate change also appears to be affecting the distribution of infectious diseases, especially those normally confined to tropical areas [Patz et al. 1996]. It is possible that an increase in ground-level UV-B might act synergistically with climate change on the frequency and severity of infectious disease [Patz et al. 1996].

5.2.6 Eye Damage

The deleterious effects of sunlight on the eye have been recorded since antiquity. It has become apparent in recent years, however, that the effects of UV radiation are more insidious and detrimental to the eye and vision than had been suspected previously. The effects may be acute (usually after a latent period), long-term after acute exposure, or chronic following long-term exposure to levels of UV below those required for an acute response [Cullen and Perera 1994].

Research on animals and fish has shown that premature aging of the lens, or cataract, has long been associated with UV radiation [Doughty and Cullen 1990; Cullen and Monteith-McMaster 1993]. A study by Cullen and Perera [1994] suggests that adverse effects such as chemosis, damaged epithelial cells, and development of inflammatory cells would result to the conjunctiva of the eye within minutes of direct exposure to sunlight at ambient levels of solar UV-B. Bergmanson et al. [1996], in their review of the clinical implications of exposure to solar UV, summarize several signs and symptoms associated with UV-induced keratoconjunctivitis. Because of the amount of new information available supporting the notion that UV radiation can harm the skin and the eye, these researchers suggest that practitioners should not hesitate to prescribe UV filters for sun glasses.

5.3 Terrestrial Ecosystems

The biological diversity of Canada, coupled with the latitude dependence of ozone layer thinning, creates a scenario for possible nutrient-driven and predator-driven disruptions to the stability of existing ecosystems. Such perturbations to population dynamics would be interwoven among terrestrial, aquatic, and wetland ecosystems.

Very little research exists on the effects of UV-B on terrestrial ecosystems within Canada. None exists for UV-B effects on flora and fauna, except for certain commercial agricultural and forest species, and these investigations have been skeletal and often conjectural. However, even this minimal research provides some insight into the potential implications of continuing increases in UV-B.

5.3.1 Agriculture

Approximately 7% of Canada's land area of 997 million hectares is arable. The agrifood sector produces 10% of Canada's gross domestic product and employs 15% of the country's 30 million people. The agro-ecosystem is unique in that most of it has been created and controlled by humans. The opportunities for mitigating the impacts of increased UV-B may be easier in such a system because it is likely to have fewer environmental variables to consider than natural systems and can be modified on an annual basis. Breeding crop varieties with increased resistance to UV-B, for instance, could be an effective mitigation strategy for agricultural systems.

In plants, UV-B radiation damages the membrane surrounding the cell, and the DNA within the cell nucleus. Other primary targets are the membrane-bound chloroplasts, which use sunlight to convert carbon dioxide and water into sugar. With damaged chloroplasts, the plant's capacity to produce energy is reduced and plant yields eventually decline. Plants do have the ability to repair damage caused by UV-B radiation; however, when the disruption exceeds the plant's ability to repair itself, permanent damage occurs.

UV-B radiation can affect a number of important plant processes and characteristics in the following ways.

- *Photosynthesis:* the ability of chloroplasts to produce sugars may be disrupted, resulting in reduced leaf productivity.
- *Growth:* leaf area, plant height, and fruit size can be altered.
- *Reproduction:* exposed pollen and eggs can be damaged, leading to reduced fertility and seed production.
- *Ecology:* differential tolerances may favour the growth of one plant type over others, an important consideration in weed-crop situations and in pasture mixtures.
- *Quality:* surface blemishes on vegetables or fruits reduce the quality of the produce. The production of pigments in response to UV-B may affect the taste of the crop. A reduction in crop quality may be far more damaging, in terms of dollars, than a reduction in yield.

5.3.1.1 Forage

Papadopoulos et al. [1996] tested the UV-B tolerance of different varieties of forage crops (alfalfa, red clover, birdsfoot, trefoil, white clover, timothy, orchard grass, bromegrass, and meadow fescue) and vegetables (carrots and broccoli). Tests were done under field conditions using filters to screen out ambient levels of UV-B. The removal of UV-B radiation from timothy grass resulted in increased rates of leaf elongation

during the second regrowth and a greater number of tillers per plant [Belanger et al. 1996]. However, the vegetative yield of legume species from the spring growing period was lower in the first year of growth when ambient UV-B radiation was filtered out. UV-B radiation had an effect on the yield of grass species in only one of the two years.

A related study, this time under greenhouse conditions, assessed the effect of increased UV-B radiation on eight varieties from two forage legume and two forage grass species [Bush et al. 1995a]. Illumination was provided by grow lights, augmented by UV lamps which provided three UV-B levels: mid-summer ambient, 2x ambient, and 3x ambient. No significant differences in plant growth among the three UV-B levels were observed.

In yet another study, four broccoli varieties were grown under filter frames. Levels of UV-B–absorbing pigments were greater in plants grown under ambient sunlight than in those grown under the filters [Goodyear et al. 1996]. The response to UV-B radiation differed somewhat with the variety.

5.3.1.2 Soybean

In 1994, eight Ontario soybean (*Glycine max* [L] Merr.) varieties were grown in the field under lamps providing a UV-B radiation dose equivalent to a 25% decrease in the ozone layer (Table 5.1). As a control, a similar group of plants was grown under lamps with the UV-B radiation removed by filters. Six of the eight cultivars had their yield reduced as a result of increased UV-B radiation. The average yield loss from the simulated 25% decrease in the ozone layer was 7%. In 1995, with the soybean crop worth over $700 million at the farm gate (information from Ontario Ministry of Agriculture Food and Rural Affairs), a 7% yield loss would equate to $49 million in lost revenue.

Table 5.1: Effect of UV-B Radiation on the Seed Yield (kg ha^{-1}) of Eight Varieties of Soybean

Soybean variety	Yield of enhanced UV-B group	Yield of control group	Percentage difference from control
Mandarin	2570	2880	11
Crest	2520	2890	13
Maple Arrow	3103	2960	–5
9061	2710	3090	12
SOO-88	3070	3620	15
PS42	3320	2770	–20
AC Bravor	3050	3670	17
9071	3020	3290	8
Average	2920	3150	7

The function of the flavonol glycosides in plant cells is unclear, although they have been implicated in growth regulation, disease resistance, and protection of the leaf mesophyll from UV radiation. The plant's capacity to produce UV-absorbing pigments is likely the first line of resistance to the damaging effects of UV radiation. These pigments, located in the hairs of soybean plants, give the plants a grey or tawny appearance, depending on the type of flavonol glycosides present. When soybean plant hair is grey, kaempferol flavonol glycosides are present in the leaves. However, when soybeans appear tawny in colour, the plants contain both quercetin and kaempferol flavonol glycosides.

In experiments done in 1995, Agriculture Canada researchers exposed soybean plants, with either grey or tawny pubescence, to UV-B radiation in controlled environmental cabinets. Leaves from the exposed plants and a control group of non-exposed plants were sampled at regular intervals. When UV-B–absorbing pigments were extracted from the leaves and measured using a spectrophotometer, concentrations of these pigments were found to be greater in the exposure cabinet than in the control cabinet. The pigment concentrations also increased for three days following UV-B exposure, then levelled off.

In addition, leaf cross-sections were scanned for UV-B–absorbing pigments using a microspectrophotometer, an instrument combining a spectrophotometer and a microscope [Pietrzak et al. 1995]. Most of the protective pigmentation was located in the palisade layer of the leaf tissue, with relatively less pigmentation in the epidermis and mesophyll regions. Concentrations of UV-B–absorbing pigments were also greater in the upper surface of the leaf than in the lower surface, which may explain why sunburn symptoms are usually more severe on the lower surface of soybean leaves.

5.3.1.3 Tomatoes

In experiments at the University of Guelph, 37 varieties of processing tomato (*Lycopersicon esculentum* Mill.) were screened for tolerance to UV-B in controlled environmental chambers. The plants were subjected to ambient UV-B, as well as UV-B levels equivalent to a 20% reduction in the ozone layer. Reductions in plant height as a result of enhanced UV-B exposure varied from 10% to 32%, while plant leaf area was reduced by 10–28%. The response to UV-B was also characterized by genetic variability within species (S. Keelan, University of Guelph, personal communication, 1995).

5.3.1.4 Maize

Maize (*Zea mays* L.) hybrids exhibited no deleterious effects on dry matter production, even when grown in controlled environmental cabinets under UV-B radiation simulating a 40% decrease in the ozone layer. Therefore, there is sufficient genotypic tolerance in Canadian maize hybrids to minimize the effects of predicted increases in UV-B [Van Doren 1995].

5.3.1.5 Canola

Researchers at the University of Guelph have screened canola (*Brassica napus* and *B. rapa* L.) varieties for tolerance to UV-B radiation in controlled environmental chambers. The plants were grown under ambient UV-B levels and levels equivalent to those arising from a 20% decrease in the ozone layer. *B. rapa* varieties were more susceptible to UV-B radiation than the *B. napus* varieties. Varietal differences for the growth parameter measured indicate that UV-B tolerance is a characteristic that can be bred into new varieties (D.J. Home, University of Guelph, personal communication, 1996).

In a related field study, researchers at the University of Guelph grew the same varieties of canola and exposed them to UV-B radiation equivalent to a reduction in the ozone layer of about 25%. The plants were exposed to UV-B from the onset of flowering to maturity. Table 5.2 shows that within both *Brassica napus* and *B. rapa* types of canola tolerance to UV-B radiation is variable. The average yield reduction from UV-B radiation was 14%. In 1996, the Canadian canola crop was worth $2.2 billion at the farm gate (data supplied by the Canola Council of Canada); thus, a 14% yield loss would equate to $308 million in lost revenue.

Table 5.2: Seed Yield (kg ha^{-1}) of Spring Canola Varieties Exposed to 10-14 kJ m^{-2} d^{-1} UV-B, Corresponding to a Decrease in the Ozone Layer of 25%.

Cultivar	Enhanced UV-B	Control	Yield reduction from control (%)
B. napus			
Bounty	1765	2440	27.7
Cyclone	2255	3052	26.1
Garrison	6630	5546	–19.6
Hyola 401	6221	5978	–4.1
Shiralee	2141	3809	43.8
Average	3802	4165	14.8
B. rapa			
AC Parkland	3521	6450	45.4
Horizon	5591	7688	27.3
Tobin	4257	3283	–29.7
Average	4457	5807	14.3

Canola adjusts to UV-B stress by synthesizing UV-screening epidermal flavonoid pigments. The increased flavonoid levels protect photosynthesis from UV change. Other research at the University of Waterloo has shown that an essential enzyme of respiration (ribulose-bisphosphate carboxylase) is photomodified to a form with a higher molecular weight by UV-B. This photomodification process is being examined *in vitro* to probe the mechanism of UV-B damage to proteins [Wilson and Greenberg 1993a, 1993b].

5.3.1.6 Wheat Straw

The straw and chaff left behind by a combine are incorporated into the soil through light tillage or, in the case of minimal tillage, left on the soil surface to decompose. The rate at which this material decomposes is increased by exposure to higher levels of UV-B [Ellert et al. 1995]. As well as providing raw material for soil humus, plant litter is an energy source for soil organisms and a nutrient source for plants.

Two recent experiments have examined the effect of UV-B on the decomposition of plant litter. In one of these, wheat straw was exposed to UV-B radiation under laboratory conditions, and the soluble carbon was measured. In the other, UV-B filters were placed over wheat straw exposed to ambient solar radiation. Solubilized carbon was extracted and measured. In both experiments, the soluble carbon concentration of the straw was enhanced by exposure to UV-B radiation, and the amount solubilized was positively related to the intensity of the UV-B. UV-B may accelerate the rate of decomposition by causing an increase in the rate of release of carbon from plant litter. This effect is of significance in arid environments or in minimum-till situations [Ellert et al. 1995].

5.3.1.7 UV-B Effects on Yield

Many factors determine yield. If a plant cannot compensate for the physical damage caused by UV-B, its yield will decrease. Krupa and Kickert [1989] examined studies of the effects of UV-B on over 100 varieties of 12 important crop species and rated crop sensitivity to UV-B on the basis of changes in biomass production. Of the varieties examined, 40% were unaffected by UV-B radiation equivalent to a 20% decrease in the ozone layer, while 60% were affected in some way. In Canada, most crops are tolerant of or have intermediate sensitivity to moderate increases in UV-B radiation (Table 5.3).

Table 5.3: UV-B Sensitivity Rating, Based on the Work of Krupa and Kickert [1989]

UV-B Sensitivity Rating		
TOLERANT	**INTERMEDIATE**	**SUSCEPTIBLE**
wheat	barley	oat
sunflower	rye	pepper
corn	soybean	cucumber
tobacco	pea	mustard
red clover	tomato	canola
alfalfa	potato	
bluegrass		
orchard grass		
cabbage		

The following approach has been used to create a simple model for predicting the effect of increased UV-B radiation on future crop yield.

- The Krupa and Kickert [1989] UV-B sensitivity rating was used to classify the major Canadian crops into tolerant, intermediate, and susceptible categories. Tolerant crops were excluded from further calculation.
- Three levels of UV-B radiation increase above the ambient level were established: 5%, 10%, and 20%.
- Three levels of yield reduction, corresponding to the three UV-B scenarios were then established. Intermediate tolerant crops had yields reduced by 1%, 2.5%, and 5% with a 5%, 10% and 20% increase in UV-B respectively. Susceptible crops had yields reduced by 2%, 5%, and 10% respectively with similar increases in UV-B.
- A farm gate dollar value, based on the 1995 yield estimates, was established for intermediate and susceptible crops.
- Other associated stresses, such as drought, or potential mitigating factors, such as increased atmospheric CO_2, were not considered.

A 5% increase in UV-B radiation would result in losses to sensitive and intermediate crops of $89 million per year (Table 5.4). With a 20% increase in UV-B, farm gate receipts would be reduced by $387 million per year. It is, however, very difficult to substantiate the conclusion that yield reductions are the result of one specific stress such as UV-B. Nevertheless, given current information on the response of plants to UV-B, it is reasonable to assume that increased UV-B will result in some crop loss.

5.3.1.8 Research needs

UV-B impacts in several areas remain unexplored or underexplored. These include:

- the soil ecosystem, including its fauna and flora
- animal production and health
- the interaction of UV-B impacts with plant diseases, weeds, and pests
- agrochemical interactions and degradation

Understanding the ramifications of effects in these areas is essential to a full understanding of the implications of UV-B increases for Canadian agriculture.

5.3.2 Forests

Canadians are custodians of 10% of the world's forest lands. Spread across 417 million hectares and covering 42% of the national landscape [CCFM 1995], Canada's forests are of huge cultural, economic, and social importance. Because of their extent and diversity, they are also of considerable ecological significance, providing habitat for wildlife and playing a major role in the global climate system and related processes such as the carbon cycle.

Table 5.4: Predicted Canadian Crop Loss for a Predicted Increase in UV-B radiation (UV-B Tolerant Crops not Included)

Crop	UV-B sensitivity	Current yield (million $)	Predicted yield (million $) with a UV-B increase		
			5%	10%	20%
canola	susceptible	2100	2048	1995	1890
oat	susceptible	226	220	215	203
soybean	intermediate	700	693	683	665
barley	intermediate	796	788	776	756
tree fruit	intermediate	230	228	224	219
soft fruit	intermediate	204	202	199	194
potato	intermediate	506	501	493	481
vegetable	intermediate	652	645	636	619
TOTAL		5414	5325	5221	5027
DIFFERENCE (TOTAL $ LOSS)			89	192	387

Forests are dynamic and continuously subjected to a changing complex of natural and anthropogenic stresses. In 1994, approximately 750,000 ha of forest in Canada were lost to fire, 11.6 million ha were defoliated by insects, and 988,960 ha were harvested [CCFM 1995]. In addition, it is estimated that 35 million ha of forest are exposed to acidic deposition and tropospheric ozone on a routine basis. The impacts of these pollutants, however, are regional in scale. On a national scale, Canada's forests are threatened by two important components of global environmental change, climate change and increases in UV-B radiation.

Unlike agricultural crops, forests are long-lived and will be exposed to increased UV-B over many years and decades. While some short-term effects have been reported, there is evidence that effects induced at the tree level are cumulative over many years [Sullivan and Teramura 1992]. Generally, not much is known concerning UV-B effects on forests, a surprising situation when one considers that forests comprise nearly 80% of total terrestrial biomass [Whittaker 1975].

The overwhelming majority of the literature on UV-B effects on plants deals with crop species and cultivars. Relatively little is known about impacts on forest tree species, and much of the limited knowledge that is available is derived from UV-B simulation experiments using species not native to Canada. A report by Loucks [1994], which linked elevated UV-B levels in 1993 to "sun-scalding" of white pine foliage in Ohio and Ontario, is the only study so far to have documented UV-B effects in the field.

5.3.2.1 Effects of UV-B on Photosynthesis in Trees

The literature on forest trees indicates that photosystem (PS) II is more affected by UV-B than PS I [Bornman and Teramura 1993]. Because of differences in experimental protocols, stage of plant and leaf development, genotypic variability, and other factors, the direction and magnitude of these effects in plants have not been consistent throughout the various studies.

Two recent, non-Canadian studies serve to illustrate the kind of research now under way into the effects of UV-B on photosynthesis. In the first of these, Naidu et al. [1993] investigated cumulative damage potential by exposing three-year-old loblolly pine (*Pinus taeda* L.) seedlings in the field to ambient (8.5 kJ m^{-2} at summer solstice) or enhanced (13.5 kJ m^{-2}) levels of biologically effective UV-B ($UV\text{-}B_{BE}$). The most recently expanded needles showed a 6% decrease in the ratio of variable to maximum fluorescence following dark adaptation, but older needles did not. No effects of enhanced UV-B on other measures of photosynthesis were noted. However, the carbon isotope ratio, which is a common time-integrated measure of photosynthesis, was more negative in two of the four needle age classes of treated seedlings, and needle length in three age classes was reduced. Because of differences in the photosynthesis measures and in the foliar chemical composition of the youngest and oldest needle age classes, the authors speculated that the differences observed between needles exposed to enhanced UV-B and those exposed to ambient levels could also reflect adaptation to shaded conditions within the canopy.

In the second study, the influence of UV-B on photosynthesis in seedlings of Norway spruce (*Picea abies* (L.) Karst.) was investigated over a two-year period by Bavcon et al. [1996]. Enhanced UV-B irradiances were extremely high (17.7 or 28 kJ m^{-2} over 8 hours) compared to maxima that might be expected from ozone depletion.The experiments also included temperature as a co-factor, since treatment was continued year-round. Synergistic effects between low temperature and enhanced UV-B were observed in the second winter. Chlorophyll concentrations were lower in one- and two-year-old needles exposed to higher UV-B levels. As temperature decreased, photochemical efficiency, vitality index, and photosynthetic activity diminished in treated plants and led to premature needle senescence.

5.3.2.2 Effects of UV-B on Tree Growth and Biomass

Sullivan and Teramura [1988] examined the effect of UV-B on seedling growth in the Pinaceae. Seedlings were grown for 22 weeks under daily doses of 0, 12.4, or 19.1 kJ m^{-2} of biologically effective UV-B. Seedling height was reduced by enhanced UV-B in lodgepole pine (*Pinus contorta* Dougl.), red pine (*Pinus resinosa* Ait.), and loblolly pine. Biomass, however, increased in Engelmann spruce (*Picea engelmannii* Parry). Fraser fir (*Abies fraseri* (Pursh) Poir), pinyon pine (*Pinus edulis* Engelm.) and black pine (*Pinus nigra* Arnold) were unaffected. Biomass reductions occurred in all other species. Effects of UV-B were less for species native to higher elevations, implying natural adaptation to higher UV-B levels at high altitude. Visual symptoms were observed, including stunting and needle discolouration, but only in three of the ten species studied.

Using older seedling material (one-year-old) and longer exposure times (seven months), the same authors [Sullivan and Teramura 1989] simulated loblolly pine exposure to 16%, 25%, and 40% ozone depletions (11.5, 13.6, and 19.1 kJ m^{-2} $UV\text{-}B_{BE}$). They found that enhanced UV-B affected growth and suggested that the effects might be cumulative throughout the growing season.

To test the cumulative effects hypothesis, Sullivan and Teramura [1992] conducted a three-year field experiment with natural and supplemented UV-B irradiances and seed sources from seven latitudes in the U.S. (31°N to 39°N). After three seasons of exposure, cumulative biomass reductions were

noted in three of the four sources, with the reductions split equally between root and shoot portions. Therefore, reductions in biomass were attributed to an overall decrease in biomass accumulation rather than a shift in carbon partitioning. The authors inferred that continued ozone depletion would affect the commercial productivity of the leading commercial species in the southeast. The inconsistencies in response between the one-year and three-year exposures highlight the need for multiyear experiments with long-lived, forest tree species.

It is well known from studies with trees [Caldwell et al. 1982] and with species from alpine areas in Europe [Rau and Hofman 1996] that plants adapted to grow at higher elevations are more resistant to UV-B than their counterparts from lower elevations. A similar relationship was seen in a study involving 38 plant species growing in natural systems along elevational gradients in Hawaii [Sullivan et al. 1992; Ziska et al. 1992]. Recent evidence also confirms that the UV-B tolerance of Canadian tree species shows a similar correlation with elevation (S. L'Hirondelle, B.C. Ministry of Forests, personal communication). Thus, not only latitude but elevation of seed source may need to be considered in any future adaptation strategy for intensively managed forest lands.

5.3.2.3 Interaction of Enhanced UV-B with Increased Atmospheric CO_2 Concentrations

Global environmental change, including increasing anthropogenic production of carbon dioxide and depletion of the stratospheric ozone layer, is altering the growth environment for forests. Some recent studies, therefore, have investigated the effects of interactions between enhanced UV-B and increased, usually doubled, CO_2 concentrations.

Stewart and Hoddinott [1993], for example, grew jack pine (*Pinus banksiana* Lamb.) seedlings for nine months in greenhouses with CO_2 concentrations of either 350 or 750 μmol mol^{-1} and low or high UV-B irradiances. High UV-B treatment decreased seedling dry weight, although dry weight was unaffected by CO_2. Carbon allocation to leaf production was favoured under high UV-B levels. High UV-B inhibited photosynthesis at 350 μmol mol^{-1} CO_2, but not at 750 μmol mol^{-1}. Interestingly, stomatal density was increased by high UV-B irradiance, but not by CO_2 enhancement.

In another study, Yakimchuck and Hoddinott [1994] examined the interactive effects of UV-B and CO_2 enrichment on the growth and physiology of seedlings of three species, jack pine, black spruce (*Picea mariana* (Mill.) B.S.P.), and white spruce (*Picea glauca* (Moench) Voss) that were grown from seed for 16 weeks. Biomass production in all species increased at high CO_2 concentrations (750 μmol mol^{-1}) but decreased at high UV-B irradiances.

A greater production of UV-B–absorbing pigments was measured in jack pine, a shade-intolerant species, than in the shade-tolerant spruces. The authors concluded that future conifer seedling growth and competitive ability will be altered by changes in ambient levels of UV-B and CO_2.

Sullivan and Teramura [1994] continued their studies with loblolly pine by investigating the effects of enhanced UV-B (13.8 kJ m^{-2} UV-B) in combination with increased CO_2 (650 μmol mol^{-1}). The higher UV-B irradiance reduced seedling biomass by 12% after 22 weeks treatment at both CO_2 levels (350 and 650 μmol mol^{-1}). However, dry matter partitioning was altered by the interaction between UV-B and CO_2, with dry matter being allocated more to shoot components by UV-B radiation when the CO_2 concentration was 350 μmol mol^{-1} and to roots when the concentration was 650 μmol mol^{-1}. The authors indicated that these subtle interactions could be important in the future to seedling establishment and competitive interactions.

These few studies indicate that UV-B impacts on forests should not be considered in isolation. Rather, the dominant components of global environmental change – UV-B and CO_2 – should be considered together as interactive stresses when considering the likely impacts of either on forests.

5.3.2.4 New Canadian Research

Currently, at least three centres are actively involved in research into UV-B effects on forest trees in Canada. Their programs are in various stages of development and are focused on different aspects of the problem.

Natural Resources Canada, Canadian Forest Service

The Fredericton-based Atlantic Forestry Centre of the Canadian Forest Service (CFS) has been conducting in-house and collaborative research into UV-B effects since 1993. In initial collaborative studies with colleagues in the UK, "model" crop species were used to provide a rapid means of determining the direction and magnitude of UV-B effects on cuticles. This information was then used to optimize experimental design for longer-term work with tree species. Responses of single crop species, transgenic mutants, and six varieties of pea (*Pisum sativum* L.) indicated that moderately enhanced UV-B had the potential to cause deleterious and specific alteration of both the surface properties of leaves and the chemical composition of the epicuticular wax [Barnes et al. 1994; Barnes et al. 1996; Gonzalez et al. 1996].

Since then, research supported by the CFS and the Natural Sciences and Engineering Research Council (NSERC) has been conducted into UV-B effects on the surface physicochemical characteristics, surface properties, ultrastructure, and physiology of leaves. In one of these studies, two-year-old seedlings of four spruce species – white spruce, red spruce

(*Picea rubens* Sarg.), black spruce, and Norway spruce – were exposed to a gradient of biologically effective UV-B (0.81–6.61 kJ m^{-2} d^{-1}) over a period of 11 weeks from bud-break to bud-set. The chemical composition of the epicuticular wax was affected in all species as the dosage increased [Gordon et al. 1995]. Effects were often induced early in the 35-day experimental period. In particular, nonacosane diol and alkyl ester proportions increased in Norway spruce needles, while fatty acids increased on black spruce needles, and estolide proportions increased in red spruce needle wax [Gordon et al. 1997a]. Norway spruce was the only species, however, to show a reduction in internode extension due to UV-B. It should be noted that the highest UV-B enhancement in this study (6.6 kJ UV-B_{BE} m^{-2} d^{-1}) was low relative to other dosages at which significant effects on conifer species have been reported.

Preliminary indications of a direct effect of UV-B at the enzyme level in wax biosynthesis were confirmed in a native deciduous species, the sugar maple (*Acer saccharum* Marsh.). *De novo* wax synthesis was studied using radiotracer techniques and leaf discs irradiated by biologically effective UV-B during [1–^{14}C] acetate uptake. Maximum incorporation of [1–^{14}C] into epicuticular waxes occurred at 6.2 kJ m^{-2} d^{-1} and decreased significantly at greater UV-B doses [Gordon et al. 1997b]. Incorporation of [1–^{14}C] into alkyl esters decreased, while incorporation into alkanes increased with increasing UV-B dose. These initial results are being followed up using radio- and heavy-isotope labelling techniques to determine the effect of UV-B on enzyme activity at a critical stage in conifer wax biosynthesis.

In the first stage of a three-phase parallel study now in progress, the New Brunswick Department of Natural Resources and Energy and the British Columbia Ministry of Forests, in partnership with CFS, are investigating the sensitivity to UV-B of 20 Canadian tree species at the juvenile seedling stage. Simultaneously, physiological growth modelling experiments with a sensitive species are underway, using both UV-B and nitrogen as co-factors. The third phase includes genetic engineering research aimed at the production of plants for use as field biomonitors for UV-B effects.

British Columbia Ministry of Forests

Research into UV-B effects has been underway at the B.C. Ministry of Forests' Glyn Road Research Station in Victoria since 1995. Three studies have been completed and one is ongoing. In one of the completed studies, three-month-old Engelmann spruce seedlings from five elevations (850–1700 m) were exposed to 0, 4.75, 9.5, or 14.25 kJ m^{-2} UV-B for six hours daily. Measurements were made of seedling morphology, biomass, chlorophyll fluorescence, membrane leakage, pigment content, and frost hardiness. Strong effects due to elevation were noted. Seedlings from the lowest elevation manifested changes in morphology and physiology at the highest UV-B dose [Binder and L'Hirondelle 1996].

In a second study, L'Hirondelle and Binder [1996] exposed Sitka spruce (*Picea sitchensis* (Bong.) Carr.) and coastal Douglas-fir (*Pseudotsuga menziesii* (Mirb.) Franco) from three elevations to UV-B dosages of 0, 4, 8, and 14 kJ m^{-2} d^{-1}. Sitka spruce seedlings were less sensitive than Douglas-fir seedlings. Within four days of exposure, Douglas-fir seedlings exposed to the highest doses were dead. At lower doses, there were strong UV-B effects on Douglas-fir height, root collar diameter, and dry weight. Dry weights of Douglas-fir seedlings decreased 34–37% as UV-B increased from 0 to 8 kJ m^{-2} d^{-1}, while the dry weight of Sitka spruce seedlings decreased 20% over the same range. There was no overall effect of elevation on response within the range studied.

Other species were investigated in a third study, similar in design to the preceding two. Frost hardiness was demonstrated to decrease with increasing UV-B dose in interior white spruce seedlings, but it increased in interior Douglas-fir seedlings (S. L'Hirondelle, B.C. Ministry of Forests, personal communication). A fourth study is underway using western red cedar (*Thuja plicata* Donn.).

Centre for Forest Biology, University of Victoria

Research work, under the leadership of Dr. D.P. Ormrod, is focused on molecular genetics, tree physiology, and anatomy and morphology. The goal is to ensure that the array of genotypes currently utilized in forest regeneration has the capability to thrive under increasing UV-B irradiation.

Short-term objectives are:

1. to compare Douglas-fir with other conifers and with model plant systems for their defence response to UV-B and other environmental stressors,
2. to define common elements of the responses among species, and
3. to make comparisons among genotypes within each species.

Growth chambers and a field simulation facility are being used. Species exposed include Douglas-fir, ponderosa pine (*Pinus ponderosa* Laws.), western red cedar, western hemlock (*Tsuga heterophylla* (Raf.) Sarg.), and white spruce. Other stressors to be applied along with UV-B include drought, heat, cold, and high visible irradiance.

5.3.2.5 Research and Monitoring Needs

Estimation of long-term UV-B impacts on the growth of natural ecosystems, unmanaged or managed forests, biodiversity structure, and forest sustainability cannot be accurately predicted with the limited knowledge base now available. With the exception of several reports from multiyear field simulations, experimental scientific research with forest trees has been conducted in the laboratory at the seedling, leaf, and cellular levels. Extrapolation of these data to the field level is not possible at this time [Percy and Hall 1997].

In order to address knowledge gaps, effort should be focused on the following areas:

- screening and identification of sensitive species, genotypes, and growth stages
- identification of biochemical and physiological attributes contributing to sensitivity or resistance
- modelling of effects on seedling growth
- multiyear field simulations of UV-B enhancement
- instrumentation of selected forest health monitoring sites for continuous UV-B measurement
- consideration of UV-B in breeding/reforestation strategies
- investigation of effects on reproduction
- assessment of potential for UV-B to alter biodiversity in forest ecosystems

The 50-year window of significant ozone depletion has sufficient potential to affect Canadian forest productivity on a large scale. Chronic UV-B damage to our long-lived, slow-growing tree species could have far-reaching consequences which are not yet apparent.

5.4 Freshwater and Wetland Ecosystems

Freshwater ecosystems within Canada have been examined for effects from UV radiation more extensively than terrestrial, wetland, and marine ecosystems. Chemical and biological effects on shallow water ecosystems, in particular, can be extensive. In combination with other stressors, enhanced UV radiation affects a wide variety of ecosystem functions and processes. Examples are depressed primary productivity, disrupted nutrient cycles, altered community structures, and modified toxic chemical patterns in the food chain. Socioeconomic impacts may also occur. Scientists are far better at describing these effects than they are at quantifying, modelling, or predicting their relative significance. This is in large part a consequence of the non-linear nature of ecosystem responses to UV-B.

5.4.1 Inland Waters

The penetration of UV-B in boreal lakes is known to be a function of the concentration of dissolved organic carbon (DOC) [Scully and Lean 1994]. As levels of DOC decline, UV-B penetration into the water column increases exponentially. Schindler et al. [1996] showed that climate warming, acid deposition, and ultraviolet radiation are intimately linked through interactions with DOC. Data taken from 46 lakes over 20 years in northwestern Ontario showed a sharp decline in DOC in the water. The average DOC level dropped 15–20%, while UV-B penetration into the water increased by between 22% and 60%. The study concluded that both climatic warming and lake acidification had produced significant declines in the DOC content of boreal lakes. In essence, UV-induced chemical and biological reactions have been responsible for changes in the aquatic ecosystems that had previously been attributed solely to acidic intrusions. Similar conclusions come from Yan et al. [1996] in their analysis of DOC decline and overall terrestrial and aquatic impacts on carbon cycle dynamics in Swan Lake, Ontario, and its basin.

Additionally, in a comprehensive empirical modelling analysis of over 2000 lakes covering eastern North America and the western United States, Williamson et al. [1996] determined relationships between DOC content and UV-B depth penetration. Their study suggested that in lakes with a DOC content less than 2 mg L^{-1}, UV-B penetration depth was more sensitive to changes in DOC levels than to changes in stratospheric ozone.

By exposing zooplankton to various levels of solar UV-B radiation, Williamson et al. [1994] showed that UV-B, even at ambient levels, inhibits some species of zooplankton from frequenting their preferred ecotones.

Through experiments in shallow flumes shielded from various wavelengths of sunlight, Bothwell et al. [1994] demonstrated that, although enhanced levels of UV light diminished the primary production of phytoplankton as expected, they reduced the size of the chironomid community that fed on the phytoplankton to an even greater extent. As a result, the accumulated phytoplankton biomass actually increased with exposure to higher UV levels, even though primary production of phytoplankton biomass was reduced. This occurred because a vital link in the food chain had been weakened and less production was being transferred to higher levels. The implications for food chain integrity and the persistence of desirable species and attributes in aquatic ecosystems are disturbing.

Recently, within the western basin of Lake Erie, blooms of the toxic blue-green alga *Microcystis* have appeared. Prior to this algal growth, dramatic colonization by the exotic zebra mussel and concurrent disruptions to algal population dynamics had resulted in increased water clarity. This, in turn, has increased the depth of the UV-B photic zone.

Polycyclic aromatic hydrocarbons (PAHs) are a ubiquitous group of toxic and mutagenic pollutants. Greenberg and colleagues at the University of Waterloo have observed that ambient UV irradiation significantly increases the toxicity of PAHs to *Lemna gibba* (an aquatic higher plant), *Daphnia magna* (an aquatic invertebrate), and aquatic bacteria. Of greater concern is their finding that PAHs are rapidly photooxidized by solar radiation to compounds with dramatically enhanced toxicity. However, since PAH loads in the environment have been calculated solely on the basis of the intact chemicals, the impacts of these substances are likely to have been underestimated [Wilson and Greenberg 1993a; Huang et al. 1995; Ren et al. 1994].

5.4.2 Amphibians

The effects of increased UV-B radiation on amphibians could be widespread. Possible direct effects include mortality, abnormal embryonic and larval development, damage to exposed organs such as the eye and skin, and systemic effects through the suppression of the immune system [van der Leun and de Gruijl 1993]. Indirect effects include changes in the relative abundance of predators, parasites, and competitors as well as toxic effects from chemicals produced or released from sediments as a result of photochemical reactions [Ovaska and Pauli 1997].

Research on UV-B effects on amphibians (frogs, toads, salamanders, etc.) within North America has been minimal. Within Canada, Grant and Licht [1995] carried out laboratory experiments on the eggs and larvae of several frog and toad species common in Ontario to establish lethal and sublethal levels of UV-A and UV-B radiation.The eggs were either exposed directly or allowed to hatch. Following the hatching of the unexposed eggs, the subsequent larval and metamorphosed forms were tested. The study concluded that current ambient levels and fluctuations of UV radiation in Ontario do not appear to adversely affect any of the life stages of the tested native amphibian species. A combination of factors, such as a copious jelly covering the eggs, photorepair mechanisms in the embryos, melanin pigmentation, and physical protection in the environment, is sufficient to protect these amphibians at current levels of exposure.

Several studies of central and northern Ontario lakes, however, suggest a potential for deleterious effects as a result of interactions between UV-B, climate change, and lake acidification [Schindler et al. 1996, Yan et al. 1996]. In one such study Mallory and co-workers described patterns of UV-B irradiance across central Ontario. They then linked these patterns with existing lake chemistries and amphibian habitat preferences to develop a preliminary risk assessment. Their modelling of UV-B patterns since 1979 suggests that exposure of amphibian eggs and embryos to UV-B has increased due to direct increases of irradiance. They concluded that, although there are no studies that provide measurements of actual mortality due to the cumulative impact of acidity, climate change, and UV-B, there is nevertheless a high potential for destructive synergistic impacts on lake food webs, habitat structure and composition, and amphibian reproduction and physiology as a result of these and other anthropogenic stresses (M.L. Mallory, personal communication).

Ovaska and Pauli [1997] have provided a brief synopsis of UV-B and amphibian research over the past two decades which reinforces conclusions about the lack of data in this area. They and other researchers also point to the importance of considering the cumulative impacts of UV-B in association with pressures such as acid rain, global warming, fungal infections, and toxic chemicals [Grant and Licht 1993; Scully and Lean 1994; Blaustein et al. 1994]. To compensate for the paucity of data on the resistance of different species, Ovaska [Ovaska and Pauli 1997] developed UV vulnerability scores for amphibians based on potential exposure at the egg, larval, and adult stages. The resulting scores reveal that many amphibian species in Canada are vulnerable to increased solar UV-B, particularly at the egg and larval stages. Vulnerable species include the western toad (*Bufo boreas*), spotted frog (*Rana pretiosa*), and Canadian toad (*Bufo hemiophrys*). For salamanders, sensitive species include the northwestern salamander (*Ambystoma gracile*), roughskin newt (*Taricha granulosa*), and tiger salamander (*Ambystoma tigrinum*). However, about 50% of the salamander species in Canada are not exposed to solar radiation at early stages of development. Relative scores such as these serve as a key tool for setting reporting, research, and monitoring priorities.

5.4.3 Research Needs

Because of the complex association of UV-B impacts with other environmental factors, research needs are varied. Foremost among these is the requirement for an integrated approach to the study of ecosystem effects which would help to identify opportunities to minimize or adapt to these impacts. This research would concentrate initially on wetlands, since they are the ecosystems that are believed to be most sensitive to changes in UV-B.

Other research needs include

- development and application of action spectra (inhibition coefficients, biological weighting functions, etc.) covering the diverse flora and fauna of Canadian ecozones;
- studies of the impacts of land use activities (e.g., clearcutting) on UV-B effects on freshwater streams;
- determination of UV-induced genetic change in Canadian flora and fauna;
- assessments of the cumulative impacts of various ecological stressors, such as climate change, acid rain, UV-B, and toxic chemicals, and of the links among them.

5.5 Marinf Ecosystems

Covering 71% of the earth's surface and accounting for some 40% of the world's primary biological productivity, the marine environment is of fundamental importance to the planet's well-being. The growth of marine plants (principally phytoplankton) fuels food webs that support fish, birds, marine mammals, and humans. As well, marine primary production plays a crucial role in global climate change by maintaining, in conjunction with physical processes, a large and variable oceanic sink for atmospheric carbon dioxide [Sarmiento and Bender 1994]. Enhanced UV-B radiation reduces marine primary productivity and might influence food web structure. It is therefore critical to assess these impacts on marine ecosystems and to understand how any large-scale changes might interact with physical and chemical processes in the ocean to influence such things as fish stocks and global climate.

UV-B is harmful to many biological processes [Vincent and Roy 1993] and it penetrates ocean waters to ecologically significant depths [Jerlov 1950; Smith et al. 1992]. UV-B also causes photochemical transformations in surface waters that can increase the availability of organic matter [Kieber et al. 1989]) and essential nutrients [Bushaw et al. 1996]. But although enhanced UV-B influences many crucial ecological processes in the ocean, the net effects are difficult to predict on the ecosystem level. Impacts of UV-B must not only be described but also quantified and evaluated in the context of ecosystem response. This is a very difficult task that is generally addressed through a series of complementary approaches, namely

- demonstration of UV-B effects on specific physiological processes as well as on the growth and survival of organisms;
- quantification of these effects in nature, as a function of UV exposure, through experimentation in the field, extrapolation of laboratory results, or direct detection of UV-B effects in the field;
- prediction of complex ecological responses to enhanced UV-B through quantification of the relative sensitivity of key ecological links or experimental observation of ecosystem responses to altered UV-B;
- synthesis of responses to UV-B in a biogeochemical context as a means of understanding the potential impacts on ecosystems, fisheries, and global climate.

Substantial progress in research related to UV-B and marine ecosystems has been made, but responses of marine ecosystems to ozone depletion cannot yet be predicted with confidence.

5.5.1 Synopsis of Research

Recent research has reinforced the conclusion that changes in UV-B exposure alter the growth, survival, and biogeochemical activities of microbes, plants, and animals in the sea. Damage to DNA is a particularly important effect of UV-B that directly influences survival [Karentz et al. 1991]. However, UV-B has other direct effects: interference with orientation (and hence the vertical movements) of motile phytoplankton [Häder and Worrest 1991], alteration of nitrogen metabolism [Döhler 1992; Göes et al. 1995] and photosynthesis [Cullen and Neale 1994] in phytoplankton, increased mortality of larvae [Vetter 1996], and negative impacts on processes ranging from viral infection to hatching success in fish eggs [Hunter et al. 1979, 1982].

Because different methods have been used to generate and quantify experimental irradiance in key studies, it is difficult to determine which physiological processes are most sensitive to solar UV-B. Comparison of results requires a biological weighting function (BWF, also called an action spectrum) to quantify biologically effective irradiance [Caldwell et al. 1986; Cullen and Neale 1996]. BWFs have been determined for key processes such as damage to DNA as well as inhibition of photosynthesis and motility in phytoplankton. The natural variability of these functions and the determination of BWFs for other processes are topics of active research. For phytoplankton [Karentz et al. 1991a; Pelletier et al. 1996], zooplankton [Williamson et al. 1994], and fish larvae [Vetter 1996], there are strong differences between species in sensitivity to UV-B.

Important responses that tend to counter UV effects have also been discovered. These include the synthesis of UV-screening agents such as mycosporine-like amino acids [Karentz et al. 1991b] and of antioxidants such as carotenoids and specific enzymes (e.g., superoxide dismutase) that protect against forms of active oxygen produced under the influence of UV radiation [Lesser 1996]. Damage to DNA, induced by UV-B, can also undergo repair: photoreactivation [Weinbauer et al. 1996; Wilhelm et al. 1996] and dark excision repair are the two major mechanisms involved [Karentz et al. 1991; Buma et al. 1995; Jeffrey et al. 1996].

Many studies have demonstrated a direct influence of altered UV-B on ecologically important processes in natural waters [Wängberg et al. 1996], and biological effects of UV-B have been detected tens of metres into the water column [Smith et al. 1992]. Perhaps the best quantified biological effect is the inhibition of short-term (hours to a day) photosynthesis of phytoplankton in the Antarctic [Helbling et al. 1994; Neale et al. 1994; Prézelin et al. 1994]. As approaches are being refined and more observations accumulate, estimates of the inhibition of photosynthesis associated with ozone depletion, though variable, are converging. Daily water column productivity is significantly decreased by both UV-A and UV-B under normal ozone, and it might be reduced a few percent further under the Antarctic ozone hole or a similarly severe depletion. Most measurements of UV effects on plankton require containment of samples for an hour to a day or more under conditions simulating fixed depths. In nature, however, planktonic organisms are commonly mixed by winds near the surface, so results for fixed depths may not apply [Cullen and Neale 1994; Helbling et al. 1994]. Despite the uncertainties associated with vertical mixing, there is growing consensus that, even under normal ozone, UV plays a major ecological role in surface waters, affecting the productivity, survival, and distribution of both bacterioplankton and phytoplankton. It follows that enhanced UV-B, due to ozone depletion, will alter ecological processes in the ocean.

5.5.2 *Prediction of Ecosystem Response*

Responses of ecosystems to increased UV-B would occur over days to years and likely involve adaptive responses, species selection, and changes in food web interactions. For example, work by Bothwell et al. [1994], described earlier in the section on inland waters, showed how enhanced UV-B exposure could result in an increase in plant biomass as a result of changes to the food web. Similar experiments can be conducted to examine the influence of UV-B on coastal or estuarine systems [Ferreyra 1995], but UV-B cannot be altered experimentally in realistic open ocean ecosystems. Consequently, researchers studying natural marine ecosystems must rely on information about the relative sensitivities of different components in these systems. Confident prediction is impossible at this time because very little quantitative information exists on the effects of vertical mixing and on the sensitivities to UV of eggs, zooplankton, and larval fish found in surface layers. Further, the net effects on microbial activity cannot be resolved. UV-B induces photochemical processes that might enhance microbial activity, but it also directly harms microbes in surface layers [Herndl et al. 1993].

Some toxic dinoflagellates show UV-photoprotective mechanisms [Carreto et al. 1989] which might give them a competitive edge in an enhanced-UV environment. Such a response to changes in UV-B might lead to a greater dominance of toxic or nuisance algae in coastal or estuarine systems. Increases in UV-B could also favour species of phytoplankton that produce dimethyl sulphide (DMS), a reactive gas implicated in cloud formation and, hence, local climate and heat balance. Indeed, UV-B has direct effects on both the synthesis of DMSP (the precursor of DMS) in estuarine phytoplankton [Sakka et al. 1996] and on photolysis rates of DMS in seawater [Crocker et al. 1995]. The influence of UV-B on species composition, and hence on DMS production and food web interactions, has also been identified in the context of competition between diatoms and the prymnesiophyte *Phaeocystis* in Antarctic waters [Davidson and Marchant 1994; Karentz and Spero 1995].

At present there are no data to disprove the suggestion that enhanced UV-B from ozone depletion can alter the species composition of phytoplankton communities and the structure of the food web. However, no such changes have been documented in the ocean. This is not surprising, given the inherent variability of marine systems and our lack of baseline information.

5.5.3 *Synthesis*

Despite the large uncertainties about UV-B impacts on primary productivity and food web structure, it is important to evaluate the global implications of changes that might occur. For example, what are the potential consequences of a hypothetical decrease (e.g., 5%) in primary productivity associated with ozone depletion? To answer such a question, one could take an estimate of annual global carbon dioxide fixation by marine phytoplankton and assume that a 5% reduction in this sink would translate directly into an equivalent (or directly proportional) reduction in atmospheric carbon dioxide stored in the ocean. This would be an overestimate, however, because only a fraction of marine primary production influences the balance between atmospheric and oceanic carbon dioxide. This fraction is called new production and consists of the organic matter that can be transported to the deep ocean by the sinking of particles or by water motions [Eppley and Peterson 1979]. But because the export of organic matter from surface layers is largely balanced by upward mixing of carbon dioxide, new production also cannot serve as a straightforward measure of the flux of atmospheric carbon to the ocean [Platt et al. 1992; Cullen and Neale 1994]. Consequently, the potential impact of ozone depletion on atmospheric carbon dioxide, mediated through inhibition of marine primary production, is unknown. However, it is likely to be much smaller than the reduction of carbon fixation *per se* [Peng 1992].

General relationships between primary production and fish production [Nixon 1988] serve to illustrate what the impacts of enhanced UV-B on fisheries might be. However, a more thorough approach is needed to estimate the extent to which the inhibition of near-surface primary production influences the productivity of major fish stocks. Enhanced UV-B inhibits phytoplankton mostly near the surface in the spring and summer, away from coastal waters that have higher levels of UV-absorbing dissolved organic matter, and in higher latitudes. How inhibition of productivity at these times and places affects the flows of energy to higher trophic levels is not known [International Arctic Science Committee 1995]. Thus, we cannot predict if ozone-related reductions in primary productivity, as opposed to a general decrease in primary production, are more or less likely to influence fish stocks.

5.5.4 Future Directions for Canadian Research

Although much progress has been made, important questions about the effects of ozone depletion on marine systems remain unanswered. Information on the effects of UV on lower trophic levels and photochemical transformations is accumulating rapidly, and an appreciation of natural variability in these processes is developing. Instruments for measuring UV in the marine environment are commercially available, experimental procedures for quantitative assessment of UV effects have been established, and techniques for detecting the physiological impacts of UV in nature have been tested.

The time has come to apply these capabilities to a comprehensive, ecosystem-based, quantitative assessment of UV effects. For productive coastal areas and estuaries, impacts of UV-B need to be evaluated in the light of UV-B–induced photochemical reactions with dissolved organic matter [Schindler et al. 1996], substrate availability for bacterioplankton and phytoplankton, and toxicity (UV-produced oxidants and metal complexes).

It is also important to determine the responses of higher trophic levels to UV. Work is progressing, and experiments on zooplankton (*Calanus*) and fish (Atlantic cod) reveal strong negative impacts as a result of near-surface exposures (Kouwenberg, Beland, Browman, and Runge, personal communication).

Predicting ecosystem response to increasing UV is linked inherently to understanding the ability of organisms and ecosystems to adapt to and ameliorate the effects of damaging radiation over short (hours to days) and long (weeks to years) time scales. In a Canadian context, this implies greater research emphasis on key ecological and economic species that may be affected by increases in UV, while recognizing that many of the effects will be global as well as regional. Part of this effort should be directed towards the identification of indicator organisms or bioassays that are sensitive to UV and may herald ecosystemic responses to increases in UV.

Information on responses to UV-B is useful for assessment only if exposures in nature are known. Thus, it is necessary to describe the climatology of UV as well as its penetration in surface waters. Presently, very few measurements of UV in Canadian marine waters exist, but this situation is changing. Interpretations of UV effects in Canadian waters require recognition of the fundamental differences that exist between the Antarctic and waters of the northern hemisphere, including the Arctic [International Arctic Science Committee 1995; Wängberg et al. 1996]. Consequently, basic research on the function of marine ecosystems in Canadian waters is essential, if immediate questions on the potential ecological effects of ozone depletion are to be answered.

5.6 MATERIALS

Degradation of materials exposed to sunlight has received considerable attention in the scientific community, particularly since the advent of synthetic polymers for outdoor use. To date, most of the research has been on these polymers, although much is also known about the nature and extent of solar damage to several other materials. Available data indicate that shorter wavelength radiation, largely within the UV-B spectrum, is mainly responsible for these effects [Andrady et al. 1995; Searle 1994].

Recent scientific reviews of the effects of photodegradation, however, indicate that the body of international knowledge, although extensive, is neither comprehensive nor adequate, even for a particular material [Andrady et al. 1991, 1995]. The mechanisms and kinetics of the degradation processes, for example, are not well understood, particularly at the molecular level. Combining photodegradation in the UV-B range with photoinduced processes at longer wavelengths and with other environmental variables adds further complexity to the issue.

In Canada, direct research into the effects of increased levels of UV-B radiation on materials has been limited, except for materials used in equipment designed for applications in space. However, several researchers are working either in areas that are specifically concerned with UV-B effects on materials or in related areas in which UV-B is a non-measured component or one of a number of specified and monitored environmental variables.

5.6.1 *Polymers*

Researchers at Lakehead University are studying the photodecomposition of several polymers, including poly(o-acetylstyrene) (POAS), poly(parapropionylstyrene) (PPPS), poly(alpha-methylvinylacetophene) (PMVAP), and poly(vinylacetophene)(PVAP) among others. The more photostable polymers tend to be POAS and PMVAP. These polymers, along with poly(o-butyrylstyrene) (POBS) and poly(o-isobutyrylstyrene) (POIS), have potential for solar energy conversion and various other outdoor applications [Weir and Whiting 1990, 1992; Weir et al. 1993, 1996a]. Researchers at the Institute for Environmental Chemistry of the National Research Council in Ottawa have been instrumental in uncovering the mechanisms of the photoinitiated oxidation of polyolefins [Lacoste and Carlsson 1992; Lacoste et al. 1993]. Photodegradation experiments with polyethylene and polypropylene films showed that, although these polymers produce different proportions of products during photooxidation, the overall oxidation occurs early and rapidly at the exposed film surface and advances into the films as exposure levels increase. Analysis of the obverse surface of polypropylene showed that this surface also oxidized rapidly [Lacoste et al. 1995].

5.6.2 *Wood and Paper*

Pulp production using relatively inexpensive thermomechanical and chemithermomechanical techniques in Canada tripled from 1982 to 1992 [Heitner 1993], primarily for the production of short-life products such as newsprint. One of the limitations to wider use of paper made from these processes is that it turns yellow on exposure to sunlight. This light-induced yellowing is due to photooxidative discolouration of lignin I in the fibre wall [Heitner 1993; Weir et al. 1994]. However, if the light-induced yellowing could be slowed by 3–36 months, the market for chemithermomechanical pulp alone would increase significantly. If the yellowing were stopped altogether, both pulps would be used in the manufacture of high brightness papers, increasing the global market for these pulps by 2.6 million tonnes [Cockram 1989].

Weir and co-workers at Lakehead University extended their earlier photodegradation work with polymers to include biopolymers such as lignin. They exposed several lignin polymers to UV light of wavelengths 300 nm and higher. The polymers underwent yellowing, which was attributed to the formation of quinonoid entities, and subsequent research defined further plausible reaction mechanisms [Weir et al. 1994a, 1994b, 1995, 1996a, 1996b]. Their work demonstrates that lignin-type compounds can undergo colouration reactions that are both totally photoinduced and independent of oxidation [Weir et al. 1996b], implying that discolouration of lignin-based pulps cannot be totally inhibited by conventional antioxidants [Weir et al. 1995].

Researchers from Paprican in Pointe Claire, Quebec, have focused on the functional groups in lignin that play a role in light-induced yellowing [Schmidt and Heitner 1991] and on lignin compounds [Schmidt et al. 1991, 1993]. Results of their experiments, in which reduced and methylated bleached thermomechanical pulp was exposed to UV radiation for two hours, show that discolouration reflects the presence of functional groups in lignin that produce coloured chromophores that are dissociated from aromatic carbonyl and phenolic hydroxyl groups [Schmidt and Heitner 1992]. Through this research, reaction pathways causing the yellowing of bleached mechanical and high-yield pulps have been identified.

Researchers at the Pulp and Paper Research Centre at McGill University in Montreal are now working with Paprican scientists and members of the Mechanical and Chemimechanical Woodpulps group of the Canadian Network of Centres of Excellence to improve the light-aging qualities of pulp and paper products. One particular study is looking into the rebound in brightness of paper that has been exposed to accelerated UV irradiation and then removed to a UV-free location [Ek et al. 1993].

Wan and co-workers at Queen's University first discovered the phototriplet mechanism in chemically induced dynamic electron polarization (CIDEP) systems in 1972. Since that time they have continued their research on the phenomenon and developed a popular technique for use in photophysical and photochemical studies. More recently, their research has examined the nature of free radical–induced photooxidation of phenols and benzenes, since both phenolic groups and methoxy-substituted phenoxy radicals play a key role in the light-induced yellowing of thermomechanical pulp. Several experiments have outlined the roles of peroxy and alkoxy radicals in initiating photooxidation processes [Wan et al. 1993].

5.6.3 *Building Materials*

Canadian research on the effects of UV-B radiation on building materials other than plastics is limited. In one of the studies currently under way, researchers at the National Research Council in Ottawa have been investigating the degradation of various building materials, such as roofing membranes and outdoor sealants, as a result of exposure to ultraviolet radiation. They are not, however, examining the potential effects of an increase in ambient levels of UV-B radiation (M. Lacasse and R. Peroli, NRC Building Materials Laboratory, personal communication). In another study,

Feldman and co-workers at Concordia University are using both accelerated and ambient weathering tests to improve the mechanical characteristics and durability of various building materials. These tests, which were carried out both with and without UV radiation and which also included temperature cycling to failure, revealed no durability differences between modified and original epoxies [Feldman and Khoury 1988; Feldman et al. 1998]. Recent studies aimed at decreasing the weather sensitivity of PVC construction materials have attempted to replace titanium dioxide with less expensive kraft lignin, both of which serve to absorb some of the incoming UV radiation [Feldman et al. 1994].

5.6.4 Paints and Coatings

Very little Canadian effort has been directed towards the effects of UV-B radiation on paints and other coatings, although Ortech International does routine testing on behalf of commercial clients to assess conformance to provincial and national standards. Typically, these are weatherability and exposure time tests for such items as automotive coatings, solar collector coatings, and other paints. These tests do not focus on UV-B impacts specifically; however, UV-B is monitored as part of the weathering studies (D. Hacker, Ortech International, personal communication). Other research laboratories across the country, for example, the Composite Materials Centre in St-Jérôme, Quebec, the Alberta Research Council in Edmonton, and the BC Institute of Technology in Vancouver, do similar client-oriented studies. However, details of these studies and their results are not available to the public.

5.6.5 Textiles and Clothing

Researchers at the University of Alberta in Edmonton have been studying the effect of light on silk. Aging studies using a xenon arc weatherometer reveal that the range of light from UV-B through to visible fades dyed silk and turns undyed silk yellow. It also decreases fibre tensile strength and extensibility and increases fabric stiffness [Halvorson and Kerr 1994].

The effectiveness of UV-B protection offered by commercially available clothing is another important area that has received recent attention. Using spectrophotometry, Capjack et al. [1994] and Davis et al. [1997] measured UV transmission through a variety of clothing materials as a function of wavelength over the 250–400 nm range. Protection generally increased with fabric weight, with closer weaves, and with darker colours. Their work demonstrates that careful selection of fabrics is necessary if a sun protection factor (SPF) of at least 15 is to be achieved. For best protection from UV radiation, dark clothing made from polyester or blends of polyester and another fibre are recommended.

5.6.6 Economic Implications

When the UNEP report on Environmental Effects of Ozone Depletion was published in 1994, understanding of the wavelength sensitivities and thus, service lifetimes of key polymeric components used in outdoor applications was incomplete, and data about other materials was even more limited. These deficiencies remain. Since the resistance of current photostabilizers and protective coatings to increased levels of UV-B radiation has still not been adequately tested, the economic implications of any strategy to counteract future potential UV-B damage to exposed materials remain speculative. However, there are economic concerns that deserve comment.

One implication of the limited level of Canadian research into the effects of UV-B radiation on materials is that Canadians will receive little direct scientific recognition and economic advantage from developments arising in this area. It is therefore legitimate to ask: Is the cost of doing nothing to offset enhanced levels of UV-B radiation higher than the cost of developing more resistant materials, paints, and coatings? However, a further question also arises, because if the Montreal Protocol is fully implemented, UV-B levels could begin to stabilize and decrease by early next century and possibly return to 1990 levels as early as the year 2020. If that were to happen, would the damage to materials inflicted by two decades of increased spring and summer exposure to UV-B radiation warrant the increased efforts and costs of developing and marketing new products that would be redundant within 30 years?

It is not obvious, however, that product research and development for these new materials would be any more expensive than current efforts to make existing polymers and other materials more photoresistant to present UV-B levels. Indeed, some product formulation costs may go down as less expensive substitutes are found. The protection of existing materials and the development of new photoresistant materials and stabilizers can, in fact, be seen as an opportunity for new business and employment generation.

If levels of UV-B radiation increase, the degradation of existing materials will be accelerated and the potential for damage hazards resulting from product failure will increase. It is impossible to make an assessment of the costs of these potential hazards with current available information, but such an assessment would need to involve safety considerations, replacement costs, and potential liability costs.

5.6.7 Data Gaps

There are several areas in which further information is needed by the international scientific community. Major priorities include:

- improved understanding of the way in which materials respond to different wavelength regions of both natural and artificial ultraviolet light sources and to simulated UV-B–enriched sunlight;
- improved and more widely distributed measurements of ambient UV radiation in the wavelength bands most responsible for the deterioration of synthetic and natural materials;
- more complete and up-to-date databases on the UV spectral response characteristics of all exposed materials, as determined by activation spectra;
- consistent quantitative relationships between field and laboratory exposure results for polymeric materials;
- more data on UV-B transmission through window glass in typical user applications.

Thus, in materials science, as in most other areas of research, much still has to be done before many of the details of UV effects can be adequately understood.

References

Andrady, A.L., M.B. Amin, S.H. Hamid, X. Hu, K. Fueki, and A. Torikai, 1991. Materials damage. Pages 45–50 in *Environmental Effects of Ozone Depletion: 1991 Update.* Nairobi: United Nations Environment Programme.

Andrady, A.L., M.B. Amin, S.H. Hamid, X. Hu, and A. Torikai, 1995. Effects of increased solar ultraviolet radiation on materials. *Ambio*, **24**(3), 191–196.

Autier, P., J.F. Dore, F. Lejeune, K.F. Koelmel, O. Geffeler, P. Hille, J.P. Cesarini, et al., 1994. Recreational exposure to sunlight and lack of information as risk factors for cutaneous malignant melanoma. *Mel. Res.*, **4**, 79–85.

Baird, E.A., P.M. McHenry, and R.M. MacKie, 1992. Effect of maintenance chemotherapy in childhood on numbers of melanocytic nevi. *Br. Med. J.*, **305**, 799–801.

Barnes, P.W., S.D. Flint, and M.M. Caldwell, 1990. Morphological responses of crop and weed species of different growth forms to ultraviolet-B radiation. *Am. J. Bot.*, **77**, 1354–1360.

Barnes, J. D., N.D. Paul, K.E. Percy, P. Broadbent, C.K. McLaughlin, and A.R. Wellburn, 1994. Effects of UV-B radiation on wax biosynthesis. Pages 196–204 in *Air Pollutants and the Leaf Cuticle* . K.E. Percy, J.N. Cape, R. Jagels, and C. Simpson, eds. NATO ASI Series G, vol. 36. Heidelberg: Springer-Verlag.

Barnes, J.D., K.E. Percy, N.D. Paul, P. Broadbent, C.K. McLaughlin, P.M. Mullineaux, G. Creissen, and A.R. Wellburn, 1996. The influence of UV-B radiation on the physico-chemical nature of tobacco (*Nicotinia tabacum L.*) leaf surfaces. *J. Exp. Bot.*, **47**, 99–109.

Bavcon, J., A. Gaberscik, and F. Batic, 1996. Influence of UV-B radiation on photosynthetic activity and chlorophyll fluorescence kinetics in Norway spruce (*Picea abies (L.) Karst.*) seedlings. *Trees*, **10**, 172–176.

Beitner, H., S.E. Norell, U. Ringborg, G. Wennerstin, and B. Matson, 1990. Malignant melanoma: aetiological importance of individual pigmentation and sun exposure. *Br. J. Dermatol.*, **122**, 43–51.

Belanger, G., Y.A. Papadopoulos, R. Gordon, N. Goodyear, K.B. McRae, R.S. Bush, E.A. Butler, and S.A.E. Fillmore, 1996. Effects of UV-B radiation on grass morphogenesis. Abstract. *Can. J. Plant Sci.*, **76**, 359.

Bergmanson, J., T. Sheldon, and A.P. Cullen, 1996. A sting in the rays. *Optician*, **212**(5560), 17–22.

Berinstain, A.B., M.K. Whittlesey, and J.C. Scaiano, 1993. Laser techniques in the study of the photochemistry of carbonyl compounds containing ligninlike moieties. Pages 111–121 in *Photochemistry of Lignocellulosic Materials*. Amer. Chem. Soc. Symposium Series 531. C. Heitner and J.C. Scaiano, eds. Washington D.C.: American Chemical Society.

Berwick, M., C. Begg, J. Fine, G. Roush, and R. Barnhill, 1996. Screening for cutaneous melanoma by skin self-examination. *J. Natl. Cancer Inst.*, **88**, 17–23.

Binder, W.D., and S.J. L'Hirondelle, 1996. Ultraviolet-B radiation effects on some British Columbia conifers: (1) Engelmann spruce from five elevations. Paper presented at The International IUFRO Meeting For Population, Ecological and Conservation Genetics, University of British Columbia, Vancouver, August 5-9, 1996.

Blaustein, A.R., P.D. Hoffman, D.G. Hokit, J.M. Kiesbecker, S.C. Walls, and J.B. Hays, 1994. UV repair and resistance to solar UV-B in amphibian eggs: a link to population declines? *Proc. Nat. Acad. Sci,*. **91**, 1791–1795.

Bornman, J.F., and A.H. Teramura, 1993. Effects of ultraviolet-B radiation on terrestrial plants. Pages 427–471 in *Environmental UV Photobiology*. A.R. Young et al., eds. New York: Plenum Press.

Bornman, J.F., and T.C. Vogelmann, 1988. Penetration of blue and UV radiation measured by fiber optics in spruce and fir needles. *Physiol. Plant.*, **72**, 699–705.

Bothwell, M.L., D.M.J. Sherbot, and C.M. Pollock, 1994. Ecosytem response to solar ultraviolet-B radiation: influence of trophic-level interactions. *Science*, **265**, 97–100.

Bouwes-Bavinck, J., D. Hardie, A. Green, S. Cutmore, A. MacNaught, B. O'Sullivan, V. Siskind, F. van der Wonde, and I.R. Hardie, 1996. The risk of skin cancer in renal transplant recipients in Queensland, Australia: a follow-up study. *Transplantation*, **61**, 715–721.

Buma, A.G.J., E.J. Van Hannen, L. Roza, M.J.W. Veldhuis, and W.W.C. Gieskes, 1995. Monitoring ultraviolet-B-induced DNA damage in individual diatom cells by immunofluorescent thymine dimer detection. *J. Phycol.*, **31**, 314–321.

Bush, R.S., Y.A. Papadopoulos, E.A. Gallant, N. Goodyear, R. Gordon, K.B. McRae, and R. Martin, 1995a. Preliminary evidence of intolerance to UV light by alfalfa cultivars. Paper presented at the annual meeting of the Atlantic Advisory Committee on Forage Crops, October 27–28, Halifax, N.S.

Bush, R.S., Y.A. Papadopoulos, R. Gordon, G. Belanger, N. Goodyear, K.B. McRae, E.A. Butler, and S.A.E. Fillmore. 1995b. Evidence of tolerance to UV-B radiation among currently cultivated alfalfa varieties. Pages 37–38 in *Proceedings of the 11th Eastern Forage Improvement Conference*, Ottawa, Ontario.

Bushaw, K.L., R.G. Zepp, M.A. Tarr, D. Schulz-Janders, R.A. Bourbonniere, R.E. Hodson, W.L. Miller, D.A. Bronk, and M.A. Moran. 1996. Photochemical release of biologically available nitrogen from aquatic dissolved organic matter. *Nature*, **381**, 404–407

Caldwell, M.M., R. Robberecht, R.S. Nowak, and W.D. Billings, 1982. Differential photosynthetic inhibition by ultraviolet radiation in species from the arctic-alpine life zone. *Arctic and Alpine Res.*, **14**, 195–202.

Caldwell, M.M., L.B. Camp, C.W. Warner, and S.D. Flint, 1986. Action spectra and their key role in assessing biological consequences of solar UV-B radiation change. Pages 87–111 in *Stratospheric Ozone Reduction, Solar Ultraviolet Radiation, and Plant Life*. R.C. Worrest and M.M. Caldwell, eds. Berlin: Springer-Verlag.

Caldwell, M.M., A.H. Teramura, and M. Tevini, 1989. The changing solar ultraviolet climate and the ecological consequences for higher plants. *Trends in Ecol. and Evol.*, **4**, 363–367.

Capjack, L., N. Kerr, S. Davis, R. Fedosejevs, K.L. Hatch, and N.L. Markee, 1994. Protection of humans from ultraviolet radiation through the use of textiles: a review. *Family and Consumer Sciences Res. J.*, **23**(2), 198–218.

Carreto, J.I., S.G. DeMarco, and V.A. Lutz, 1989. UV-absorbing pigments in the dinoflagellates *Alexandrium excavatum* and *Prorocentrum micans*. Effects of light intensity. Pages 333–336 in *Red Tides: Biology, Environmental Science, and Toxicology*. T. Okaichi, T.M. Anderson, and T. Nemoto, eds. Elsevier.

CCFM (Canadian Council of Forest Ministers), 1995. *Compendium of Canadian Forestry Statistics*. Ottawa: Canadian Council of Forest Ministers.

Clark, J.B., and G.R. Lister, 1975. Photosynthetic action spectra of trees. II: The relatiobship of cuticle structure to the visible and ultraviolet spectral properties of needles from coniferous species. *Plant Physiol.*, **55**, 407–413.

Cockram, R.A. 1989. CTMP in fine papers. *Proceedings of the International Mechanical Pulping Conference*. Helsinki: Finnish Pulp and Paper Research Institute.

Crocker, K.M., M.E. Ondrusek, R.L. Petty, and R.C. Smith, 1995. Dimethylsulfide, algal pigments, and light in an Antarctic *Phaeocystis* sp. *Mar. Biol.*, **124**, 335–340.

Cullen, A.P., and S. Monteith-McMaster, 1993. Damage to the rainbow trout (*Oncorhyncus mykiss*) lens following acute dose of UVB. *Curr. Eye Res.*, **12**, 97–106.

Cullen, A.P., and S.C. Perera, 1994. Sunlight and human conjunctival action spectrum. Ultraviolet radiation hazards. *SPIE Proceedings*, **2134**, 24–30.

Cullen, J.J., and P.J. Neale, 1994. Ultraviolet radiation, ozone depletion, and marine photosynthesis. *Photosyn. Res.*, **39**, 303–320.

Cullen, J.J., and P.J. Neale, 1996. Biological weighting functions for describing the effects of ultraviolet radiation on aquatic systems. In *Effects of Ozone Depletion on Aquatic Ecosystems*. D-P. Häder, ed. R.G. Landes.

Davidson, A.T., and H.J. Marchant, 1994. The impact of ultraviolet radiation on *Phaeocystis* and selected species of Antarctic marine diatoms. Pages 187–205 in *Ultraviolet Radiation in Antarctica: measurements and biological effects*. C.S. Weiler and P.A. Penhale, eds. Washington, D.C.: American Geophysical Union.

Davis, S., L. Capjack, N. Kerr, and R. Fedosejevs, 1997. Clothing as protection from ultraviolet radiation: which fabric is most effective? *International J. Dermatology*, in press.

Day, T.A., T.C. Vogelmann, and E.H. DeLucia, 1992. Are some plant life forms more effective than others in screening out ultraviolet-B radiation? *Oecologia*, **92**, 513–519.

Day, T.A., G. Martin, and T.C. Vogelmann, 1993. Penetration of UV-B radiation in foliage: evidence that the epidermis behaves as a non-uniform filter. *Plant Cell Environ.*, **16**, 735–741.

Day, T.A., B.W. Howells, and W.J. Rice, 1994. Ultraviolet absorption and epidermal-transmittance spectra in foliage. *Physiol. Plant.*, **92**, 207–218.

DeLucia, E.H., T.A. Day, and T.C. Vogelmann, 1992. Ultraviolet-B and visible light penetration into needles of two species of subalpine conifers during foliar development. *Plant Cell Environ.*, **15**, 921–929.

DeLucia, E.H., S.L. Naidu, and J. Chen, 1994. Effects of simulated stratospheric ozonr depletion on seedling growth of several species of hardwood trees. *Erigenia*, **13**, 132–140.

Dillenberg, L.R., J.H. Sullivan, and A.H. Teramura, 1995. Leaf expansion and development of photosynthetic capacity and pigments in *Liquidambar styraciflua (Hamamelidaceae)* – Effects of UV-B radiation. *Am. J. Bot.*, **82**, 878–885.

Döhler, G., 1992. Impact of UV-B radiation on uptake of 15N-nitrate by phytoplankton of the Wadden Sea. *Mar. Biol.*, **112**, 485–489.

Doughty, M.J., and A.P. Cullen, 1990. Long-term effects of a single dose of ultraviolet-B on albino rabbit cornea – II. Deturgescence and fluid pump assessed *in vitro*. *Photochem. and Photobiol.*, **51**, 439–449.

Dunning, C.A., L. Chalker-Scott, and J.D. Scott, 1994. Exposure to ultraviolet-B radiation increases cold hardiness in Rhododendron. *Physiol. Plant.*, **92**, 516–520.

Ek, M., H. Lennholm, G. Linblad, T. Iverson, and D.G. Gray, 1993. Photochromic behaviour of UV-irradiated mechanical pulps. Pages 147–155 in *Photochemistry of Lignocellulosic Materials*. Amer. Chem. Soc. Symp. Series 531. C. Heitner and J.C. Scaiano, eds. Washington, D.C.: Amer. Chem. Soc.

Ellert, B.H., H.H. Janzen, and E.G. Gregorich, 1995. Environmental driving variables and plant litter decomposition in Canada. Page 74 in *Driven by Nature: Plant Litter Quality and Decomposition*. Proceedings of an international conference held at Wye College, U. of London, England. September 17–20, 1995.

Elwood J.M., and R.P. Gallagher, 1983. Site distribution of malignant melanoma. *Can. Med. Assoc. J.*, **128**, 1400–1404.

Elwood J.M., and T.G. Hislop, 1982. Solar radiation in the etiology of cutaneous malignant melanoma in Caucasians. *Natl. Cancer Inst. Monograph*, **62**, 167–171.

Elwood J.M., R.P. Gallagher, G.B. Hill, and J. Pearson, 1985a. Cutaneous melanoma in relation to intermittent and constant sun exposure: the Western Canada Melanoma Study. *Int. J. Cancer* **35**, 427–433.

Elwood, J.M., R.P. Gallagher, J. Davison, and G.B. Hill, 1985b. Sunburn, suntan, and risk of cutaneous malignant melanoma: the Western Canada Melanoma Study. *Br. J. Cancer*, **51**, 543–549.

Eppley, R.W., and B.J. Peterson, 1979. Particulate organic matter flux and planktonic new production in the deep ocean. *Nature*, **282**, 677–680.

Falkowski, P.G., 1994. The role of phytoplankton photosynthesis in global biogeochemical cycles. *Photosyn. Res.*, **39**, 235–258.

Feldman, D., and M. Khoury, 1988. Epoxy-lignin polyblends. Part II: Adhesive behaviour and weathering. *J. Adhesion Sci. Technology*, **2**(2), 107–116.

Feldman, D., M. Lacasse, and D. Banu, 1988. Contribution to the modification of an acrylic sealant with lignin. *J. Polymeric Materials*, **5**, 131–139.

Feldman, D., D. Banu, and S. El-Raghi, 1994. Poly(vinyl chloride)-lignin blends for outdoor application in building. *J. Macromolecular Sci. Part A: Pure and Applied Chem.*, **A31(5)**, 555–571.

Fernbach, E., and H. Mohr, 1990. Coaction of blue/ultraviolet-A light and light absorbed by phytochrome in controlling growth of pine (*Pinus sylvestris*). *Planta*, **180**, 212–216.

Fernbach, E., and H. Mohr, 1992. Photoreactivation of the UV light effects on growth of Scots pine (*Pinus sylvestris* L.) seedlings. *Trees*, **6**, 232–235.

Ferreyra, G. A., 1995. Effets du rayonnement ultraviolet sur le plancton des régions froides tempérées et polaires. Dept. of Oceanography, Laval University.

Finsen, N.R., 1901. The treatment of *lupus vulgaris* by concentrated chemical rays. Pages 73–75 in *Phototherapy*. London: Edward Arnold.

Gallagher, R.P., J.M. Elwood, and G.B. Hill, 1986. Risk factors for cutaneous malignant melanoma: the Western Canada Melanoma Study. *Rec. Results Cancer Res.*, **102**, 38–55.

Gallagher, R.P., J.M. Elwood, W.J. Threlfall, J.J. Spinelli, S. Fincham, and G.B. Hill, 1987. Socioeconomic status, sunlight exposure, and risk of malignant melanoma: the Western Canada Melanoma Study. *J. Nat. Cancer Inst.*, **79**, 647–652.

Gallagher, R.P., D.I. McLean, C.P. Yang, A.J. Coldman, H.K.B. Silver, J.J. Spinelli, and M. Beagrie, 1990a. Anatomic distribution of acquired melanocytic nevi in white children. *Arch. Dermatol.*, **126**, 466–471.

Gallagher, R.P., D.I. McLean, C.P. Yang, A.J. Coldman, H.K.B. Silver, J.J. Spinelli, and M. Beagrie, 1990b. Suntan, sunburn, and pigmentation factors and the frequency of acquired melanocytic nevi in children. *Arch. Dermatol.*, **126**, 770–776.

Gallagher, R.P., G.B. Hill, C.D. Bajdik, S. Fincham, A.J. Coldman, and D.I. McLean, 1995a. Sunlight exposure, pigmentation factors, and risk of non-melanocytic skin cancer: I – basal cell carcinoma. *Arch. Dermatol.*, **131**, 157–163

Gallagher, R.P., G.B. Hill, C.D. Bajdik, S. Fincham, A.J. Coldman, and D.I. McLean, 1995b. Sunlight exposure, pigmentation factors, and risk of non-melanocytic skin cancer: II – squamous cell carcinoma. *Arch. Dermatol.*, **131**, 164–169.

Garbe, C., S. Kruger, R. Stadler, I. Guggenmoss-Holzmann, and C.E. Orfanos, 1989. Markers and relative risk in a German population for developing malignant melanoma. *Int. J. Dermatol.*, **28**, 517–523.

Garssen, J., W. Goettsch, F. de Gruize, W. Slob, and H. Van Loveren, 1996. Risk assessment of UVB effects on resistance to infectious diseases. *Photochem. Photobiol.*, **64**, 269–294.

Göes, J. I., N. Handa, S. Taguchi, T. Hama, and H. Saito, 1995. Impact of UV radiation on the production patterns and composition of dissolved free and combined amino acids in marine phytoplankton. *J. Plankton Res.*, **17**, 1337–1362.

Gonzalez, R., N.D. Paul, K. Percy, M. Ambrose, C.K. McLaughlin, J.D. Barnes, M. Areses, and A.R. Wellburn, 1996. Responses to ultraviolet-B radiation (280–315 nm) of pea (*Pisum sativum*) lines differing in leaf surface wax. *Physiol. Plant.*, **98**, 852–860.

Goodyear, N., R.R. Bush, R. Gordon, Y.A. Papadopoulos, G. Belanger, K.B. McRae, E.A. Butler, and S.A.E. Fillmore, 1996. Growth and physiological responses of four broccoli cultivars to ambient and reduced levels of UV-B radiation during two seasons. *Abstract. Can. J. Plant Sci.*, **76**, 358.

Gordon, D.C., K.E. Percy, and R.T. Riding, 1995. Effect of UV-B radiation on cuticular characteristics in four spruce species. Abstract. In *Solar Ultraviolet Radiation: Modeling and Measurement*. Proceedings of a NATO Advanced Study Institute workshop, Halkidiki, Greece, October 2–11, 1995.

Gordon, D.C., K.E. Percy, and R.T. Riding, 1997a. Effect of enhanced UV-B radiation on four *Picea* species. *New Phytol.*, forthcoming.

Gordon, D.C., K.E. Percy, and R.T. Riding, 1997b. Effect of enhanced UV-B radiation on adaxial leaf surface micromorphology and epicuticular wax biosynthesis of sugar maple. *Chemosphere*, in press.

Granstein, R.D., and D.N. Sauder, 1987. Whole body exposure to ultraviolet radiation results in increased serum interleuken-1 activity in humans. *Lymphokine Res.*, **6**, 187–193.

Grant, K.P., and L.E. Licht, 1993. Acid tolerance of anuran embryos and larvae from central Ontario. *J. Herpetol.*, **27**, 1–6.

Grant, K. P., and L.E. Licht, 1995. Effects of ultraviolet radiation on life-history stages of anurans from Ontario, Canada. *Can. J. Zool.*, **73**, 2292–2301.

Green, A., V. Siskind, C. Bain, and J. Alexander, 1985. Sunburn and malignant melanoma. *Br. J. Cancer*, **51**, 393–397.

Green, A., C. Bain, R. MacLennan, and V. Siskind, 1986. Risk factors for cutaneous melanoma in Queensland. *Rec. Results Cancer Res.*, **102**, 76–97.

Grob, J.J., J. Gouvernet, D. Aymer, A. Mostaque, M.H. Romano, A.M. Collet, M.C. Noe, M.P. Dicostanzo, and J.J. Bonerandi, 1990. Count of benign melanocytic nevi as a major indicator of risk for non-familial nodular and superficial spreading melanoma. *Cancer*, **66**, 387–395.

Häder, D-P. and R.C. Worrest, 1991. Effects of enhanced solar ultraviolet radiation on aquatic ecosystems. *Photochem. Photobiol.*, **53**, 717–725.

Halvorson, B.G., and N. Kerr, 1994. Effect of light on the properties of silk fabrics coated with Parlene-C. *Studies in Conservation*, **39**, 45–56.

Harrison, S.L., R. McLennan, R. Speare, and I. Wrongski, 1994. Sun exposure and melanocytic nevi in young Australian children. *Lancet*, **344**, 1529–1532.

Heitner, C., 1993. Light-induced yellowing of wood-containing papers. Pages 2–25 in *Photochemistry of Lignocellulosic Materials*, Amer. Chem. Soc. Symposium Series 531. C. Heitner and J.C. Scaiano, eds. Washington, D.C.: American Chemical Society.

Helbling, E. W., V. Villafañe, and O. Holm-Hansen, 1994. Effects of ultraviolet radiation on Antarctic marine phytoplankton photosynthesis with particular attention to the influence of mixing. Pages 207–227 in *Ultraviolet Radiation in Antarctica: Measurements and Biological Effects*. C.S. Weiler and P.A. Penhale, eds. Washington, D.C.: American Geophysical Union.

Herndl, G. J., G. Müller-Niklas, and J. Frick, 1993. Major role of ultraviolet-B in controlling bacterioplankton growth in the surface layer of the ocean. *Nature*, **361**, 717–719.

Hoddinott, J, 1994. Impacts of UV-B and CO_2 on boreal forest seedlings. Pages 23–27 in *International conference on ozone depletion and ultraviolet radiation: preparing for the impacts*, April 27–29, 1994, Victoria, B.C. Proceedings. K. Heidorn and B. Torrie, eds. Victoria: The Skies Above Foundation.

Holly, E.A., J.W. Kelly, S.N. Shpall, and S-H Chiu, 1987. Number of melanocytic nevi as a major risk factor for malignant melanoma. *J. Amer. Acad. Dermatol.*, **17**, 459–468.

Holly, E.A., D.A. Aston, R.D. Cress, D. Ahn, and J. Kristiansen, 1995. Cutaneous melanoma in women. I: Exposure to sunlight, ability to tan and other risk factors related to ultraviolet light. *Amer. J. Epidemiol.*, **141**, 923–933.

Holman, C.D.J., B.K. Armstrong, and P.J. Heenan, 1983. A theory of the etiology and pathogenesis of human cutaneous malignant melanoma. *J. Natl. Cancer Inst.*, **71**, 651–656.

Holman, C.D.J., B.K. Armstrong, and P.J. Heenan, 1986. Relationship of cutaneous malignant melanoma to individual sunlight exposure habits. *J. Natl. Cancer Inst.*, **76**, 403–414.

Huang, X-D., D.G. Dixon, and B.M. Greenberg, 1995. Toxicity of polycyclic aromatic hydrocarbons to the duckweed *Lemna gibba* L. G-3 in natural sunlight. *Ecotoxicol. Environ. Safety*, **32**, 194–200.

Hunter, J. R., J.H. Taylor, and H.G. Moser, 1979. Effect of ultraviolet radiation on eggs and larvae of the northern anchovy, *Engraulis mordax*, and the Pacific mackerel, *Scomber japonicus*, during the embryonic stage. *Photochem. Photobiol.*, **29**, 325–338.

Hunter, J. R., S.E. Kaupp, and J.H. Taylor, 1982. Assessment of effects of UV radiation on marine fish larvae. Pages 459-497 in *The Role of Solar Ultraviolet Radiation in Marine Ecosystems*. J. Calkins, ed. London: Plenum.

International Arctic Science Committee. 1995. *Effects of Increased Ultraviolet Radiation in the Arctic*. IASC Secretariat.

Jeffrey, W. H., R.J. Pledger, P. Aas, S. Hager, R.B. Coffin, R. Von Haven, and D.L. Mitchell, 1996. Diel and depth profiles of DNA photodamage in bacterioplankton exposed to ambient solar ultraviolet radiation. *Mar. Ecol. Prog. Ser.*, **137**, 293–304.

Jenkins, G.I., J.M. Christie, G. Fuglevand, J.C. Long, and J. Jackson, 1995. Plant responses to UV and blue light: biochemical and genetic approaches. *Plant Sci.*, **112**, 117–138.

Jerlov, N.G., 1950. Ultraviolet radiation in the sea. *Nature* **166**, 111–112.

Jungblut, T.P., J-P. Schnitzler, W. Heller, N. Hertkorn, J.W. Metzger, W. Szymczak, and H. Sandermann, Jr., 1995. Structures of UV-B induced sunscreen pigments of the Scots Pine (*Pinus sylvestris* L.). *Angew. Chem.*, Int. Ed. Engl., **34**, 312–314.

Karentz, D., and H.J. Spero, 1995. Response of natural *Phaeocystis* population to ambient fluctuations of UVB radiation cased by Antarctic ozone depletion. *J. Plankton Res.*, **17**, 1771–1789.

Karentz, D., J.E. Cleaver, and D.L. Mitchell, 1991a. Cell survival characteristics and molecular responses of Antarctic phytoplankton to ultraviolet-B radiation. *J. Phycol.*, **27**, 326–341.

Karentz, D., F.S. McKuen, M.C. Land, and W.C. Dunlap, 1991b. Survey of mycosporine-like amino acid compounds in Antarctic marine organisms: potential protection from ultraviolet exposure. *Mar. Biol.*, **108**, 157–166.

Kelly, J.W., J.K. Rivers, R. MacLennan, S. Harrison, A.E. Lewis, and B.J. Tate, 1994. Sunlight: a major risk factor associated with development of melanocytic nevi in Australian school children. *J. Amer. Acad. Dermatol.*, **30**, 40–48.

Kerr, J.B. and C.T. McElroy, 1993. Evidence for large upward trends of ultraviolet radiation linked to ozone depletion. *Science*, **262**, 1032–1034.

Khlat, M., A. Vail, M. Parkin, and A. Green, 1992. Mortality from melanoma in migrants to Australia: variation by age at arrival and duration of stay. *Amer. J. Epidemiol.*, **135**, 1103–1113.

Kieber, D.J., J. McDaniel, and K. Mopper, 1989. Photochemical source of biological substrates in sea water: implications for carbon cycling. *Nature*, **341**, 637–639.

Kossuth, S.V., and R.H. Biggs, 1981. Ultraviolet-B radiation effects on early seedling growth of Pinaceae species. *Can. J. For. Res.*, **11**, 243–248.

Kricker, A., B.K. Armstrong, D.R. English, and P.J. Heenan, 1995. Does intermittent sun exposure cause basal cell carcinoma? A case-control study in Western Australia. *Int. J. Cancer* **60**, 589–494.

Krupa, S.V., and R.N. Kickert, 1989. The greenhouse effects: impact of UV-B, CO_2, and O_3 on vegetation. *Env. Pollut.*, **61**, 263–393.

Lacoste, J., and D.J. Carlsson, 1992. Gamma-, photo- and thermally-initiated oxidation of linear low density polyethylene: a quantitative comparison of oxidation products. *J. Polymer Sci. Part A: Polymer Chem.*, **30**, 493–500.

Lacoste, J., D. Vaillant, and D.J. Carlsson, 1993. Gamma-, photo-, and thermally-initiated oxidation of isotactic polypropylene. *J. Polymer Sci. Part A: Polymer Chem.*, **31**, 715–722.

Lacoste, J., Y. Deslandes, P. Black, and D.J. Carlsson, 1995. Surface and bulk analyses of the oxidation of polyolefins. *Polymer Degradation and Stability* **49**, 21–28.

Lesser, M. P., 1996. Acclimation of phytoplankton to UV-B radiation: oxidative stress and photoinhibition of photosynthesis are not prevented by UV-absorbing compounds in the dinoflagellate *Prorocentrum micans*. *Mar. Ecol. Prog. Ser.*, **132**, 287–297.

L'Hirondelle, S.J. and W.D. Binder, 1996. Ultraviolet-B radiation effects on some British Columbia conifers. 2: Sitka spruce and coastal Douglas-fir from three elevations. Paper presented at the International IUFRO Meeting for Population, Ecological, and Conservation Genetics, University of British Columbia, Vancouver, August 5–9, 1996.

Loucks, O.L., 1994. Sun-scald on 1993 foliage of white pine (*Pinus strobus*) linked to UV-B radiation in Ohio and Ontario. Pages 39–47 in *International conference on ozone depletion and ultraviolet radiation: preparing for the impacts*, April 27–29, 1994, Victoria, B.C. Proceedings. K. Heidorn and B. Torrie, eds. Victoria: The Skies Above Foundation.

MacKie, R.M., T. Freudenberger, and T.C. Aitcheson. 1989. Personal risk factor chart for cutaneous melanoma. *Lancet II*, 487–490.

Madronich, S., R.L. McKenzie, M.M. Caldwell, and L.O. Bjorn, 1995. Changes in ultraviolet radiation reaching the earth's surface. *Ambio*, **24**, 143–164.

Marrett, L.D., W.D. King, S.D. Walter, and L. From, 1992. Use of host factors to identify people at high risk for cutaneous malignant melanoma. *Can. Med. Assoc. J.*, **147**, 445–453.

McKenzie, R.C., E.S. Park, E.S. Brown, W.R. Brown, G.S. Shivji, and D.N. Sauder, 1994. Effect of ultraviolet inducible cytokines on melanoma growth *in vivo*: stimulation of melanoma growth by interleukin 1 and 6. *Photoderm., Photoimmunol. Photomed.*, **10**, 74–79.

McLean, D.I., R.P. Gallagher, A.J. Coldman, and V.C. Ho., 1995. The Vancouver Mole Study: nevi in children. *Ann. RCPSC*, **28**, 297–300.

Miyagi, T., A. Bhutto, and S. Nonaka, 1994. The effects of sunscreens on UVB erythema and Langerhans cell depression. *J. Invest. Dermatol.*, **21**, 645–651.

Naidu, S.L., J.H. Sullivan, A.H. Teramura, and E.H. DeLucia, 1993. The effects of ultraviolet-B radiation on photosynthesis of different aged needles in field-grown loblolly pine. *Tree Physiol.*, **12**, 151–162.

Neale, P. J., M.P. Lesser, and J.J. Cullen, 1994. Effects of ultraviolet radiation on the photosynthesis of phytoplankton in the vicinity of McMurdo Station, Antarctica. Pages 125–142 in *Ultraviolet Radiation in Antarctica: Measurements and Biological Effects*. C.S. Weiler and P. Penhale, eds. Washington, D.C.: American Geophysical Union.

Nelemans, P., H. Groenendal, L. Kiemoney, F.H.J. Rampen, D.J. Ruiter, and A.L.M. Verbeek, 1993. Effect of intermittent exposure to sunlight on melanoma risk among indoor workers and sun-sensitive individuals. *Environ. Health Persp.*, **101**, 252–255.

Nixon, S.W., 1988. Physical energy inputs and the comparative ecology of lake and marine ecosystems. *Limnol. Oceanogr.*, **33**, 1005–1025.

Østerlind. A., M.A. Tucker, B.J. Stone, and O.M. Jensen, 1988. The Danish case-control study of cutaneous malignant melanoma. Importance of UV light exposure. *Int. J. Cancer*, **42**, 319–324.

Ovaska, K., and B. Pauli, 1997. *Vulnerability of Amphibians in Canada to Climate Warming and Increased UV-B Radiation.* Canadian Wildlife Service Report. Hull: Environment Canada, forthcoming.

Papadopoulos, Y.A., N. Goodyear, R. Belanger, G. McRae, K.B. Bush, R.R. Butler, E.A. Butler, and S.A.E. Fillmore, 1996. Impact of current UV-B radiation on forage grass and legume production in northern latitudes. Abstract. *Can. J. Plant. Sci.*, **76**, 358–359.

Patz, J.A., P.R. Epstein, T.A. Burke, and J.M. Balbus, 1996. Global climate change and emerging infectious diseases. *J. Amer. Med. Assoc.*, **275**, 217–223.

Pelletier, H., W.W.C. Gieskes, and A.G.J. Buma, 1996. Ultraviolet-B radiation resistance of benthic diatoms isolated from tidal flats in the Dutch Wadden Sea. *Mar. Ecol. Prog. Ser.*, **135**, 163–168.

Peng, T-H., 1992. Possible effects of ozone depletion on the global carbon cycle. *Radiocarbon*, **34**, 772–779.

Percy, K.E., and J.P. Hall, 1997. Enhanced UV-B: A threat to Canada's forests? In *Proceedings of the Ontario Climate Advisory Committee workshop on atmospheric ozone: issues, science, impacts, policy and programs*, September 30–October 1, 1996, Toronto. In press.

Pietrzak, L.N., J. Dorell, M.J. Morrison, and J. Fregeau-Reid, 1995. In situ microspectral characterization of flavonoids in soybean leaves. Abstract. Page 172 in *Proceedings of the 80th annual meeting of Am. Ass. Cereal Chemists*, San Antonio, Texas, November 5–9, 1995.

Platt, T., P. Jauhari, and S. Sathyendranath, 1992. The importance and measurement of new production. Pages 273–284 in *Primary Productivity and Biogeochemical Cycles in the Sea*. P.G. Falkowski and A. Woodhead, eds. London: Plenum.

Prézelin, B.B., N.P. Boucher, and R.C. Smith, 1994. Marine primary production under the influence of the Antarctic ozone hole: Icecolors '90. Pages 159–186 in *Ultraviolet Radiation in Antarctica: Measurements and Biological Effects*. C.S. Weiler and P.A. Penhale, eds. Washington, D.C.: American Geophysical Union.

Rau, W., and H. Hofman, 1996. Sensitivity to UV-B of plants growing in different altitudes in the Alps. *J. Plant Physiol.*, *148*, 21–25.

Ren, L., X-D. Huang, B.J. McConkey, D.G. Dixon, and B.M. Greenberg, 1994. Photoinduced toxicity of three polycyclic aromatic hydrocarbons (fluoranthene, pyrene, and naphthalene) to the duckweed *Lemna gibba* L. G-3. *Ecotoxicol. Environ. Safety*, **28**, 160–171.

Rivers, J.K., P.C. Frederiksen, and C. Dibdin, 1990. A prevalence survey of dermatoses in the Australian neonate. *J. Amer. Acad. Dermatol.*, **23**, 77–81.

Robberecht, R., and M.M. Caldwell, 1978. Leaf epidermal transmittance of ultraviolet radiation and its implications for plant sensitivity to ultraviolet-radiation induced injury. *Oecologia*, **32**, 277–287.

Rosso, S., R. Zanetti, C. Martinez, M. Tormo, S. Schraub, H. Sancho-Garnier, S. Franceschi, L. Gafa, et al., 1996. The multicentre South European Study "Helios" II: different sun exposure patterns in the aetiology of basal cell and squamous cell carcinomas of the skin. *Br. J. Cancer*, **73**, 1447–1454.

Runeckles, V.C., and S. Krupa, 1994. The impact of UV-B radiation and ozone on terrestrial vegetation. *Environ. Pollut.*, **83**, 191–213.

Sakka, A., M. Gosselin, M. Levasseur, S. Michaud, and S. Demers, 1996. Effects of reduced ultraviolet radiation on concentrations of dimethylsulfoniopropionate and dimethylsulfide during a microcosm study in the lower St. Lawrence estuary. *Mar. Ecol. Prog. Ser.*, in press.

Sarmiento, J.L., and M. Bender, 1994. Carbon biogeochemistry and climate change. *Photosyn. Res.*, **39**, 209–234.

Scaiano, J.C., J.C. Netto-Ferreira, and V. Wintgens, 1991. Fragmentation of ketyl radicals derived from alfa-phenoxyacetophenone: an important mode of the decay for lignin-related radicals. *J. Photochem. and Photobiol.*, **59**, 265.

Schindler, D.W., P.J. Curtis, B.R. Parker, and M.P. Stainton, 1996. Consequences of climate warming and lake acidification for UV-B penetration in North American boreal lakes. *Nature*, **379**, 705–708.

Schmidt, J.A., and C. Heitner, 1991. Light-induced yellowing of mechanical and ultra-high yield pulps: Part 1, effects of methylation, $NaBH_4$ reduction, and ascorbic acid on chromophore formation. *J. Wood Chem. Tech.*, **11**(4), 397.

Schmidt, J.A., and C. Heitner. 1992. Light-induced yellowing of mechanical and ultra-high yield pulps; Part 2, the role of etherified guaiacylglycerol-beta-arylether groups. *Proceedings of the Second European Workshop on Lignicellulosics and Pulp*, Grenoble.

Schmidt, J.A., A.B. Berinstain, F. de Rege, C. Heitner, C. Johnston, and J.C. Scaiano, 1991. Photodegradation of the lignin model alfa-guaiacoxyacetoveratrone: unusual effects of solvent, oxygen, and singlet state participation. *Can. J. Chem.*, **69**, 104.

Schmidt, J.A., E. Goldszmidt, C. Heitner, J.C. Scaiano, A.B. Berinstain, and L.J. Johnston, 1993. Photodegradation of alfa-guaiacoxyacetoveratrone. Pages 122–128 in *Photochemistry of Lignocellulosic Materials*. Amer. Chem. Soc. Symposium Series 531. C. Heitner and J.C. Scaiano eds. Washington, D.C.: American Chemical Society.

Schnitzler, J-P., T.P. Jungblut, W. Heller, C. Langbartels, M. Kofferlein, and H. Sandermann. 1994. Effects of ozone and UV-B radiation on Scots pine. *Acta Hort.*, **381**, 463–469.

Schnitzler, J-P., T.P. Jungblut, W. Heller, M. Köfferlein, P. Hutzler, U. Heinzmann, E. Schmezler, D. Ernst, C. Langbartels, and H. Sandermann, 1996. Tissue localization of UV-B–screening pigments and of chalcone synthase mRNA in needles of Scots pine seedlings. *New Phytol.*, **132**, 247–258.

Scotto, J., T.R. Fears, and J.F. Fraumeni Jr., 1983. *Incidence of Non-melanoma Skin Cancer in the United States*. NIH Publ. No. 82-2433. Washington, D.C.: U.S. Public Health Service, National Institutes of Health.

Scully, N.M., and D.R.S. Lean, 1994. The attenuation of the ultraviolet radiation in temperate lakes. *Arch. Hydrobiol. Beih. Ergebn. Limnol.*, **43**, 135–144.

Searle, N.D., 1994. Effect of light source emission on durability testing. Pages 52–67 in *ASTM STP 1202: Accelerated and Outdoor Durability testing of Organic Materials*. W.D. Ketola and D. Grossman eds. Philadelphia: American Society for Testing Materials.

Smith, C., J.M. McGregor, J.N.W. Barker, R.W. Morris, S.P.A. Rigden, D.M. MacDonald, 1993. Excess melanocytic nevi in children with renal allografts. *J. Amer. Acad. Dermatol.*, **28**, 51–55.

Smith, R.C., B.B. Prézelin, K.S. Baker, R.R. Bidigare, N.P. Boucher, T. Coley, D. Karentz, S. MacIntyre, H.A. Matlick, D. Menzies, M. Ondrusek, Z. Wan, and K.J. Waters, 1992. Ozone depletion: ultraviolet radiation and phytoplankton biology in Antarctic waters. *Science*, **255**, 952–959.

Spruance, S.L., 1985. Pathogenesis of herpes simplex labialis: experimental induction of lesions with UV light. *J. Clin. Microbiol.*, **22**, 366–368.

Stewart, J.D., and J. Hoddinott, 1993. Photosynthetic acclimation to elevated atmospheric carbon dioxide and UV irradiation in *Pinus banksiana*. *Physiol. Plant.*, **88**, 493–500.

Sullivan, J.H., and A.H. Teramura, 1988. Effects of ultraviolet-B radiation on seedling growth in the Pinaceae. *Amer. J. Bot.*, **75**, 225–230.

Sullivan, J.H., and A.H. Teramura, 1989. The effects of ultraviolet-B radiation on loblolly pines. 1: Growth, photosynthesis, and pigment production in greenhouse grown saplings. *Physiol. Plant.*, **77**, 202–207.

Sullivan, J.H., and A.H. Teramura, 1992. The effects of ultraviolet-B radiation on loblolly pine. 2: Growth of field seedlings. *Trees*, **6**, 115–120.

Sullivan, J.H., and A.H. Teramura, 1994. The effects of UV-B radiation on loblolly pine. 3: Interaction with CO_2 enrichment. *Plant Cell Environ.*, **17**, 311–317.

Sullivan, J.H., A.H. Teramura, and L.H. Ziska, 1992. Variation in UV-B sensitivity in plants from a 3,000-m elevation gradient in Hawaii. *Am. J. Bot.*, **79**, 737–743.

Sullivan, J.H., B.W. Howells, C.T. Ruhland, and T.A. Day, 1996. Changes in leaf expansion and epidermal screening effectiveness in *Liquidambar stryaciflua* and *Pinus taeda* in response to UV-B. *Physiol. Plant.* **98**, 349–357.

van der Leun, J.C., and F.R. de Gruijl, 1993. Influences of ozone depletion on human and animal health. Pages 95–123 in *UV-B Radiation and Ozone Depletion: Effects on Humans, Animals, Plants, Microorganisms, and Materials*. M. Tevini, ed. Boca Raton: Lewis.

Van Doren, K.S., 1995. Effect of enhanced UV-B radiation on Ontario soybean cultivars and maize hybrids. M.Sc. Thesis, U. of Guelph.

Vetter, R. D., 1996. UV-B irradiance and DNA damage in pelagic fish eggs and larvae: temperate and polar habitats. *Eos*, **76**, OS164.

Vincent, W. F., and S. Roy, 1993. Solar ultraviolet-B radiation and aquatic primary production: damage, protection, and recovery. *Environ. Rev.*, **1**, 1–12.

Wan, J.K.S., I.A. Shkrob, and M.C. Depew, 1993. Primary photophysical and photochemical processes of alpha-guaiacoxyacetoveratrone. Pages 99-110 in *Photochemistry of Lignocellulosic Materials*. Amer. Chem. Soc. Symposium Series 531. C. Heitner and J.C. Scaiano eds. Washington, D.C.: American Chemical Society.

Wängberg, S-A., J-S. Selmer, N.G.A. Eklund, and K. Gustavson, 1996. UV-B effects on Nordic marine ecosystems – a literature review. *TemaNord*, **515**, 1–45.

Warfel, A.H., J.A. Moy, T. Meola, M. Sanchez, N.A. Soter, and D.V. Belsito, 1993. Effect of ultraviolet B (UVB) on the expression of human immunodeficiency virus (HIV) in mice and humans. *Photochem. Photobiol.*, **57**, 755–759.

Weinbauer, M. G., S.W. Wilhelm, and C.A. Suttle, 1996. Significance of photoreactivation for maintaining high concentrations of infectious viruses in the sea. Abstr. Amer. Soc. Microbiol. New Orleans, LA, May 1996.

Weinstock, M.A., G.A. Colditz, W.C. Willett, M.J. Stampfer, B.R. Bronstein, M.C. Mihm, and F.E. Speizer, 1989a. Moles and site specific risk of non-familial cutaneous malignant melanoma in women. *J. Natl. Cancer Inst.*, **81**, 948–952.

Weinstock, M.A., G.A. Colditz, W.C. Willett, M.J. Stampfer, B.R. Bronstein, M.C. Mihm, and F.E. Speizer, 1989b. Non-familial cutaneous melanoma incidence in women associated with sun exposure before 20 years of age. *Pediatrics*, **84**, 199–204.

Weir, N.A., and K. Whiting, 1990. Studies of poly(ortho-acetylstyrene)s II: Photoreactions of poly(o-acetylstrene), *J. Polymer Sci. Part A: Polymer Chem., 28*, 1935–1945.

Weir, N.A., and K. Whiting, 1992. Photolysis of poly(o-acetylstyrene) in solution. *J. Polymer Sci. Part A: Polymer Chem.*, **30**, 1601–1608.

Weir, N.A., J. Arct, and A. Ceccarelli, 1993. Photoreactions of poly(o-butyrylstyrene) in the long wave region. *J. Photochem. and Photobiol. Part A: Chem.*, **72**, 87–93.

Weir, N.A., J. Arct, and A. Ceccarelli, 1994a. Photodecomposition of lignin model compounds. Part I. *Polymer Degradation and Stability*, **43**(3), 409-414.

Weir, N.A., J. Arct, A. Ceccarelli, and A. Siren, 1994b. Some photoreactions of substituted poly(acrylophenomes). *European Polymer J.*, **30**(6), 701–706.

Weir, N.A., J. Arct, and A. Ceccarelli, 1995. Chromophore production in lignin model compounds – anaerobic reactions. *Research Chemistry Intermediate*, **21**(3–5), 353–371.

Weir, N.A., J. Arct, A. Ceccarelli, and K. Whiting, 1996a. Polymers with enhanced photostability: photoreactions of poly(o-isobutylstyrene) in the long wave region. *J. Photochem. and Photobiol. Part A: Chem.*, **96**, 203–209.

Weir, N.A., J. Arct, and A. Ceccarelli, 1996b. Long-wave photodegradation of poly(3,5-dimethooxyacrylophenone) in the solid state. *European Polymer J.*, **32**(7), 805–810.

Weir, N.A., J. Arct, A. Ceccarelli, and D. Puumala, 1996c. Long-wave photochemistry of dimethoxylated compounds related to lignin. *Polymer Degradation and Stability*, **52**, 119–129.

Wellburn, A., 1994. Effects of UV-B radiation on wax biosynthesis. Pages 195–204 in *Air Pollutants and the Leaf Cuticle*. NATO ASI Series G, vol. 36. K.E. Percy, J.N. Cape, R. Jagels, and C. Simpson, eds. Heidelberg: Springer-Verlag.

White, E., C.S. Kirkpatrick, and J.A.H. Lee, 1994. Case-control study of malignant melanoma in Washington State. I: Constitutional factors and sun exposure. *Amer. J. Epidemiol.*, 139, 857–868.

Whittaker, R.H., 1975. *Communities and Ecosystems*. 2nd ed. New York: Macmillan.

Wilhelm, S. W., M.G. Weinbauer, D.R. Garza, K.M. Rodda, and C.S. Suttle, 1996. In situ light-mediated destruction and repair of marine virus communities and isolates. *Eos*, **76**, OS208.

Williamson, C.E., P.C. Schulze, B.R. Hargreaves, and J. Seva, 1994. The impact of short-term exposure to UV-B radiation on zooplankton communities in northern temperate lakes. *J. Plankton Res.*, **16**, 205–218.

Williamson, C.E., R.S. Stemberger, D.P. Morris, T.M. Frost, and S.G. Paulsen, 1996. Ultraviolet radiation in a North American lake: attenuation estimates from DOC measurements and implications for plankton communities. *Limnol. Oceanogr.*, **41**, 1024.

Wilson, M.I., and B.M. Greenberg, 1993a. Protection of the DI photosystem II reaction center protein from degradation in ultraviolet radiation following adaptation of *Brassica napus* L. to growth in UV-B. *J. Photochem. and Photobiol.*, **57**, 556–563.

Wilson, M.I., and B.M. Greenberg, 1993b. Specificity and photomorphogenic nature of UV-B induced cotyledon curling in *Brassica napus* L. *Plant Physiol.*, **102**, 671.

Wolf, P., C. Donawho, and M. Kripke, 1993. Analysis of the protective effect of different sunscreens on ultraviolet radiation induced local and systemic suppression of contact hypersensitivity and inflammatory responses in mice. *J. Invest. Dermatol.*, **100**, 254–259.

Yakimchuck, R., and J. Hoddinott, 1994. The influence of ultraviolet-B light and carbon dioxide enrichment on the growth and physiology of seedlings of three conifer species. *Can. J. For. Res.*, **24**, 1–8.

Yan, N.D., W. Keller, N.M. Scully, D.R.S. Lean, and P.J. Dillon, 1996. Increased UV-B penetration in a lake owing to drought-induced acidification. *Nature*, **381**, 141–143.

Zanett, R., S. Rosso, C. Martinez, C. Navarro, S, Schraub, H. Sancho-Garnier, S. Fraceschi, L. Gafa, et al., 1996. The multicentre South European Study "Helios" I: skin characteristics and sunburns in basal cell and squamous cell carcinomas of the skin. *Br. J. Cancer*, **73**, 1440–1446.

Ziska, L.H., A.H. Teramura, and J.H. Sullivan, 1992. Physiological sensitivity of plants along an elevational gradient to UV-B radiation. *Am. J. Bot.*, **79**, 863–871.

Zmudzka, B.Z., and J.Z. Beer, 1990. Activation of human immunodeficiency virus by ultraviolet radiation. *Photochem. Photobiol.*, **52**, 1153–1162.

APPENDIX

ACRONYMS AND ABBREVIATIONS

ADEOS	Japanese spacecraft, launched 1996
AES	Atmospheric Environment Service
AGCM	Atmospheric General Circulation Model
ASHOE	Airborne Southern Hemisphere Ozone Experiment
ATMOS	Atmospheric Trace Molecule Spectroscopy
BCC	Basal Cell Carcinoma
BUV	Backscattered Ultraviolet
BWF	Biological Weighting Factor
CCCma	Canadian Centre for Climate Modelling and Analysis
CFC	Chlorofluorocarbon
CIE	Commission Internationale de l'éclairage
CLAES	Cryogenic Limb Array Spectrometer, on UARS
CMAM	Canadian Middle Atmosphere Model
CMC	Canadian Meteorological Centre
CMOS	Canadian Meteorological and Oceanographic Society
CRISTA	Cryogenic Infrared Spectrometers and Telescopes for the Atmosphere
CSA	Canadian Space Agency
CTM	Chemical Transport Model
DMS	Dimethyl Sulphide
DMSP	Dimethylsulphoniopropionate
DNA	Deoxyribonucleic Acid
DOC	Dissolved Organic Carbon
ECC	Electrochemical Concentration Cell
ECMWF	European Centre for Medium Range Weather Forecasting
ENSO	El Niño Southern Oscillation
ENVISAT	ESA satellite scheduled for launch in 1999
ER-2	High altitude research aircraft operated by NASA
ERS-2	Earth Resources Satellite 2, of the ESA
ESA	European Space Agency
FASCD	Fast Atmospheric Signature Code
FTIR	Fourier Transform Infrared spectrometer
GCM	General Circulation Model
GOME	Global Ozone Monitoring Experiment
GSFC	Goddard Space Flight Center, NASA
HALOE	Halogen Occultation Experiment, on UARS
HCFC	Hydrogenated Chlorofluorocarbon
IPCC	Intergovernmental Panel on Climate Change
IR	Infrared
ISTS	Institute for Space and Terrestrial Science
JPL	Jet Propulsion Laboratory, California
LITE	Lidar In-space Technology Experiment
MAESA	Measurements for Assessing the Effects of Supersonic Aircraft
MAI	Middle Atmosphere Initiative
MOPITT	Measurement of Pollution in the Troposphere
NASA	National Aeronautics and Space Administration
NDSC	Network for the Detection of Stratospheric Change
NOAA	National Oceanic and Atmospheric Administration
NWP	Numerical Weather Prediction
OA	Objectively Analysed
ODIN	Satellite of the Swedish Space Corporation
OSIRIS	Optical Spectrograph and Infrared Imaging System
PSC	Polar Stratospheric Cloud
QBO	Quasi-Biennial Oscillation
RAF	Radiometric Amplification Factor
SAGE	Stratospheric Aerosol and Gas Experiment
SBUV	Solar Backscatter Ultraviolet
SCC	Squamous Cell Carcinoma
SEF	Spectral Finite Element forecast model
SPADE	Stratospheric Photochemistry, Aerosols, and Dynamics Experiment
SPARC	Stratospheric Processes and their Role in Climate
STE	Stratospheric-Tropospheric Exchange
STRAT	Stratospheric Tracers of Atmospheric Transport
TOMS	Total Ozone Mapping Spectrometer
TOVS	Tiros Operational Vertical Sounder
UARS	Upper Atmosphere Research Satellite
UNEP	United Nations Environment Programme
UQAM	University of Quebec at Montreal
UV	Ultraviolet
VOC	Volatile Organic Compound
WHO	World Health Organization
WMO	World Meteorological Organization
WOUDC	World Ozone and UV Data Centre

GLOSSARY

Aerosol A suspension, in a gaseous medium, of solid particles, liquid particles, or solid and liquid particles.

Albedo The ratio of the amount of electromagnetic radiation reflected by a body to the amount incident upon it, commonly expressed as a percentage.

Atmospheric General Circulation Model (AGCM) Computer simulations of the global atmosphere's general circulation.

Brewer Brewer Total Ozone Spectrophotometer.

Calibration The determination, by measurement or comparison with a standard, of the accuracy of a measuring instrument.

Characterization The assessment of the response of an instrument to variations in factors other than those intended to be measured (e.g., temperature response, time constant, linearity of response).

Chlorofluorocarbons (CFCs) Hydrocarbons in which the hydrogen atoms have been replaced by chlorine and fluorine atoms.

Dobson Dobson Total Ozone Instrument

Dobson Unit (DU) The standard unit for total ozone (100DU = 1mm at standard temperature and pressure).

Flux Transfer of power onto, or across, a surface, expressed in watts. Flux is often used incorrectly in place of irradiance. However, flux density, being power per unit area, is the same as irradiance.

Greenhouse Effect Heating effect exerted by the atmosphere upon the earth because the atmosphere absorbs and reemits infrared radiation. The functional analogy to a greenhouse is false.

Greenhouse Gas A gas in the atmosphere that emits infrared radiation.

Halons Proprietary trade name for brominated CFCs.

Infrared Radiation (IR) Electromagnetic radiation whose wavelengths lie in the range of 0.8 μm to 10,000 μm (see also short-wave and long-wave).

Intensity Same as radiance.

Interferometer Optical instrument using the twin-beam or multibeam interference of light to make measurements with high spectral resolution. Also known as a Fourier Transform Spectrometer.

Irradiance The power transferred onto, or across, a unit area of surface by radiation from all directions within a hemisphere. The surface is usually horizontal. Measured in Wm^{-2}.

Irradiation The energy transferred onto, or across, a unit area of surface by radiation from all directions within a hemisphere during some specified period (e.g., per day). Measured in Jm^{-2}.

Lidar Optical equivalent of radar, in which pulsed radiation from a laser is transmitted upwards into the atmosphere and the return radiation is measured as a function of time.

Long-wave Radiation Radiation in the 4–100 μm wavelength range, usually referring to what is emitted by the earth or atmosphere.

Methane (CH_4) A colourless, odourless gas that is lighter than air, having strong infrared absorption bands at 3.3, 3.8, and 7.7 μm.

Nadir The point on the celestial sphere vertically below the observer, or 180 degrees from the zenith.

Nitrous Oxide (N_2O) A colourless, sweet-tasting gas that is slightly soluble in water. It has strong infrared absorption bands at 4.5 and 7.8 μm.

Optical Depth A measure of atmospheric transmission, specifically the negative of the natural logarithm of the transmission of the direct beam.

Ozone (O_3) A gaseous allotrope of oxygen with three atoms per molecule.

Ozone Hole A dramatic if not precise description of the area of low ozone values that has developed during spring in the Antarctic since about 1980.

Potential temperature The temperature a parcel of air would acquire if compressed to standard pressure (101.325 kPa).

Radiance The electromagnetic power originating from a given direction and transferred across a unit surface normal to that direction. Measured in $Wm^{-2}\ sr^{-1}$. Also called Intensity.

Radiative Transfer Transmission of energy by electromagnetic radiation.

Radiometer Instrument for measuring radiation.

Short-wave Radiation Radiation with wavelengths less than 4.0 μm. In atmospheric physics this is mostly solar radiation.

Spectral Irradiance Spectrally resolved irradiance, i.e. power per unit area per unit wavelength interval. Units $Wm^{-2}\,\mu m^{-1}$.

Spectral Radiance Spectrally resolved radiance, i.e., power per unit area per unit wavelength interval per unit solid angle. Measured in $Wm^{-2}\,sr^{-1}\,\mu m^{-1}$.

Spectroradiometer An instrument used to measure spectral radiance or irradiance at many wavelengths.

Spectrometer An instrument used to measure spectral radiance or irradiance at many wavelengths (i.e., the same as a spectroradiometer).

Spectrophotometer An instrument that measures spectral irradiance or spectral radiance at a few wavelengths.

Stratosphere Region of the atmosphere extending approximately from 10 km to 50 km in altitude. Temperature generally increases with height, and the radiation balance controls the temperature distribution in this region.

Total Ozone Usually specified as the thickness of a layer of pure ozone at standard temperatue and pressure that would contain the same number of ozone molecules as that in the vertical atmospheric column above a given point on the earth's surface. A typical value is 3 mm or 300 DU.

Tropopause The atmospheric boundary between the troposphere and the stratosphere, usually characterized by an abrupt change in the lapse rate. The altitude of the tropopause varies between 15–20 km in the tropics and 8 km in polar regions.

Troposphere The lower layers of the atmosphere extending from the surface to a height of between 8 and 20 km. The region is characterized by a general decrease in temperature with altitude.

Ultraviolet (UV) Radiation with wavelengths in the range of 100–400 nm, commonly divided into UV-A (400–315 nm), UV-B (315–280 nm), and UV-C (280–100 nm).

Umkehr Effect The term Umkehr (German, meaning reversal or return) comes from the description of the graph of the logarithm of the ratio of zenith sky radiances at two UV wavelengths plotted against the solar zenith angle. The graph has a stationary value and can be used to infer the ozone profile (Umkehr method).

Window (spectral) A region of the spectrum where there is little atmospheric absorption.

Zenith Angle The angle between a particular direction and the local vertical.